ON THE IMPLICATIONS OF VARIOUS APPROACHES TO GROUNDWATER SOURCE PROTECTION

by

Rengina Rahman

A thesis
presented to the University of Waterloo
in fulfillment of the
thesis requirement for the degree of
Doctor of Philosophy
in
Earth Sciences

Waterloo, Ontario, Canada, 2008

© Rengina Rahman 2008

I hereby declare that I am the sole author of this thesis. This is a true copy of the thesis, including any required final revisions, as accepted by my examiners.

I understand that my thesis may be made electronically available to the public.

Abstract

Protection of groundwater sources has become an important issue in Canada. Over the last decade many approaches to the protection of groundwater sources have evolved. Some approaches provide qualitative information while others give quantitative values with respect to protection measures. The objective of the thesis is to examine the existing approaches of source water protection (SWP) using a complex geological setting, and introduce new methodologies towards the quantitative measurement of the various steps of SWP. The information obtained from the studies can be used to set up future guidelines for SWP.

The first step in SWP is to assess the vulnerability of an aquifer. In this thesis, we compare three approaches for evaluating aquifer vulnerability: the Index Approach (Intrinsic Susceptibility Index, or ISI), the Hydraulic Resistance (HR) Approach (similar to the Aquifer Vulnerability Index, or AVI) and the Travel Time Approach (Surface to Aquifer Advective Time, or SAAT). The ISI approach uses the thickness and vertical hydraulic conductivity of the layers overlying an aquifer, and the vulnerability is expressed as a numerical score which is related to these parameters but is not physically based. The HR approach is physically based, uses the same parameters as ISI with the addition of porosity, and results are in the form of travel time under a unit gradient. SAAT extends the physically based approach by including the unsaturated zone and using the actual downward gradient; results are given in terms of advective travel time from surface to aquifer. These three approaches are compared, using two different aquifer systems.

The second step in SWP is the delineation of wellhead protection areas (WHPAs). The WHPA delineates the area within which a source of contamination could have an impact on the well. The actual impact on the well depends not only on the source, but also on the characteristics of the groundwater system. Important considerations include the dimensionality of the system, the uncertainty in the system characteristics, and the physical processes that could affect the impact. The conventional approach is to define different time of travel (TOT) zones based on backward advective particle tracking. An alternative approach is to apply backward advective-dispersive solute transport modelling, in which dispersion can be taken as representing the uncertainty in defining the hydrogeologic characteristics (e.g. hydraulic conductivity) of the aquifer. The outlines of the TOT zones in the backward advective particle tracking approach is obtained by drawing an envelope around the respective tracks, which may require considerable guesswork. In the

backward-in-time transport modelling, the outline of the TOT zones are developed using mass balance principles.

The third step is the assessment of well vulnerability. Well vulnerability is based on the source-pathway-receptor concept which analyses the transport and fate of the contaminants along its path from the source to the receptor, and the interaction of the well itself with the flow system, and thus determines the actual impact on the well. The impact can be expressed in terms of the contaminant concentration in the well water. The mapping of the impact can be carried out by using a standard advective-dispersive transport model in either a forward-in-time mode (for a known contaminant source) or in a backward-in-time mode (for unknown sources). Thus, the well vulnerability concept goes beyond the conventional approach of WHPA, which is based solely on advective transport, neglecting dispersion and chemical processes.

For any known point or non-point time-varying contaminant sources located arbitrarily within the well capture zone, the expected concentration at the well can simply be evaluated by convoluting the source mass with the results of the well vulnerability without further use of the model. Convolution is a well-known and effective superposition method to deal with arbitrary inputs in time and space for linear systems. The information of the contaminant concentration in the well water can be used to quantify the risk of a well becoming contaminated.

Risk can be expressed in terms of the exposure value of the contaminant concentration exceeding the allowable limit and the time frame within which the well becomes contaminated. The exposure value can be integrated with the time element to set up a ranking of priorities, or to calculate the investment that must be made today in order to have the required funds available for remediation at the time it becomes necessary. The concept is applied to a well using hypothetical contaminant sources located arbitrarily within the capture zone.

Well vulnerability maps can be used as a powerful tool to identify the optimal locations for Beneficial Management Practices (BMPs). A case study addressing the problem of elevated nitrate levels in a drinking water supply well is used to demonstrate the principle. The reduction of nitrate input concentration within the most vulnerable areas shows the largest impact at the well.

Acknowledgements

I would like to express my sincere gratitude to my co-supervisors Professors Emil Frind and Dave Rudolph for introducing me to interesting research projects related to this thesis. I am very grateful to Professor Emil Frind for his insightful guidance, patience and support for my work. I would like to express sincere thanks to Professor Dave Rudolph for his insightful advice and encouragement throughout this research. I like to thank Professor Neil Thomson for providing important suggestions for certain phases of my research work. Special thanks to Dr. John Molson for explaining various aspects of modelling on many occasions and for always making himself available for discussions. I like to thank Dr. Michel Robin for serving as the external examiner and for his many useful comments on the thesis. I also thank Dr. Jon Paul Jones for his helpful discussions.

I am grateful to Rob McLaren for sharing his expertise to run groundwater models. I would like to acknowledge Dr. Fabien Cornaton for sharing his views on well vulnerability. Thanks are due to Richard Wootton of the Region of Waterloo for providing nitrate data. I like to also thank my fellow graduate students Sunyoung, Tapesh, Marcelo, Ben, Rasheeda, Ed Cey, Rudy, Eric, Paulo, Muhammad and Showmin, with whom I had discussions many times.

Finally this thesis might not exist at all without the love and support of my husband Anwar and two lovely daughters Zara and Tanisha. I can never thank my parents and sisters enough for their love and encouragement.

My research was supported in part through grants awarded to Professors Frind and Rudolph by the Natural Sciences and Engineering Research Council of Canada, and the Best in Science program of the Ontario Ministry of Environment.

Dedication

To my husband and our two daughters.

Contents

List of Tables

List of Figures

Chapter 1

Introduction

1.1 General

Groundwater provides a significant portion of the drinking water supply in many communities. The Region of Waterloo in Southern Ontario, Canada, for example, receives approximately 75% of the municipal water supply from groundwater resources. A network of over 100 supply wells most clustered in well fields, pump water from three main aquifers [Region of Waterloo, 2007]. The quality of this water source has been excellent; however, over the last decade, rapid development has increased the threat to water quality. As a result, the protection of groundwater has become more important in recent years.

Harmful substances (both natural and synthetic) released at point sources or areal (non-point) sources are the major sources of groundwater contamination. Point sources include landfill leachate, and oil or gasoline spills, while non-point sources originate from agricultural activities and road salt. In groundwater environments, some contaminants are dissolved in the water or are highly mobile and persistent, while others break down rather quickly or readily adhere to soil particles. The different types of behavior cause large variations in the time taken for contaminants to reach a water supply well.

The largest anthropogenic non-point source of contamination worldwide is nitrate originating from fertilizer application on farm fields [Bouchard et al., 1992]. Nitrogen fertilizer that is not taken up by plants on the farm fields is volatilized or carried away by surface runoff and the rest leaches to the groundwater in the form of nitrate. This not only makes the nitrogen unavailable to crops, but can also elevate

the nitrate concentration in groundwater above the level acceptable for drinking water quality. Other sources of nitrate contamination are septic systems, manure storage, or spreading operations. Similarly, nitrogen from manure can be lost from fields, barnyards, or storage locations. Septic systems can elevate groundwater nitrate concentrations because they remove only half of the nitrogen in wastewater, leaving the remaining half to percolate to groundwater. Exposure to drinking water with a nitrate level at or just above the health standard of 10 mg/L nitrate-N is a potential health problem, primarily for infants. Epidemiological evidence linking intake of nitrate and nitrite with cancer occurrences in human beings is equivocal [Ward et al., 2003], [Roos et al., 2003], and [Weyer et al., 2001].

An example of nitrate contamination is the Thornton Well Field which supplies about half the drinking water demand for the City of Woodstock in Southern Ontario. Nitrate concentrations in extracted water from this well field have been steadily increasing since 1980. The water in some wells started to exceed Ontario′s Maximum Allowable Concentration (MAC) of 10 mg-N/L in 1994 [Haslauer, 2005]. To satisfy the MAC, groundwater of different compositions from different sources has been blended before distribution. However, the problem has been worsening in recent years. In order to reduce nitrate contamination in the wells, the County of Oxford has purchased an area of farmland within the 2-year capture zone of the Thornton well field, renting it back to farmers with restrictions placed on the amount of nitrate fertilizer that can be applied. The county grants the farmers compensation by renting the land for less than market value [Haslauer, 2005].

The environmental impact of road de-icing salt has also been a growing concern over the past decade in Canada [Howard et al., 1993]; [Jones et al., 1986]; [Bester et al., 2006]. For groundwater-dependent areas like Waterloo Region, the impacts of road salt on groundwater resources are a significant concern. Since 1997, 13 municipal drinking water wells in Waterloo Region have tested higher than the 250 mg/L drinking water standard for chloride [Region of Waterloo, 2006]. The water from these wells is diluted with water from other wells through the municipal drinking water system. However, the continued trend of increasing chloride levels is a concern for the region.

The major elements of source water protection (SWP) are the identification of critical contributing areas that are likely to become contaminated, the identification of potential threats and sources of contamination within those areas, and

the assessment of the risk of groundwater sources becoming contaminated. This information can be put together to provide usage restrictions or to focus greater attention within the more sensitive areas in order to prevent contamination of the underlying groundwater resources.

Over the last decade, procedures have evolved in developing methods to protect drinking water resources. The first step is usually to evaluate the vulnerability of groundwater resources to surface or subsurface contamination. The concept of aquifer vulnerability/susceptibility was first introduced by Trotta [Trotta, 1985]. Aquifer vulnerability/susceptibility is defined as the protective effect of overlying layers on an actual or potential drinking water aquifer. The detailed history and concept of aquifer vulnerability is given later in this thesis.

The next step in groundwater protection is to delineate wellhead protection areas (WHPAs) around the water supply wells. To date, a large number of analytical and numerical approaches have been employed to facilitate the delineation of WHPAs. The typical analytical approach involves the simplification of a groundwater system to a single aquifer in two dimensions, neglecting recharge. Analytical techniques are usually valid in simple homogeneous systems. Numerical approaches are utilized primarily for complex aquifer systems where recharge plays a vital role. The numerical approach can provide estimates for both transient and steady-state scenarios.

The most commonly used technique for WHPA delineation is the application of backward advective particle tracking using a simulated steady-state flow field. In this approach, particles may be tracked for a given time period to generate a time-dependent capture zone, or particles may be tracked until they meet the water table or any of the domain boundaries to generate a maximum extent of the capture zone. Examples of 3D capture zone modelling are given by Kinzelbach et al. (1992), Martin and Frind (1998), Frind et al. (2002), and others. As an alternative to particle tracking, transport modelling can be used to delineate a capture zone. While standard particle tracking considers only the advective component of flow, transport modelling considers both the advective and the dispersive component. The dispersive component can be interpreted as representing the uncertainty in the hydrogeologic parameters [Frind et al., 2002].

Chin and Chittaluru (1994) used a random walk approach to delineate capture

zones around pumping wells. Vassolo (1998) applied stochastic inverse modelling to the delineation of the capture zone of a well in Germany. Kunstmann and Kinzelbach (2000) used Kolmogorov's backward equation with a first-order second-moment method to obtain the probabilistic capture zones that account for uncertainty in the model parameters for the same aquifer. In 2001, Feyen introduced the generalized likelihood uncertainty estimation methodology to the problem of capture zone uncertainty [Feyen et al., 2001].

The delineation of capture zones by standard particle tracking methods, however, is based solely on advective time of travel (TOT) and thus neglects a number of processes that tend to affect the actual impact of contamination on a well. These processes include dispersion, chemical reactions, and dilution at the well by mixing of contaminated water with clean water. These processes are included in the concept of well vulnerability. Well vulnerability is based on the source-pathway-receptor concept which analyses the processes acting on a contaminant travelling through a groundwater system thus providing the actual impact on the well. The impact can be expressed in terms of the mass flux reaching the well or the contaminant concentration in the well water. This information is more useful in a decision-making process than time of travel alone.

In 1992, Bagtzoglou obtained backward location probabilities for identifying sources of contamination by reversing the flow field in a random walk method [Bagtzoglou et al., 1992]. Wilson and Liu used a heuristic method to obtain a backward probabilistic continuum model from the forward advective-dispersive equation [Wilson and Liu, 1995]. In 1999, Neupauer and Wilson used backward transport models to improve the characterization of known sources of groundwater contamination, to identify previously unknown contamination sources, and to delineate capture zones [Neupauer and Wilson, 1999]. Cornaton (2003) used backward transport modelling to delineate vulnerability maps for a single well for unknown sources within a 2D hypothetical system. Frind et al. (2006) used backward transport model to develop well vulnerability maps for the Greenbrook well field, which is part of the well system of the Regional Municipality of Waterloo in Southern Ontario [Frind et al., 2006].

In addition to the development of well vulnerability maps, protection of groundwater sources also requires the assessment of risk of well contamination. The risk of well contamination from potential contaminant sources can be assessed using the

Environment Protection Agency (EPA) Priority Setting Approach [EPA, 1990]. In this approach, a risk score is calculated by multiplying two risk components which are the likelihood of the well becoming contaminated, and the severity of the well contamination. In 2001, Harman linked GIS with the priority setting approach to make the approach more flexible and efficient [Harman et al., 2001].

Worrall et al. (2000) used statistical methods to assess the risk of pesticides to contaminate groundwater based on their chemical properties (mainly adsorption and degradation). Any pesticide found to occur above the drinking water limit was considered as a "leacher". The information obtained from the approach provides a prior indication of whether a new pesticide is a leacher or not. Butt and Oduyemi (2003) used a holistic approach and an accompanying knowledge-based computer model to assess the risk of the drinking water sources due to a nearby landfill. Nobre et al. (2007) assessed the risk of groundwater resource contamination based on a source-pathway-receptor approach. In their approach, the risk score is calculated by integrating information on intrinsic groundwater vulnerability (based on the index method), source zone mapping, and capture zone delineation.

The Government of Ontario has introduced an approach known as semi-quantitative risk assessment (SQRA) to determine the risk of specific threats entering the drinking water supply wells [Ontario Ministry of Environment (MOE), 2006]. The SQRA approach is performed primarily on an individual parcel-based scale. The parcel-based risk assessment relies on the information of the vulnerability and the threats inventory. The SQRA approach multiplies scores for threats and vulnerability to produce a risk rating. The risk rating is divided into four categories: significant, moderate, low, and negligible.

1.2 Objectives and Goals

Various steps of SWP, namely aquifer vulnerability, the delineation of wellhead protection areas (WHPAs), well vulnerability, and the assessment of risk of a well become contaminated, and the optimal application of Beneficial Management Practices (BMPs) within WHPAs are discussed in this study. One of the objective is to analyze the existing approaches of aquifer vulnerability in detail to show which approaches give the better representation of the physical processes of the groundwater system, and introduce alternative approaches. The standard approach for delineating WHPAs is to apply the backward advective particle tracking. An alter-

native approach is to apply the backward advective-dispersive transport modelling [Muhammad, 2000] and [Frind et al. 2002]. WHPAs delineated using the two approaches are compared in this study. The second objective is to advance the concept proposed by Frind et al. (2006) by defining well vulnerability for multiple wells within a well field in terms of concentrations of the unit pulse sources of contamination in the extracted well water, including dilution with clean water [Einarson and Mackay, 2001]. The concept of the well vulnerability is further used as a basis for risk assessment of a well becoming contaminated. Here we advanced the presently available approaches of risk assessment by introducing a quantitative approach based on the cost of well contamination. Well vulnerability can be used to identify the optimal location for the application of BMPs. The approaches are applied to simple hypothetical systems, as well as within a more complex real geological settings, to understand the accuracy and limitations of the methodologies. The goal of the research is to present complete as well as improved methodologies towards the quantitative measurement of the various steps of SWP. The information obtained from the methodologies can be used to set up future guidelines for SWP.

1.3 Organization of the Thesis

The remainder of the thesis is organized into eight chapters:

- Chapter 2 describes the study area and reviews the basic principles forming the basis for the groundwater flow and transport models applied in this thesis.
- Chapter 3 discusses standard approaches of the mapping of aquifer vulnerability and introduces alternative approaches. The mapping of aquifer vulnerability due to surface sources of contamination is one of the key elements in assessing groundwater vulnerability.
- Chapter 4 involves the delineation of WHPAs around the well based on the travel time of the contaminant particles from the ground surface to the well. The conventional approach for delineating WHPAs is to apply backward advective particle tracking in a steady-state flow field. An alternative approach is to apply backward advective-dispersive transport modelling. The study compares the WHPAs delineated using the two approaches for a hypothetical system as well as for the complex geological setting.

- In Chapter 5, a powerful approach known as the well vulnerability concept is reviewed, which provides more useful information than the conventional approaches used to delineate WHPAs. Well vulnerability describes the impact of a source in terms of the maximum expected concentration in the extracted well water, the time to reach maximum concentration, the time required to reach some predefined threshold value, and the time the concentration stays above the threshold value in the well water. The impact of a source at a known location can be determined using standard advective-dispersive transport modelling, which is known as the forward approach.

- Chapter 6 develops a systematic approach for mapping well vulnerability for sources at unknown locations using backward-in-time transport modelling. A sensitivity analysis on the well vulnerability map is also carried out in this chapter.

- Chapter 7 introduces a quantitative approach of risk assessment of a well becoming contaminated due to potential sources within the WHPA. This approach is based on the concept of well vulnerability. The results provide the exposure value and the time frame within which the well will become contaminated, and can be expressed in terms of the investment that must be made to cover the future cost of well remediation.

- The well vulnerability concept is also very useful for identifying the location of BMP areas. Chapter 8 presents a methodology and examples for identifying the best possible location within the WHPA to apply BMPs for reducing contamination at the well water.

- Chapter 9 is a summary of the thesis with some concluding remarks. It also includes recommendations for future work.

Chapter 2

The Waterloo Moraine Study Area: Conceptual Model

In this chapter, first we describe the geographical area that we area considering for applying various techniques of groundwater protection. A description of the groundwater flow and transport model used in the analysis is also provided.

2.1 Description of the Study Area

This study focuses on the Mannheim well field as an example for developing groundwater protection measures including vulnerability maps, delineation of the WHPA, and assessment of the risk of the well becoming contaminated. To a lesser extent, the neighbouring Greenbrook well field is also used.

The Mannheim well field is one of the most important well fields located within the Regional Municipality of Waterloo (RMOW) (Figure 2.1). The RMOW covers an area of approximately 1360 km^2 including the cities of Cambridge, Kitchener, and Waterloo and four townships: Wellesley, Wilmot, Woolwich, and North Dumfries. The RMOW has a population of $>$ 400,000 and derives 75% of its water supply from groundwater. One of the primary sources of water for the municipal water supply system is the Waterloo Moraine, a complex multi-aquifer system of glacial origin. As presented in Figure 2.1, the Waterloo Moraine is part of the Grand River watershed.

Glaciation of the Waterloo Region in the late Wisconsinan period ($23,000$ to $10,000$

years ago) was responsible for both the shape of the bedrock topography and the structure of the overlying Quaternary sediments. The area is underlain by layers of soft, sedimentary limestones, shales and sandstones. The sediments have been described as either till or kame moraines, with little sedimentological description of the internal composition and geometry of these strategic landforms [Karrow, 1987]. Kame or stratified moraines are composed of gravel, sand, and silt, deposited at the margin of inactive ice. Till moraines are mapped as massive sediment bodies and thought to be deposited by advancing ice. These till units act as protective barriers for the underlying materials except where the high permeability materials known as "windows" provide pathways for contamination to enter the aquifers. Glaciofluvial sand and gravel deposits located between the major till units form the major aquifers in the system. A detailed description of the glacial geology is given by Chapman and Putnam (1984) and Karrow (1993).

Because of its importance to the water supply of the Region of Waterloo, the Waterloo Moraine system has been studied in considerable detail by Martin and Frind (1998) as well as other researchers. The original study site of Martin and Frind (1998) covers approximately 750 km^2, including the Waterloo Moraine and the immediate area surrounding the Moraine. As shown in Figure 2.2, the study area is bounded approximately by the Nith River in the west, the Grand River in the east, Boomer Creek in the north and Roseville Swamp along the south-eastern edge. The site has a number of important municipal well fields including Mannheim, Parkway, and Greenbrook. Some wells within the well field were removed from service in the past due to contamination, while some others are currently facing the risk of an increasing level of contamination.

Martin and Frind (1998) developed a conceptual hydrogeological model of the Waterloo Moraine consisting of four continuous aquifer/aquitard sequences (Figure 2.3). The individual model layers are spatially continuous, but contain numerous discontinuities such as windows in the aquitards and sandy till lenses in the aquifers. The high-permeability zones within the aquitard units allow recharge into deep aquifers from surface infiltration or cross-formational flow. The upper aquifer is the most extensive and regionally continuous unit, and the most productive source of water. The two lower aquifers have pockets of discontinuous sand and gravel which are productive locally.

The individual well fields within the Waterloo Moraine use different aquifers of

the system as a water source; for example, Aquifer 1 supplies the Mannheim well field, Aquifer 2 the Greenbrook well field, and Aquifer 3 the Parkway well field. Aquifer 1, also known as the Mannheim aquifer, provides baseflow to Alder Creek and supplies water for domestic wells, the Mannheim municipal well fields as well as other well fields in the region. The Mannheim well field consists of two parts, Mannheim North and Mannheim South. The Mannheim North well field has seven wells: K21, K25, K29, K91, K92, K93, and K94; Mannheim South well field has four wells: K22, K23, K24, and K26. The Mannheim aquifer consists of about 60 m of mostly unconfined coarse sand and gravel. The wells, which are screened at a depth of about 50-60 m, have supplied water to the Region since the 1950s.

The Greenbrook well field, on the eastern flanks of the Waterloo Moraine, was the primary source of water for the city of Kitchener prior to the addition of other well fields in the 1950s. The Greenbrook wells currently provide 10% of the drinking water for the Region of Waterloo. Over the past few decades, the extracted water from the wells has shown steadily increasing chloride concentrations due to application of road salt [Bester et al., 2006]. Besides the Greenbrook well field, wells within the Strange St. and William St. well fields are screened in Aquifer 2. Aquifer 2 is fully confined, but there are some windows in the overlying layers allowing direct communication between ground surface and the aquifer.

2.2 Flow Modelling

A detailed understanding of the groundwater flow system is the first step in the analysis of various groundwater protection measures. Three-dimensional modelling of the system is the accepted approach to develop this understanding. This section will review the basic principles.

WATFLOW [Molson et al., 2002] is a finite element model based on the solution of the 3D groundwater flow equation. The model solves the continuity equation for flow which can be expressed as [Bear, 1972]:

$$\frac{\partial}{\partial x_i}\left[K_{ij}\left(\frac{\partial h}{\partial x_j}\right)\right] - \sum_{k=1}^{N} Q_k(t)\cdot\delta(x_k, y_k, z_k) = S_s\frac{\partial h}{\partial t} \tag{2.1}$$

where K_{ij} [LT^{-1}] is the hydraulic conductivity tensor, h [L] is the hydraulic head, Q_k [$\mathrm{L}^3\mathrm{T}^{-1}$] is the fluid volume flux for a source or sink located at ($x_k,\ y_k,\ z_k$), S_s

[L^{-1}] is the specific storage and t [T] is the time.

WATFLOW uses triangular prismatic finite elements which provide maximum flexibility in grid refinement to fit irregular or sloping stratigraphies with variable layer thicknesses. As one option in the model, GRIDBUILDER [McLaren, 1999] can be used as a pre-processor to generate a preliminary finite element grid in the two-dimensional horizontal plane. In WATFLOW, the 2D finite element grid is extended in the vertical direction according to the surface elevations of the various hydrostratigraphic units and the number of element layers. The Waterloo Moraine conceptual model (Fig. 2.3) uses a total of 29 element layers and 30 nodal surfaces. A recharge spreading layer (RSL) option is also applied which distributes recharge into high hydraulic conductivity layers without causing excessive mounding. In addition, one-dimensional line elements are used to represent well screens within the finite element grid [Sudicky, 1989].

The development of the 3D flow system is the basis for the source water protection studies. In this study, only steady-state groundwater flow is considered which reduces the RHS of equation (2.1) to zero. The solution of equation (2.1) requires that either Type 1 or Type 2 boundary conditions are specified all around the domain. The boundary conditions for the flow model are shown in Figure 2.4. The top boundary of the model is chosen at the ground surface.

The unsaturated zone in the WATFLOW model is generated by using a simplified form of the unsaturated flow equation [Beckers, 1998]. In this approach, a pseudo-saturated subroutine is used to approximate physical processes in the unsaturated zone. The elemental water content θ is derived based on the elemental pressure head p according to the van Genuchten relationship [Van Genuchten, 1986]:

$$\theta = \begin{cases} \theta_r + \frac{\theta_s - \theta_r}{[1+|\alpha p^n|]^m} & p < 0 \\ \theta_s & p \geq 0 \end{cases} \tag{2.2}$$

where θ_r is the residual water content, θ_s is the saturated water content, α is an index of capillary fringe height, and n and m are dimensionless fitting parameters with the connection $m = 1 - \frac{1}{n}$, given that $n > 1$. For regional-scale applications, where vertical discretization in the unsaturated zone might be too coarse to accurately represent the pressure head-saturation relationship above the water table, the following equation may be used to calculate an average water content, $\overline{\theta}$:

$$\overline{\theta} = \frac{1}{(p_t - p_b)} \int_{p_b}^{p_t} \theta(p) dp \tag{2.3}$$

where p_t and p_b represent the pressure head at the top and bottom faces of each prismatic element. Under these conditions, the relative permeability (k_r) and effective saturation (S_e) can be derived according to [Mualem, 1976]:

$$k_r = S_e^{\frac{1}{2}} \left[1 - \left(1 - S_e^{\frac{1}{m}} \right) \right]^{-2} \tag{2.4}$$

$$S_e = \frac{\overline{\theta} - \theta_r}{\theta_s - \theta_r} \tag{2.5}$$

The pseudo-unsaturated subroutine can be applied only under steady-state conditions.

The final matrix equations for flow are solved using an efficient preconditioned conjugate gradient (PCG) matrix solver. In practice, the PCG solver has performed exceptionally well, even under highly heterogeneous conditions (with up to 5 orders of magnitude conductivity contrast between adjacent elements), with high accuracy and rapid convergence. Elemental velocity components are then derived from the nodal heads using Darcy's equation.

Figure 2.5(a) shows the 2D finite element grid for the Waterloo Moraine, while Fig. 2.5(b) shows an enlargement for the area of the Mannheim well field. The pumping wells of the Mannheim well field are shown on the enlargements. Figure 2.6 shows the thickness of Aquifer 1, ranging from 10 to about 40 m. The hydraulic conductivity values for the Waterloo Moraine were estimated locally based on a geologic correlation with lithologic descriptions taken from well logs. These local values were then interpolated areally using kriging to produce a three-dimensional hydraulic conductivity field [Martin, 1994]; [Martin and Frind, 1998]. This three-dimensional field was further refined using an automated calibration routine [Beckers, 1998]; [Beckers and Frind, 2002]. In the calibration, observed subsurface hydraulic heads and stream baseflow were used as calibration targets. To calculate the equivalent horizontal hydraulic conductivity of Aquifer 1, the arithmetic mean in the horizontal direction over the six layers was calculated. Figure 2.7 shows the areal distribution of horizontal hydraulic conductivity K_x for Aquifer 1 within the Mannheim area, ranging from 10^{-6} to 10^{-3} m/s, with some of the highest values found in the area of the Mannheim well field (see cross-section A-A$'$ in Fig. 2.7).

2.3 Transport Modelling

Once the groundwater velocities are generated for the study area, the Waterloo Transport Code (WTC) [Molson and Frind, 2004], an advective-dispersive time-marching transport model, is used to simulate transport processes within the Mannheim well field. WTC is an advanced numerical model for solving complex three-dimensional groundwater mass transport problems. As in the flow model, WTC uses 3D triangular prism elements to resolve the spatial domain. The symmetric-matrix time-integration scheme of Leismann and Frind (1989) is employed in combination with a standard Galerkin finite element method (e.g. see Huyakorn and Pinder, 1983). The Leismann Scheme is particularly efficient since it generates a symmetric coefficient matrix for the transport problem, which saves memory and execution time. The final matrix equation for the mass transport problem is solved using the same efficient PCG solution for symmetric matrices as is used for the solution of the flow problem. A solution obtained in this way is inherently time marching because the response is advanced discretely through time from one time step to the next.

Numerical errors in the transport code were controlled by observing the grid Peclet and Courant criteria given by [Daus et al., 1985]:

$$P_e = \frac{v\Delta x}{D} \leq 2 \tag{2.6}$$

$$C_r = \frac{v\Delta t}{\Delta x} \leq \frac{P_e}{2} \leq 1 \tag{2.7}$$

where Δx is the grid spacing, Δt is the size of the time step, v is the average pore water velocity, and D is the dispersion coefficient.

The transport equation has advection and dispersion terms, the advective term in the transport equation can lead to numerical dispersion if the above two constraints are violated. Numerical dispersion may be difficult to identify, but it typically takes the form of a smeared concentration profile, a lagging concentration front appears or as oscillations resulting in negative concentrations or concentrations exceeding the source concentration [Frind, 1997].

The WTC code is applied in this study to develop WHPAs, intrinsic well vulnerability maps and to assess the risk of well contamination. WTC can simulate advective-dispersive transport in both the forward (known source location) and the backward (unknown source location) mode (see Chapters 5 and 6).

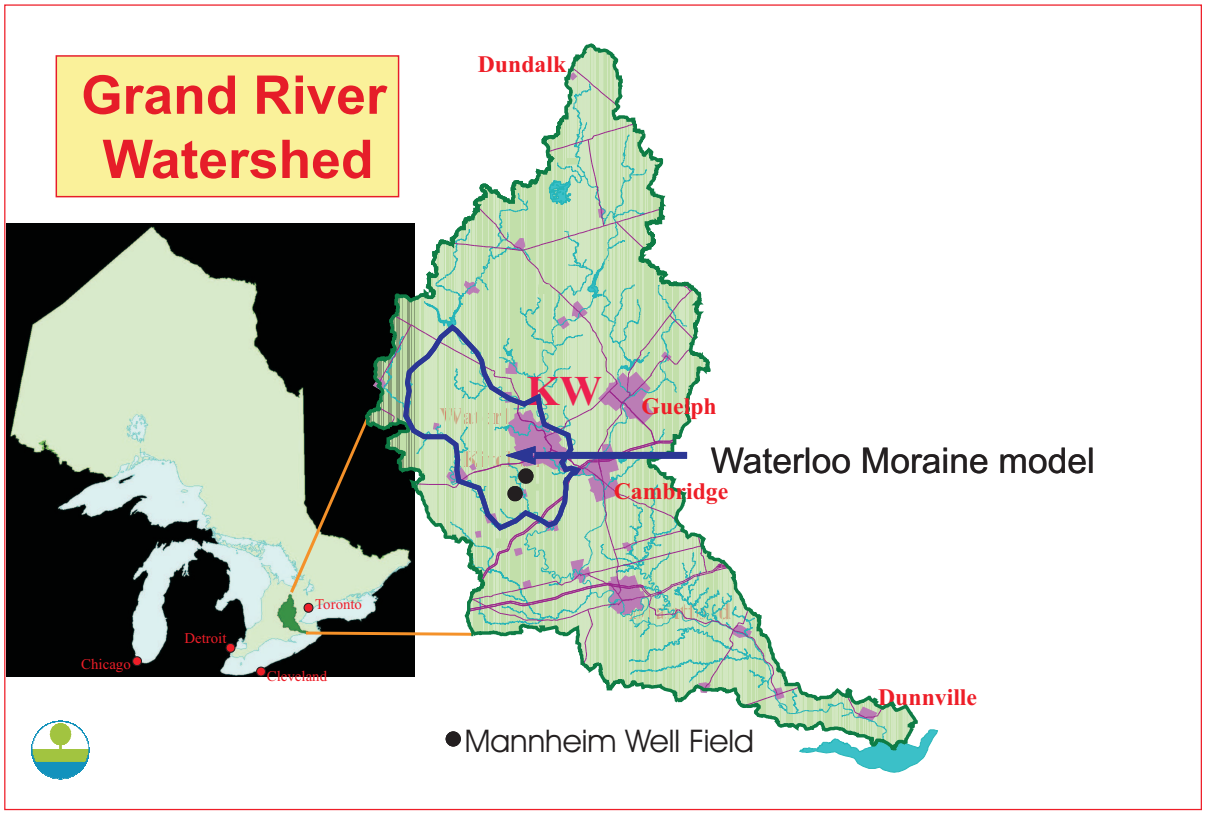

Figure 2.1: Grand River Watershed showing the Waterloo Moraine study area and the Mannheim well field (from the Grand River Conservation Authority).

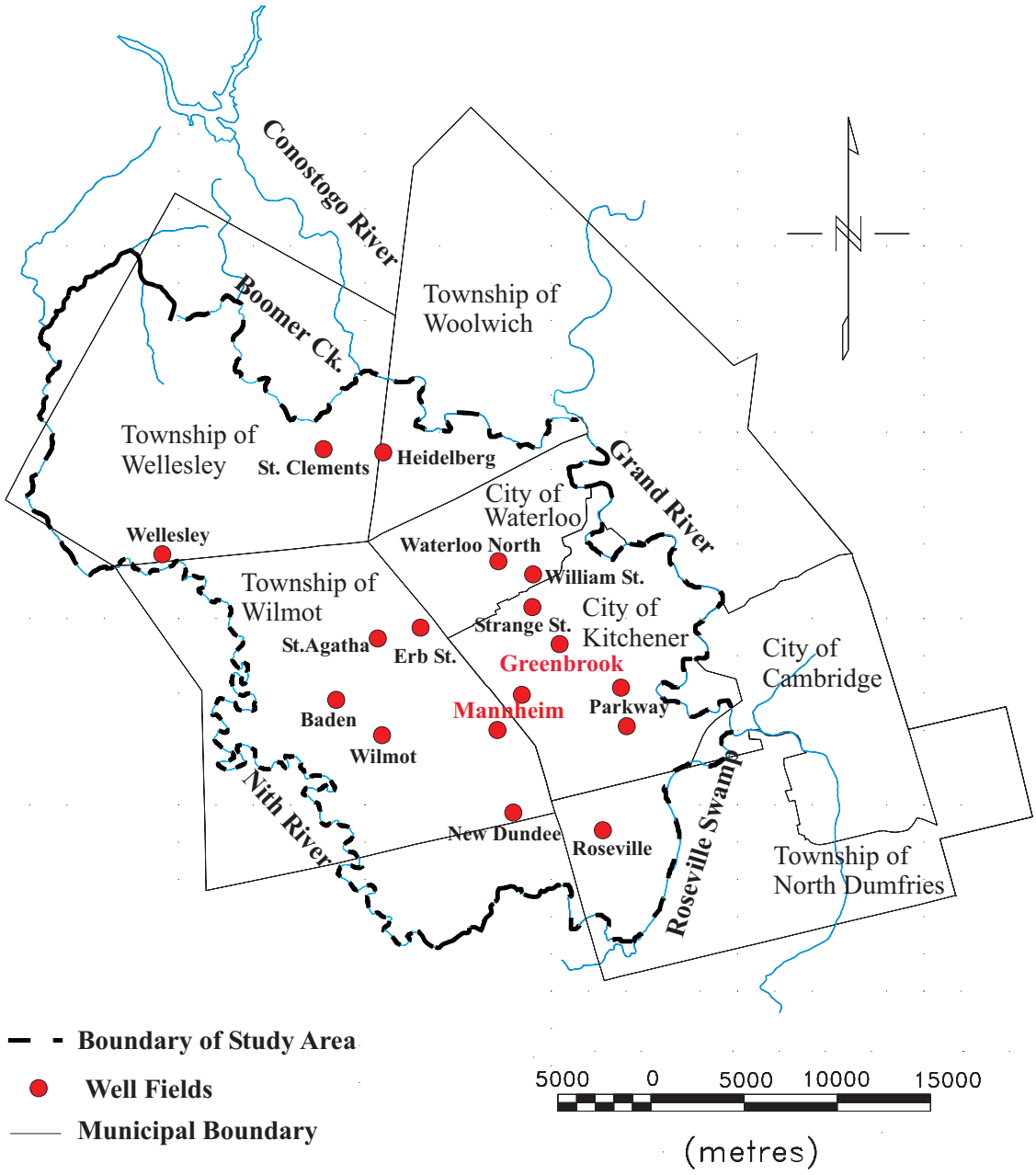

Figure 2.2: Waterloo Moraine study area and well fields (after Frind et al., 2002).

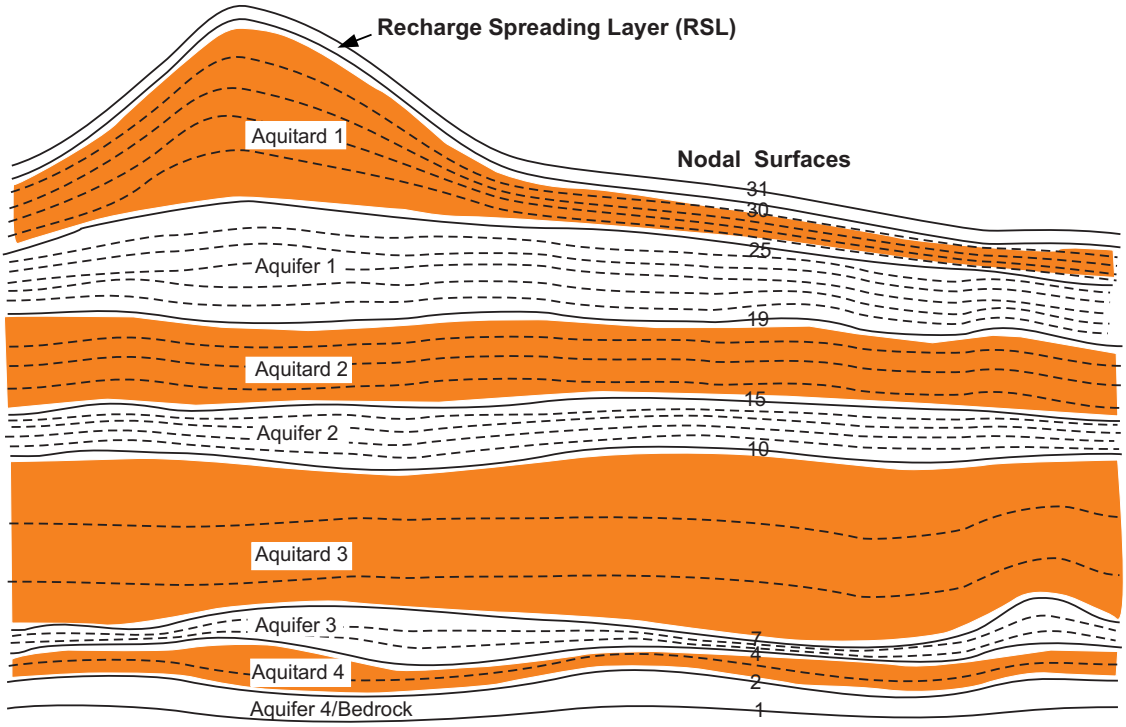

Figure 2.3: Hydrogeological conceptual model of the Waterloo Moraine (after Martin and Frind, 1998).

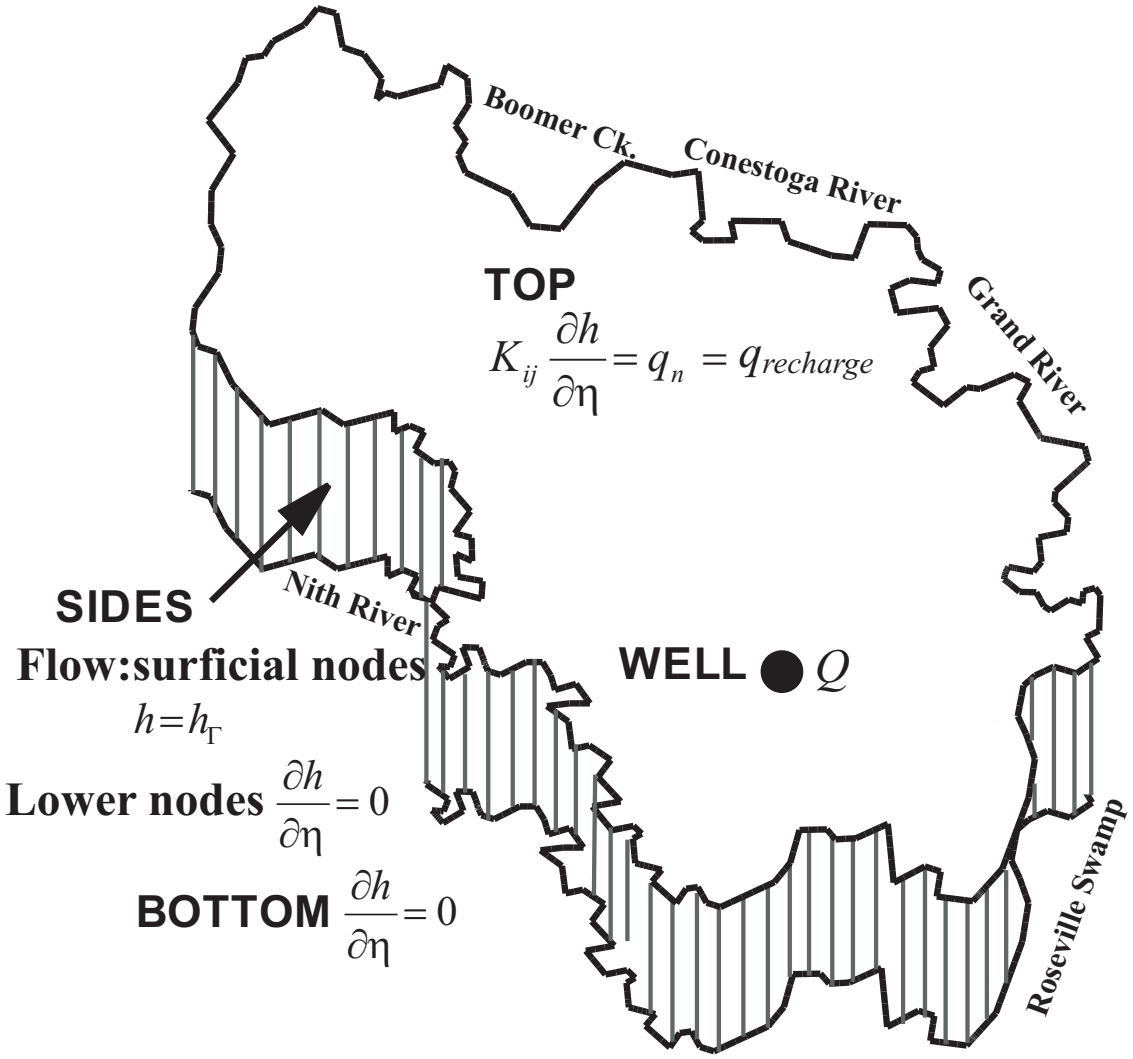

Figure 2.4: Boundary conditions for the flow model (after Muhammad, 2000).

(a)

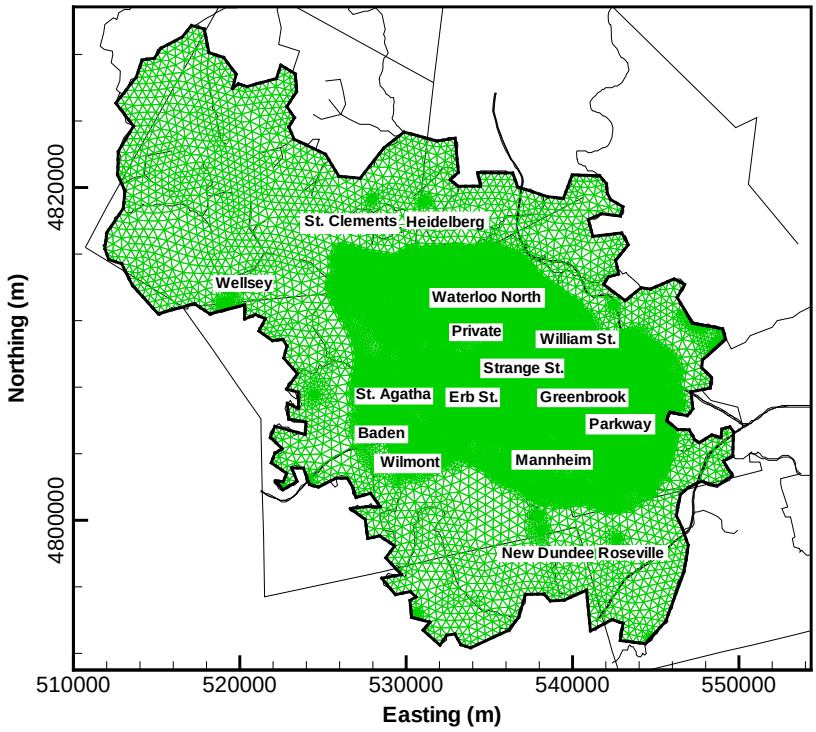

(b)

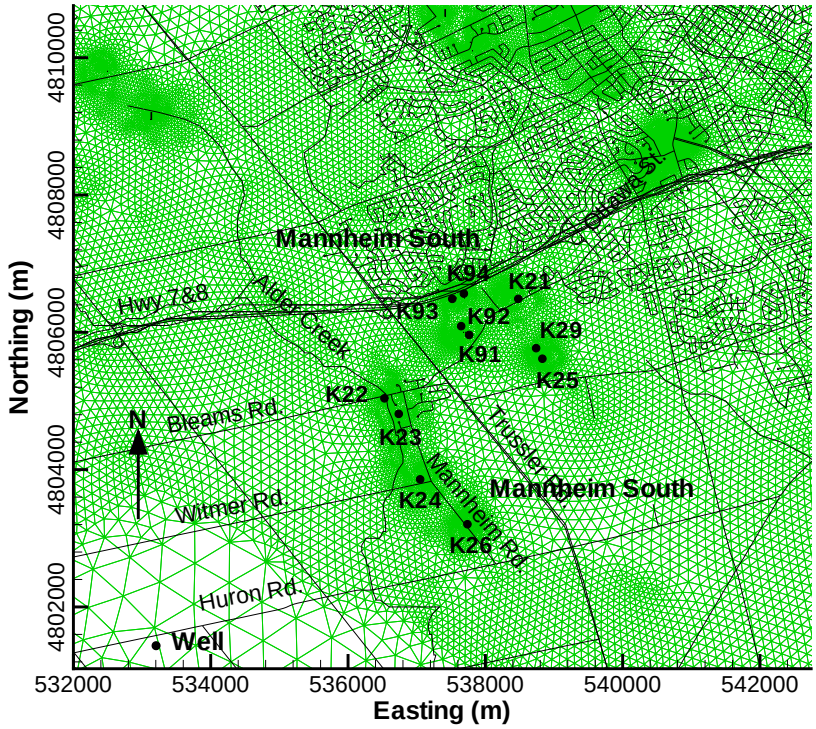

Figure 2.5: 2D Finite element mesh (a) Waterloo Moraine, (b) Mannheim area.

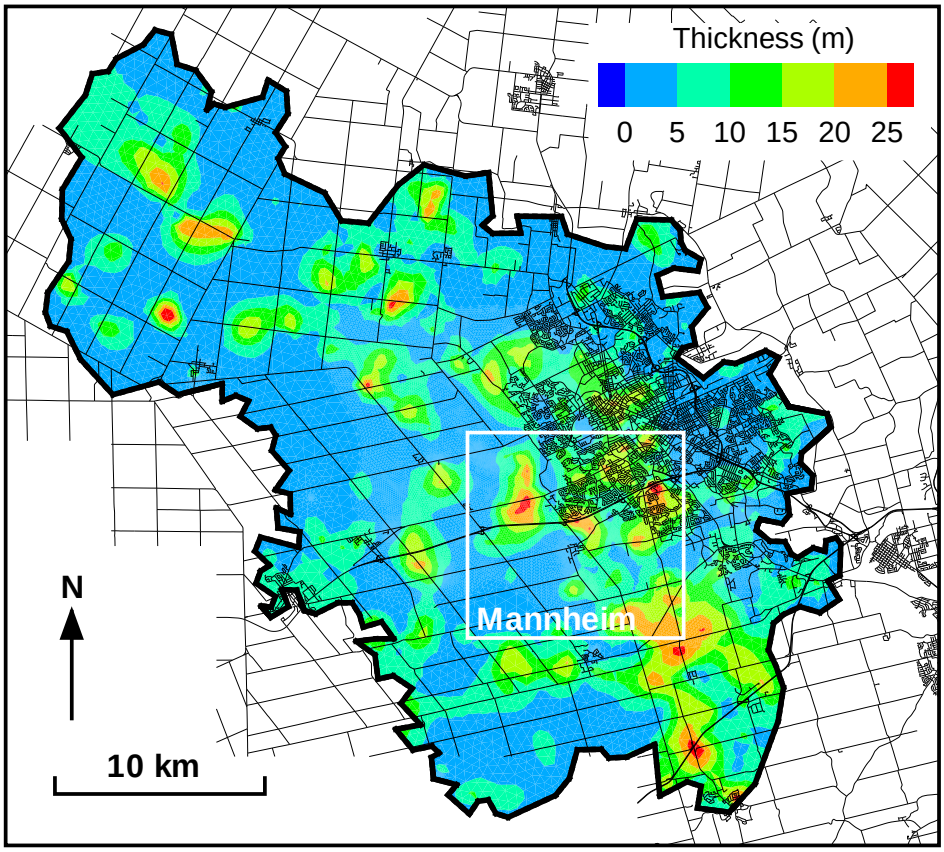

Figure 2.6: Thickness of Aquifer 1 within the Waterloo Moraine, (after Martin and Frind, 1998).

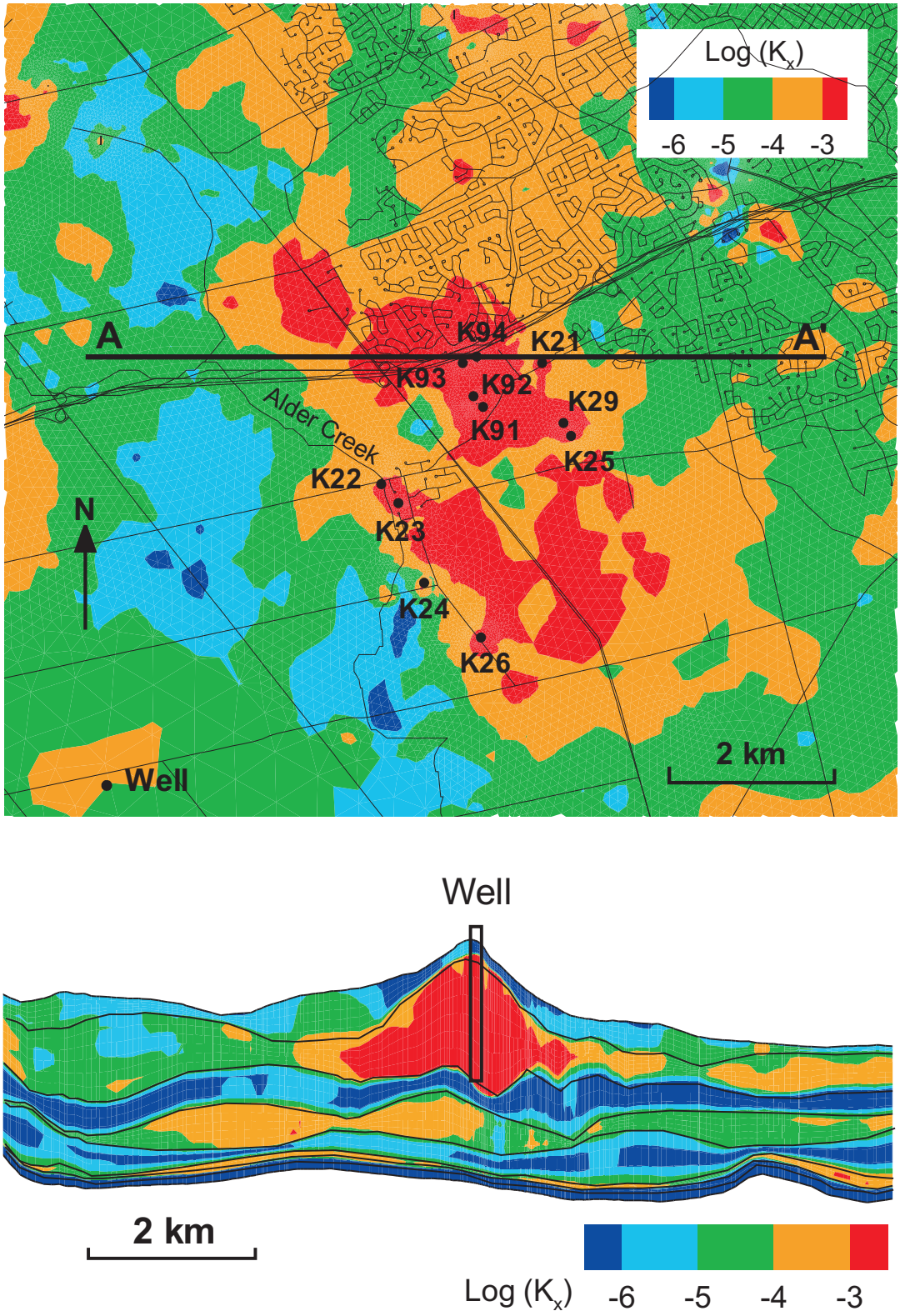

Figure 2.7: Hydraulic conductivity K_x of Aquifer 1, (K_x in m/s) (after Martin and Frind, 1998): Mannheim area, and along the vertical section A-A′.

Chapter 3

Aquifer Vulnerability: A Comparison of Approaches

Providing safe drinking water is a high-priority challenge in industrialized countries including Canada. Following the Walkerton tragedy of 2000, the Province of Ontario made a commitment to the long-term protection of Ontario′s present and future drinking water resources. A major element towards this protection is the evaluation of the vulnerability of groundwater resources to contamination originating at ground surface. This chapter provides a brief background on the aquifer vulnerability concept, discusses standard approaches for the assessment of aquifer vulnerability currently in use in the Province of Ontario, introduces alternative approaches, and presents the results of a case study focused on the Mannheim and Greenbrook well field areas.

3.1 History, Concepts, and Terminology

Aquifer "vulnerability", along with the related term "susceptibility", expresses how vulnerable or susceptible a groundwater resource is to surface sources of contamination. Next to the contamination source itself, the most important factor is the protection provided to the resource by overlying geologic layers. Various approaches to define vulnerability, along with different terminology, have emerged over the last 20 years or so. A recent summary is given by Frind et al. (2006).

The earliest contribution to the topic of aquifer vulnerability/susceptibility may have been by Trotta (1985), who pioneered the use of Arc/Info GIS mapping using

digitized data to develop a state-wide map of groundwater susceptibility for the State of Wisconsin. At about the same time and within the context of the same project, Schmidt (1987) defined groundwater "susceptibility" as the ease with which the contaminant can be transported from the land surface to the water table. This work also provided the impetus for the development of the DRASTIC approach for the assessment of aquifer vulnerability, which aims to provide a means to combine relevant attributes that may have a bearing on aquifer vulnerability, such as hydrogeology, soil texture, and depth to water table, to produce aquifer vulnerability maps, usually with the help of GIS overlay techniques [Aller et al., 1987].

A similar approach is described by Foster (1987), who uses the term aquifer pollution vulnerability and defines it as the intrinsic characteristics of the strata which separate the saturated aquifer from the land surface, while determining its sensitivity to being adversely affected by a surface-applied contaminant load. This author further defines an integrated index of aquifer pollution vulnerability in terms of vulnerability classes based on the different classes of pollutants (nutrients, pathogens, organics, heavy metals, etc). The method for delineating aquifer pollution vulnerability based on this approach is known as the GOD method [Foster, 1987]; [Foster and Hirata, 1992]. The GOD vulnerability index characterizes aquifer pollution vulnerability on the basis of Groundwater hydraulic confinement, Overlying strata and Depth to water table. It should be noted that these methods usually require assigning weights to the various attributes, so the final outcome will depend on the various weights assigned. More recently, on behalf of the World Bank, the same authors have developed a comprehensive practical guide aimed at decision makers, planners, and practitioners in the World Bank client countries [Foster et al., 1991].

The U.S. EPA (1987); (1997) defined intrinsic susceptibility of an aquifer as relating to the hydrogeologic characteristics of the overlying layers (e.g. hydraulic conductivity, layer thickness, porosity), and aquifer vulnerability as a more comprehensive term relating also to the effect of land-use practices, contaminant characteristics, and loading. These original definitions are still purely qualitative, with no attempt at quantification. Similar definitions were given by the U.S. National Research Council (NRC) in 1993.

Similarly, Vrba and Zoporozec (1994) defined vulnerability as an intrinsic property of a groundwater system that depends on the sensitivity of the system to human and/or natural impacts. These authors further distinguish between intrin-

sic vulnerability being solely a function of the hydrogeological factors, namely, the characteristics of the aquifer and the overlying soil and geologic materials, and specific vulnerability describing potential impacts of land uses and contaminants or groups of contaminants, as well as hydrological and hydrogeological factors.

Focazio et al. (2002) further expanded on the USEPA definition by including in the definition of intrinsic susceptibility all aquifer system properties (hydraulic conductivity, porosity, gradients) as well as the associated stresses on the system (recharge, interaction with surface water, travel through the unsaturated zone, well discharge). In the definition of vulnerability, they included the characteristics of contaminant sources, relative location of wells, fate and transport of contaminants, as well as all of the characteristics included under intrinsic susceptibility. All of these terms are understood to be qualitative. Comparing the definitions of Focazio (2002) with those of Vrba and Zoporozec (1994) shows that the terms intrinsic susceptibility and intrinsic vulnerability have basically the same meaning.

The counties of the European Union have adopted a common approach for classifying the vulnerability of aquifers. The main concepts of this approach are described by Daly et al. (2002), who focus on Karst aquifers. They define intrinsic vulnerability as the vulnerability of the groundwater to contaminants, taking into account the inherent geological, hydrological, and hydrogeological characteristics, but independent of the nature of the contaminants. In this sense, the European intrinsic vulnerability would be similar to the USEPA susceptibility. However, although the European term does not refer to a specific contaminant, it considers the properties that are relevant for all types of contaminants, including advective transport time, relative quantity of contaminants which can reach the target, and physical attenuation such as dispersion, dilution, dual porosity, etc. Specific vulnerability additionally takes into account the chemical behaviour of the contaminant and the vulnerability of the groundwater to a particular contaminant or group of contaminants [Brouyère et al., 2001].

The European approach introduces one important principle, namely the idea of the hazard-pathway-target model, which bases vulnerability on the protective effect of the material encountered by a contaminant along the complete pathway from source to target. The approach distinguishes between the groundwater resource (the aquifer) and the water source (the well). For resource vulnerability mapping, the target is either the water table or the top of the aquifer and the path is the vertical

path through the overlying layers, while for source vulnerability mapping, the target is the well and the path is the total path from the hazard to the well. The main difference between the USEPA and the European terminology lies in the terms susceptibility (USEPA) and intrinsic vulnerability (EU) [Brouyère et al., 2001].

The first to use the source-pathway-hazard model in Canada were van Stempvoort et al. (1992). This type of model allows a fully physically based quantitative assessment of aquifer vulnerability, which is based on the vertical advective travel time from a surface source through the overlying material layers to the target aquifer. It makes use of the fact that a measure of the protective capacity of overlying layers is the hydraulic resistance, and since the unit of hydraulic resistance is time, the total hydraulic resistance of a series of layers is the same as the advective travel time of a particle through these layers. To keep data requirements to a minimum, these authors use only the hydraulic conductivity and the thickness of overlying strata, so the resulting travel time is understood to be for a unit gradient and unit porosity.

For practical use, van Stempvoort et al. (1992) recommend the use of a vulnerability index based on the log of advective travel time. In this way, a low index value (short travel time) indicates high vulnerability; while a high index value (long travel time) indicates low vulnerability. This method was applied for groundwater protection mapping in the Prairie Provinces of Canada as well as in other parts of North America and Europe [Van Stempvoort et al., 1992]. A more refined approach using actual gradients and accounting for the unsaturated zone is the surface to aquifer advection time (SAAT) approach proposed by the MOE Technical Experts Committee (2004), discussed in detail below.

3.2 Review of Approaches for Aquifer Vulnerability Mapping

Two methods are currently used in Ontario: the "Intrinsic Susceptibility Index" (ISI) and the "Surface to Aquifer Advection Time" (SAAT); where the former is an index method and the latter a travel time method. The latter is a refined form of the Hydraulic Resistance approach (HR) which is the basis of the earlier Aquifer Vulnerability Index (AVI) method introduced by van Stempvoort et al. (1992). We will here review the theoretical basis of these methods and, in the next section, illustrate their use by application to the Mannheim and Greenbrook aquifers.

3.2.1 Intrinsic Susceptibility Index (ISI)

The Intrinsic Susceptibility Index (ISI) has been introduced by the Ontario Ministry of the Environment (MOE) in 2006 for use in Ontario. In this method, the ISI-value for a target aquifer is determined by multiplying the thickness of each overlying layer by a number called the K-factor for the layer, and by summing the values over the layers to obtain an overall score. K-factors for common hydrogeologic materials (essentially related to the negative exponent of the hydraulic conductivity, K, except for K greater than or equal to 10^{-6} m/s) are provided in Table 3.1. The K-factor represents the degree of protection offered by each respective geologic material that overlies the aquifer.

ISI results provide a dimensionless index value which can be calculated point-by-point over an area, depending on the available data, and which can be mapped over a source water protection (SWP) area. For example, a 5 m layer of clay till (K = 10^{-9} m/s, tabulated K-factor = 8) has an ISI value of 40. In the ISI approach, a score of less than 30 indicates the aquifer is highly vulnerable, 30 to 80 signifies moderate vulnerability, while values greater than 80 denote low vulnerability.

It should be noted that although the values going into the calculation of the ISI (thickness and hydraulic conductivity) are physical, the calculation itself is not a physically based operation because the exponential nature of the hydraulic conductivity is not considered; therefore the results are non-physical. Consequently, the ISI values cannot be combined with any other physical quantity (such as travel time). ISI values can only be used as relative values in relation to other ISI values, and to provide a rough idea about areas of high or low vulnerability within a source protection area.

ISI values can also be misleading in some circumstances. For example, consider a gravel aquifer overlain by (a) a 2 m layer of clay till, and (b) a 20 m layer of silty sand:

(a) $K = 10^{-9}$ m/s, K-factor = 8, ISI score = $2 \times 8 = 16 \rightarrow$ high vulnerability

(b) $K = 10^{-4}$ m/s, K-factor = 3, ISI score = $20 \times 3 = 60 \rightarrow$ moderate vulnerability.

So the ISI approach would suggest that an aquifer overlain by 2 m of clay till

is more vulnerable than one overlain by 20 m of silty sand (or in other words, the silty sand is more protective than the clay till). If we apply a physically based approach and express vulnerability in terms of travel time T (assuming a porosity of 0.3 and a gradient of 0.01 for both systems), we would get:

Table 3.1: K-factors for common hydrogeologic materials [MOE, 2006].

Geomaterial	K-fac.	K-value (m/s) @75% range**	Highest K-Value (m/s)
gravel	1	1.00E-01	0.1
weathered dolomite/limestone		1.00E-06	
karst		1.00E-03	
permeable basalt		1.00E-03	
sand	2	1.00E-02	1.00E-02
peat(organics)	3	1.00E-03	1.00E-03
silty sand		1.00E-04	
weathered clay <5 m below surface		1.00E-04***	
shrinking/fractured & aggregated clay		1.00E-04***	
fractured igneous metamorphic rock		1.00E-05	
weathered shale		1.00E-05***	
silt	4	1.00E-06	1.00E-06
loess		1.00E-06	
limestone/dolomite		1.00E-06	
weathered/fractured till	5	1.00E-07	1.00E-07
diamicton (sandy, silty)		1.00E-07***	
diamicton (sandy, clayey)		1.00E-08***	
sandstone		1.00E-07	
clay till	8	1.00E-09***	1.00E-09
clay (unweathered marine)		1.00E-10	
unfractured igneous and metamorphic rock	9	1.00E-13	1.00E-13

** Correspondence with descriptors of observed K-values in Freeze & Cherry (1979), Prentice-Hall. Derived using the length of the line to determine the 75% value and rounding to the highest K-value.
*** Estimated value based on field studies in Ontario.

(a) $T = (2 \times 0.3) / (0.01 \times 10^{-9}) = 6 \times 10^{+10}$ sec = 1900 years $\rightarrow$ low vulnerability

(b) T = (20 × 0.3) / (0.01 × 10^{-4}) = 6 × 10^{+6} sec = 0.19 years → high vulnerability.

Therefore, the clay layer actually offers a four-order-of-magnitude better protection than the silty sand, as would be expected. The physically based approach actually reverses the results of the index approach in this case. This example shows that the ISI method should be used with caution.

3.2.2 The Hydraulic Resistance Approach (HR)

Van Stempvoort et al. (1992) proposed the use of hydraulic resistance of the layers overlying an aquifer as a physically based measure of aquifer vulnerability, coining the term Aquifer Vulnerability Index (AVI). Because the term AVI is also used in the MOE Mannual [Ontario Ministry of Environment (MOE), 2006] to denote an index method similar to ISI, but entirely different from the original physically based van Stempvoort approach, we will here use the generic term Hydraulic Resistance (HR) approach to avoid confusion. The van Stempvoort approach can be seen as consisting of the HR approach, plus a subjective scheme by which the HR results are interpreted in terms of qualitative vulnerability ranges from low to high.

The HR approach requires the vertical hydraulic conductivity and the thickness of the overlying layers (i.e. the same quantities as used in the ISI approach) as input parameters. The HR results determine the intrinsic vulnerability of the target aquifer, a characteristic that is independent of the flow system and the contaminant. Unsaturated conditions are not considered.

The HR method is based on the well-known physical principle of series flow, which is often used in electricity and hydraulics applications. In series flow, the resistances of the individual members (i.e. geologic layers acting as resistors) can be shown to be additive [Bear, 1972]; [Kruseman and de Ridder, 1990]. The hydraulic resistance, C_i of a geologic layer i can be written as

$$C_i = \frac{d_i}{K_i} \tag{3.1}$$

where d_i is the thickness and K_i is the vertical hydraulic conductivity of the i^{th} geologic layer. The total hydraulic resistance, C_q, of the n layers above the target

aquifer is:

$$C_q = \sum_{i=1}^{n} \frac{d_i}{K_i} = {T_q}^u \tag{3.2}$$

C_q [T] is numerically equal to the total advective travel time of a non-reactive contaminant, ${T_q}^u$ [T], when the downward vertical Darcy flux q [T^{-1}] is under unit vertical gradient and the porosity is unity. ${T_q}^u$ has the same units of time as used in K, but for practical use these are normally converted to years.

Because contaminants normally travel at the pore velocity rather than the Darcy velocity, we can also write the above equations in terms of the hydraulic resistance of the pore space C_v within the medium. In that case, equation 3.2 becomes:

$$C_v = \sum_{i=1}^{n} \frac{d_i \eta_i}{K_i} = {T_v}^u \tag{3.3}$$

where η_i is the porosity, and ${T_v}^u$ is the advective time taken by a non-reactive particle travelling at the average pore velocity, again under a unit downward vertical gradient. Because porosities normally vary only over a narrow range, an average value will normally be adequate.

Both C_q and C_v are intrinsic characteristics of the layers overlying an aquifer. The calculation requires the hydraulic conductivity and the thickness of the layers, which is the same data as used in the ISI method, plus the porosity.

Van Stempvoort et al. (1992) suggest the use of the log of the hydraulic resistance (C_i) to express vulnerability ranges. In this study, the log of the hydraulic resistance of the pore space (C_v) is used to express vulnerability ranges. These are shown in Table 3.2 ranging from extremely low to extremely high.

Table 3.2: Aquifer vulnerability index in terms of hydraulic resistance [van Stempvoort et al., 1992].

Hydraulic resistance (C_v)	Log (C_v)	Vulnerability ranges
0 to 10 y	< 1	extremely high
10 to 100 y	1 to 2	high
100 to 1000 y	2 to 3	moderate
1000 to 10,000 y	3 to 4	low
$>$ 10,000 y	> 4	extremely low

The advective time ${T_v}^u$ (under unit gradient) can easily convert to an actual advective travel time by dividing the downward vertical gradient, the motivation being that the actual travel time through the aquitard can then be compared with (or possibly added to) the horizontal travel time in the aquifer to get the total travel time from a contaminant source to the well. However, since the gradient is not an intrinsic characteristic of the medium, it can change over time. Therefore, actual travel time is no longer an intrinsic characteristic of the system. An alternative is the European approach which includes the temporal averaging gradient as input of the intrinsic vulnerability. We will discuss this approach in the next section.

3.2.3 Surface to Aquifer Advection Time (SAAT)

Aquifer vulnerability can also be assessed using the travel time approach called the Surface to Aquifer Advective Time (SAAT). The SAAT approach recommended by the MOE Technical Experts Committee (2004) is a refinement of the resistance method proposed by van Stempvoort et al. (1992), differing from the latter by using the actual gradient and incorporating the unsaturated zone.

Dividing equ. (3.3) by the downward vertical gradient ∇h_z yields the actual advective travel time T_{adv}:

$$T_{adv} = \frac{1}{\nabla h_z} \sum_i \frac{d_i \eta_i}{K_i} \qquad \nabla h_z \neq 0 \tag{3.4}$$

where it should be remembered that this equation is not applicable in areas where the gradient is zero or upward.

To show that only the overall gradient is needed (not the individual gradients for each layer), we consider the advective flux reaching the target aquifer [Bear, 1972]; [Frind, 1997]:

$$q = v\eta = \frac{\sum d_i}{\sum (d_i/K_i)} \frac{\sum \triangle h_i}{\sum d_i} \tag{3.5}$$

where q is the Darcy velocity, v is the average pore water velocity, η is the weighted average porosity, and $\triangle h_i$ is the head change over layer i. The first term on the right-hand side of this equation is the harmonic mean conductivity over all the layers and the second term is the total gradient. This equation can also be written as:

$$q = \frac{D}{{T_q}^u} \nabla h_z \tag{3.6}$$

where D is the total thickness. Knowing that time = distance/velocity, we can also write

$$T_{adv} = \frac{D}{v} = \frac{D}{q/\eta} = \frac{T_q{}^u \eta}{\nabla h_z} = \frac{1}{\nabla h_z} \sum_i \frac{d_i \eta_i}{K_i} \qquad \nabla h_z \neq 0 \tag{3.7}$$

Accordingly, to convert the travel time under a unit gradient and unit porosity to actual travel time, we divide by the overall vertical gradient and multiply by the average porosity. Equation 3.7 provides the travel time through the saturated zone.

In places where the depth of the water table is greater than 3 m, the time of travel for water and contaminants through the unsaturated zone is significant and should be accounted for [MOE, 2006]. The estimation of the travel time through the unsaturated zone is more complex. For example, in the case of a thick unsaturated zone, contaminants will take a relatively long time to reach the water table. On the other hand, if the unsaturated zone is thin and becomes fully saturated during a major rainstorm, the contaminants will reach the water table instantaneously under a unit gradient.

To account for unsaturated flow, the unsaturated part of the travel time, T_{unsat}, can be written as:

$$T_{unsat} = \frac{1}{\nabla h_z} \left(\frac{d_{wt} \theta}{K(\theta)} \right) \qquad \nabla h_z \neq 0 \tag{3.8}$$

where d_{wt} is the depth to the water table and θ is the moisture content. In Equation (3.8) the unsaturated hydraulic conductivity, $K(\theta)$ is not constant and is a function of the moisture content, θ. As θ increases, $K(\theta)$ also increases. The values of moisture content and unsaturated hydraulic conductivity are different for different types of material. For example for coarse material such as sand and gravel, the pores are large and water drains quickly. At lower moisture contents, there may be very few saturated pores. On the other hand, finer-grained soils such as clay may have most of the pores still saturated. So at higher moisture content the sandy soil has a greater hydraulic conductivity; however, at low moisture content, the clay has a greater hydraulic conductivity.

A potential problem with equ. (3.8) is that the function $K(\theta)$ is rarely known. For this case, the equation can be rewritten in terms of the infiltration rate. Assuming that flow is at an average steady-state throughout the year, and using the fact that the infiltration rate $q_z = K \nabla h_z$, the advective travel time through the

unsaturated zone can be simplified to:

$$T_{unsat} = \frac{d_{wt}\theta_m}{q_z} \qquad q_z \neq 0 \tag{3.9}$$

Equation (3.9) is not valid where the infiltration rate is zero or exfiltration occurs. The infiltration rate, q_z, can be estimated with a soil moisture balance model like HELP [Schroeder et al., 1994] or the simpler Thronthwaite Method [Thornthwaite, 1948] or any suitable flow model (for example WATFLOW [Molson et al., 2002]). The mobile moisture content of the surface material, θ_m, is used as a substitute for the average moisture content of the soil under steady-state drainage at the infiltration rate. The value can be taken from locally known information or it can be estimated from a map of the Quaternary geology and the following approximate Table 3.3. In the presence of multiple layers within the unsaturated zone, the equivalent θ_m is calculated as the arithmetic mean value of θ_m, weighted by the layer thickness. The depth to the water table (d_{wt}) can be obtained by subtracting the water table elevation from the ground surface elevation. The water table elevation can be determined from the record of the static water table at the observation wells.

Table 3.3: Moisture content for hydrogeologic material [MOE, 2006].

Overburden texture	Mobile moisture content
Sand	10%
Loam	25%
Clay	40%

The advective travel time in the saturated zone together with an estimate of the unsaturated zone travel time can be used to assess the intrinsic vulnerability of the aquifer to surface contamination.

3.3 Aquifer Vulnerability in the Mannheim well field

For the purposes of this comparison, we will focus on the Mannheim well field and designate Aquifer 1 as the target aquifer. As mention in Chapter 2, Aquifer 1 is the most extensive and regionally continuous unit, and the most productive source of water.

3.3.1 Aquifer Vulnerability Parameters

Figure 3.1(a) shows the thickness of Aquitard 1, ranging from mostly 10 to about 40 m, while Fig. 3.1(b) shows again an enlargement for Mannheim. As shown in Figure 2.3, Aquitard 1 has been subdivided into 5 discrete layers for the purpose of model discretization. The hydrogeologic properties vary throughout each of these layers. To calculate the equivalent vertical hydraulic conductivity of Aquitard 1, the harmonic mean in the vertical direction over the five layers was calculated. Figure 3.2(a) shows the areal distribution of vertical hydraulic conductivity K for Aquitard 1 for the entire Moraine area, ranging from 10^{-4} to 10^{-8} m/s, while Fig. 3.2(b) shows an enlargement for the area of the Mannheim well field.

Figure 3.3 shows the depth to the water table, which gives the thickness of the unsaturated zone needed in the SAAT analysis, and which varies between about 10 and 50 m within Mannheim area. Aquifer 1 is mostly unconfined, however some areas are confined over the study area. The confined areas are overlain by relatively thick portions of Aquitard 1 and therefore will be expected to have a low vulnerability. Conversely, some unconfined parts will have a high vulnerability.

3.3.2 The Index Approach: ISI

Figure 3.4 shows the results of the ISI vulnerability analysis for the Mannheim area. The resulting index values range from 0 to 300, which gives a vulnerability range from high (values between 0 to 30) to moderate (values between 30 to 80) and into the low range (values above 80). The areas of high vulnerability (red to orange) in the southern part of the study area correlate well in general with the areas where Aquifer 1 is unconfined (blue in Fig. 3.4). The area of lower vulnerability in the north (blue) coincides with an area where Aquifer 1 is also unconfined (Fig. 3.4). The thickness of the overlying layers above Aquifer 1 within those areas is in the range of 20 to 40 m and the vertical hydraulic conductivity is in the range of 10^{-7} to 10^{-8} m/s.

The ISI map shows some correlation with the hydraulic conductivity map (Fig. 3.2(b)). However, the ISI-values are mostly dominated by the aquitard thickness (Fig. 3.1(b)) as is evident from the ISI calculation method. By contrast, the hydraulic conductivity, which varies over orders of magnitude and which therefore should have the greatest impact on the protective capacity of the aquitard, is un-

derrepresented. For example, the high conductivity zones (windows) in Aquitard 1 in the NW (Northwest) quadrant appearing as orange spots in Fig. 3.2(b), and serving as conduits for recharge and for contaminants, are not correctly represented. This suggests that the ISI method may give misleading results if the aquitard consists of materials with widely varying hydraulic conductivity, as is already apparent from the simple example in Section 3.2.1.

3.3.3 The Hydraulic Resistance Approach: HR

The HR approach is conceptually simple as it uses the same data as the ISI approach, albeit in a different way, to calculate the resistance of the overlying layers. It considers only the geologic stratum above the target aquifer, making no distinction between confined and unconfined aquifers, and it does not account for the unsaturated zone as a distinct barrier.

Van Stempvoort et al. (1992) recommend that the HR results as calculated by equ. (3.2) be represented as the log of the aquitard resistance C_v in years (= advective travel time in years under a unit gradient). These results are shown in Figure 3.5. The HR vulnerability shows a good visual correlation with the hydraulic conductivity (Fig. 3.2(b)), with the important windows in the NW quadrant correctly represented. The vulnerability classification suggested by van Stempvoort et al. (1992) is also shown on the colour bar. The figure shows that most of the Mannheim area has a resistance of 10 years (1 on the log scale) or less; this is classified as an extremely high vulnerability, which is fully consistent with the aquitard characteristics. In the area to the north of the well field, where the hydraulic resistance is over 100 years (2 on the log scale), the aquitard is both thick (20 to 50 m; Fig. 3.1(b)) and has a low hydraulic conductivity of around 10^{-7} m/s (Fig. 3.2(b)). The hydraulic resistance over 100 years represents moderate vulnerability.

A concern, however, is the subjective part. In order to qualify as "low vulnerability" the aquitard must have a resistance of 1000 to 10,000 years, whereas the highest resistance values attained in the Waterloo Moraine are of the order of 100 to 1000 years. Accordingly, none of the areas of the Waterloo Moraine qualifies as having low vulnerability according to the HR method. This would suggest that a subjective vulnerability range might depend on the context, meaning that the appropriate range for the Waterloo Moraine might differ from that for, say, a high-level radioactive waste repository site.

3.3.4 The Travel Time Approach: SAAT

The SAAT approach calculates the travel time through the saturated zone using eqn. (3.4). To calculate the travel time through the unsaturated zone, we have two options: (a) using equ. (3.8) with the unsaturated flow properties and the downward gradient, and (b) using equ. (3.9) with the infiltration rate q_z and tabulated values for the residual moisture content (Table 3.3). Since in most practical situations the infiltration rate will be easier to obtain than the unsaturated soil characteristics, we will here focus on option (b).

To obtain the required input values for option (b), hydraulic conductivity values were extracted from the top layer of the WATFLOW model and translated into corresponding soil types by using Table 3.1; these soil types were then entered into Table 3.3 to select appropriate values of residual moisture content. Likewise, infiltration rates required in equ. (3.9) were taken from the results of the detailed WATFLOW modelling of Martin and Frind (1998) and Muhammad (2000). A uniform recharge rate of 530 mm/year was applied at the ground surface, which satisfies the overall water balance, was allowed to redistribute by means of the RSL in the model (as shown in Figure 2.3) from areas of low hydraulic conductivity to areas of high conductivity or to streams. During calibration, it was found that the RSL shunted approximately 260 mm/year of the recharge out of the system via stream runoff, while the remaining 270 mm/year was redistributed according to the hydrogeological characteristics of the subsurface. Thus the actual infiltration is spatially variable, and in some parts, the model shows a small amount of exfiltration. In situations where information on the spatially variable infiltration rate is not available, an average value can be used to calculate travel time through the unsaturated zone.

The total advective travel time through the layers above the Aquifer 1 can be calculated using the travel time within the unsaturated and the saturated zone. The 1D vertical travel time through the saturated zone is estimated using equ. (3.4). In equ. (3.4), the vertical gradient within the saturated zone is estimated using the head difference between the water table and the top of Aquifer 1.

We will consider two options for developing vulnerability map: (a) the areally variable infiltration rate and gradient obtained from WATFLOW, and (b) an average infiltration rate of 270 mm/yr and average gradient of 0.9 over the Mannheim area. In the SAAT method, a travel time between 0 and 5 years represents a highly vulnerable area, a travel time between 5 and 25 years means medium vulnerability,

and a travel time greater than 25 years gives low vulnerability [MOE, 2006].

The results under option (a) in terms of advective travel time are shown in Fig. 3.6. The associated vulnerability ranges are also shown on the colour bar. In some areas zero, close to zero, and upward gradients were encountered (white areas); this means that the SAAT approach is not applicable in these areas. The zero or upward gradients are due to the presence of wetland or streams within the study area (as shown in Figure 3.3). Some of the white areas have resulted from the exfiltration, since the flow is controlled by the topography and the heterogeneity of the system, where recharge occurs at topographic highs and discharge occurs at topographic lows. The map shows good correlation with the aquitard thickness, and the aquitard hydraulic conductivity. As can be seen from Figure 3.6 the northern part of the study area gives high travel times which is also evident in Figure 3.4 and Figure 3.5. The important windows in the NW quadrant within the hydraulic conductivity map (Fig. 3.2(b)) are correctly represented in Figure 3.6. The depth to the water table which gives the thickness of the unsaturated zone shows good correlation with Figure 3.6. In areas where the water table is shallow gives high vulnerability and the deep water table means low vulnerability. In the area of the Mannheim South well field, the vertical travel times are in the range of 1 to 30 years, whereas in the Mannheim North well field, they are in the range of 30 to 300 years.

The results under option (b) are shown in Figure 3.7. Compared to Figures 3.1(b), 3.2(b), and 3.3, Figure 3.7 shows that there is some visual correlation with the thickness, and good correlation with the hydraulic conductivity and the depth to the water table. As should be expected in areas where the aquifer is unconfined and the depth to the water table is about 30-50 m, vulnerability is low with advective travel times of 100 years, whereas in areas where the depth to water table is about 0-20 m, vulnerability is between high and moderate with advective travel times in the 1-30 year range. There seems to be little recognizable correlation with the ISI results (Fig. 3.4) and with the HR results (Fig. 3.5).

In most SWP studies, detailed information at the level used above may not be available. In the case where unsaturated-zone characteristics are not available, a reasonable approach would be to neglect the protective effect of the unsaturated zone and to assume saturated conditions up to ground surface. This assumption would in any case be a conservative one. The SAAT equation applicable in this

case will be equ. (3.4) and an average gradient over the Mannheim area of 0.9 is used.

Figure 3.8 shows the vulnerability map using the saturated condition and the average gradient. The white areas have now disappeared. Compared to Fig. 3.6, the overall vulnerability has increased in Fig. 3.8. Because the data used for Fig. 3.8 differ from those used in the HR model (Fig. 3.5) only the magnitude of the gradient (0.9 vs. 1.0), Figures 3.8 and 3.5 are identical except the scale factor of 1.0/0.9.

3.4 Aquifer Vulnerability at the Greenbrook Well Field

For the purposes of this comparison, we also focus on the Greenbrook well field, and designate Aquifer 2 as the target aquifer. Aquifer 2 is fully confined, but there are some windows in the overlying layers allowing direct communication between the surface and the aquifer.

3.4.1 Aquifer Vulnerability Parameters

Figures 3.9, 3.10 and 3.11 show the data providing the input for the aquifer vulnerability calculations for the Greenbrook well field area. The combined thickness of the overlying layers within the Waterloo Moraine and the Greenbrook area ranges mostly from 10 to 70 m (Fig. 3.9). The vertical hydraulic conductivity map (Fig. 3.10) represents the harmonic mean values of the layers overlying Aquifer 2; these range from 10^{-8} to 10^{-6} m/s over most of the area, with the exception of a high-K window in the SW (Southwest) quadrant. In the area of the Greenbrook well field itself, the water table is shallow (Fig. 3.11), while to the southwest, the water table is much deeper; this is also the area of the Mannheim well field which pumps from partly unconfined Aquifer 1.

3.4.2 The Index Approach: ISI

Figure 3.12 shows the resulting vulnerability map for Aquifer 2 obtained by the ISI approach. The map is a close reflection of the thickness map (Fig. 3.9(b)),

but it shows little similarity with the hydraulic conductivity map (Fig. 3.10(b)). This is explained by the basic flaw in the ISI calculations, which neglects the fact that hydraulic conductivity varies exponentially. As a result, the most dominant factor influencing aquifer vulnerability is underrepresented in the ISI calculations. In a realistic vulnerability map, the hydraulic conductivity would be expected to dominate.

3.4.3 The Hydraulic Resistance Approach: HR

Figure 3.13 shows the vulnerability map obtained with the HR approach. This map shows good correlation of the thickness map (Fig. 3.9(b)) and a close reflection of the hydraulic conductivity distribution (Fig. 3.10(b)). The window in Aquitard 1 in the SW quadrant that provides a shorter travel path for the contaminants is correctly represented. The orange area in the centre represents a hydraulic resistance C_v of about 1.8 to 3 years, which corresponds to an advective travel time (divide by average gradient = 0.13) of about 18 to 30 years. Since the unsaturated zone is neglected by assuming saturated conditions up to ground surface, this would be a conservative estimate. Thus Fig. 3.13 is a realistic and credible representation of the vulnerability of Aquifer 2.

3.4.4 The Travel Time Approach: SAAT

Figure 3.14 shows the vulnerability map obtained with the SAAT approach, using the tabulated values of mobile moisture content for the unsaturated zone calculations. The map is very similar to that in Fig. 3.13, as would be expected, except for some blanked-out spots. These blanked-out spots represent areas where the gradient is either upward or zero or very close to zero. Some of these areas are explained by wetlands forming groundwater discharge areas. The large white area near the south border is the Mannheim well field (i.e. wells K93 and K94) which pumps from Aquifer 1, with the result that the gradient in the layers overlying Aquifer 2 are upward and some the area the gradient is zero or very close to zero. In the orange areas in the centre of the map, the advective travel time is 30 to 60 years, which agrees well with the HR results in Fig. 3.13 if the effect of the unsaturated zone is taken into account.

Figure 3.15 shows the vulnerability using an average infiltration rate of 270 mm/year and an average gradient of 0.13. The white areas disappear and the extremely long

travel times (500 years) become moderate (160 years).

Figure 3.16 shows the SAAT results obtained by assuming saturated conditions up to ground surface and an average vertical gradient of 0.13. Compared to Fig. 3.14, Fig. 3.16 shows that the overall vulnerability is increased within the study area. This map now corresponds almost exactly to the HR results (Fig. 3.13), with the orange area in the centre being in the 18 to 30 years range except for a scale factor of 1.0/0.13.

3.5 Discussion

For the Mannheim area, the target aquifer is the water table aquifer. Essentially all of the ISI map area has moderate to low vulnerability, which agrees with the HR and SAAT results. However, most of the detail in particular the windows in the NW quadrant, is not seen in the ISI map. This suggests that aquitard heterogeneities may not be represented well by the ISI method, as expected. In the Greenbrook well field, in which the wells are pumping from the deeper aquifer, the ISI results cannot be compared to the results of SAAT and HR except in a rough qualitative way.

In the SAAT approach, the importance of the unsaturated parameters in the calculated travel time is more dominant in the Mannheim area (target aquifer, Aquifer 1) than that in the Greenbrook area (target aquifer, Aquifer 2). SAAT, however, does not apply where the gradient is zero or close to zero. Although an upward gradient (for example at groundwater discharge areas) in the SAAT approach means that the aquifer is not vulnerable, it can appear as vulnerable in the ISI or HR approach.

To overcome uncertainties in obtaining accurate unsaturated zone parameters, the unsaturated zone can be treated as saturated, which is a conservative assumption in the context of vulnerability. With these assumptions, the quantitative SAAT and HR results are in excellent agreement except for a scale factor.

However, the qualitative labelling assigned to HR (based in Table 3.2 for the van Stempvoort AVI method) appears to be tilted toward the high side; for example, for the area in the centre, the SAAT vulnerability is labelled as "moderate to low", while the HR vulnerability is labelled "high to extremely high", for the same numerical values. Thus the HR vulnerability ranges should be used with caution.

3.6 Conclusions

In this chapter, we considered the concept of aquifer vulnerability as a measure of the barrier effect of a protective layer overlying a target aquifer, taking into account only the characteristics of the geologic materials and the flow system. The source-pathway-receptor approach is used. Specific contaminant characteristics are not considered.

For the source-pathway-receptor approach, the results show that a quantitative measure of vulnerability such as advective travel time, as used in the SAAT method, is to be preferred over a non-quantitative index approach, such as used in the ISI method. While the ISI method tends to give misleading results for heterogeneous systems, advective travel time is always physically representative of the actual system. It can also serve as a link between a vulnerability model and a 2D groundwater flow model.

The HR method includes all time-invariant characteristics of overlying materials and is applicable to all situations. It uses the same data as ISI except porosity. Although the results are given in terms of advective travel time under a unit gradient, it can easily be converted to true advective travel time. The user should also be aware that qualitative vulnerability ranges (low-moderate-high) in the HR method are subjective and may depend on the specific situation. However, vulnerability ranges are useful as supplementary information along with quantitative measures such as travel time.

A drawback of the SAAT method is its dependence on a downward vertical gradient. In reality, gradients can be upward, zero or near-zero, or variant in time. A near-zero gradient will give very long advective travel times, while zero gradient means the method is not applicable in that area. Under invariant conditions, an upward gradient (i.e., upward flow) means that water will not reach the aquifer, so the aquifer is not vulnerability.

In the SAAT approach, if adequate data on the unsaturated characteristics are not available, the unsaturated zone can be treated as saturated, resulting in a consistently conservative estimate of vulnerability. If the unsaturated zone is treated as saturated and an average gradient is used, the SAAT method is identical to the HR method, except for a constant scale factor.

(a)

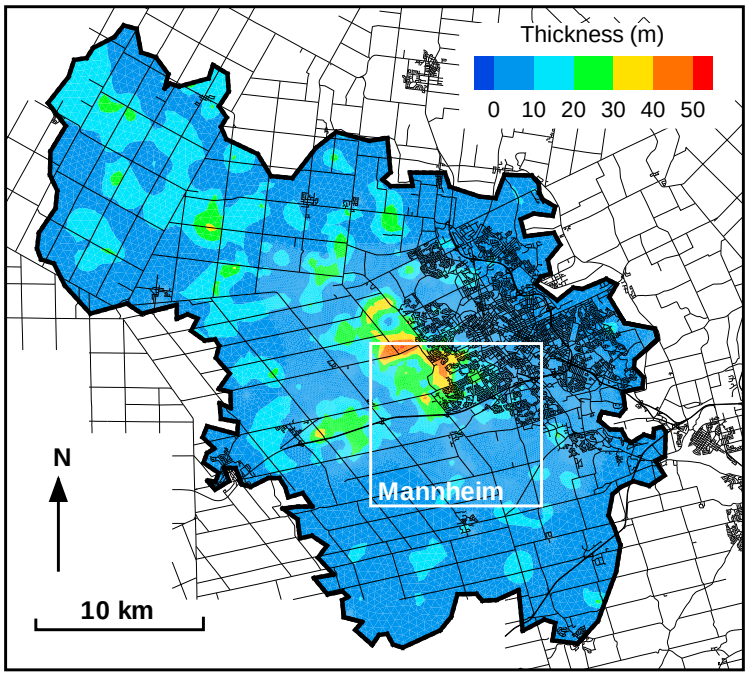

(b)

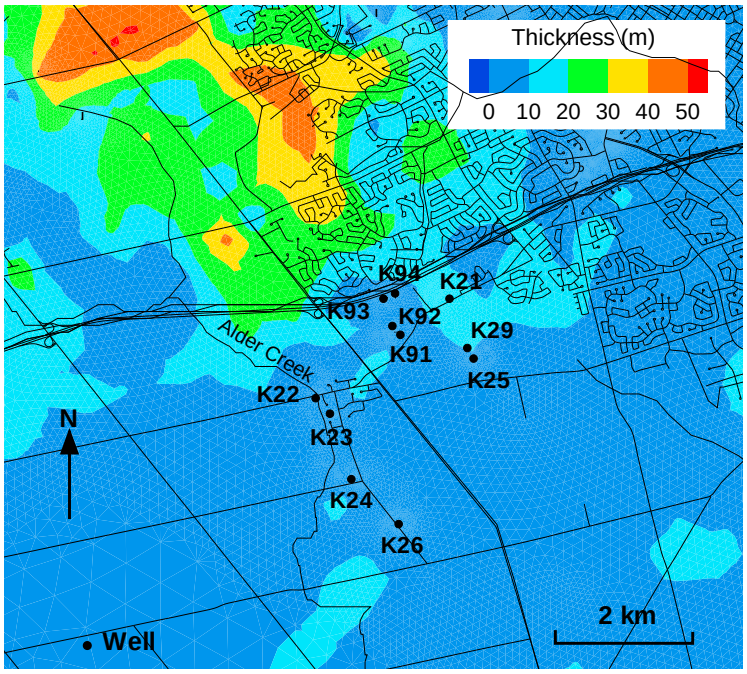

Figure 3.1: Thickness of Aquitard 1 (a) Waterloo Moraine, (b) Mannheim area.

(a)

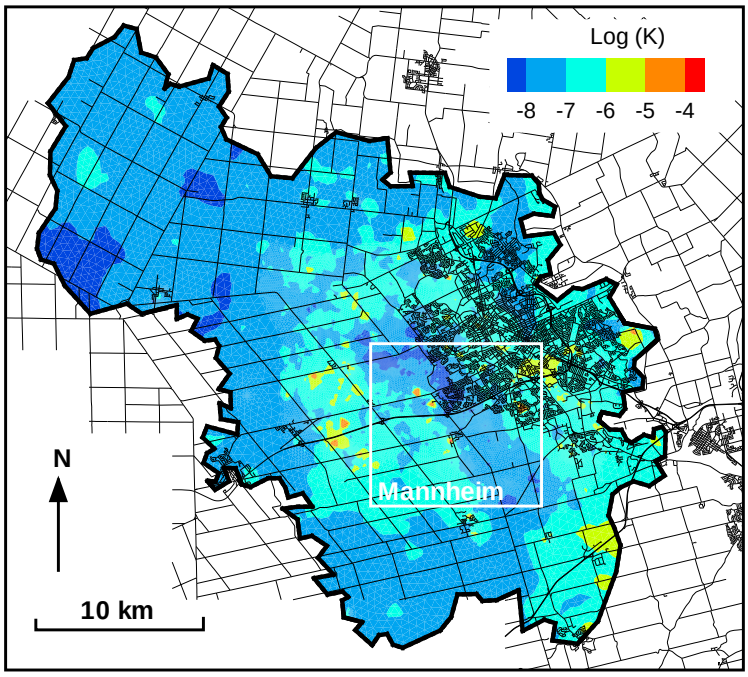

(b)

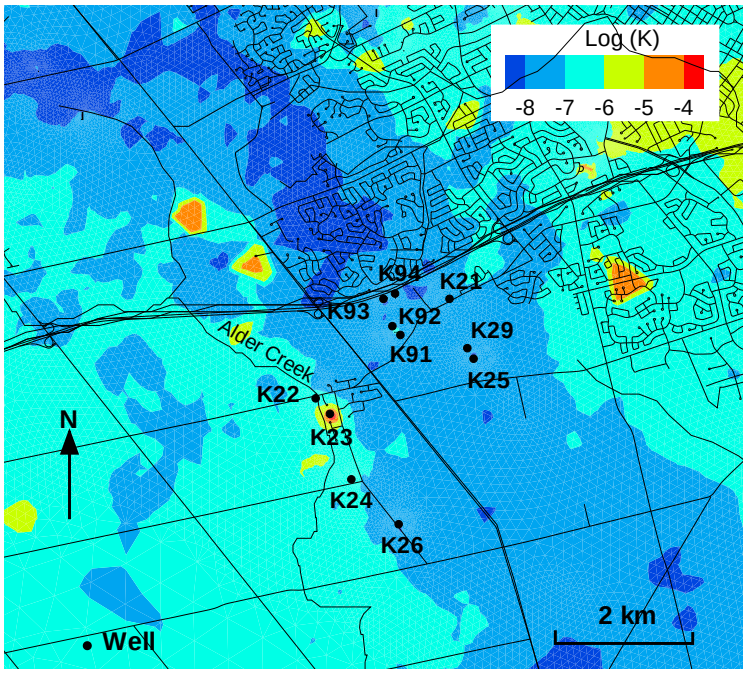

Figure 3.2: Vertical hydraulic conductivity K of Aquitard 1 (K in m/s) (a) Waterloo Moraine, (b) Mannheim area.

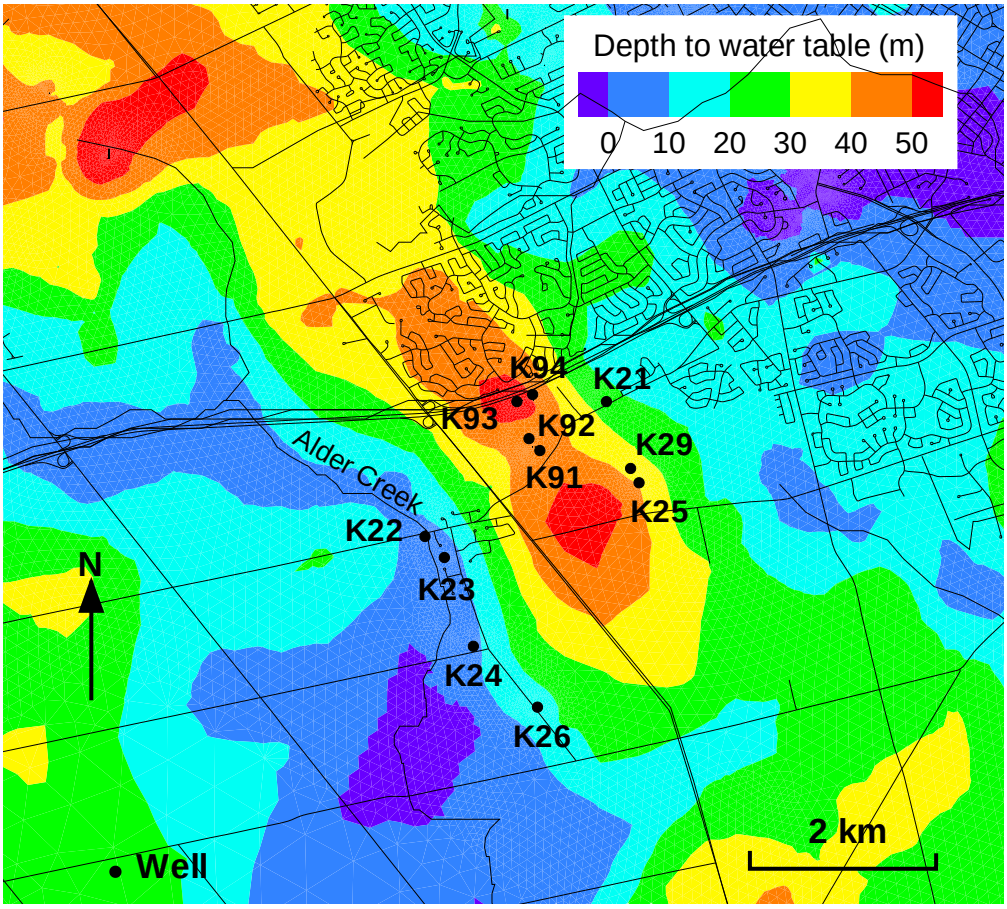

Figure 3.3: Depth to water table, Mannheim area.

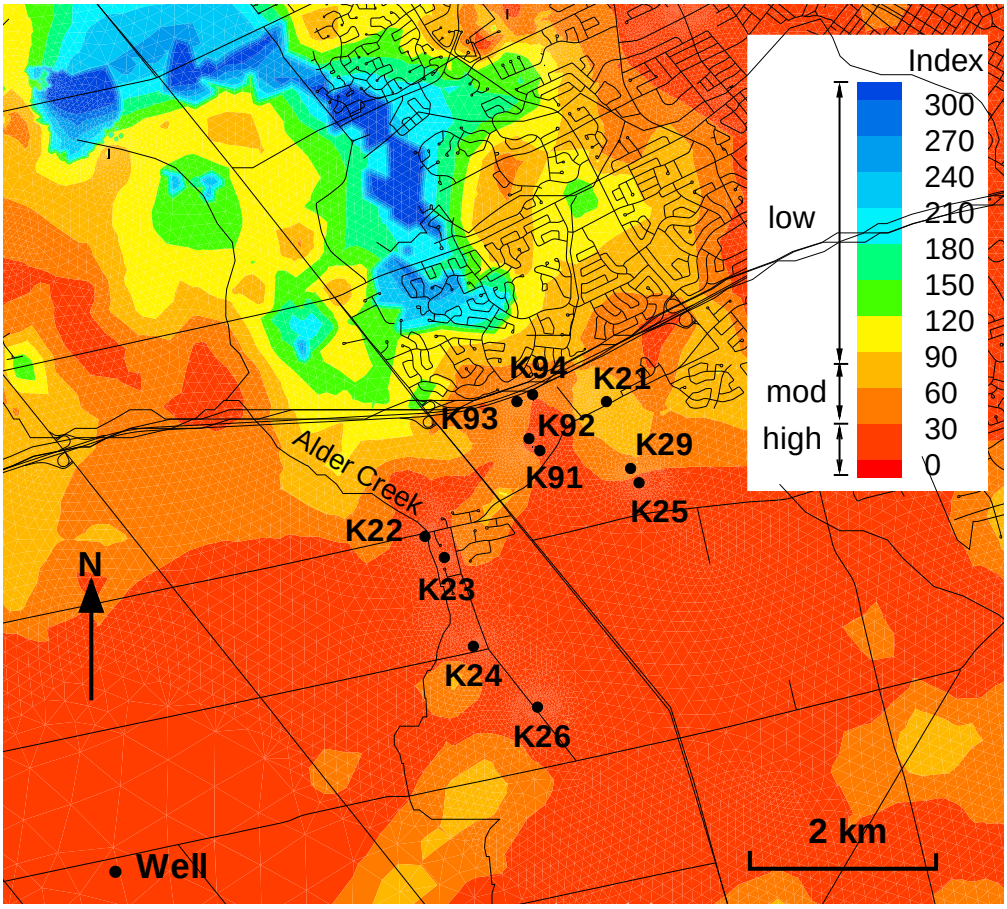

Figure 3.4: Vulnerability map for Aquifer 1, Mannheim area, using the ISI method.

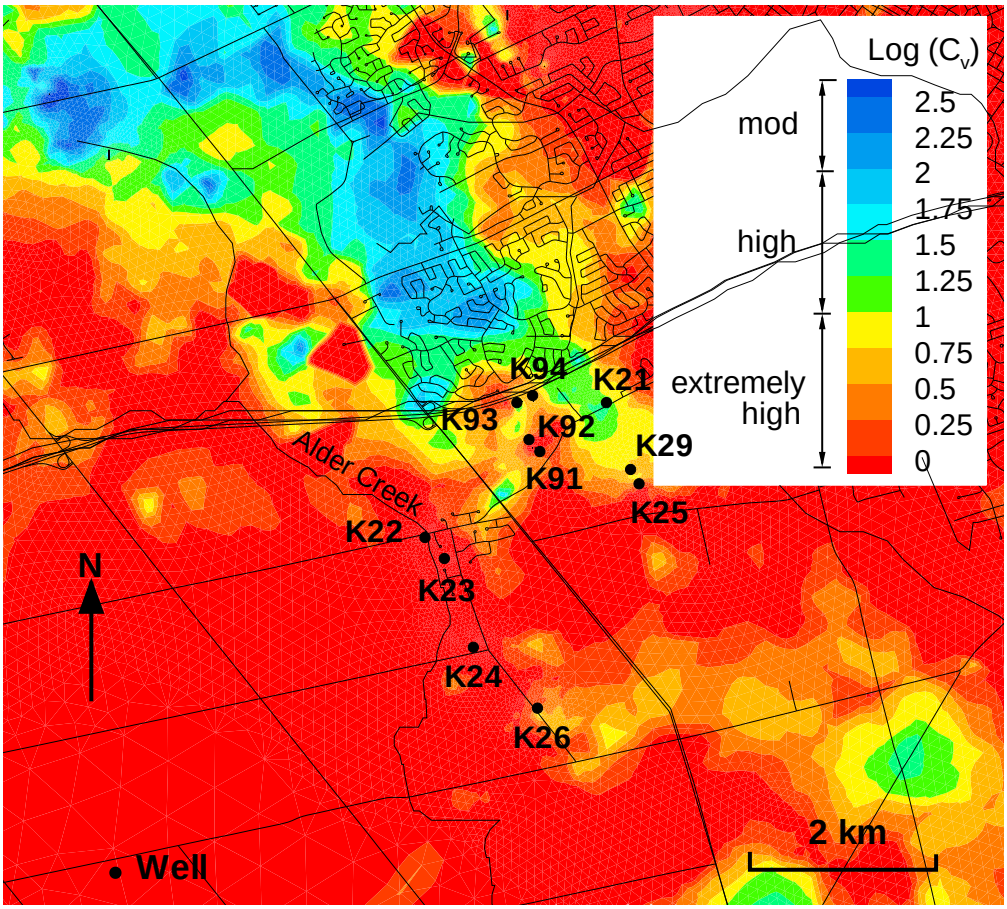

Figure 3.5: Vulnerability map for Aquifer 1, Mannheim area, using the HR method (color bar showing AVI values according to van Stempvoort et al., 1992)

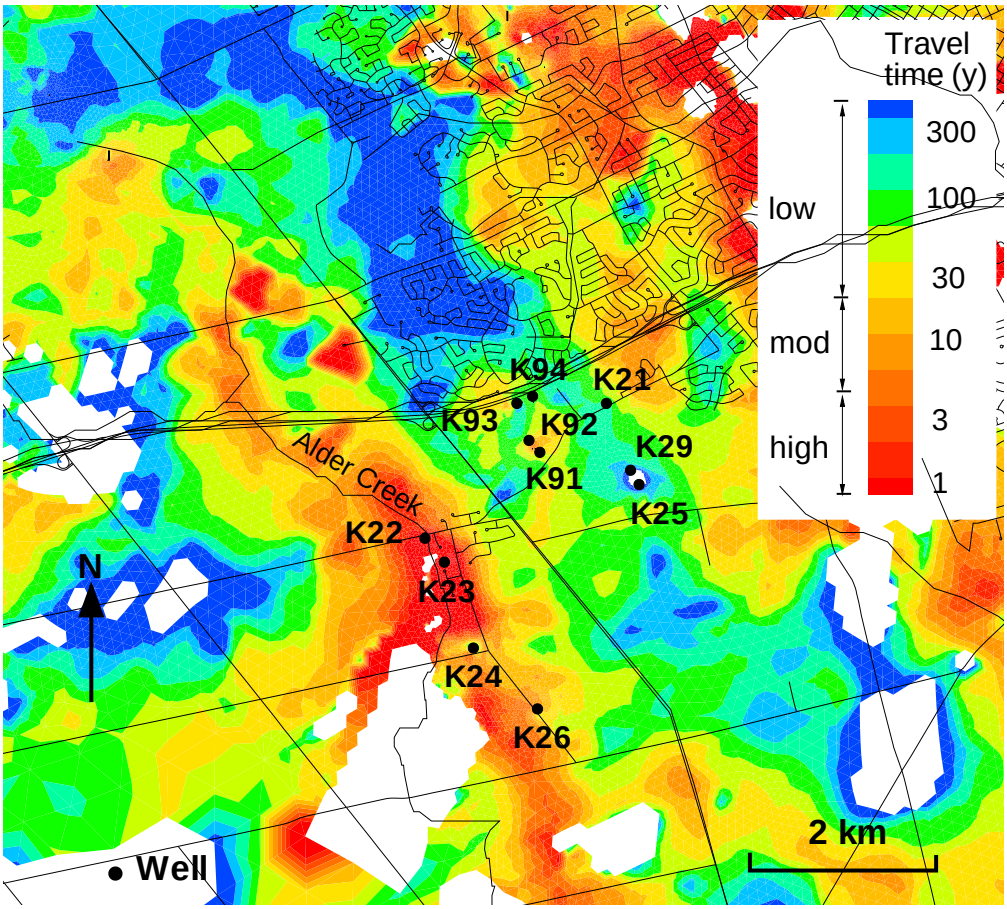

Figure 3.6: Vulnerability map for Aquifer 1, Mannheim area, using the SAAT approach based on equation 3.4, with spatially varying gradient, and equation 3.9, with θ_m values taken from Table 3.3 and spatially varying infiltration rate (white areas indicate zero or upward gradient and exfiltration).

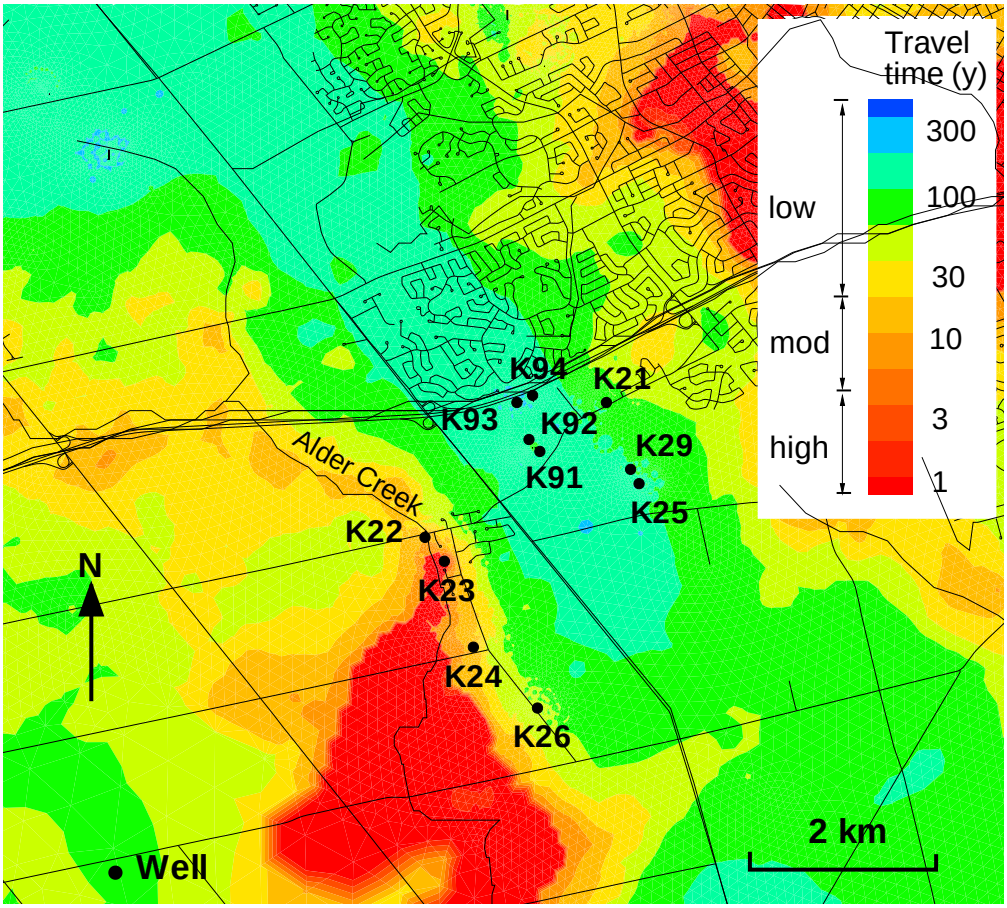

Figure 3.7: Vulnerability map for Aquifer 1, Mannheim area, using the SAAT approach based on equation 3.4 with an average gradient of 0.9 and equation 3.9, with θ_m values taken from Table 3.3, average infiltration rate of 270 mm/year.

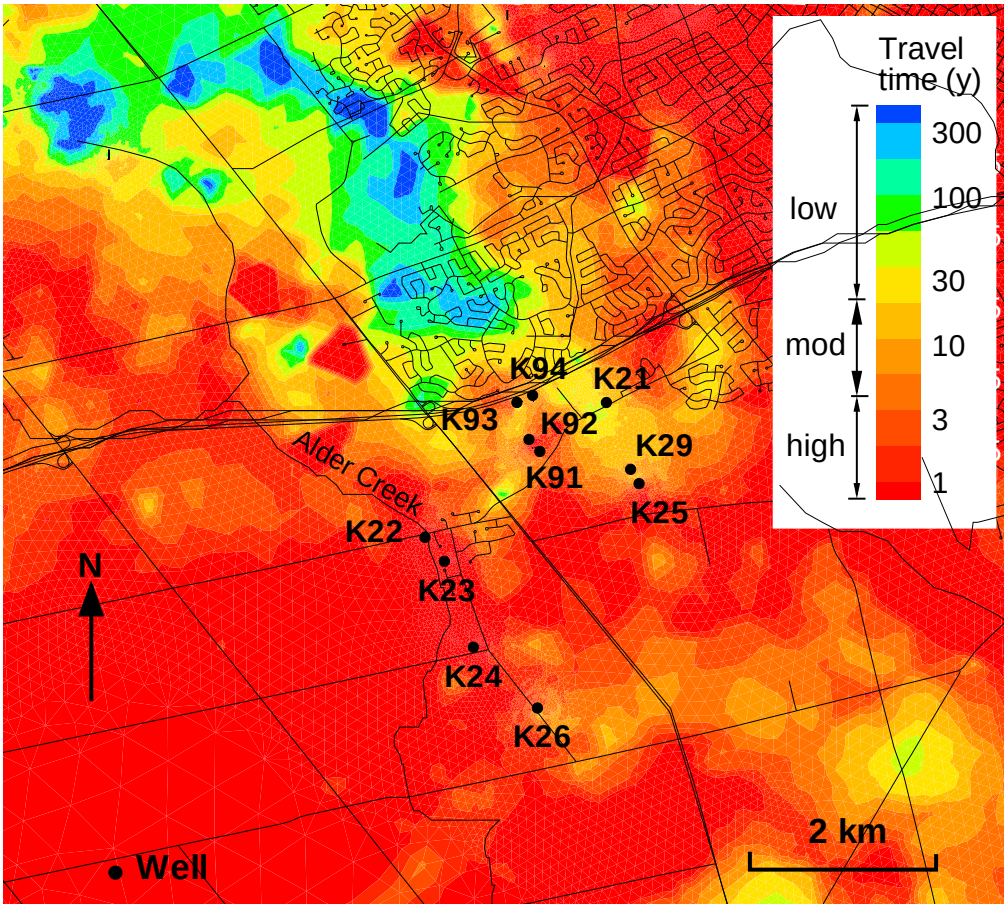

Figure 3.8: Vulnerability map for Aquifer 1, Mannheim area, using the SAAT approach based on equ. (3.4), assuming fully saturated conditions, average gradient 0.9.

(a)

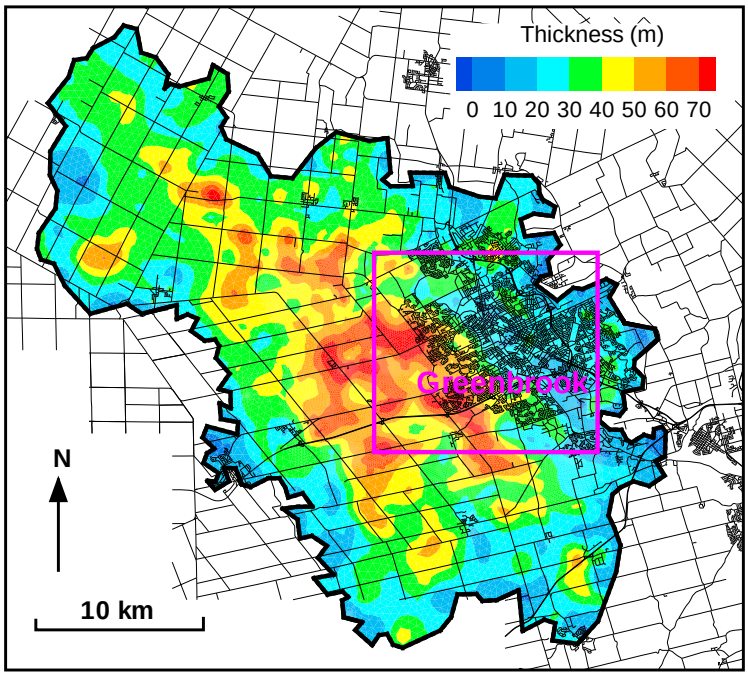

(b)

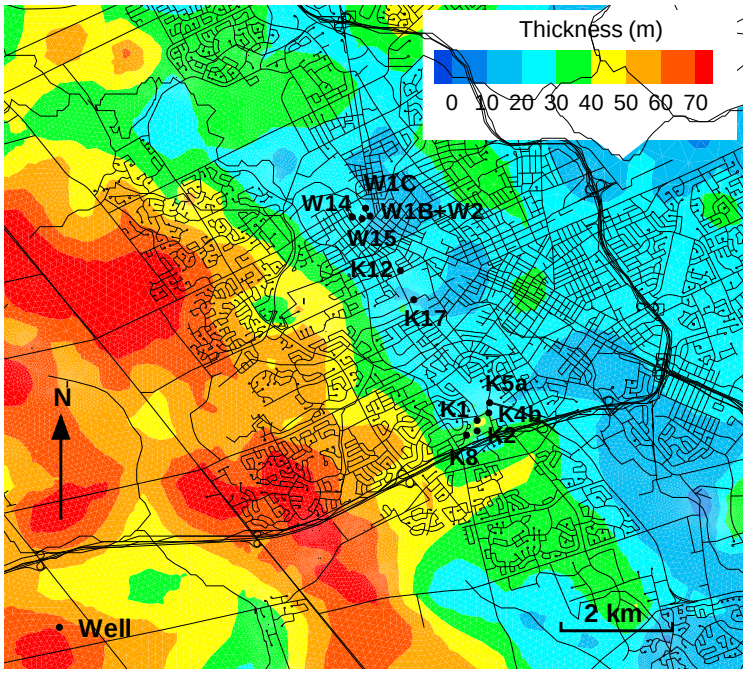

Figure 3.9: Thickness of the overlying layers above Aquifer 2 (a) Waterloo Moraine, (b) Greenbrook and surrounding area.

(a)

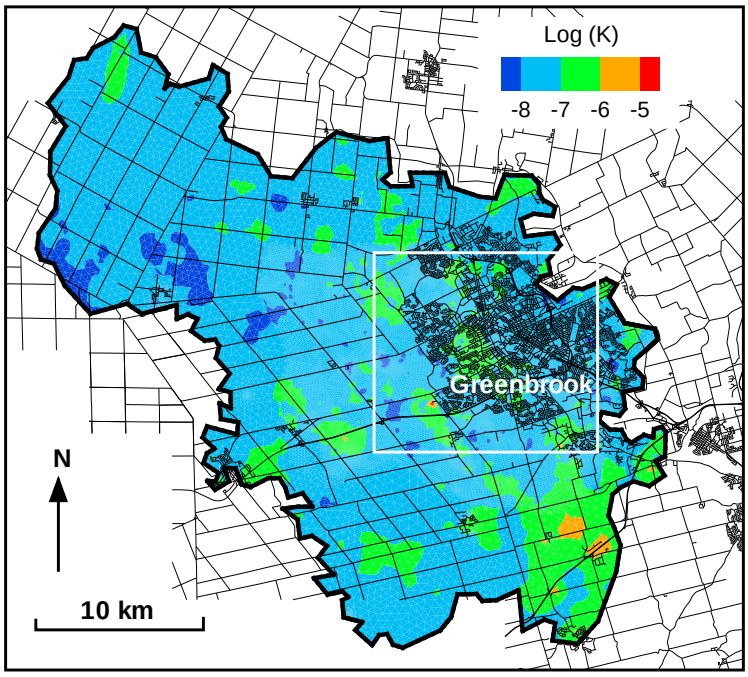

(b)

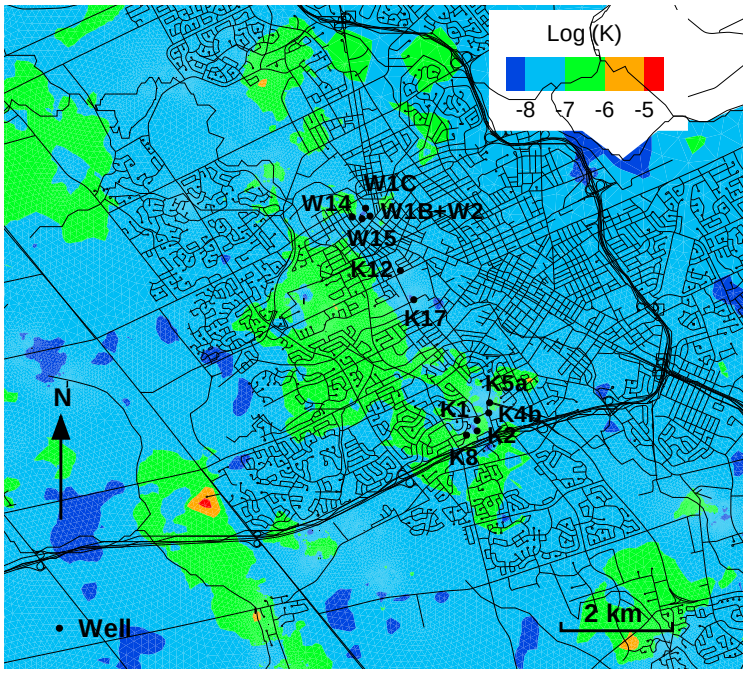

Figure 3.10: Vertical hydraulic conductivity K of the overlying layers above Aquifer 2 (K in m/s) (a) Waterloo Moraine, (b) Greenbrook and surrounding area.

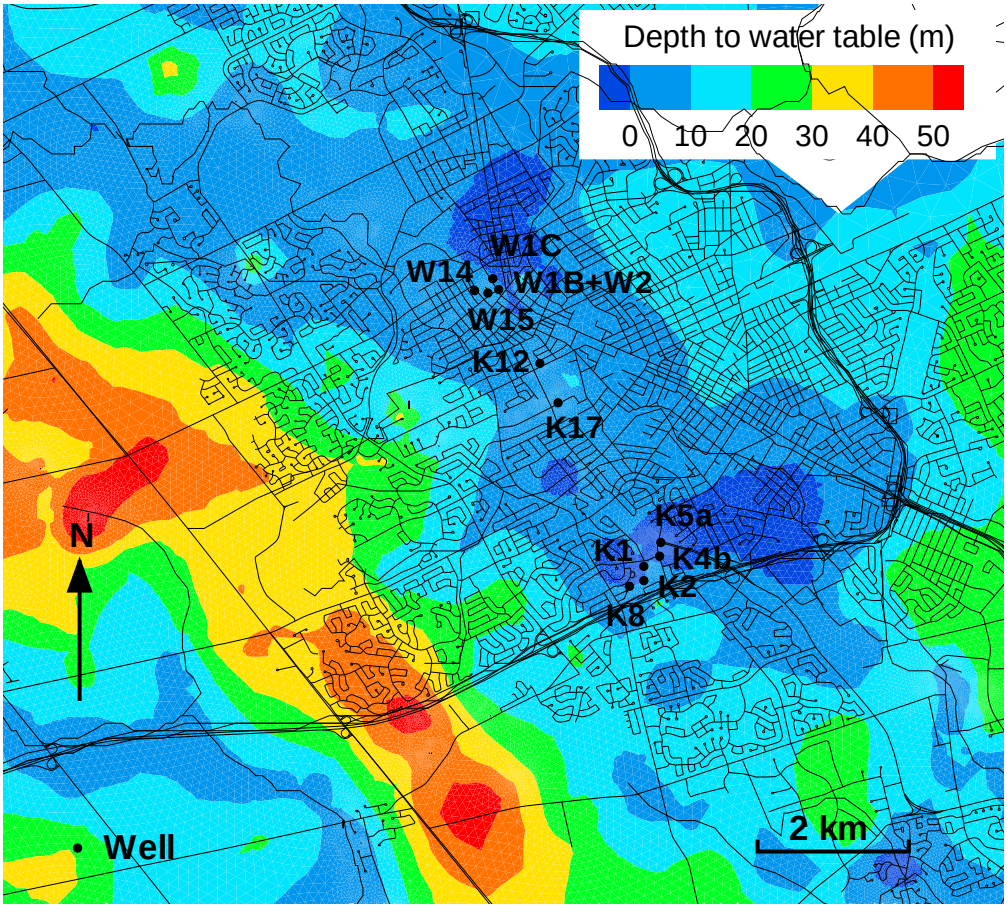

Figure 3.11: Depth to water table, Greenbrook and surrounding area.

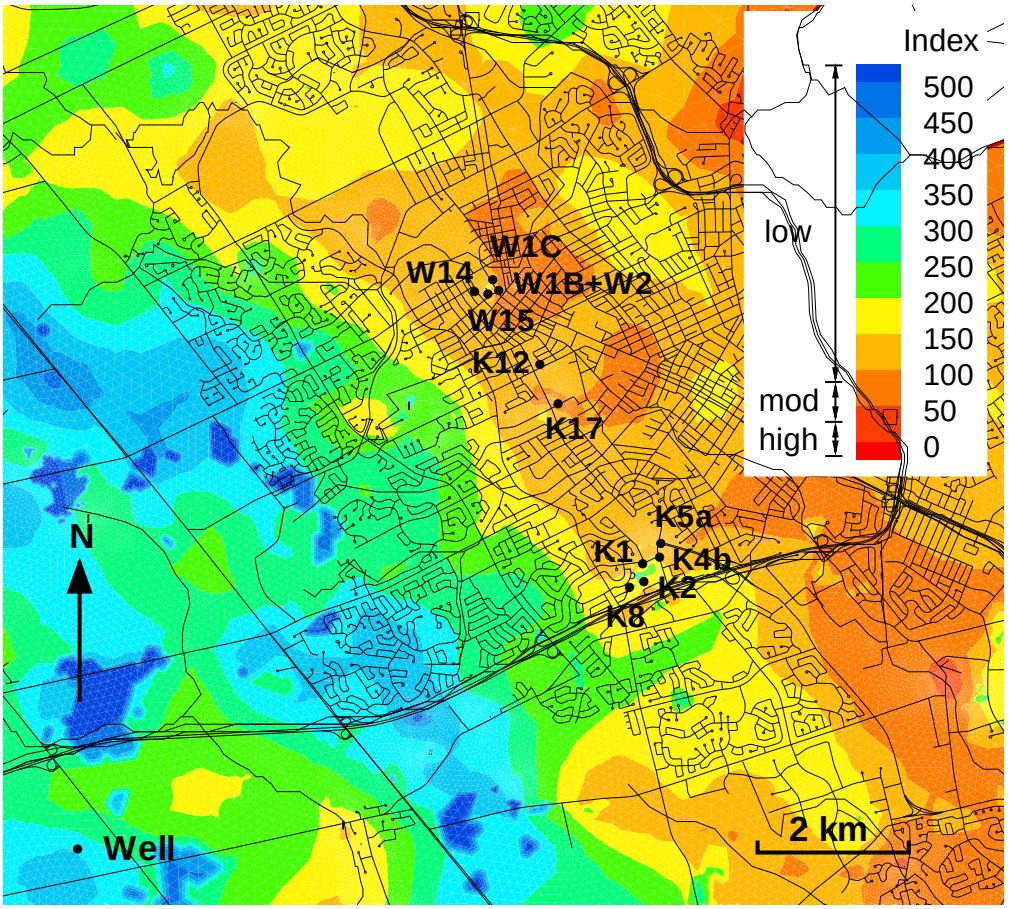

Figure 3.12: Vulnerability map for Aquifer 2, Greenbrook area, using the ISI method.

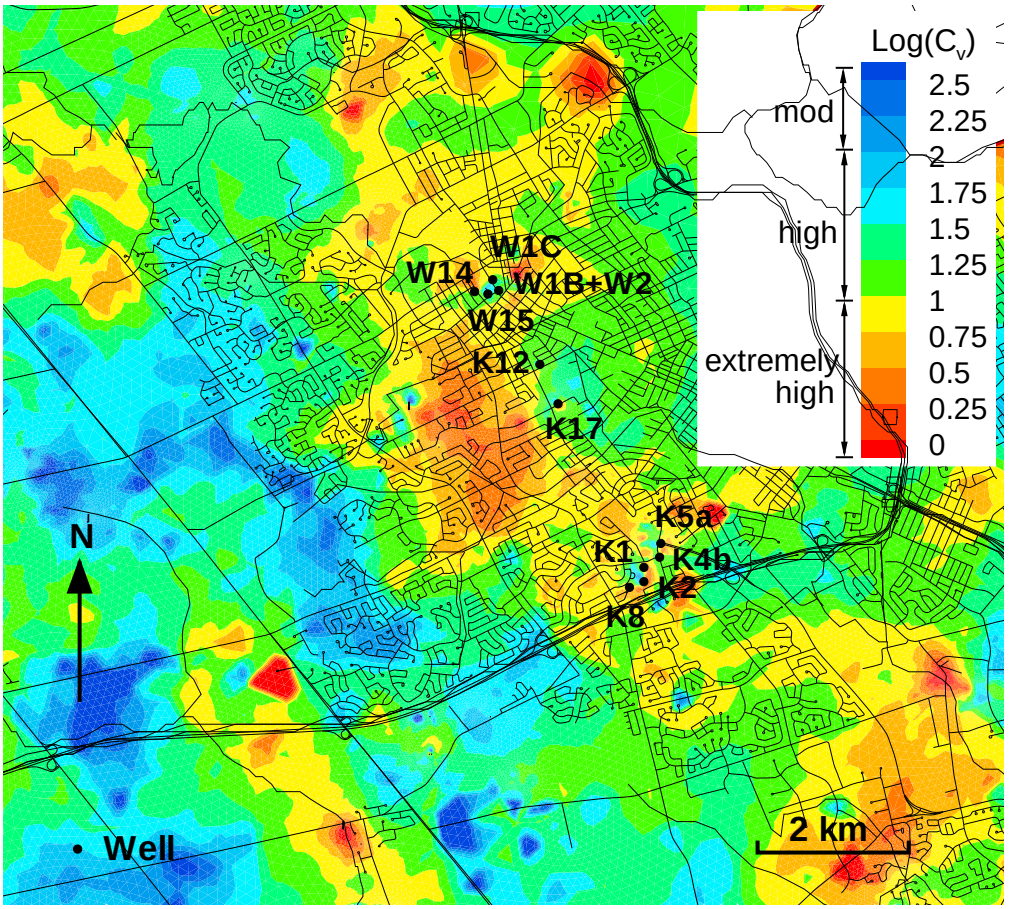

Figure 3.13: Vulnerability map for Aquifer 2, Greenbrook area, using the HR method (color bar showing AVI values according to van Stempvoort et al., 1992).

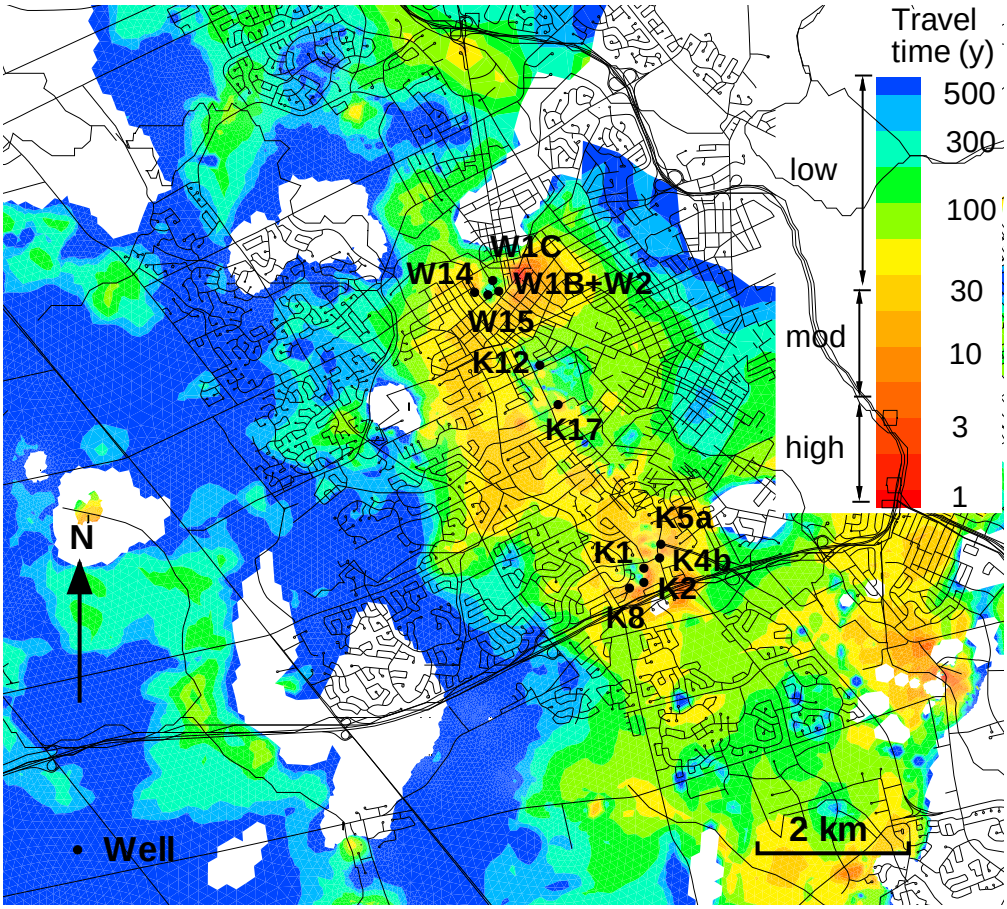

Figure 3.14: Vulnerability map for Aquifer 2, using the SAAT approach based on equation 3.4, with spatially varying gradient, and equation 3.9, with θ_m values taken from Table 3.3 and spatially varying infiltration rate (white areas indicate zero or upward gradient and exfiltration).

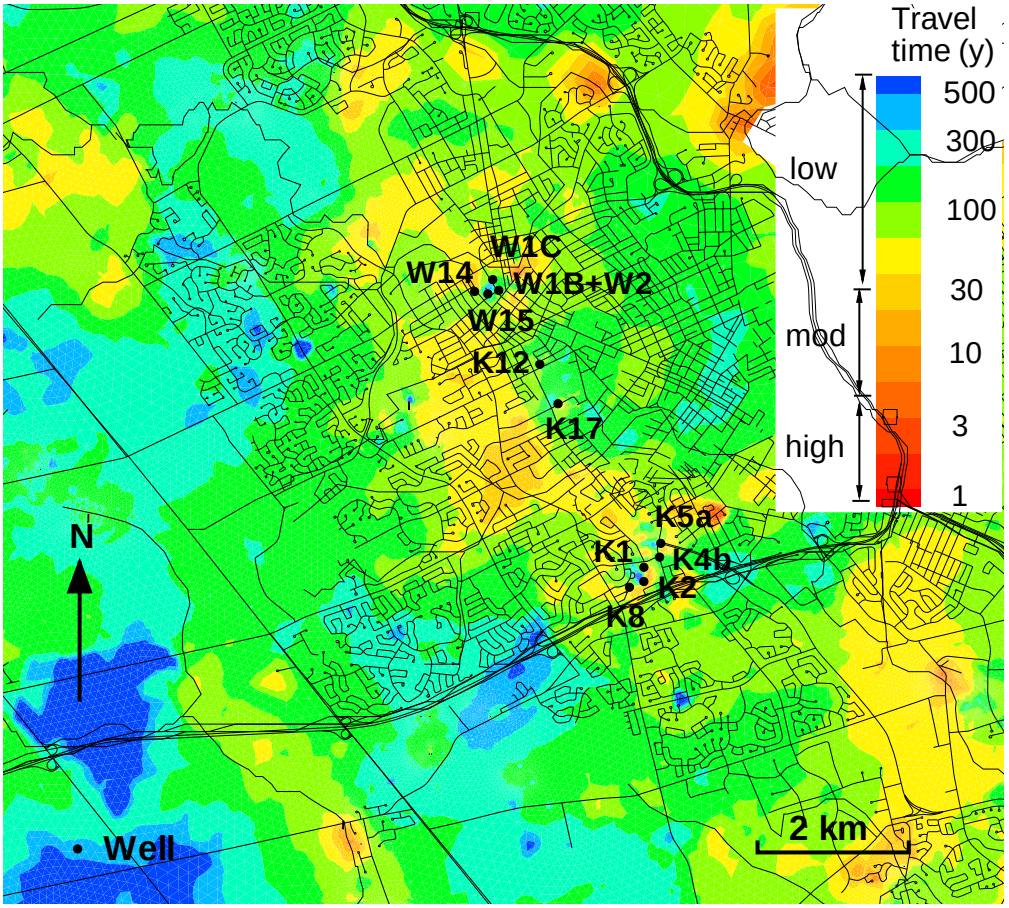

Figure 3.15: Vulnerability map for Aquifer 2, using the SAAT approach based on equation 3.4 using an average gradient of 0.13 and equation 3.9, with θ_m values taken from Table 3.3, average infiltration rate of 270 mm/year.

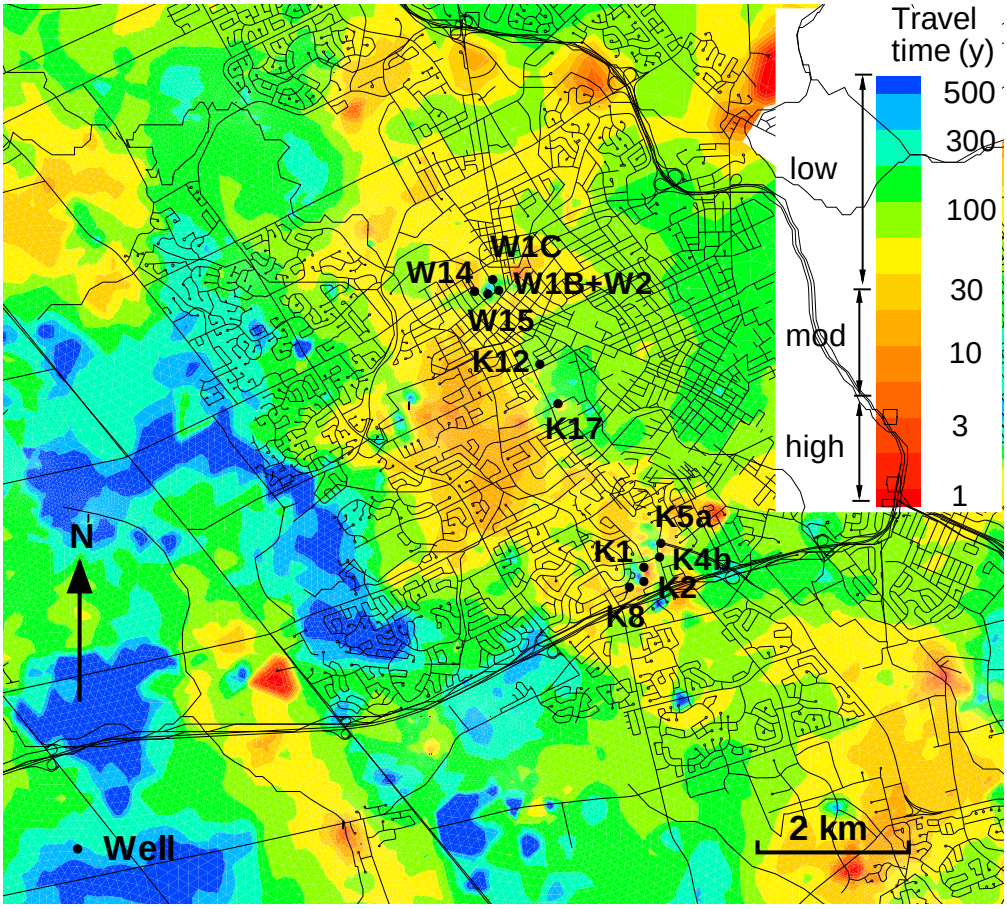

Figure 3.16: Vulnerability map for Aquifer 2, Greenbrook area, using the SAAT approach based on equ. (3.4), assuming fully saturated conditions, average gradient 0.13.

Chapter 4

Wellhead Protection Areas

The second component of source protection is the concept of the wellhead protection area (WHPA). The standard way to delineate a WHPA is by backward particle tracking from the well, either for a specified time, or to emergence of the particle on the surface. WHPAs can also be delineated using the advective-dispersive transport approach.

In this chapter, a comparison is made between a 3D backward advective-dispersive approach and a 3D particle tracking approach using a hypothetical system. The 3D advective-dispersive approach and the particle tracking approach are also demonstrated by application to the Mannheim well field.

4.1 Background

According to the U.S. Environmental Protection Agency (EPA), a WHPA is defined as "the surface and subsurface area surrounding a water well or well field, supplying a public water system, through which contaminants are reasonably likely to move toward and reach such a water well or well fields" [EPA, 1987]. The WHPA can be all or a part of the well's capture zone. The size of a WHPA varies from site to site depending on a number of factors, including the geologic and hydrogeologic features of the area and the goals of the protection program.

The conventional approach for delineating WHPAs is based on the time of travel (TOT) of a contaminant in the groundwater from the source to the well. In Ontario, Canada, TOT is an established and accepted method to delineate WHPAs.

According to a report of the Ministry of Environment submitted by the Technical Experts Committee (TEC) in 2004, the following are to be identified: (1) a 100 m radius pathogen security area immediately surrounding a wellhead, (2) a 2-year pathogen management zone around a wellhead, (3) a 5-year TOT zone for dense non-aqueous phase liquids (DNAPLs)/contaminant protection, (4) a 25-year TOT zone to protect against persistent contaminants. The total capture zone for the drinking water supply well is also added as a required component for WHPA analysis. Similar regulations are in use in other jurisdictions throughout North America and Europe.

The TOT is usually determined by applying the advective particle tracking technique in a steady-state flow field. In a typical particle tracking analysis, the steady-state flow field of the system is determined first by running a suitable flow model with the appropriate parameters and boundary conditions, then placing a sufficient number of particles at the well and tracking them advectively in the upgradient direction; this procedure is known as backward tracking. If the analysis is done in 3D, the particles can be tracked until they reach the ground surface to obtain the ultimate capture zone, or for a specific time period to obtain a time-dependent capture zone. Alternatively, particles can be placed at the ground surface or water table and tracked in the downgradient direction until captured by the well; this is known as forward tracking. As an alternative to particle tracking, transport modelling in either a forward or a backward mode can be used. While particle tracking considers only the advective component of flow, transport modelling considers both the advective and the dispersive component. The dispersive component can be seen as representing the uncertainty in the hydrogeologic parameters [Frind et al., 2002].

For any modelling undertaken to delineate a realistic WHPA, it is important to verify the applicability of the hypotheses related to the model and to ensure that the model integrates all the major characteristics of the aquifer system. Paradis et al. used methods ranging from simple approaches to complex computer models to generate WHPAs for simple groundwater flow systems [Paradis et al., 2007]. These methods provide a relatively wide range of WHPAs for the same system. The importance of the geologic structure is demonstrated in a classical paper by Fogg, who has found that for complex aquifer systems, flow is not so much controlled by the hydraulic conductivity of the more permeable units, but by their continuity and interconnectedness, particularly in the vertical direction [Fogg, 1986]. He has also noted that for such systems, the 3D representation is important since the

vertical interconnectedness would be lost in a 2D model. Therefore, 3D modelling should be encouraged wherever there is a significant vertical component of velocity, which must be present if there is surface recharge. Martin and Frind also highlighted the controlling influence of aquitard windows in the capture zone delineation [Martin and Frind, 1998]. The use of 3D models has also been demonstrated as necessary in highly anisotropic and heterogeneous settings [Marquis and Stewart, 1992]; [Springer and Bair, 1994]; [Barlow, 1994]; [Foster, 1987].

4.2 Dimensionality

By definition, a WHPA is an area delineated on the ground surface. However, this does not mean that the delineation can be simplified to the 2D horizontal plane. All groundwater flow systems, being part of the hydrologic cycle, are inherently three-dimensional, and 3D processes will ultimately determine the shape of the WHPA on the surface. With backward particle tracking, the particles are injected at the well and they travel in the 3D system in the upgradient flow direction until they reach the ground surface, thus defining the steady-state or ultimate capture zone. Alternatively, particles starting at the well can travel for a specified time period, defining a time-dependent TOT zone. In each case the capture zone or WHPA is delineated by drawing an envelope around the particle end positions. The requisite flow field is determined by running a groundwater flow model in at steady state.

In situations where sufficient 3D data are not available, a two-dimensional analysis is sometimes used where the aquifer is considered as 2D and particles are tracked horizontally in the plane of the pumped aquifer for the required time period to obtain a time-dependent capture zone in the aquifer. This capture zone is then projected to the ground surface. The fundamental drawback with this method is that the particles cannot reach the ground surface; therefore an ultimate capture zone cannot be delineated. Also, the recharge contribution to flow in the aquifer is neglected, which will change the flow system if the recharge is significant. These drawbacks suggest that a 2D analysis should only be used if the recharge over the area of the WHPA is so small as to have no effect on the flow system in the area considered for the TOT analysis. Such situations can occur if the aquifer receives all of its recharge in a recharge area far upstream of the well area, for example an outcrop area. For the more general situation, the flow system should always be modelled as 3D in order to obtain a realistic WHPA.

4.3 Physical Processes and Uncertainty

In standard particle tracking, the movement of each particle is governed solely by advective flow, assuming the flow system is known. A number of processes that are relevant to the transport of contaminants are neglected, such as: a) dispersion, b) dilution at the well, and c) chemical reactions. A method that can account for some of the processes neglected by advective particle tracking is backward-in-time advective-dispersive transport modelling [Uffink, 1989]; [Wilson and Liu, 1995]; [Kunstmann and Kinzelbach, 2000]; [Neupauer and Wilson, 2001]; [Frind et al., 2002]; [Cornaton, 2003]. A particularly important process is macrodispersion, which can be taken as representing the uncertainty in defining the hydrogeologic characteristics (e.g. hydraulic conductivity) of the aquifer [Gelhar and Axness, 1983]. Another is dilution in the well by mixing of contaminated water with clean water, which tends to moderate concentrations [Einarson and Mackay, 2001]. Both of these processes can be handled by the methodology discussed here. Chemical reactions (except for simple sorption and decay reactions) are beyond the scope of this study.

The transport approach can easily be implemented in the context of WHPA delineation by using a standard advective-dispersive transport model in a backward-in-time mode. The results of backward-in-time transport modelling appear in the form of a 3D plume, which can be projected onto the ground surface to show the probability of capture. This probability plume is the backward equivalent of a contaminant plume obtained by forward modelling. The probability plume can be easily transformed into a conventional capture zone by using mass balance principles (see [Frind et al., 2002]). However, it should be noted that by applying this type of transformation, an important characteristic of the probabilistic form is lost, namely the absence of a sharp boundary between the area of capture within the WHPA and the area of non-capture outside of the WHPA. A gradual transition from capture to non-capture areas is clearly more realistic than a sharp boundary. With a sharp WHPA boundary line, groundwater protection guidelines will apply on one side of the line and not apply on the other side of the line, creating the potential for land use conflicts. Moreover, the line will change if pumping rates and recharge change.

An alternative approach to account for uncertainty is to use a stochastic analysis, where a number of different realizations of a hydraulic conductivity field are generated on the basis of statistical parameters, and the model is used to test these

different realizations to obtain the final result. This type of approach is beyond the scope of the present work.

4.4 Approaches to Delineate WHPA

Figure 4.1 shows a drinking water supply well within a system consisting of an aquifer and aquitard layer. In the delineation of the WHPA, the target is the well and the travel path is from the ground surface to the well. Backward advective particle tracking is the most commonly used method for WHPA delineation. An alternative approach is the advective-dispersive transport modelling which includes dispersion in addition to advection ([Uffink, 1989], [Wilson and Liu, 1995], [Kunstmann and Kinzelbach, 2000], [Neupauer and Wison, 2001], [Frind et al., 2002], and [Cornaton, 2003]. The dispersion coefficient, which is spatially variable and velocity-dependent, can be considered to represent the uncertainty in the position of the particle due to local-scale heterogeneities in the hydraulic conductivities. Because the effect of local heterogeneities is included in the transport approach, the latter can provide arguably more realistic TOT zones than advective particle tracking [Frind et al., 2002] and [Frind et al., 2006].

4.4.1 3D Backward Advective Particle Tracking

The 3D flow system is used as a basis for the delineation of WHPA in the advective particle tracking approach. In this approach, a number of particles are placed along a circle centered on the well. These particles are then tracked upstream in the direction of the negative velocity field until they reach the water table or the ground surface. Time-of-Travel zones as well as maximum extent of capture zones can be determined in this way.

The Pollock method, a semi-analytical method, is commonly used to calculate time-dependent locations of particles within the given flow field [Pollock, 1994]. In this method, the velocity across a cell or block can be interpolated linearly on the basis of the head distribution, and given the particle's entry point, its exit point can be located on the basis of the shortest travel time within the cell or block.

4.4.2 3D Backward Advective-Dispersive Approach

The governing equation of the backward-in-time advective dispersive transport model is similar to the standard advective-dispersive equation except the flow field is reversed. The standard advective-dispersive equation is solved for concentration whereas the backward equation is solved for the travel time probability density function (pdf) of a water particle. The governing equation for the three-dimensional backward model can be written in backward time, τ as:

$$\frac{\partial \psi^*}{\partial \tau} = \frac{\partial}{\partial x_i}\left(D_{ij}\frac{\partial \psi^*}{\partial x_j} + v_i \psi^*\right) \tag{4.1}$$

where ψ^* is the travel time probability density function (pdf) which gives the intensity of probability that the water particles situated at the position x will be absorbed by the outlet boundary at time τ. In equation (4.1), x_i denotes the spatial directions (i =1,2,3) (L), D_{ij} is the $(i,\ j)^{th}$ entry of the dispersion tensor (LT^{-2}) expressed in terms of longitudinal dispersivity α_L (L), the transverse horizontal dispersivity α_{TH} (L), the transverse vertical dispersivity α_{TV} (L), and the molecular diffusion coefficient D_m (LT^{-2}) [Burnett and Frind, 2002], and v_i is the groundwater velocity (LT^{-1}) in the direction of x_i.

The initial and boundary conditions are:

$$\psi^*(x,0) = 0 \qquad \text{in } \Omega$$

$$\psi^*(x,\tau) = g(\tau) \qquad \text{on } \Gamma_1$$

$$(v_i\psi^* + D_{ij}\frac{\partial \psi^*}{\partial x_j}).n_i = q.g(\tau).n \qquad \text{on } \Gamma_1$$

$$(D_{ij}\frac{\partial \psi^*}{\partial x_j}).n_i = 0 \qquad \text{on } \Gamma_1 \cap \Gamma_0$$

$$\text{Free exit boundary condition} \qquad \text{on } \Gamma_2$$

In the above conditions, Ω is the three-dimensional domain space, q is the water flux vector, and n designates the normal at the boundary, $g(\tau)$ is a specific function, Γ_1 is the inflow boundary, Γ_2 is the outflow boundary, and Γ_0 is the no-flow boundary. At the outflow boundary, the free exit boundary condition will occur where neither the concentration nor the mass flux is known [Frind, 1988]. At the free exit boundary, the boundary term $(v_i\psi^* + D_{ij}\frac{\partial \psi^*}{\partial x_j}).n_i$ is built into the solution with all quantities treated as unknowns. The detailed descriptions of the continuous and discrete backward equations are given in Appendix A.

The TOT zones relative to a given temporal reference τ_r is obtained by solving the backward travel time pdf using Equation 4.1 with the above boundary conditions, and by evaluating the cumulative probability density function (cdf) at each point for time τ_r.

4.5 Comparison of 3D Advective-Dispersive Model and Advective Model

The aquifer system is 250 m×125 m× 32 m in the x, y, and z directions, respectively. The thickness of the aquifer is 24 m and the thickness of the aquitard is 8 m. The initial head is 32 m. A constant head boundary of 36 m on the left side and 32 m on the right hand side is applied at the top layer. The base of the model domain is impermeable. The hydraulic conductivity of the aquifer and aquitard layers is set at 10^{-3} m/s and 10^{-5} m/s in the x and y direction and 10^{-5} m/s and 10^{-6} m/s in the z direction respectively. A steady-state pumping rate of 6.9 m^3/day is used for the capture zone analysis. A recharge rate of 2200 mm/year is applied at the top boundary.

The steady-state head distribution and elemental velocities are obtained using the flow model WATFLOW [Molson et al., 2002]. The maximum extent of capture zone for the hypothetical system is generated using the WTC model [Molson and Frind, 2004]. WTC is an advective-dispersive time-marching transport code used for solving complex three-dimensional groundwater mass transport problems. The transport parameters used in the equation are $\alpha_L = 10$ m, $\alpha_{th} = 1$ m, $\alpha_{tv} = 0.01$ m, and $D_m = 1\times10^{-10}$ m^2/s. In order to generate the capture zone, the velocity field is reversed and a constant concentration of 1 is applied at the well. The transport model was run in a backward mode with a negative velocity field until the plume stabilized, which occurred at about 750 days.

As shown in Figure 4.2, the results of backward-in-time transport modelling appear in the form of a 3D plume of capture probability. The intersection of the 3D plume with the land surface (Figure 4.2(b)) gives the probability of capture of a drop of water falling onto the surface which is also related to the concentration at the ultimate point (pumping well). For WHPA delineation, the 3D projection onto the ground surface as shown in Figure 4.2(a) (rather than the intersection with the

ground surface) is generally used. The plume of capture probability can also be converted into a conventional capture zone outline by using mass balance principles (see next section).

For the 3D particle tracking analysis, the particle tracking module WATRAC [Frind and Molson, 2004] is used, which is part of the 3D finite element model WATFLOW [Molson et al., 2002]. WATRAC is a finite element adaptation of the Pollock method [Pollock, 1994]. WATRAC uses a trilinear interpolation of the velocity field within each triangular prismatic element, and it allows particles to change direction at material interfaces, producing physically realistic particle tracks. WATRAC accepts the nodal heads from WATFLOW, and tracks particles in either the backward or forward mode for either a specified time period or until all particles reach the ground surface.

To delineate the capture zone, 108 particles are placed on a circle of 3 m radius around the well screen. The particles are tracked in the upgradient direction until they reach the ground surface or top of the model domain. The results are shown in Fig. 4.3. The maximum extent of the capture zone can be delineated by drawing an envelope curve around the respective particle tracks. Comparison of Figures 4.2 and 4.3 shows that the probability plume using advective-dispersive transport modelling is sightly larger than the envelope obtained by particle tracking.

4.6 Case Study: The Mannheim Well Field

We will select the Mannheim well field in the Regional Municipality of Waterloo as a demonstration case study and we will apply the two key methods, namely 3D backward particle tracking and 3D backward advective-dispersive transport modelling, to delineate the capture zones and TOT areas for this well field.

4.6.1 Flow Model

The hydrology of the Mannheim well field is described in Chapter 2. As mentioned in Chapter 2, the well field consists of two parts: Mannheim North, including wells K21, K25, K29, K91, K92, K93 and K94, and Mannheim South, including wells K22, K23, K24 and K26. The pumping rates for the individual wells (as of November, 1999) are listed in Table 4.1; the total for Mannheim South is 17,260

m^3/day and that for Mannheim North is 16,780 m^3/day, for an overall total of 34,040 m^3/day. All eleven wells are screened in Aquifer 1, known as the Mannheim aquifer, which is the shallowest aquifer in the system and whose extensive sand and gravel layers make it the main aquifer in the Waterloo Moraine. The most productive zones are the coarse gravels found at the base of the aquifer in some locations. The Mannheim site was chosen for study because the Mannheim wells have historically exhibited high nitrate (NO_3^-) concentrations as well as elevated chloride concentrations [CH2M-Hill, and Papadopulous and Associates Inc., 2003]. As such, WHPA work conducted in the Mannheim well field is an area of intense focus.

The horizontal hydraulic conductivity distribution in Aquifer 1 is calculated as the arithmetic mean values of the hydraulic conductivities of the individual layers within the aquifer weighted by the layer thickness. The hydraulic conductivity for the Mannheim area is shown in Chapter 2, and ranges from about 10^{-6} to 10^{-3} m/s.

Table 4.1: Mannheim well field: Summary of pumping rates (after Muhammad, 2000).

Well field	Wells	Pumping rate, m^3/day
M. South	K22, K23	7350
M. South	K24	2960
M. South	K26	6950
M. North	K93, K94	1870
M. North	K91, K92	1680
M. North	K21	3970
M. North	K25, K29	9260

The 3D steady-state flow system in the Waterloo Moraine was simulated by Martin and Frind (1998) using the Finite Element model WATFLOW [Molson et al., 2002]. For the flow simulation, the eight layers of the conceptual model were further subdivided into 29 element layers, and the distribution of hydraulic conductivity within each of these layers was obtained by 3D kriging using the lithologic data from hundreds of boreholes within the area. The recharge function was obtained by first applying a uniform recharge rate of 530 mm/yr over the entire ground surface and then redistributing this recharge according to local soil conditions by means of a thin (0.1 m) highly permeable Recharge Spreading Layer (RSL), which is part of

the model. The RSL redistributes the recharge away from areas of low hydraulic conductivity that might not be able to accept the given amount toward areas of higher conductivity which can accept it, and to streams.

Beckers (1998) calibrated the Waterloo Moraine model by subdividing the area and adjusting the net average recharge rates and hydraulic conductivities in each subarea until an acceptable match was found between the simulated and observed hydraulic heads. In the course of the calibration, it was found that the RSL diverts approximately 260 mm/yr of recharge out of the system via stream runoff, while the remainder was redistributed according to the hydrogeologic characteristics of the subsurface. The calibration procedure with respect to the Waterloo Moraine is described in a report by Waterloo Hydrogeologic (2000).

The resulting hydraulic head distribution in Aquifer 1 is shown in Fig. 4.4(a) for the Moraine as a whole, and in Fig. 4.4(b) for the Mannheim area. As can be seen, groundwater flow is generally from the northwest to southeast toward the major rivers which form the boundaries of the model. Figure 4.4(b) shows a drawdown cone of about 40 m in the northwest corner; this is due to pumping at the Erb St. well field which is not part of Mannheim. Corresponding head distributions in the other aquifers of the system are shown by Martin and Frind (1998). The 3D steady-state head distribution throughout the aquifer system is used as a starting point for the capture zone delineation.

4.6.2 WHPAs Delineation using 3D Backward Particle Tracking

For the 3D particle tracking analysis we will use the particle tracking module WATRAC [Frind and Molson, 2004]. WATRAC was used for the delineation of most of the WHPAs for the Region of Waterloo well fields; the procedure is described in a report by Waterloo Hydrogeologic (2000).

To initiate the tracking procedure, particles are uniformly placed at a 40 m radius around the well screen. With 11 wells, 5 layers over the screen lengths, and 32 particles per layer, this amounts to a total of $11 \times 5 \times 32 = 1760$ particles. The particles are tracked backward in time for specified time periods, or until most of the particles reached ground surface. The final configuration with most of the particles having arrived at ground surface is accepted as the maximum extent of

capture zone. The time periods selected were 2, 5, and 25 years, and the time to steady-state was found to be approximately 100 years. The corresponding results, as projections of the 3D particle tracks onto the ground surface, are shown in Figs. 4.5, 4.6, 4.7, and 4.8. The particle statistics provided with the plots show the percentage of particles reaching the specified time limit, those reaching the top without reaching the time limit, and those reaching a side boundary. It can be seen that the proportion of particles reaching the top increases from 6% at 2 years to 82% at 100 years, showing how the system approaches steady-state. The 18% of particles remaining in the system at 100 years are found to move rather slowly upward through low-permeability material, so their effect on the final capture zone will be minimal. Accordingly, 100 years was accepted as the steady-state travel time for this system under the given pumping regime.

It is also evident from the tracks that more particles reach the surface in a shorter time in the Mannheim South area than in the Mannheim North area. This is due to the higher vulnerability of the aquifer in the Mannheim South area (see Fig. 3.6). The irregular shape of the TOT zones is due to the heterogeneity of the system. Also noteworthy is that in Mannheim South, the particles tend to move to the surface rather quickly, while in Mannheim North, they tend to travel through the aquifer for some distance before emerging. This is mainly due to the lower hydraulic conductivity of the overlying aquitard in the Mannheim North area (see Fig. 3.2(b)). Accordingly, although the pumping rate for Mannheim South is slightly higher, the capture zone for Mannheim North is larger.

On the basis of the particle tracks, the individual TOT zones are obtained by manually drawing envelope curves around the tracks. Note that while the envelope curve is drawn on the plane of the ground surface, it will encompass all subsurface 3D tracks throughout the system. The resulting outline will be somewhat subjective, depending on how one decides to smooth out the irregularities of the 3D tracks. We will not use this manual approach here; instead we will outline an alternative approach in the next section.

4.6.3 WHPAs Delineation using 3D Backward-in-Time Transport Modelling

Application of the backward-in-time transport modelling approach is conceptually similar to standard advective-dispersive transport modelling except that the flow

field and boundary conditions are reversed and the results are given in terms of capture probability instead of concentration. Any standard advective-dispersive transport model can be used, and reversing the flow field and adapting the boundary conditions are a simple operation. The dispersion parameters are the same in the forward or backward mode. The backward transport modelling approach has been previously used in the delineation of the WHPA for the Greenbrook well field of the Region of Waterloo [Frind et al., 2002].

As in the particle tracking approach, we start again with the steady-state flow field obtained from the flow model WATFLOW. The backward transport simulation is done with the 3D Waterloo Transport Code (WTC) [Molson and Frind, 2004]. The transport parameters used in the simulations are $\alpha_L = 20$ m, $\alpha_{TH} = 5$ m, $\alpha_{TV} = 0.02$ m, and $D_m = 1{\times}10^{-10}$ m^2/s, where α_L, α_{TH}, α_{TV}, and D_m represent longitudinal dispersivity, transverse horizontal dispersivity, transverse vertical dispersivity and the molecular diffusion coefficient, respectively. These values are the same as those used in previous studies of this system, and are consistent with a spatial transport scale of about 10 to 15 km [Gelhar et al., 1992]. A continuous source of concentration ($C_0 = 1$) is applied at each well within the well field, and WTC is run in a backward mode using the negative velocity field. The simulation continues until the plume stabilizes, which in this case occurs after approximately 100 years of simulation time. The projection of the resulting probability plume onto ground surface is shown in Fig. 4.9. The individual contours represent the probability of a particle of water falling on a contour being captured by the well.

The capture probability by itself would be a rational basis for delineating a WHPA on a probabilistic basis, without the need for a sharp boundary where different rules apply inside and outside of the boundary. However, most regulatory systems today require a WHPA delineated by a line drawn on a map. This is done by means of a simple mass balance calculation, where the total pumping is balanced by the infiltration into the aquifer through a representative control surface over a given area. The infiltration is calculated by selecting a suitable element layer just above the water table, where flow will be essentially vertical, and element-wise summing the contributions (where infiltration = pore velocity $\times$ porosity $\times$ saturation $\times$ element area). The contour satisfying this mass balance is the required capture zone outline.

For the Mannheim well field, the area enclosed by the 0.1 contour of the probability plume is found to balance the pumping rate at the prevailing influx through

the ground surface. Having established this value, we can now also delineate any other TOT zone for the well field by selecting the corresponding probability plume and extracting the same contour. Figure 4.10 shows the resulting TOT zones for 2, 5, 25, and 100 years.

We can now superimpose the above TOT zone outlines obtained by transport modelling onto the particle tracks obtained earlier. The results are shown in Figures 4.11, 4.12, 4.13, and 4.14. In general we would expect that, due to dispersion, the TOT zones obtained by transport modelling should be somewhat larger than the area covered by the corresponding particle tracks. We note that this is generally the case for the Mannheim system, but that the spread occurs mostly in the up-gradient areas towards the west. This is due to macrodispersion having its largest value in the longitudinal direction. According to Gelher (1983) macrodispersion can be taken as representing the uncertainty in the hydrogeologic parameters, which is lacking in the particle tracking approach. Therefore, the TOT outlines can arguably be taken to be more realistic than envelope curves that might be drawn subjectively around the particle tracks. For example, the most westerly extent of the 100-yr TOT zone is about 1 km to the west of the most westerly particle tracks. As noted above, the capture zone for Mannheim South is smaller than that for Mannheim North, although the pumping rate is slightly larger. As already shown by the particle tracks, the disparity is due to the fact that the vulnerability is slightly higher in the southern area, because particles reach the surface faster, and because the water is drawn from a smaller area.

4.7 Conclusions

This chapter focuses on the delineation of wellhead protection areas (WHPAs). The purpose of WHPA delineation is to define the area within which a source of contamination could have an impact on the well. The actual impact on the well will depend not only on the source, but also on the characteristics of the groundwater system. The best way to assess the impact is by means of a source-pathway-receptor approach where all relevant processes acting on a migrating contaminant particle are analyzed. Important considerations include the dimensionality of the system, the uncertainty in the system characteristics, and the physical processes that could affect the impact. Since a WHPA delineation can rarely be independently validated, it is important that all relevant processes be included in the delineation.

The most commonly used approach to WHPA delineation is backward particle tracking on the basis of a 3D steady-state flow system simulation. This approach is simple, cost-effective, and straightforward and it generally leads to useful results. However, it neglects important process such as dispersion. The alternative approach, backward advective-dispersive transport modelling, does not have these limitations. The transport approach produces a capture zone in the form of a Probability-of-Capture plume (a contaminant plume in reverse), which can be easily converted into a standard WHPA outline. The dispersive component in the transport model represents uncertainty in the flow characteristics (i.e. hydraulic conductivity) in the form of macrodispersion.

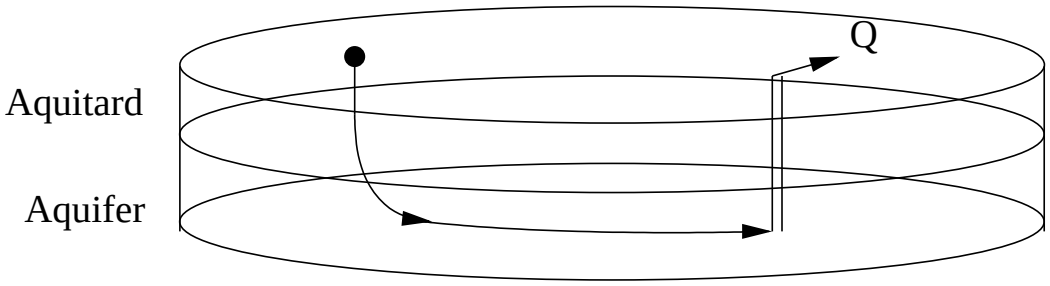

Figure 4.1: 3D travel path of a water particle within a aquifer system.

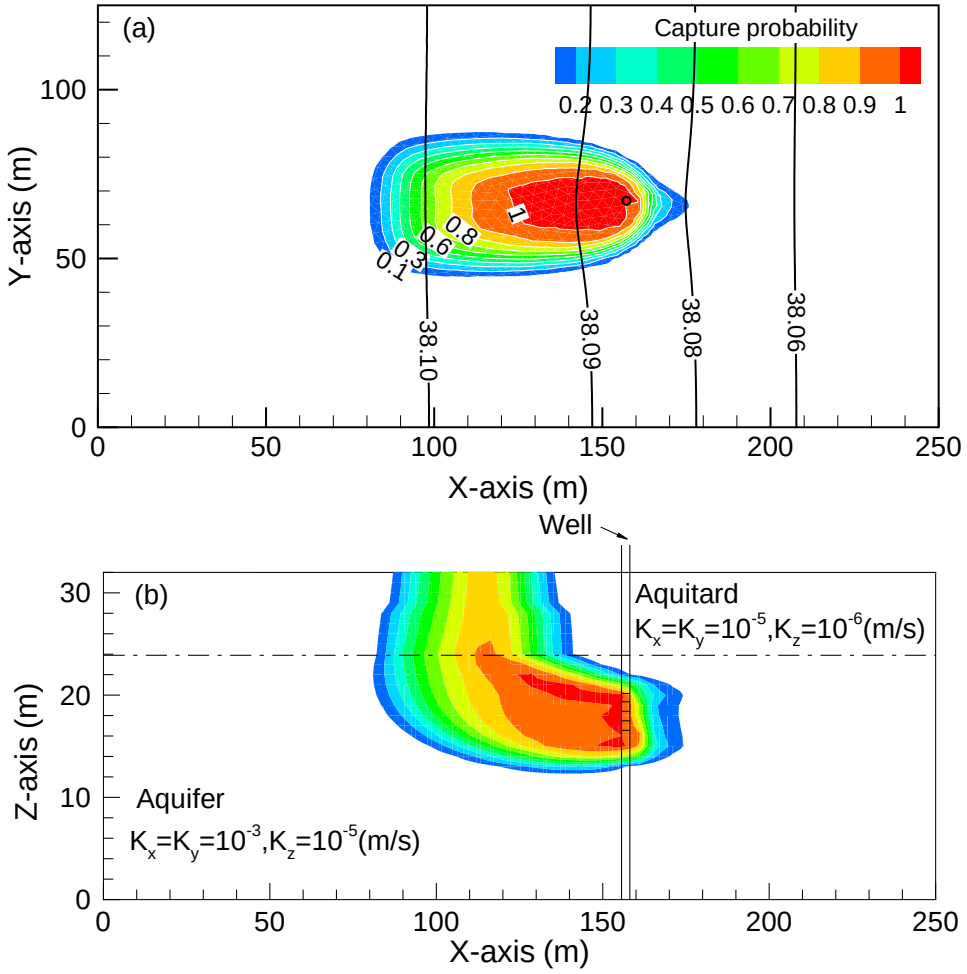

Figure 4.2: 3D advective dispersive maximum extent of capture zone (a) plan view, (b) cross-section (vertical exaggeration of 3.5).

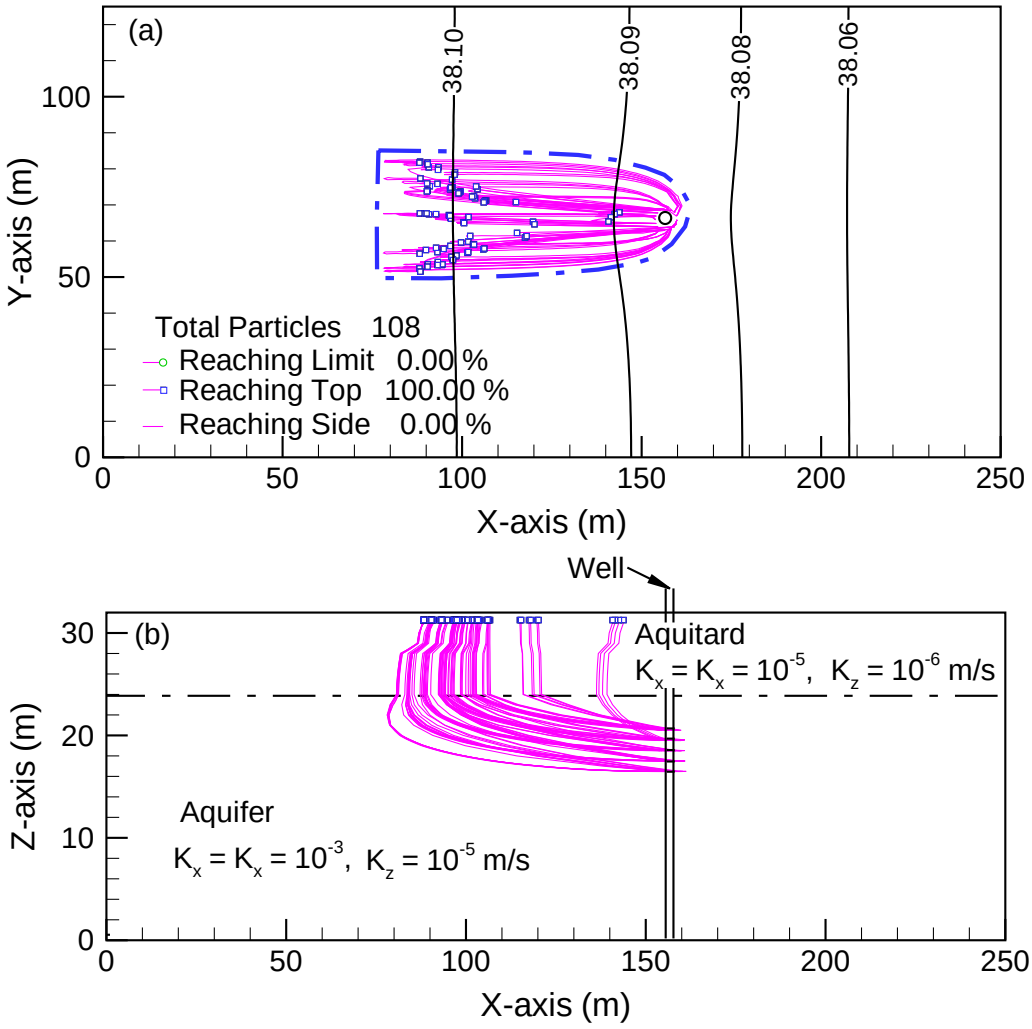

Figure 4.3: 3D advective maximum extent of capture zone (a) plan view (plume projected onto ground surface), (b) cross-section (vertical exaggeration of 3.5).

(a)

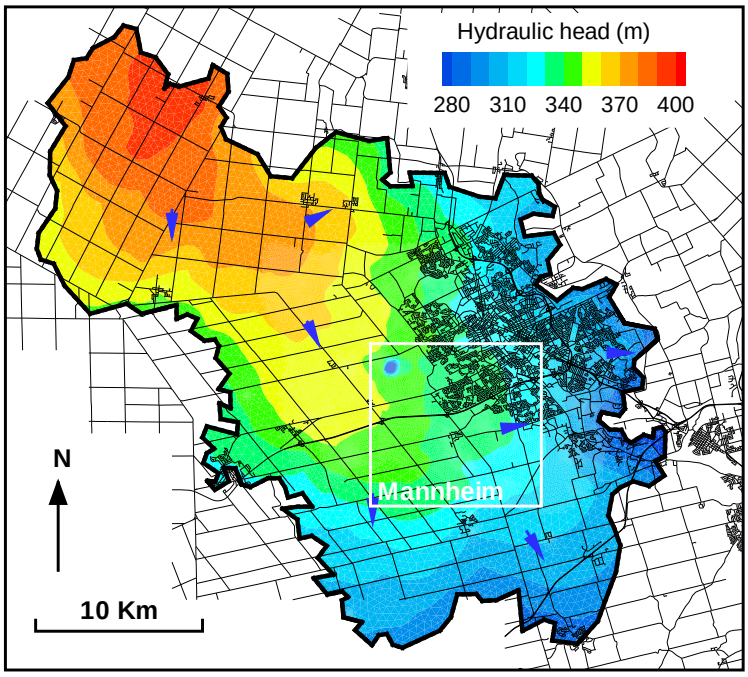

(b)

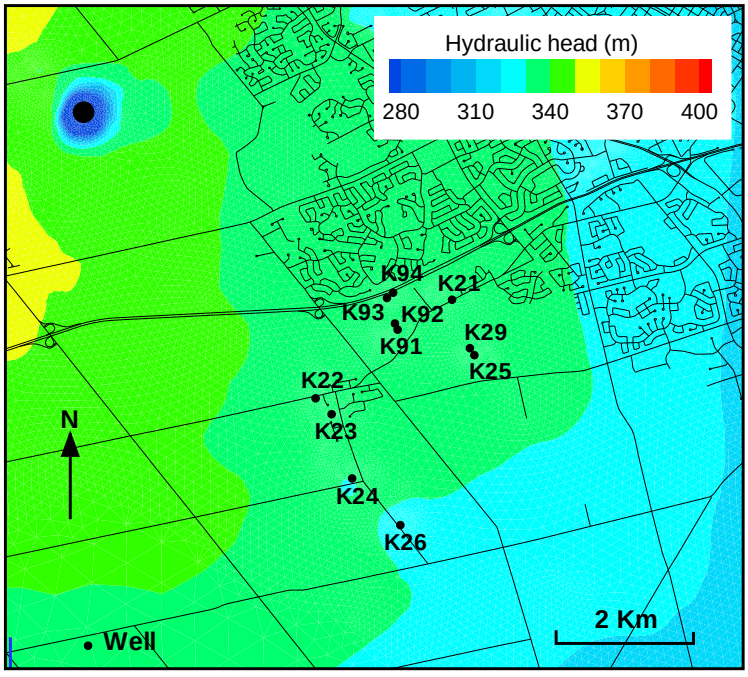

Figure 4.4: Hydraulic head distribution in Aquifer 1 (after Martin and Frind, 1998) (a) Waterloo Moraine, (b) Mannheim area.

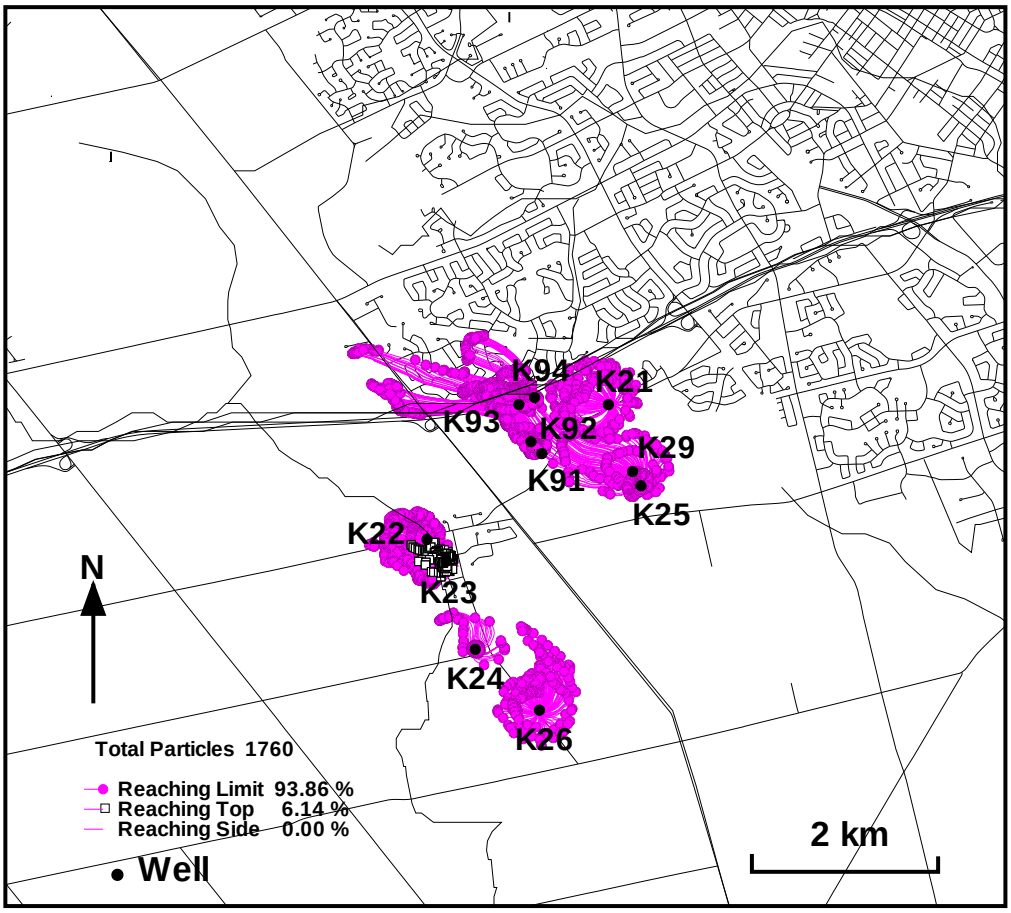

Figure 4.5: 2-year particle tracks, Mannheim well field.

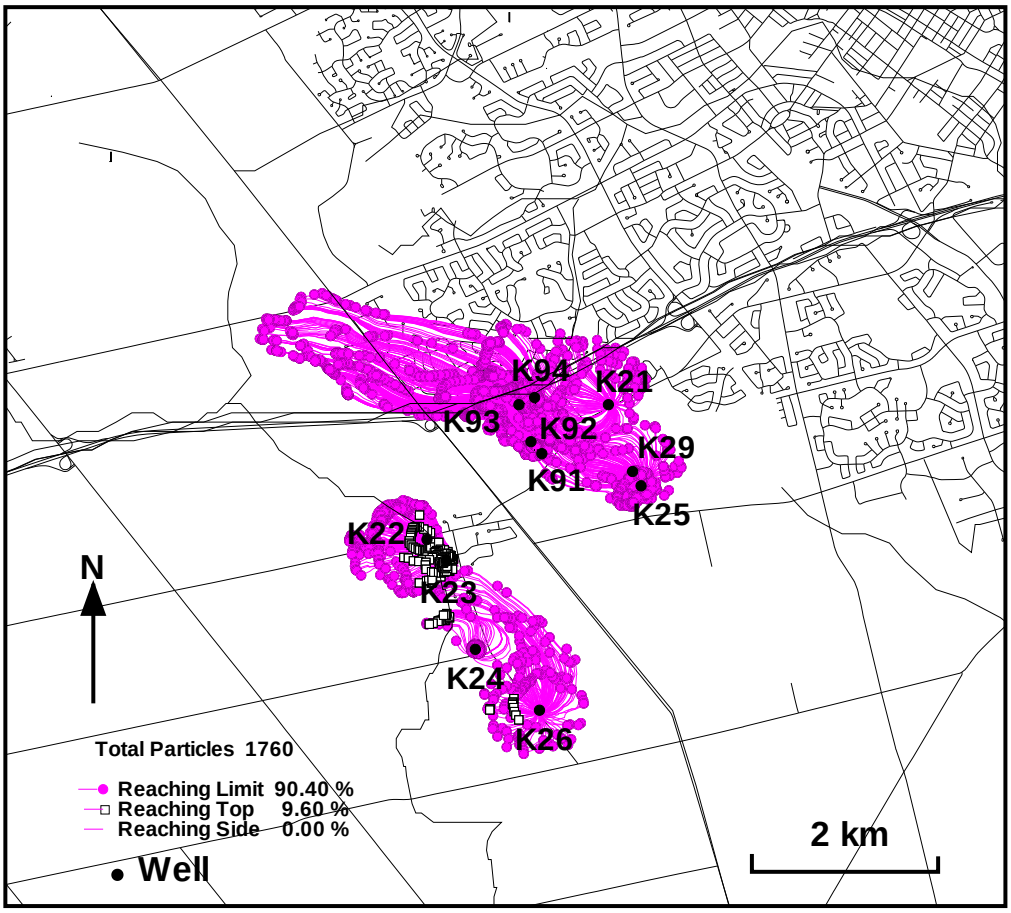

Figure 4.6: 5-year particle tracks, Mannheim well field.

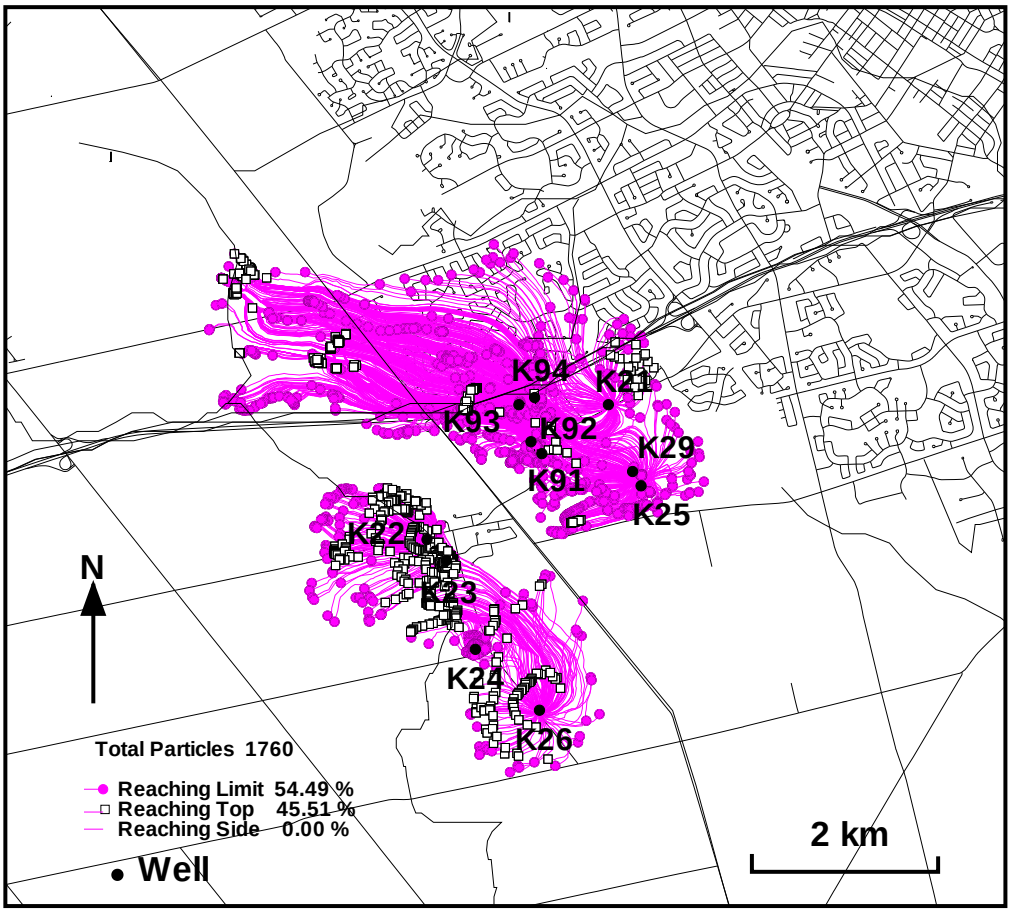

Figure 4.7: 25-year particle tracks, Mannheim well field.

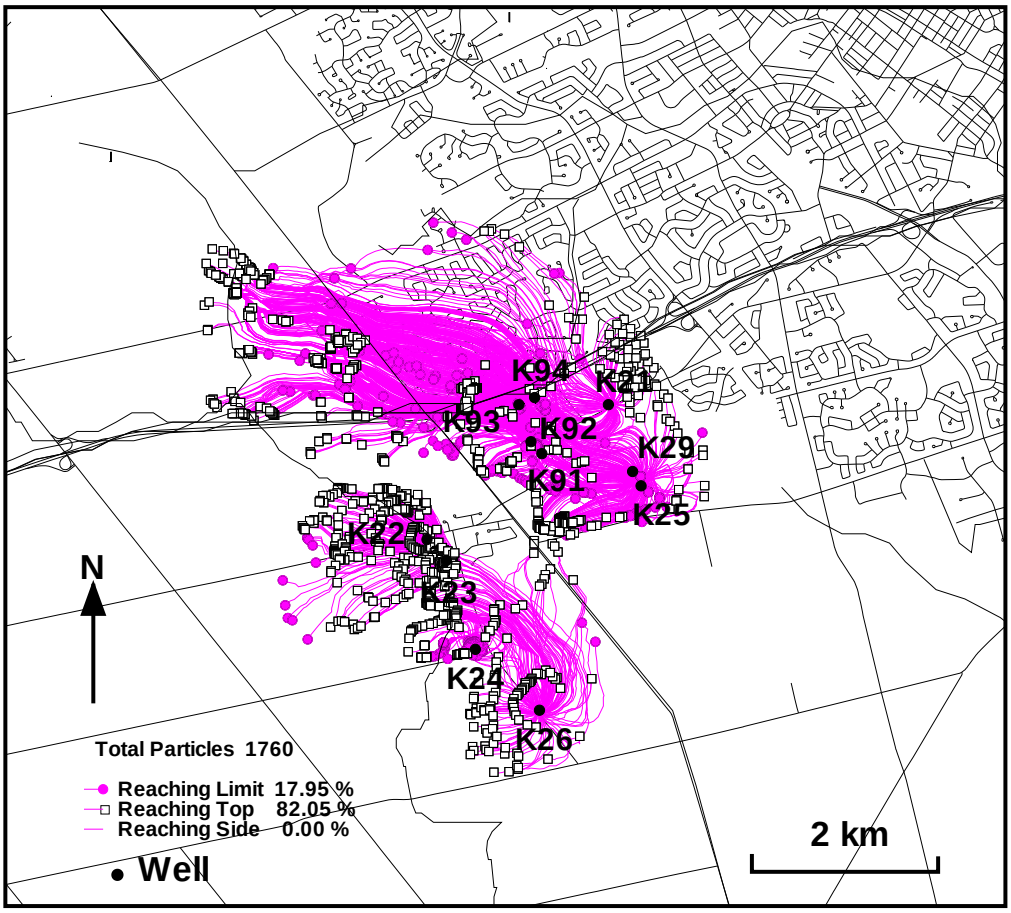

Figure 4.8: 100-year particle tracks for ultimate capture zone, Mannheim well field.

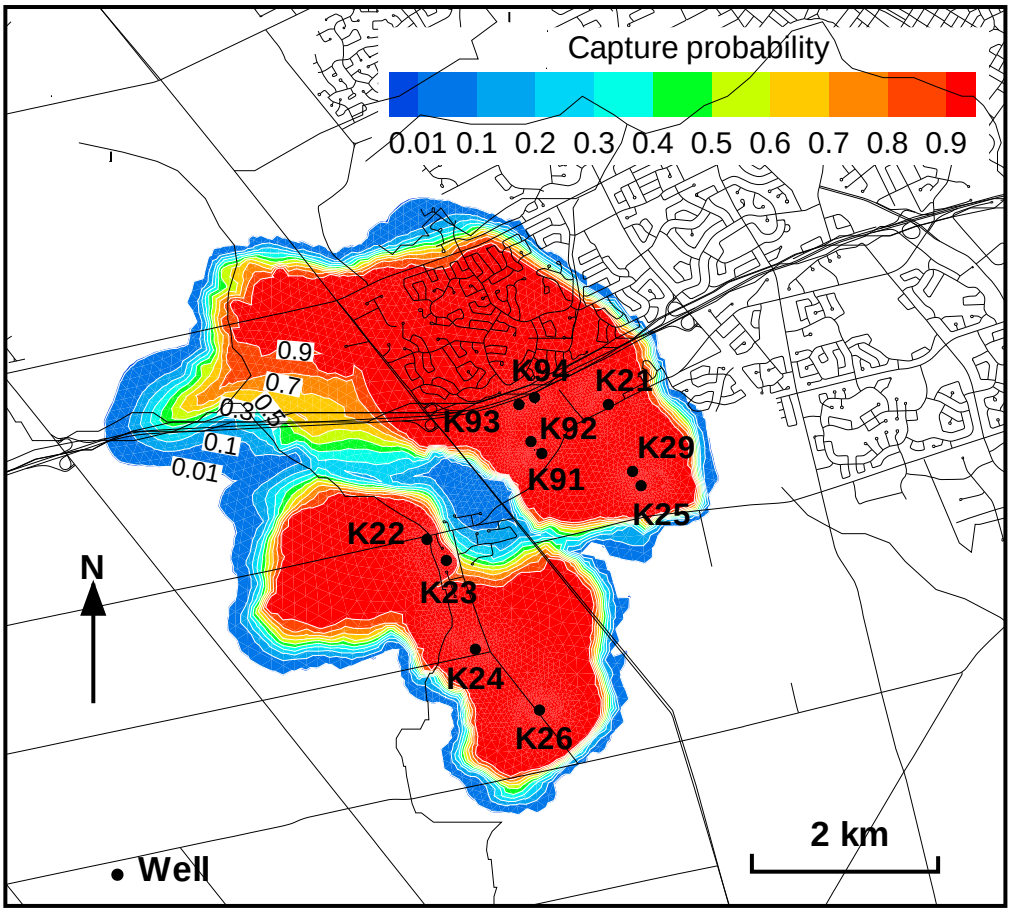

Figure 4.9: Probability-of-Capture plume, from projection of 3D plume onto ground surface, Mannheim well field.

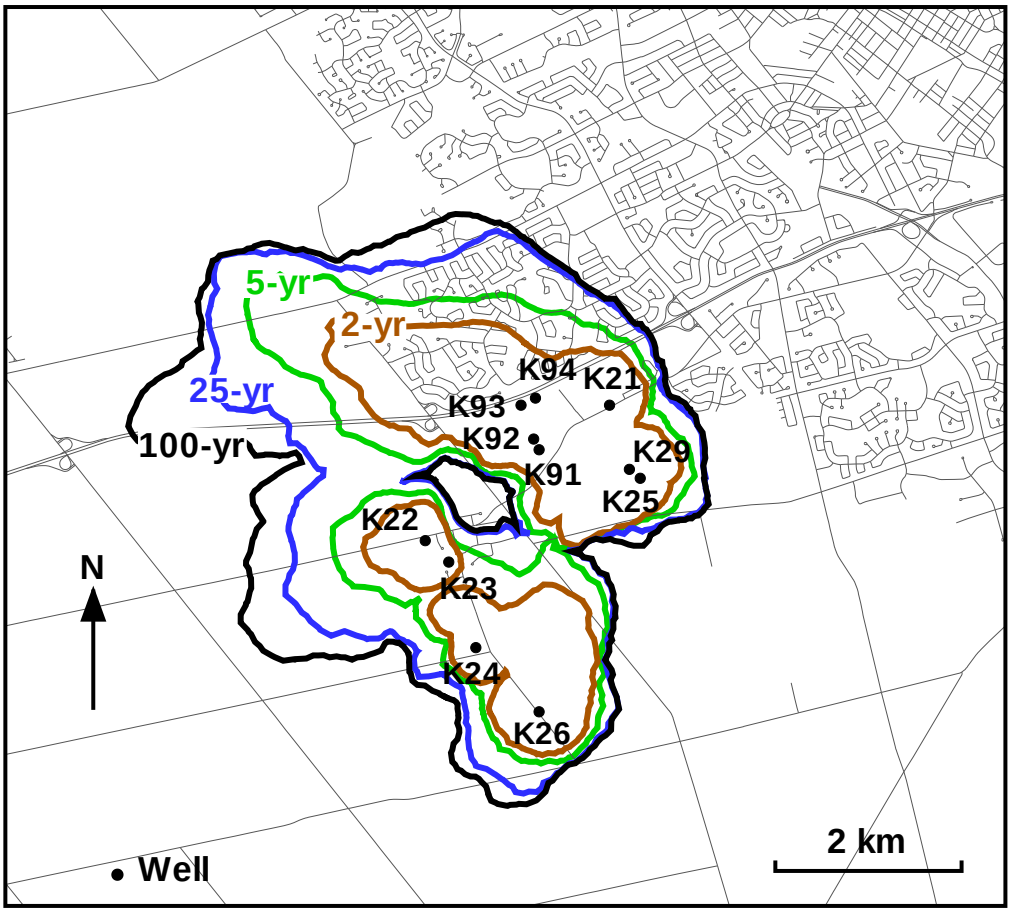

Figure 4.10: TOT zone outlines for 2, 5, 25, and 100 years, extracted from Probability-of-Capture plume, Mannheim well field.

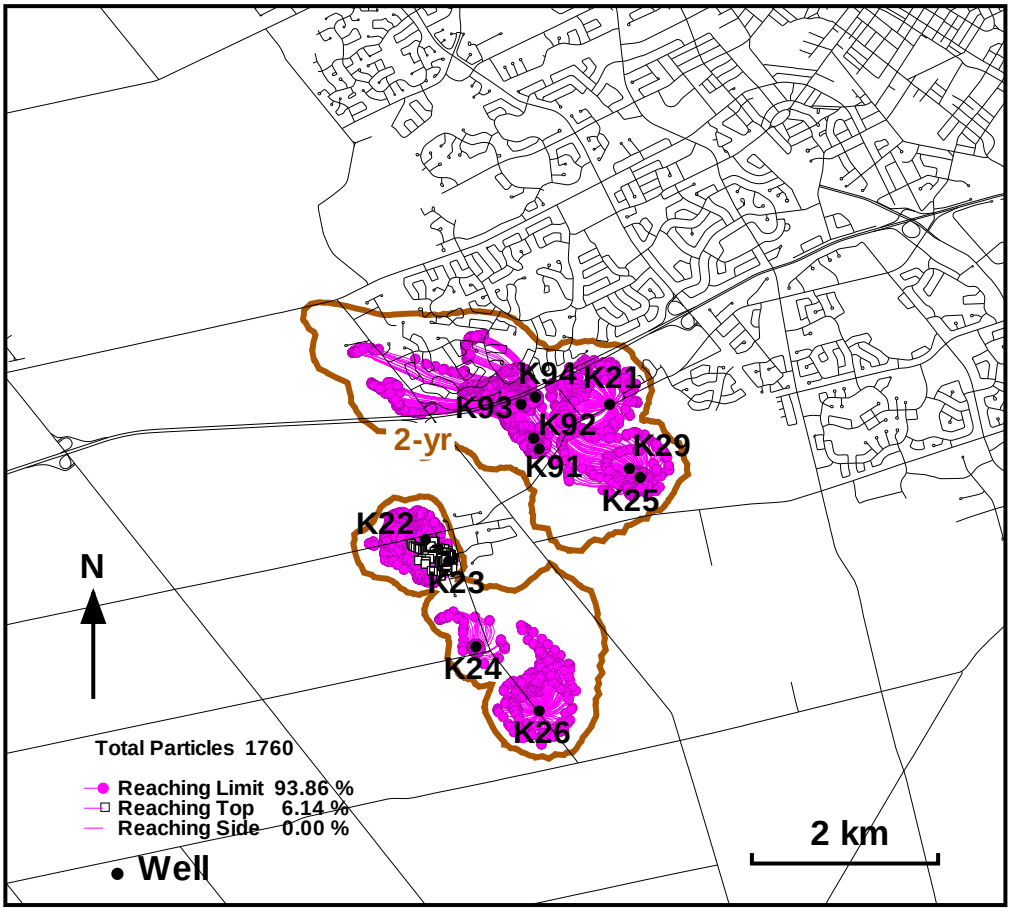

Figure 4.11: 2-year TOT zone outlines with corresponding particle tracks, Mannheim well field.

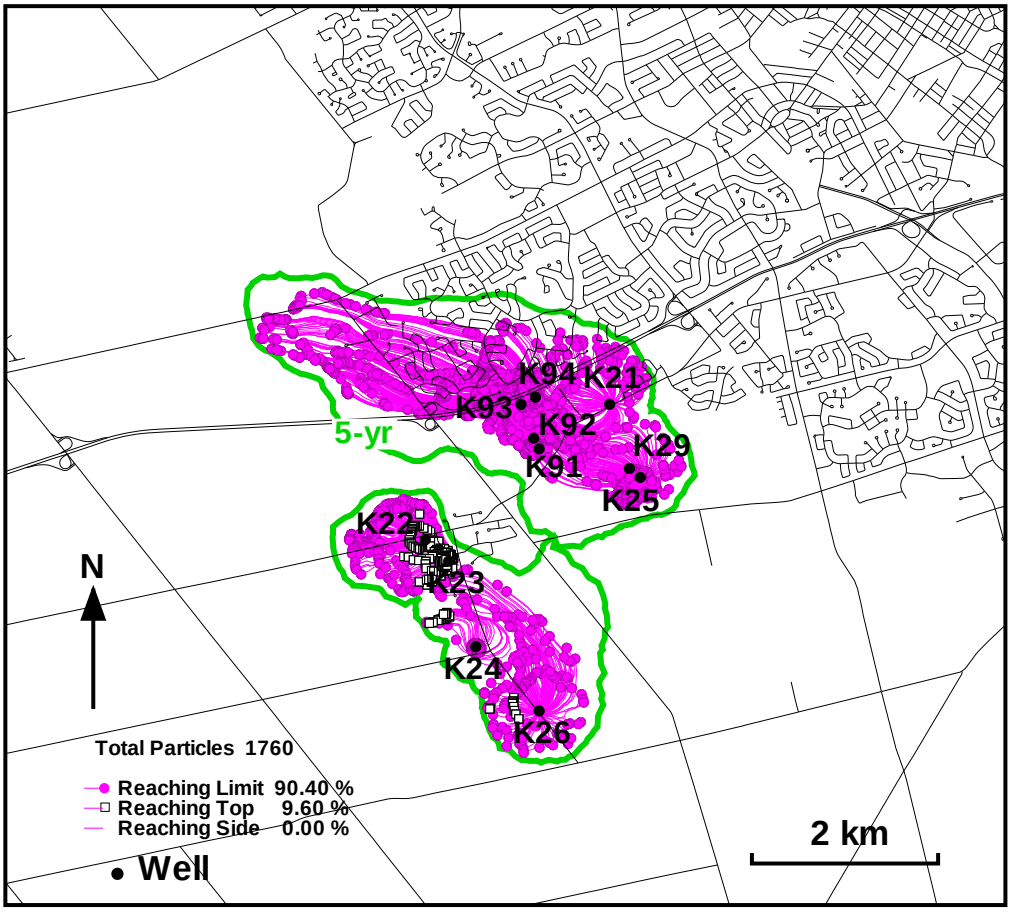

Figure 4.12: 5-year TOT zone outlines with corresponding particle tracks, Mannheim well field.

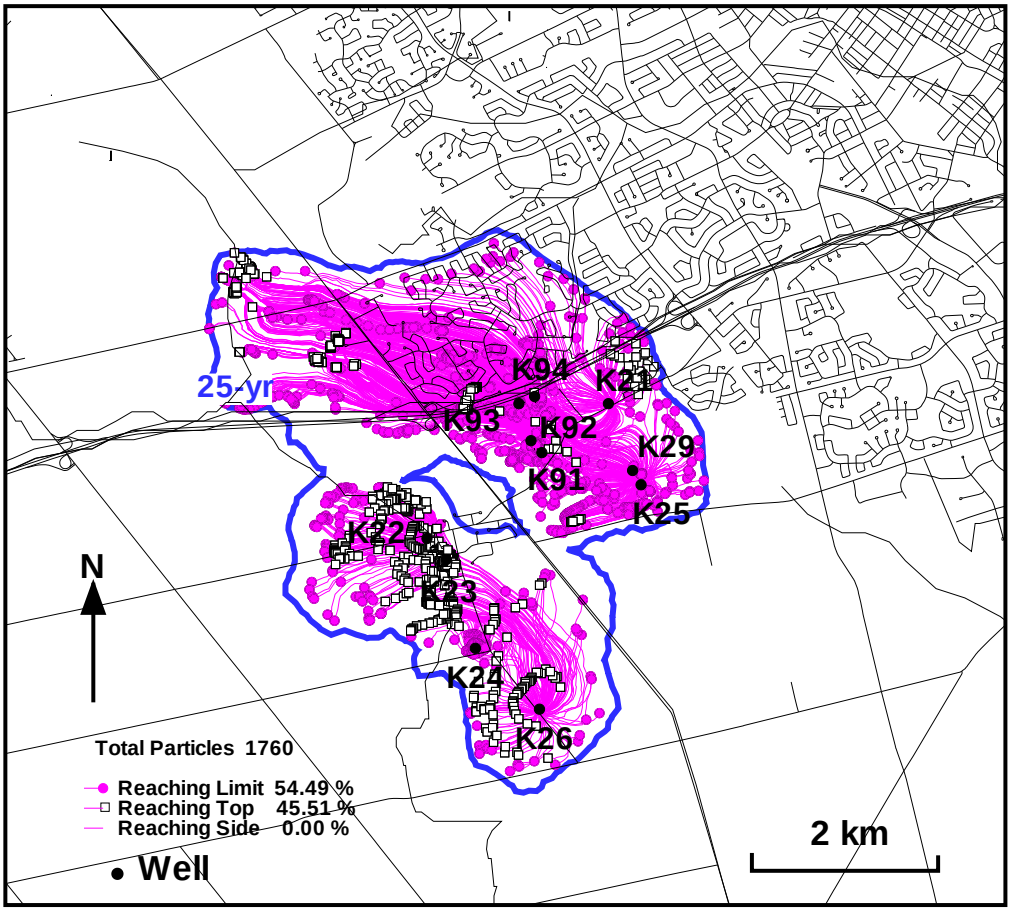

Figure 4.13: 25-year TOT zone outlines with corresponding particle tracks, Mannheim well field.

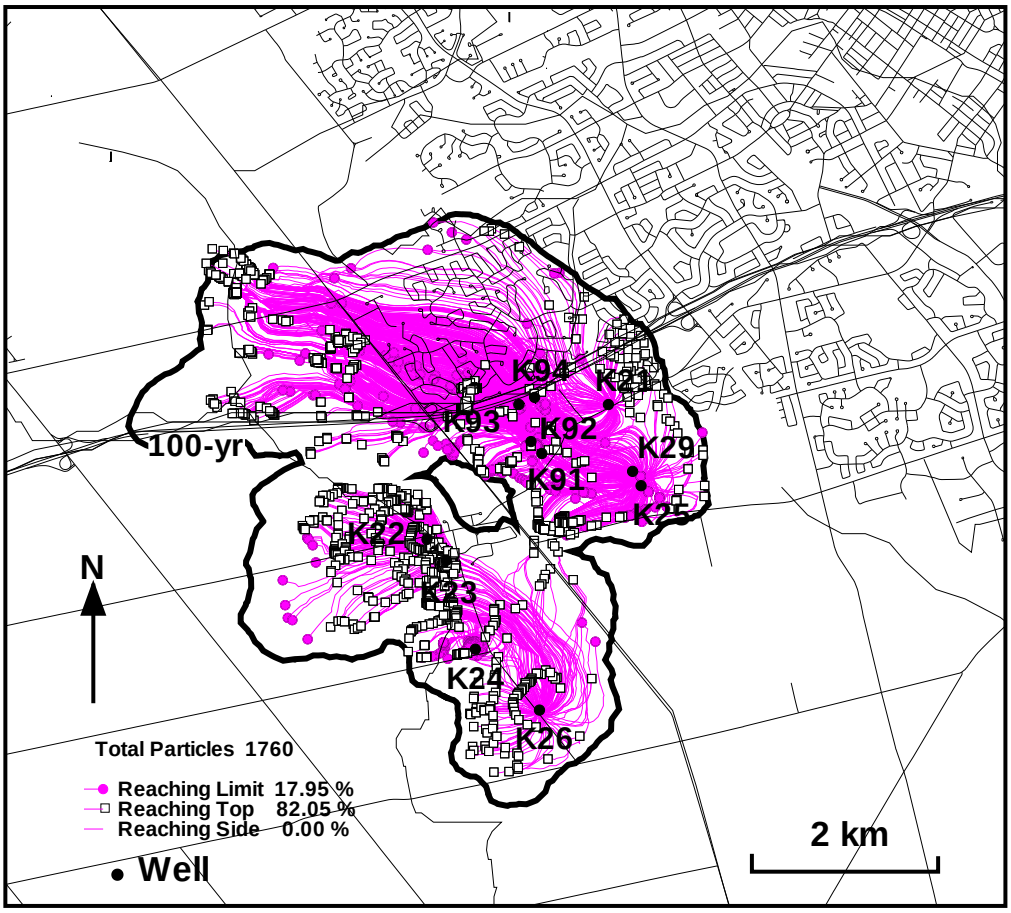

Figure 4.14: 100-year TOT zone for maximum extent of capture zone, with corresponding particle tracks, Mannheim well field.

Chapter 5

Well Vulnerability

In this chapter, we will focus on the vulnerability of the well itself. Well vulnerability modelling is a fully quantitative approach based on the source-pathway-receptor principle that combines the advantages of quantitative aquifer vulnerability with those of quantitative capture zone delineation.

5.1 The Concept of Well Vulnerability

Existing approaches to groundwater protection are generally based on the conventional concept of a WHPA, delineated on the basis of the average time a contaminant will take to reach the well. Different TOTs are specified for the exclusion or containment of a given contaminant species.

The TOT concept is based solely on advective transport and thus neglects a number of processes that tend to affect the actual impact of contamination on a well. These processes include dispersion, chemical reactions, and dilution at the well by mixing of contaminated water with clean water. Thus it tends to fall short of providing a rational and credible assessment of the actual impact on a water supply well. The actual impact and the ensuing risk depends not only on the advective travel time, but also on the nature of the source, the transport and fate of the contaminant along its path from the source to the receptor (i.e. a well), and the interaction of the well itself with the flow system.

The issue of dilution at the well is particularly important. For example, researchers Einarson and Mackay (2001) have found that high concentrations measured in mon-

itoring wells near a production well may, due to dilution, result in a low mass flux into the well, and actual concentrations in the well water may be below detection. The issue of dispersion is also important, as it can result in lower concentrations at the well, but also in earlier arrival times of critical concentrations relative to the advective TOT.

The concept of well vulnerability provides a means to take into account this additional information. Well vulnerability is based on the analysis of the pathway a contaminant travels in a multiple barrier system from a contaminant source to a receptor while being influenced by various processes along the way, and it quantitatively describes the expected impact of a contamination event on a well by means of certain measures. Well vulnerability differs from the conventional concept of aquifer vulnerability in that the target is the well (rather than the drinking water aquifer), and the pathway is the complete pathway from the contamination source to the well (rather than just the layers overlying the drinking water aquifer). They can be defined in terms of concentration at the well or mass flux reaching the well with dilution experienced by the contaminant. The measures include the maximum expected value, time to reach the maximum value, the time for drinking water standards at the well to be breached, and the exposure time of the well to the contamination. The impact on a well can be assessed on the basis of this method by applying a standard advective-dispersive transport model including all relevant physical and chemical processes, and determining the corresponding contaminant concentration breakthrough at the well.

A more detailed discussion of the Well Vulnerability concept is given by Frind et al. (2006). That study distinguishes between the forward approach, which is used to assess the impact of a source at a known location on a well, and a backward approach, which applies to potential sources at unknown locations within the WHPA. The backward approach is based on the adjoint principle, which is explained in detail in Chapter 6. Either way, the impact assessment is done on the basis of the breakthrough curve at the well. We will here focus on the forward approach with a known source.

To demonstrate the qualitative assessment of well vulnerability, we assume a pulse source of specified strength C_{source} applied at some specified point within the capture zone for one unit of time, and observe the corresponding breakthrough curve at the well. Since we assume a linear process, the breakthrough curve is scalable

according to the source strength. From the analysis of the breakthrough curve, the four measures of well vulnerability are defined as (see Figure 5.2):

- Peak concentration (C_{peak}): This value represents the maximum concentration value measured in the well. Generally, C_{peak} will be lower than C_{source} on account of dispersion, degradation, and dilution due to mixing with clean water.
- Time to peak concentration (T_{peak}): This is the time taken to reach the maximum concentration C_{peak}. For a pulse source, T_{peak} should be similar to the arrival time of most particles in a standard advective particle tracking model.
- Time to exceed a defined concentration value (T_{exceed}): This is the time taken to exceed a certain predefined concentration level C_{DWS}, which could be the drinking water standard for a certain contaminant.
- Exposure time to above-threshold concentrations (T_{expo}): The exposure time is the difference between the time to breach a specified threshold concentration in the well water and the time at which the concentration drops back below the threshold concentration.

5.2 Forward Approach

A basic approach to simulate well vulnerability is to apply a pulse source at some point within the WHPA and run a forward simulation to assess the impact of the source in the well. This will yield a breakthrough curve at the well, for which the above-defined key parameters expressing vulnerability can be described. The forward model is based on the standard advective-dispersive equation and can be written as:

$$\frac{\partial(RC)}{\partial t} = \frac{\partial}{\partial x_i}\left(D_{ij}\frac{\partial C}{\partial x_j} - v_i C\right) - \frac{q_0}{\theta}C + \frac{q_I}{\theta}C_I - R\lambda C \tag{5.1}$$

where $C(x,t)$ is the resident concentration (ML^{-3}), t is the time (T), x_i denotes the spatial dimensions (i =1,2,3) (L), D_{ij} is the $(i,j)^{th}$ entry of the dispersion tensor (LT^{-2}) expressed in terms of longitudinal dispersivity α_L (L), transverse horizontal dispersivity α_{TH} (L), transverse vertical dispersivity α_{TV} (L), the molecular diffusion coefficient D_m (LT^{-2}) [Burnett and Frind, 2002], and v_i is the groundwater

velocity (LT^{-1}) in the direction of x_i. In equation (5.1) q_0 is the outflow or sink rate per unit of volume, q_I is the inflow or source rate per unit volume, C_I is the source strength, θ is the volumetric moisture content, and R is the retardation factor. The retardation factor can be defined as

$$R = 1 + \frac{\rho_b K_d}{\theta} \tag{5.2}$$

where ρ_b is the bulk density of the porous medium, and K_d is the distribution coefficient that governs the partitioning of the solute into dissolved and sorbed phases. To represent radioactive or biological decay, we assume a first-order reaction of the following form:

$$\frac{dC}{dt} = \lambda C \tag{5.3}$$

where λ is the decay constant.

The boundary conditions are:

$$C(x,0) = C_0(x) \qquad \text{in } \Omega$$

$$C(x,t) = g(t) \qquad \text{on } \Gamma_1$$

$$(v_i C - D_{ij}\frac{\partial C}{\partial x_j})n_i = q.n.g(t) \qquad \text{on } \Gamma_1$$

$$(v_i C - D_{ij}\frac{\partial C}{\partial x_j})n_i = 0 \qquad \text{on } \Gamma_0$$

$$\text{Free exit boundary condition} \qquad \text{on } \Gamma_2$$

In the above, Γ_1 is the inflow boundary, Γ_2 is the outflow boundary, Γ_0 is the no-flow boundary, and $g(t)$ is a known source function. At the outlet boundary, the free exit boundary condition will occur where neither the concentration nor the mass flux is known [Frind, 1988]. At the free exit boundary, the boundary term is built into the solution with all quantities treated as unknowns.

5.3 Demonstration of Well Vulnerability Concept

The concept is demonstrated by means of a hypothetical example (Figure 5.1). The conceptual domain is 600 m × 350 m × 5 m in the x, y, and z directions, respectively. The system has one aquifer of 4 m thickness and one aquitard of 2 m thickness. It has a constant-head boundary of 20 m on its right side (x = 600 m). The base of the domain is impermeable. The pumping well located at (x, y) = (428 m, 174

m) is pumped at the rate of 51.84 m^3/day from the middle of the aquifer. The length of the well screen is 1 m. The hydraulic conductivity, K, of the aquifer and aquitard is 10^{-3} and 10^{-4} m/s respectively. A uniform recharge flux of 20 cm/yr is applied over the top of the model. In the transport model, the numerical values of the chosen dispersivities are those that would normally be used for a system of the given scale. The values are $\alpha_L = 10$ m, $\alpha_{th} = 1$ m, $\alpha_{tv} = 0.01$ m, respectively.

The 3D finite element model WATFLOW [Molson et al., 2002] is first used to obtain the nodal steady-state head distribution and elemental velocities. A unit pulse source is applied for 1 day at the source location upstream of the well at (x, y) = (223 m, 174 m) and the transport model WTC [Molson and Frind, 2004] is applied to solve for the concentration distribution. The resulting breakthrough curve is shown in Figure 5.2. Figure 5.2 shows the maximum expected concentration (C_{peak}) at the well, the time taken to reach maximum (T_{peak}), the time taken to reach a drinking water standard (DWS) of 10^{-4} relative to the source concentration (T_{exceed}), and the time taken for the concentration in the well to remain above the DWS (T_{expo}).

Similar measures can be obtained from the breakthrough curve corresponding to a non-pulse source. Promising results from the application of the forward well vulnerability approach to a municipal well field setting have been obtained by Piersol (2005).

5.4 Application to the Mannheim Well Field

The same procedure can be applied to the Mannheim well field. A hypothetical source is placed over an area of 0.06 km^2 within the Mannheim South well field upgradient from the wells K22 and K23, as shown in Figure 5.3. The source concentration ($C_0 = 1$) is applied for one day as a type 3 (specific flux) boundary condition and the propagation of the plume from the source to the well is simulated.

Figure 5.4 shows the plume along the vertical cross-section A-A′ after 10 days, 2 years, and 10 years. After penetrating the thin aquitard in the source area, the one-day pulse moves along Aquifer 1 to reach the wells in about 10 years. The resulting breakthrough curves, shown in Fig. 5.5, represent the expected concentration in the well water. Figure 5.5 shows that the maximum concentration about 6×10^{-6} g/m^3 will show up at well K22 in 5 years and the concentration of 7.2×10^{-6}

g/m^3 will show up at well K23 in 7 years. Using the resulting breakthrough curve, one can also determine the time taken to exceed a certain DWS and the time the concentration of the well water will remain above the DWS.

The four key well vulnerability characteristics apply to a contaminant source placed as shown in Fig. 5.3. By placing similar sources elsewhere within the capture zone, the vulnerability characteristics can be mapped over the WHPA. This approach would require a large number of forward transport model runs. A more efficient approach is discussed in the next section.

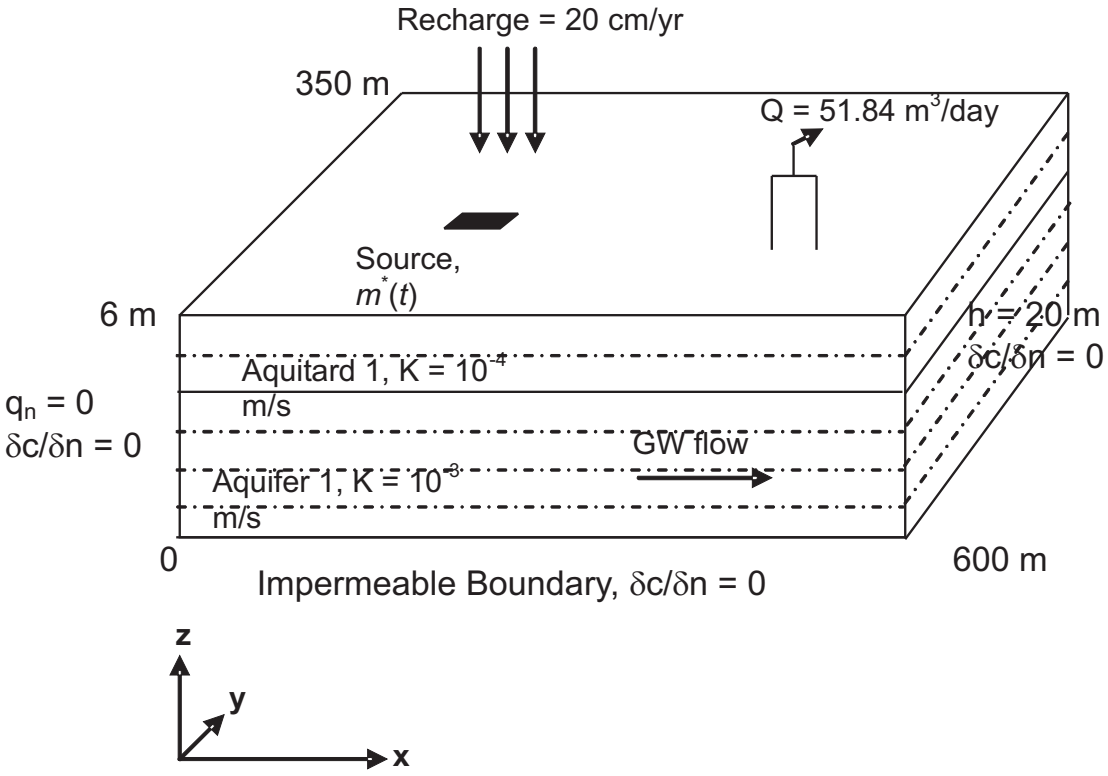

Figure 5.1: 3D conceptual domain of a layered system with single well.

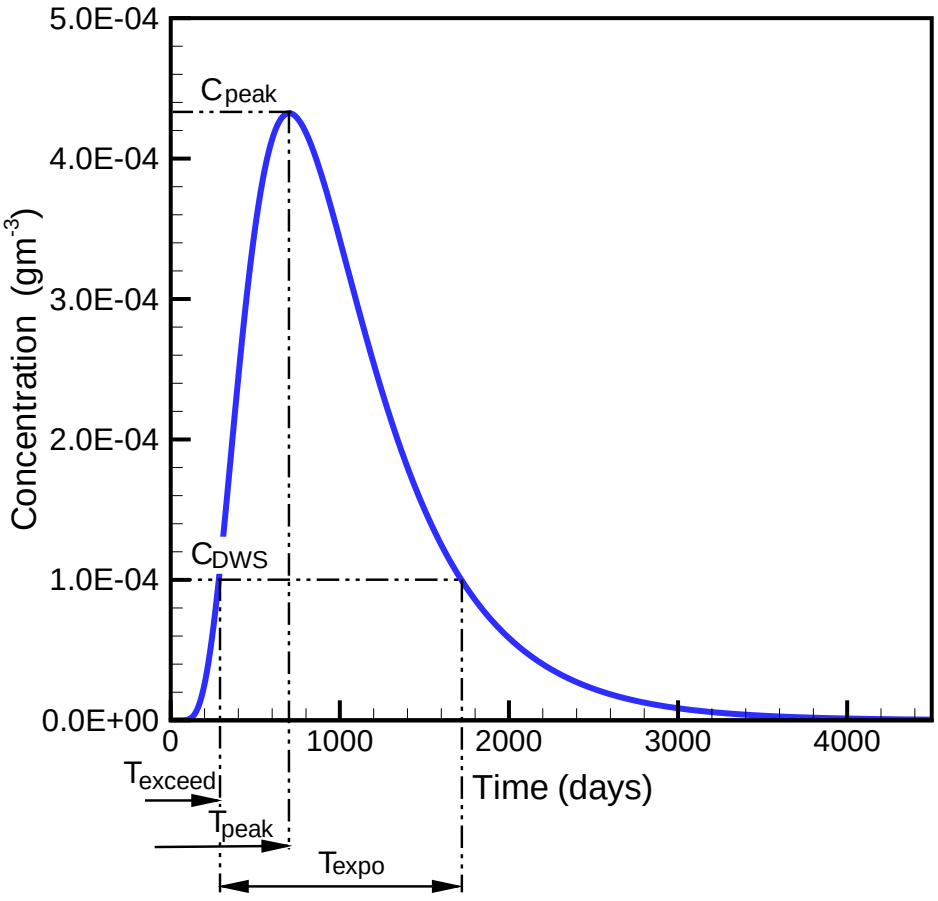

Figure 5.2: Breakthrough curve at well and well vulnerability measures for a pulse source.

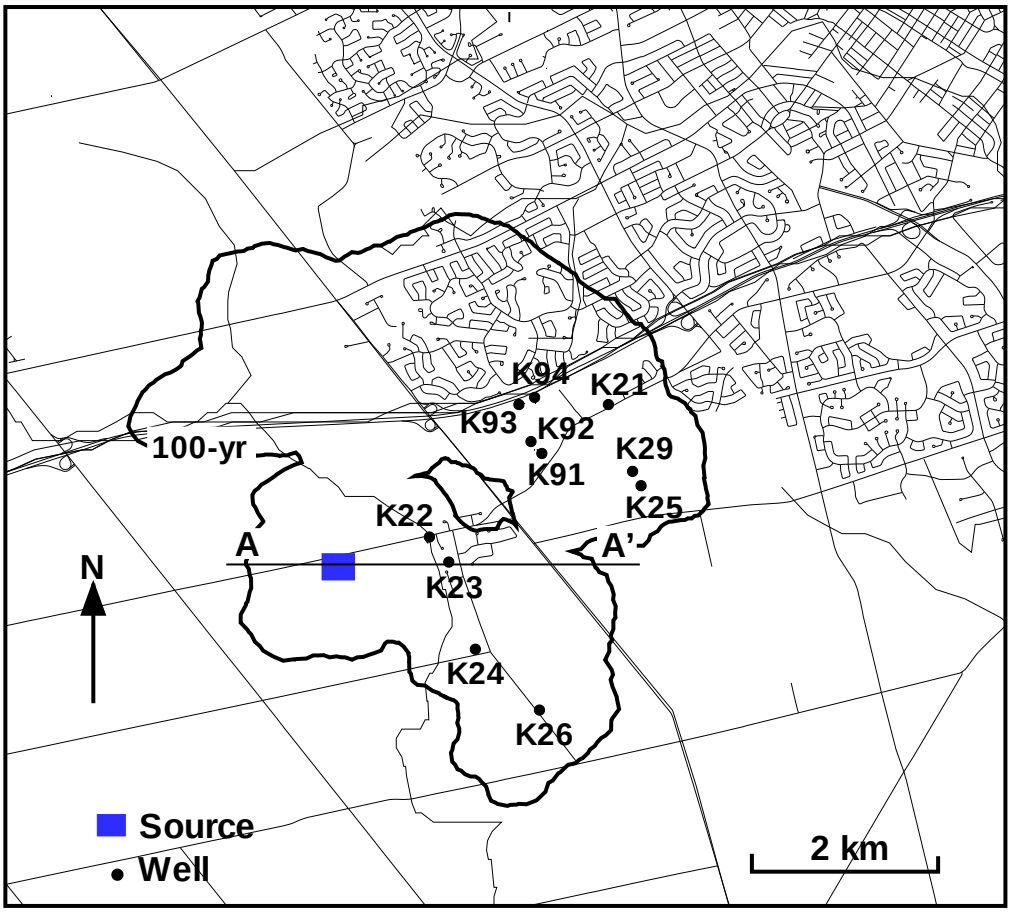

Figure 5.3: Location of the unit pulse sources within Mannheim well field to demonstrate the concept of well vulnerability.

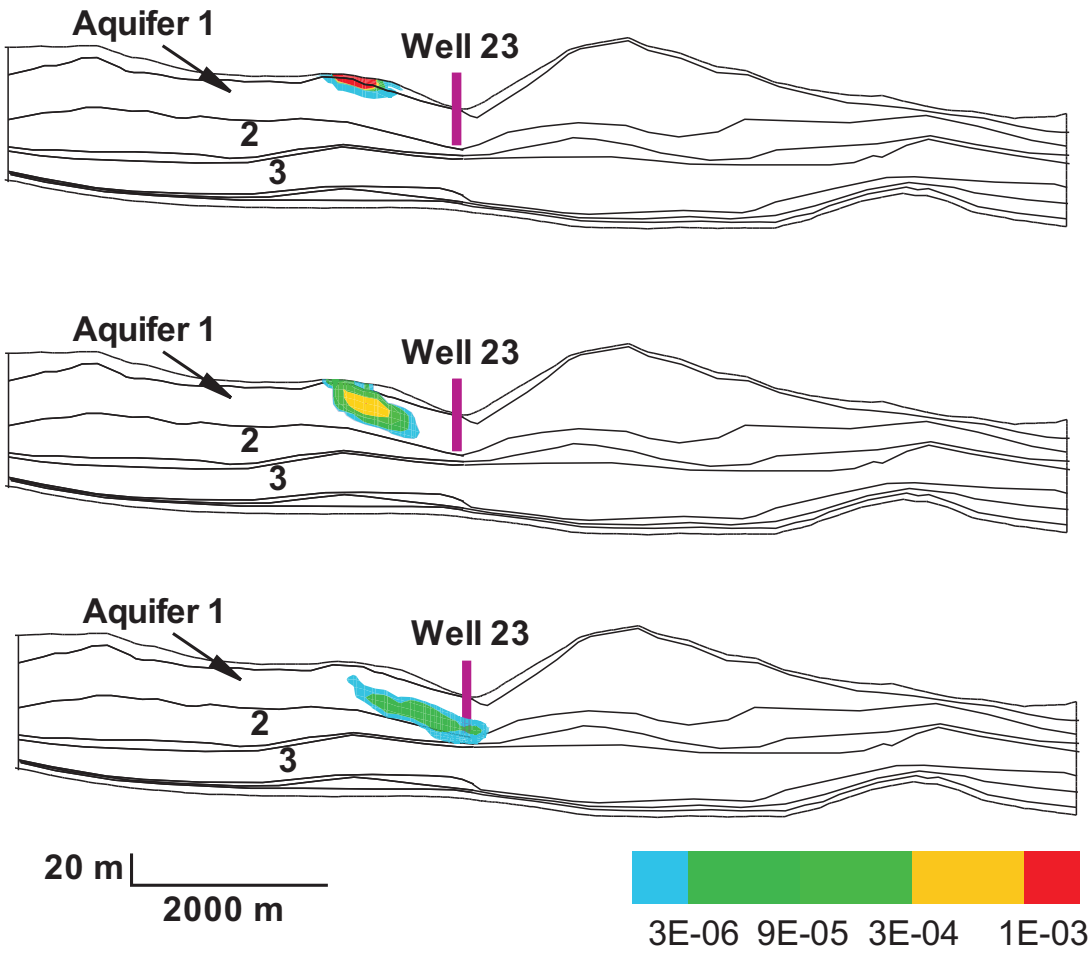

Figure 5.4: Contaminant plume at 10 days, 2 years, and 10 years, along the section A-A′ (see Fig. 5.3).

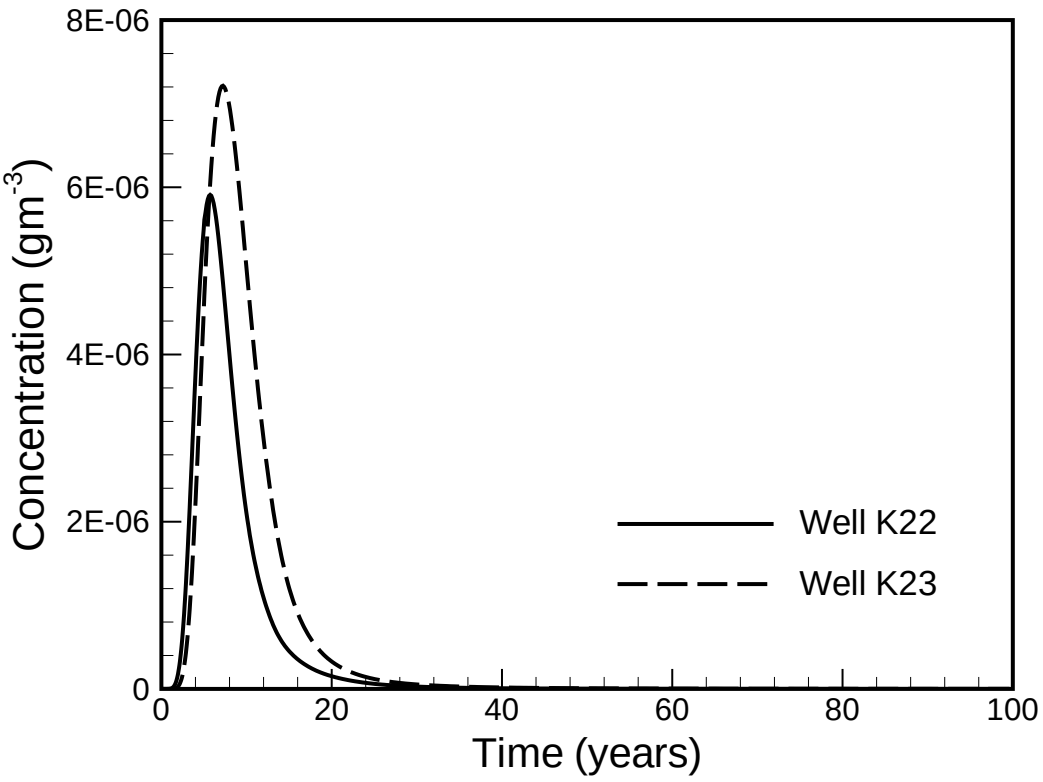

Figure 5.5: Expected concentration distribution at well K22 and well K23 due the unit pulse sources within Mannheim well field.

Chapter 6

Well Vulnerability for Unknown Sources: Backward-in-Time Transport Modelling

Well vulnerability maps for unknown sources can be developed using a backward-in-time transport model. While the forward model is solved for concentration, the backward equation is solved for the travel time probability density function (pdf) of a particle in backward time. The information provided by the well vulnerability maps is useful in the protection and management of groundwater sources and hence a high reliability of the expected concentration values is essential. A sensitivity analysis of the maximum expected concentration at the well water is carried out in this chapter. Part of this work has appeared in the proceedings of the IAH Groundwater Specialty Conference [Rahman et al., 2006].

6.1 Background

The backward-in-time transport modelling for unknown sources is similar to that used for the backward approach for capture zone delineation (see Chapter 4). The theory is based on the work by Uffink (1989); Wilson and Liu (1995); Kunstmann and Kinzelbach (2000); Neupauer and Wilson (2001); and Cornaton (2003). The governing equation for the backward model is similar to that for the forward model for contaminant transport with some modifications to account for the upgradient movement of probability. The forward modelling approach requires large number of model runs for each source within the capture zone of the well, whereas the

backward model requires only one simulation for each observation to obtain probabilities for all possible sources.

Cornaton (2003) has shown that the travel distance pdf at the well, which is obtained using the forward model, is equivalent to the flow-rate-scaled life-expectancy-to-well pdf at the contaminant injection point acquired using the backward model. The travel distance pdf is the resident concentration breakthrough at the well, which is normalized by the injected mass at the source location. The life-expectancy-to-well pdf is defined as the time required for the water particles to travel from the source location to the well. These definitions are based on the assumption of a steady-state flow field. Cornaton has developed vulnerability maps of the groundwater resource using the life-expectancy-to-well pdf scaled by the pumping rate for a hypothetical system of a single well.

The scaled backward travel time pdf has been used by Frind et al. to develop vulnerability maps for the Greenbrook well field [Frind et al., 2006]. In their approach, the problem of multiple wells within a well field was solved by placing a fence line a short distance upgradient of the well field and defining well vulnerability in terms of concentrations in the aquifer at the fence line. A single forward concentration breakthrough curve was first obtained by injecting a mass pulse at an arbitrary contaminant source within the capture zone and recording the breakthrough curve at the well fence. Multiple backward breakthrough curves were then generated by injecting another pulse at the wells and recording the corresponding breakthrough curves at all points of interest within the capture zone. The backward breakthrough curves were scaled by matching their magnitude to the normalized forward breakthrough curve, utilizing the principle of equivalence between the forward and backward curves [Neupauer and Wilson, 2001]; [Cornaton, 2003].

In this chapter we advance the concept proposed by Frind et al. (2006) by defining well vulnerability for multiple wells within a well field in terms of concentrations in the extracted well water, including dilution with clean water [Einarson and Mackay, 2001]. The approach avoids the need for a fence in the case of well fields with multiple wells. The information of contaminant concentration in the extracted well water is very useful in assessing potential impacts and determining the risks posed by contaminant plumes drawn into the water supply wells. A 3D conceptual aquifer system is used to demonstrate the methodology. To demonstrate practical usefulness, the method is also applied to generate vulnerability maps for a real well field

consisting of multiple wells.

6.2 Backward Adjoint Approach

For unknown potential sources that could be located anywhere within the capture zone, we can utilize the adjoint principle [Uffink, 1989]; [Wilson and Liu, 1995]; [Kunstmann and Kinzelbach, 2000]; [Neupauer and Wilson, 2001]; [Neupauer and Wilson, 2002]; [Cornaton, 2003] to assess the impact of the source in the well. The governing equation for the backward model is the adjoint equation of the forward transport model. The backward equation can be written in terms of backward time, τ as:

$$\frac{\partial \psi^*}{\partial \tau} = \frac{\partial}{\partial x_i}\left(D_{ij}\frac{\partial \psi^*}{\partial x_j} + v_i \psi^*\right) - \frac{q_0}{\theta}\psi^* - R\lambda\psi^* \tag{6.1}$$

In the above, the dependent variable ψ^* characterizes the pdf for the time required for a decaying contaminant initially situated at a given point within the capture zone to reach the well. This approach allows us to substitute a single backward run for a large number of forward runs. The source is now placed at the well; the model is run in backward mode with a negative velocity field and the same dispersivity values as in the forward run. The breakthrough curves are recorded at a number of detection points within the capture zone.

In the forward model we inject a pulse at the source location and record the concentration breakthrough curve at the well, while in backward-in-time transport modelling, we inject a unit pulse at the well and record the travel time pdf at the source location. If the concentration breakthrough curve at the well for the forward run is normalized by the injected mass, and the backward travel time pdf is scaled by the well pumping rate, both curves will be equivalent and of dimension (L^{-3}).

6.3 Well Vulnerability Maps: Hypothetical Example

This example demonstrates the approach for a group of wells that are part of a hypothetical well field sharing a common capture zone. The approach involves applying one forward run with a pulse source at an arbitrary location within the well capture zone, and with breakthrough curves recorded at each well, plus one backward run with a pulse source proportional to the ratio of the well flow rate

to the total flow rate applied at each well, and breakthrough data recorded at all points within the capture zone. The capture zone is assumed to cover the entire conceptual model.

The hypothetical conceptual domain (Figure 6.1) is 600 m × 350 m × 10 m in the x, y, and z directions, respectively. The system is separated into 10 horizontal layers. It has no-flow boundaries on the left side (x = 0) and a constant-head boundary of 20 m from layer 1 (bottom) to layer 6 and no-flow boundaries for layer 7 to 10 on the right side (x = 600 m). The base of the domain is impermeable. Three pumping wells located at (x_1, y_1) = (409 m, 219 m), (x_2, y_2) = (432 m, 178 m) and (x_3, y_3) = (399 m, 141 m) are pumped at the rate of 5.18 m^3/day, 8.64 m^3/day and 4.32 m^3/day, respectively, from layers 2 and 3. The hydraulic conductivity, K, of the aquifer and aquitard layers is 10^{-3} m/s and 10^{-4} m/s, respectively. A uniform recharge flux of 12 cm/yr is applied over the top of the model. The transport parameters are $\alpha_L = 10$ m, $\alpha_{TH} = 1$ m, $\alpha_{TV} = 0.01$ m, $D_m = 1 \times 10^{-10}$ m^2/s and R = 1.

The 3D finite element model WATFLOW [Molson et al., 2002] is first used to obtain the nodal steady-state head distribution and elemental velocities, and the corresponding transport model WTC [Molson and Frind, 2004] is then used to solve the forward and backward transport equations. For the forward transport problem, we applied a mass of 10000 mg for 1 day at the source (for location see Figure 6.1). The forward breakthrough curves (normalized using the mass applied) are recorded at each of the three wells and are then summed to a single forward breakthrough curve. For the backward problem, we applied a unit pulse source at the wells. The pulse source is distributed among the wells proportional to the ratio of the well flow rate to the total flow rate at each well. The backward travel time pdf is observed at the source location. The resulting backward curve is then scaled by the well pumping rate. As shown in Figure 6.2, the scaled backward travel time pdf at the source location is equivalent to the forward breakthrough curve at the well except for some small numerical errors at the tail of the curve. The backward model is then used to map the vulnerability measures within the well field.

The vulnerability maps are created by post-processing the scaled backward travel-time pdfs at each point in the system. Figure 6.3 shows the resulting vulnerability maps for the three wells considered together. The maximum expected relative concentration at the wells due to unit pulse sources is shown in Figure 6.3(a). Figure 6.3(b) shows the time taken (in years) for the maximum expected concentration to

appear at the wells, while Figure 6.3(c) shows the time taken to breach a threshold value of 10^{-4}. Finally, Figure 6.3(d) shows the exposure time to concentrations above the threshold value. For example, for a source located at point A (Fig. 6.3(a)), the maximum expected relative concentration will be about 4×10^{-2} and the time taken to reach that maximum will be 18 years (Fig. 6.3(b)). However, the threshold value will be reached in about 8 years (Fig. 6.3(c)), and the wells will be exposed to above-threshold values for about 14 years (Fig. 6.3(d)). These values relate to the contaminant in the extracted well water, taking into account dilution with clean water.

As expected, the maximum relative concentration decreases with the distance of the source from the well, whereas the time taken to reach the maximum, as well as the time taken to breach the threshold value, increase with distance. However, the exposure time of about 20 years to above-threshold concentrations is highest for source locations about 80 m upstream of the well, and lower for points closer to and farther from the well. The reason for this is that for a source located very close to a well, the breakthrough curve will be very sharp and pass quickly, while for very long distances, the breakthrough curve will be much dispersed and most of it may be below the threshold value, resulting again in only a short time of exposure. Therefore, the intermediate distances yield the largest exposure time.

6.4 Well Vulnerability Maps: Mannheim Well Field

The 3D flow system of the Waterloo Moraine developed by Martin and Frind (1998) is used as a basis for the well vulnerability maps. The steady-state flow system and the WHPAs for the Mannheim well fields are shown in Chapter 4. Figures 4.4 and 4.10 show the head distribution and 100-yr capture zone are reproduced here as Figure 6.4.

For the purpose of the analysis, the two Mannheim well fields are divided into clusters of neighbouring wells. The Mannheim South well field is arranged into three well clusters (1, 2, 3; wells K22 and K23, well K24, well K26) and the Mannheim North well field is arranged into four clusters (4, 5, 6, 7; wells K93 and K94, wells K91 and K92, well 21, and wells K25 and K29), as shown in Figure 6.4. For each cluster, a non-reactive unit pulse source is applied for 1 day. For the individual wells within the cluster, the pulse is proportional to the ratio of the well flow rate to the total flow rate of the cluster.

The impact of the pulse sources at the wells is expressed in terms of the maximum expected relative concentration in the well water, the time required to reach the maximum expected relative concentration, the time required to breach an arbitrary threshold concentration of 10^{-9}, and the contaminant exposure time to above-threshold concentrations. In this example we have chosen a threshold value of 10^{-9} since the impact of the unit pulse source reaches a maximum concentration of 10^{-7} at the well. The contamination level at the well due to the pulse sources is related to the scaled backward travel time pdf. Individual vulnerability maps for well cluster 1 to 7 are developed by post-processing the scaled backward travel time pdf at each point within the capture zones. Figures 6.6 to 6.18 show the well vulnerability maps for each cluster.

The resulting maps show that if a unit pulse source of contamination is applied at point X′ for one day within the Mannheim South well field, the impact of the source will reach a maximum expected relative concentration of 1×10^{-8} at well cluster 1 (Fig. 6.6(a)) in about 5 years (Fig. 6.6(b)), the contaminant concentration will take less than 5 years to reach the threshold value of 10^{-9} (Fig. 6.6(c)), and the exposure time at well cluster 1 is about 20 years (Fig. 6.6(d)). For the same source the impact will reach below the threshold value at well cluster 2 (Fig. 6.8(a)). The impact of the source at point X′ also reaches at well cluster 3 but at a lower magnitude than well cluster 1. As shown in Figure 6.10(a) a relative peak concentration of more than 1×10^{-9} will arrive in well cluster 3 in less than 20 years (Fig. 6.10(b)), will reach the threshold value in 5 years (Fig. 6.10(c)), and will remain in the well water for about 40 years (Fig. 6.10(d)).

On the other hand, in case of a unit pulse source at point X within the Mannheim North well field, well cluster 4 will see a maximum expected relative concentration of 5×10^{-8} (Fig. 6.12(a)) in less than 5 years (Fig. 6.12(b)), the contaminant concentration will reach the threshold value in about 1 year (Fig. 6.12(c)) , and the exposure time above the threshold concentration is 20 years (Fig. 6.12(d)). For the same source the impact will also reach well clusters 5, 6 and 7 (see Figures 6.14, 6.16, and 6.18).

The vulnerability maps for the seven clusters within the Mannheim well field contain all the useful information of the conventional capture zone delineation, plus the selected quantitative measures expressing the vulnerability of the well. All values

in the vulnerability maps are relative to unit pulse sources of contamination. The composite well vulnerability maps for the Mannheim well field can be obtained by superimposing these seven maps. One drawback of this approach is that it may be difficult to extract the overall vulnerability information for a point within the capture zone.

6.5 Well Vulnerability Maps: Mannheim Well Field (Lumped Approach)

To overcome the above problem, we will develop an approach that will lump all wells within a well field together. This approach has the advantage that it requires only one simulation run for each well field; however, the impact at each well is expected to be the same as that of the lumped well. It should be noted that both approaches differ from the approach used by Frind and others (2006) in that the concentrations mapped are actual concentrations in the well water, taking into account mixing with clean water in the well, rather than concentrations in the aquifer near the well.

The vulnerability maps are developed by following the procedure laid out in the previous section. In the backward model, a unit pulse source is placed at the wells. The unit pulse source is distributed among the wells proportional to the ratio of the individual well flow rates to the total flow rate for the well field. The backward pdf is recorded for all nodal points in the corresponding well field. All curves are scaled with the total pumping rate in the corresponding well field, and the scaled backward travel time pdfs are post-processed to extract the desired vulnerability measures for each well.

This approach is again applied to the Mannheim well field, and the results are shown in Figure 6.20. In this example, the wells within a well field are treated together. If a source of contaminant is located close to a well, the impact of the contaminant will be observed only in that well, however for distant sources, the expected impact on a well as predicted by the vulnerability maps is the lumped impact on all wells.

For example, a pulse source of contaminant at location A (Fig. 6.20) in the Mannheim South well field will be expected to show up in the nearest wells at

a maximum concentration of 5×10^{-8} (Fig. 6.20(a)) in about 1 year (Fig. 6.20(b)). For the same source, and a threshold concentration of 10^{-9}, the time required will be less than 1 year (Fig. 6.20(c)) and the contaminant will remain at above-threshold concentrations for about 20 years (Fig.6.20(d)). Likewise, the impact of a source at point B will be a maximum concentration more than 1×10^{-9} in about 20 years at the wells K22, K23 and K24 of Mannheim South, a time to breach the threshold value in 5 years, and an exposure time of about 40 years.

Similarly, for a source at location C within the Mannheim North well field, the contaminant will reach the two nearest wells at a maximum concentration of 5×10^{-8} in about 1 year, the time to breach the threshold will be less than 1 year, and the exposure time will be less than 20 years. For a source at point D, the effect will be a maximum concentration of about 5×10^{-9} in about 5 years at each of the seven wells of this well field, a threshold value of 10^{-9} will be reached at about 1 year, and the exposure time to above-threshold concentrations will be 20 years.

In the vulnerability maps, the time to reach maximum concentration should be equivalent to the corresponding time-dependent capture zone at ground surface [Frind et al., 2002]. Figure 6.20(b) shows that the agreement between the 100-yr contour from the vulnerability assessment and the 100-yr capture zone outline is fairly good, with small discrepancies due to differences in the respective numerical procedures.

The vulnerability maps for the Mannheim North well field show an anomaly in the western part of the capture zone (see for example Fig. 6.20(a)). If we take a vertical cross-section along the wells K93 and K94, the cause of this anomaly is evident in the cross-section (Fig. 6.21). Figure 6.21 reveals a window in the aquitard overlying Aquifer 1. This window provides a preferred pathway for contaminant migration to the wells within that well field. Therefore, the area of this window represents a high-risk zone where a spill would pose a serious threat to the wells.

6.6 Sensitivity of Well Vulnerability Map

There is a large body of literature on the topic of uncertainty in the delineation of capture zones. Most of this work is based on the assumption of a 2D capture zone. For example, Van Leeuwen and others (1998) used an approach based on random space functions and using Monte Carlo analysis to determine the probability dis-

tribution of stochastic capture zones. Guadagnini and Franzetti (1999) extended the stochastic approach to time-related capture zones. More recently, Feyen and others (2001) introduced the generalized likelihood uncertainty estimation (GLUE) methodology to the problem of capture zone uncertainty, also addressing uncertainty resulting from imperfect knowledge of the parameters defining the correlation structure, in addition to the variations due to different realizations.

The Waterloo Moraine aquifer system consists of multiple discontinuous aquifers and aquitards, and a major source of uncertainty is the location of windows in the aquitards which provide interconnecting pathways between the different aquifer units, and have a controlling influence on the capture zones [Martin and Frind, 1998]. By using the transport equation, smaller-scale uncertainties are represented as macrodispersion. The impact of larger-scale uncertainties can be investigated by scenario analysis, where a small number of feasible scenarios is created and calibrated by means of an automatic calibration tool [Merry et al., 2000].

In this study a limited sensitivity analysis of the maximum expected relative concentration due to the pulse sources of contaminations is performed by increasing the hydraulic conductivity of the lenses of Aquifer 1 close to well cluster 5 (i.e., wells K91 and K92). Well cluster 5 is approximately located in the north western part of the Mannheim North well field. As shown in Figure 6.22(a), the horizontal hydraulic conductivity of Aquifer 1 ranges mostly from 10^{-6} to 10^{-3} m/s within the areas of the well cluster 5. The conductivity values are increased by 1 to 2 order of magnitude within the area indicated by the red circle (as shown in Fig. 6.22(b)). The water table changes only slightly as a result of increased conductivities; the groundwater flow model is therefore not recalibrated.

Figure 6.23 shows the maximum expected relative concentration for well cluster 5 both with the original and the increased hydraulic conductivity. The increased hydraulic conductivity is shown to result in a very significant change in the maximum expected concentration at the well in that both the area impacting the wells increases and the concentration itself increases. This result illustrates that the maximum expected relative contaminant concentration at the wells is highly sensitive to the presence large-scale of heterogeneities.

6.7 Summary

Well vulnerability maps provide quantitative information about the threat to a well due to pulse sources of contamination within its capture zone. The concept can also be formulated for well fields with multiple wells. For simplicity, the wells within a well field can be lumped together in the vulnerability analysis, but the mapping of individual well vulnerability is also possible. Vulnerability maps provide important information such as the maximum expected relative concentration at the well by including the dilution of the contaminated water with the clean water. The information on concentration in the extracted well water is the primary interest from the users point of view in assessing potential impacts. The vulnerability maps also provide the time history of the contamination, including the time required for a contaminant to reach the maximum concentration at the well, the time to reach a threshold value of the contaminant, and the exposure time of the concentration above the threshold value.

The impact of all potential but unknown pulse sources can be assessed using the backward-in-time transport approach, which requires a single model simulation run. The information gained goes much beyond that obtained from the conventional approach which is based on the advective time of travel of the contaminant. The results also illustrate that the value of maximum expected relative concentration at the wells is highly sensitivity to the material heterogeneity. The presence of windows in the aquitard that control flow and transport can lead to a shorter time for the contaminant migration to the wells with a higher maximum relative concentration. The study shows that large-scale heterogeneities and connectivity of aquifer units are controlling parameters.

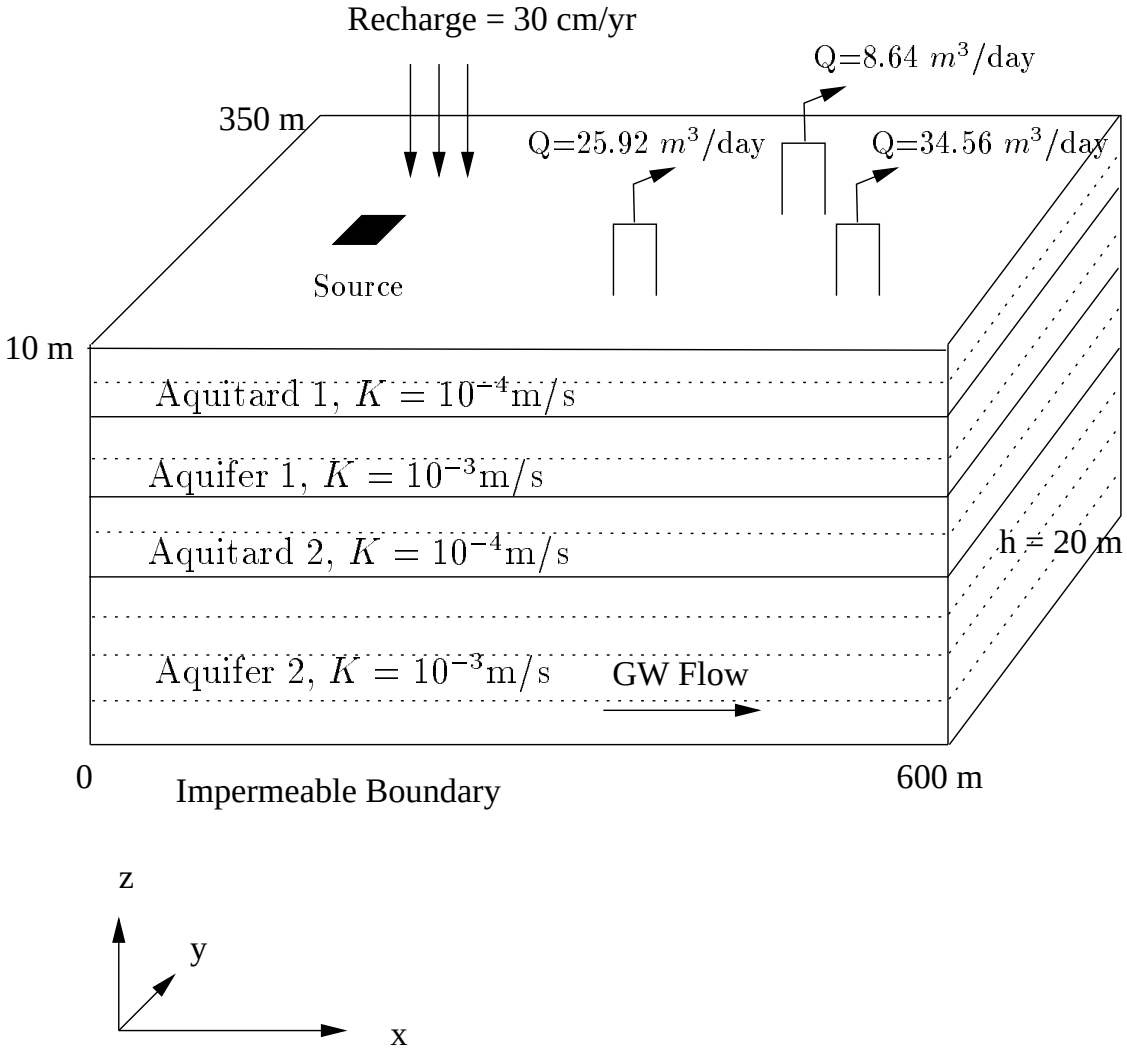

Figure 6.1: 3D conceptual domain of a layered system with multiple wells.

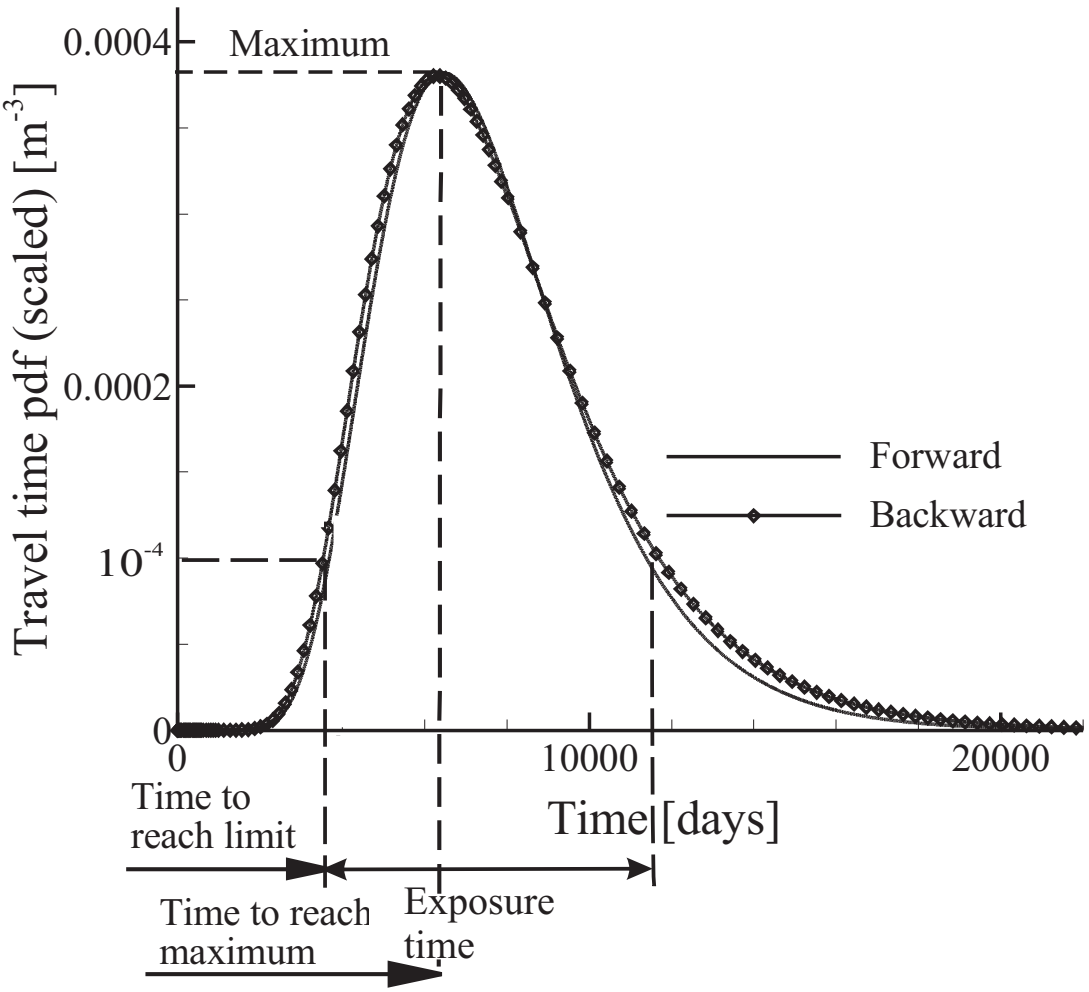

Figure 6.2: Forward and backward breakthrough curves from the test simulation showing the impact of a pulse source, with vulnerability characteristics.

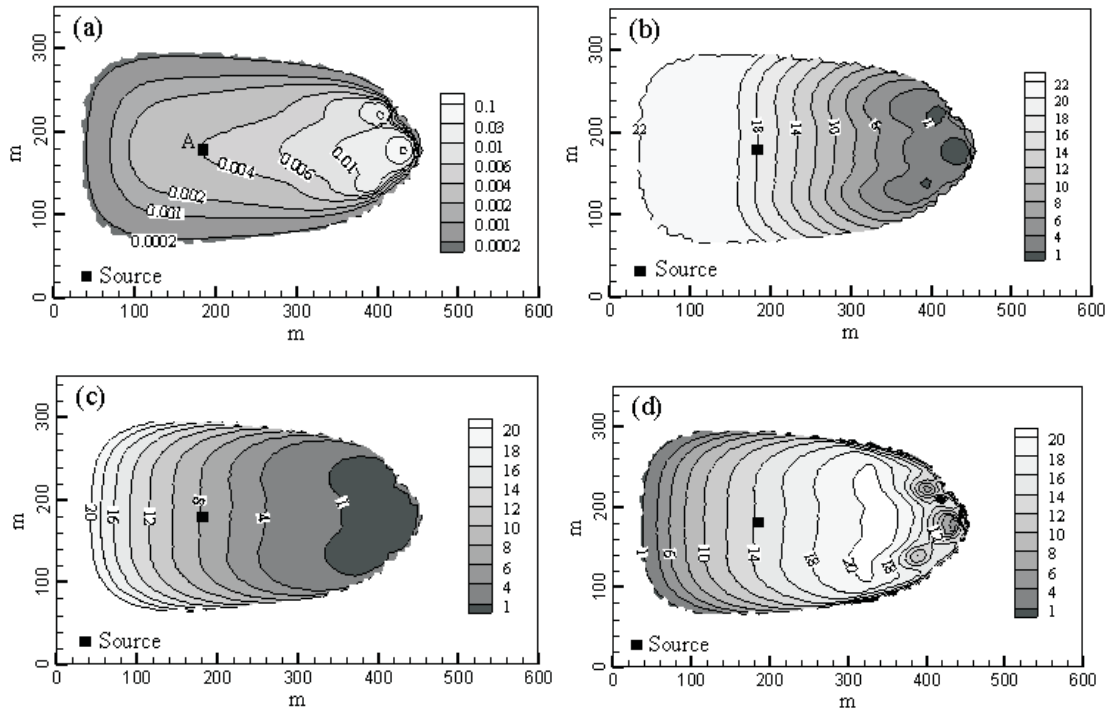

Figure 6.3: Vulnerability maps for the test case with multiple wells: (a) maximum expected concentration at the wells, (b) time taken for the maximum concentration to reach the wells, (c) time taken to breach a threshold concentration of 10^{-9}, (d) exposure time to above-threshold concentrations.

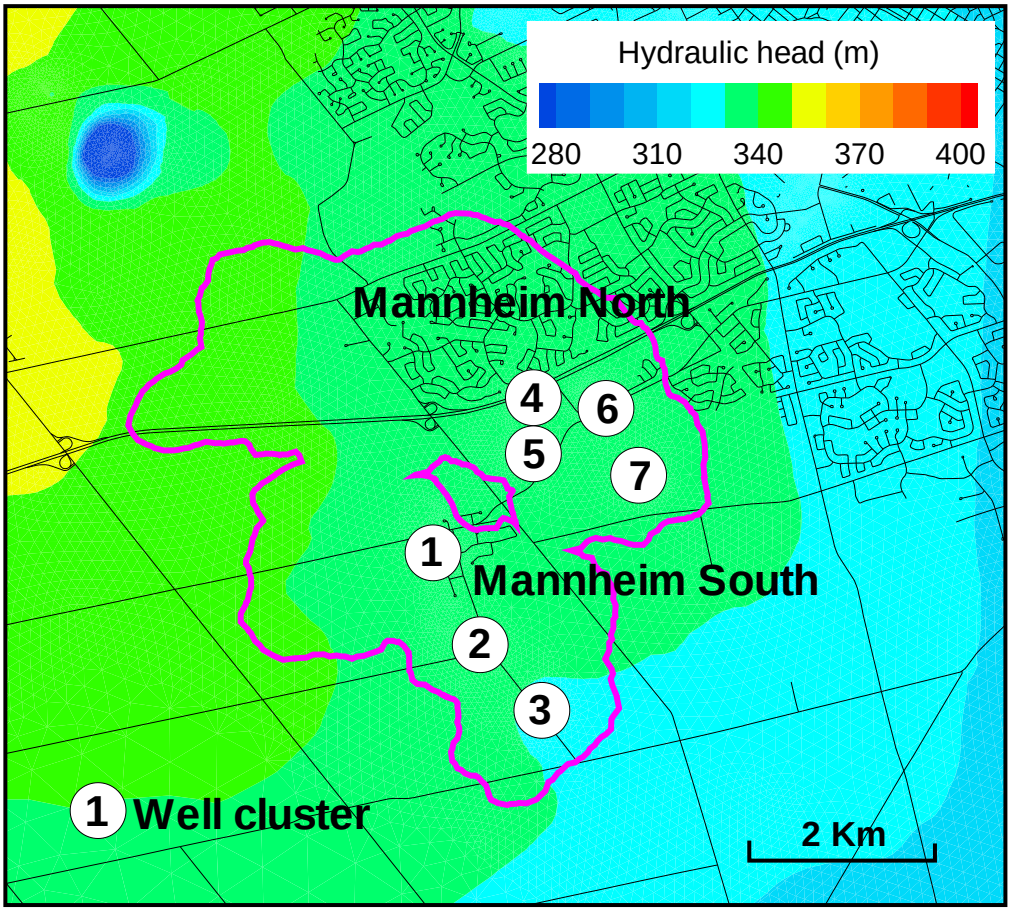

Figure 6.4: Mannheim well field: steady-state head distribution and 100-year capture zone.

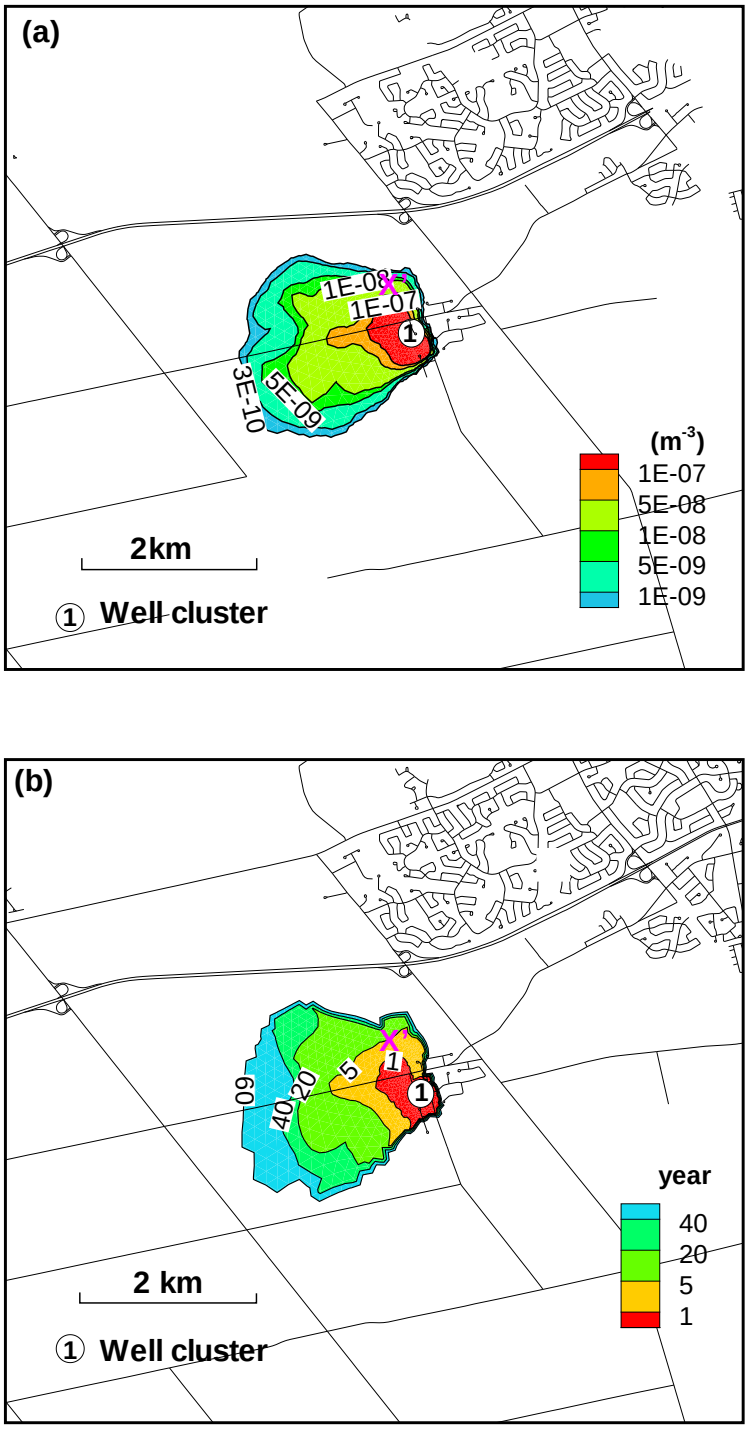

Figure 6.5: Well vulnerability maps for well cluster 1: (a) maximum expected concentration at the wells, and (b) time taken for the maximum concentration to reach the wells.

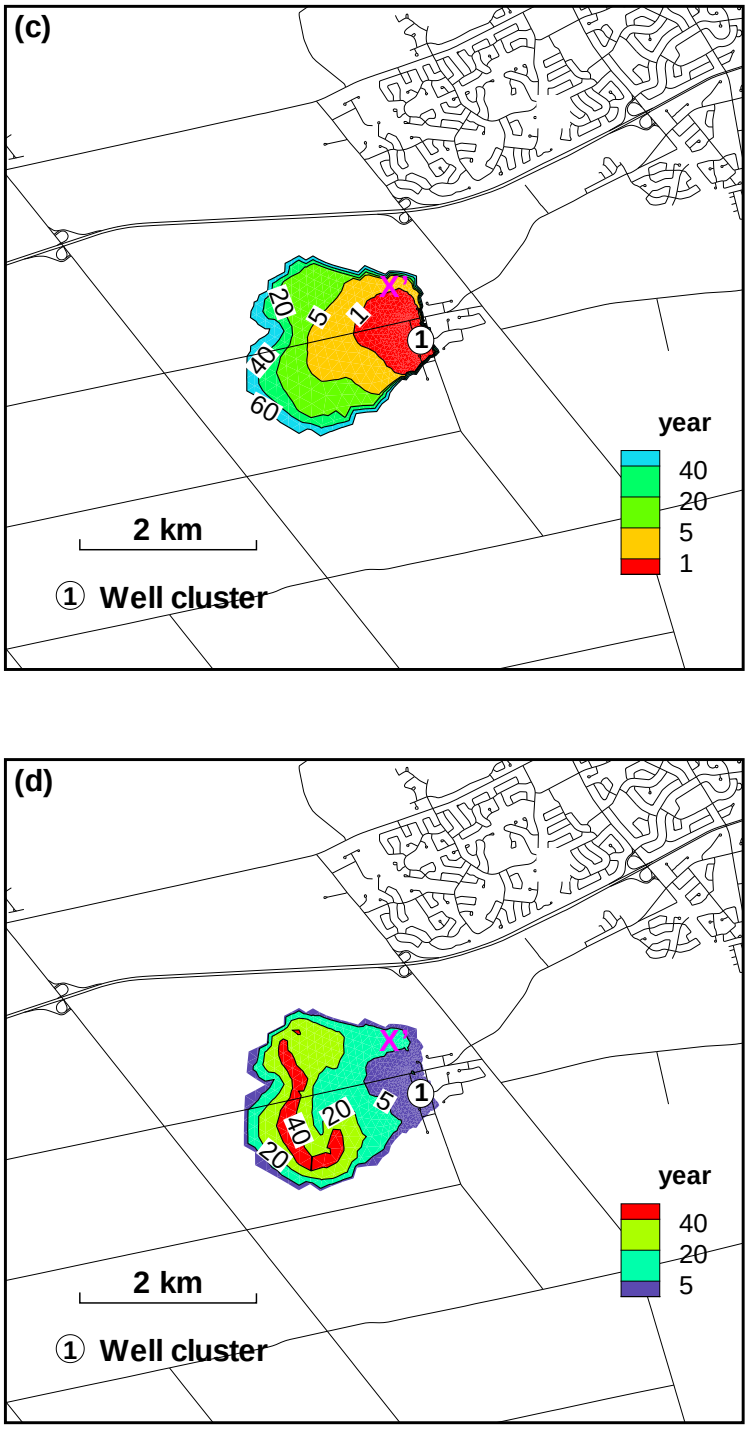

Figure 6.6: Well vulnerability maps for well cluster 1: (c) time taken to breach a threshold concentration of 10^{-9}, and (d) contaminant duration at the wells to above-threshold concentration.

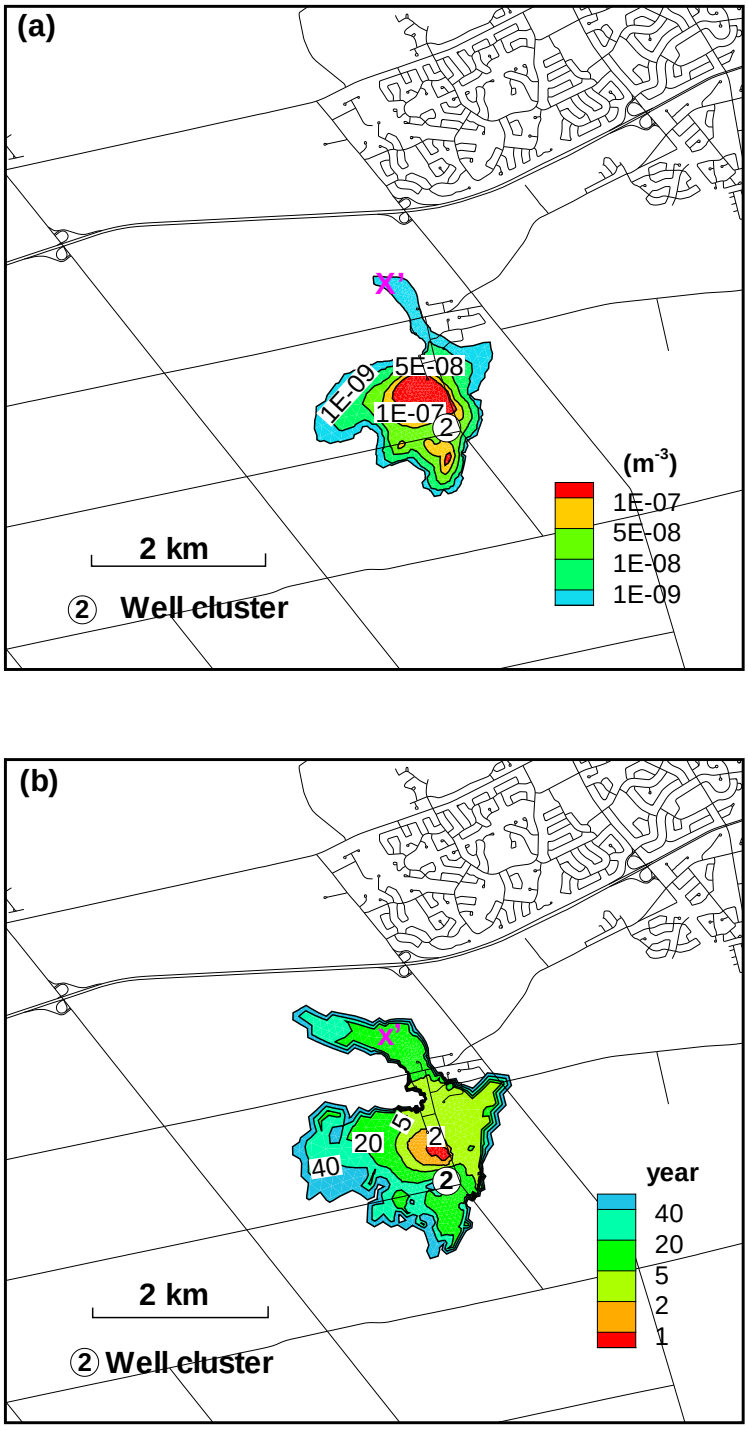

Figure 6.7: Well vulnerability maps for well cluster 2: (a) maximum expected concentration at the wells, and (b) time taken for the maximum concentration to reach the wells.

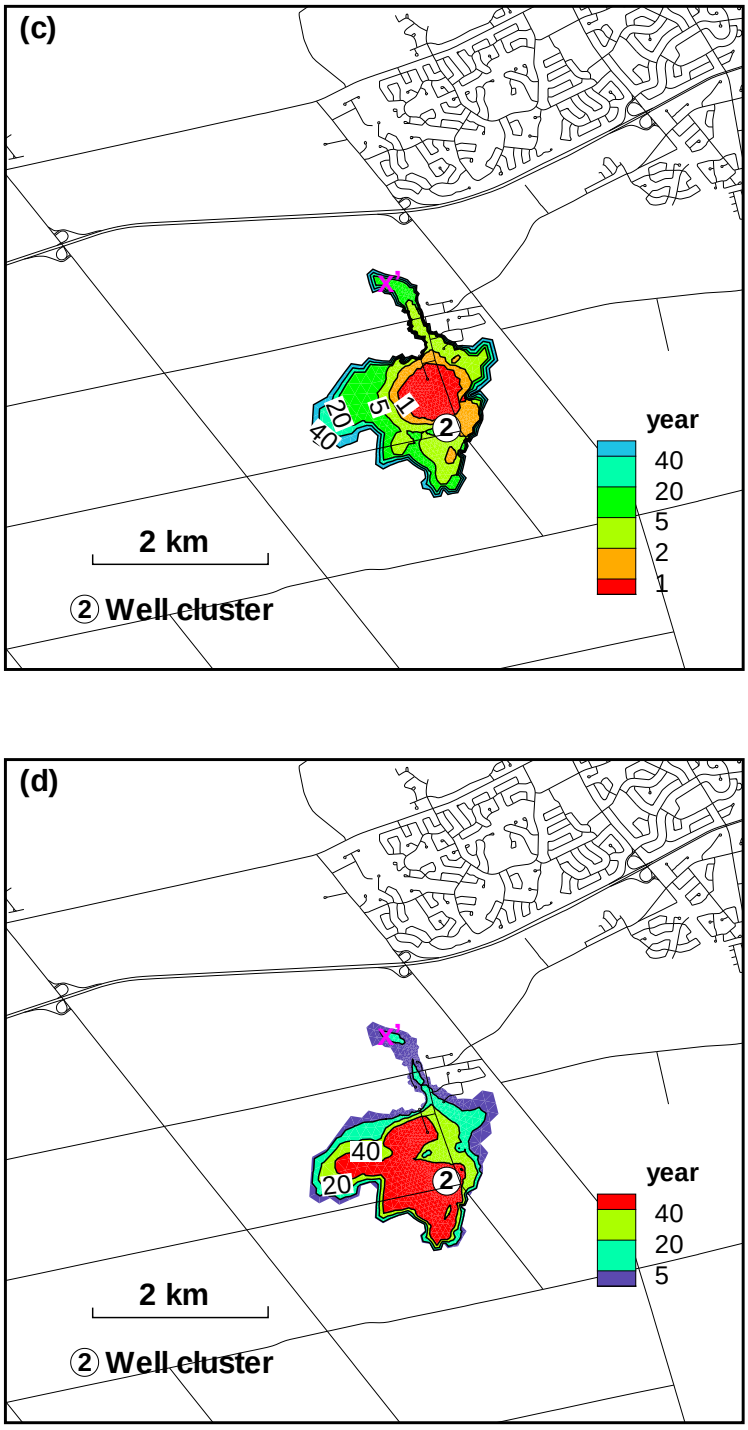

Figure 6.8: Well vulnerability maps for well cluster 2: (c) time taken to breach a threshold concentration of 10^{-9}, and (d) contaminant duration at the wells to above-threshold concentration.

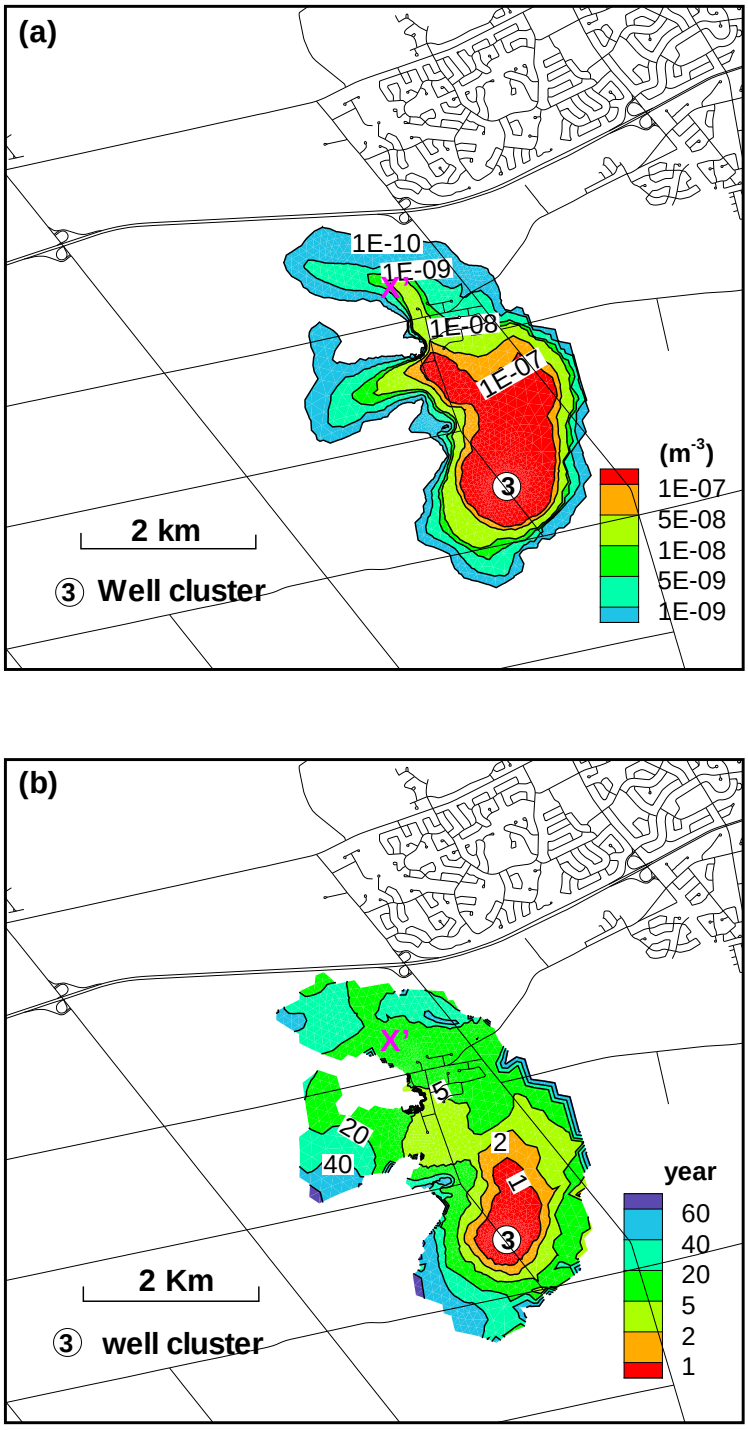

Figure 6.9: Well vulnerability maps for well cluster 3: (a) maximum expected concentration at the wells, and (b) time taken for the maximum concentration to reach the wells.

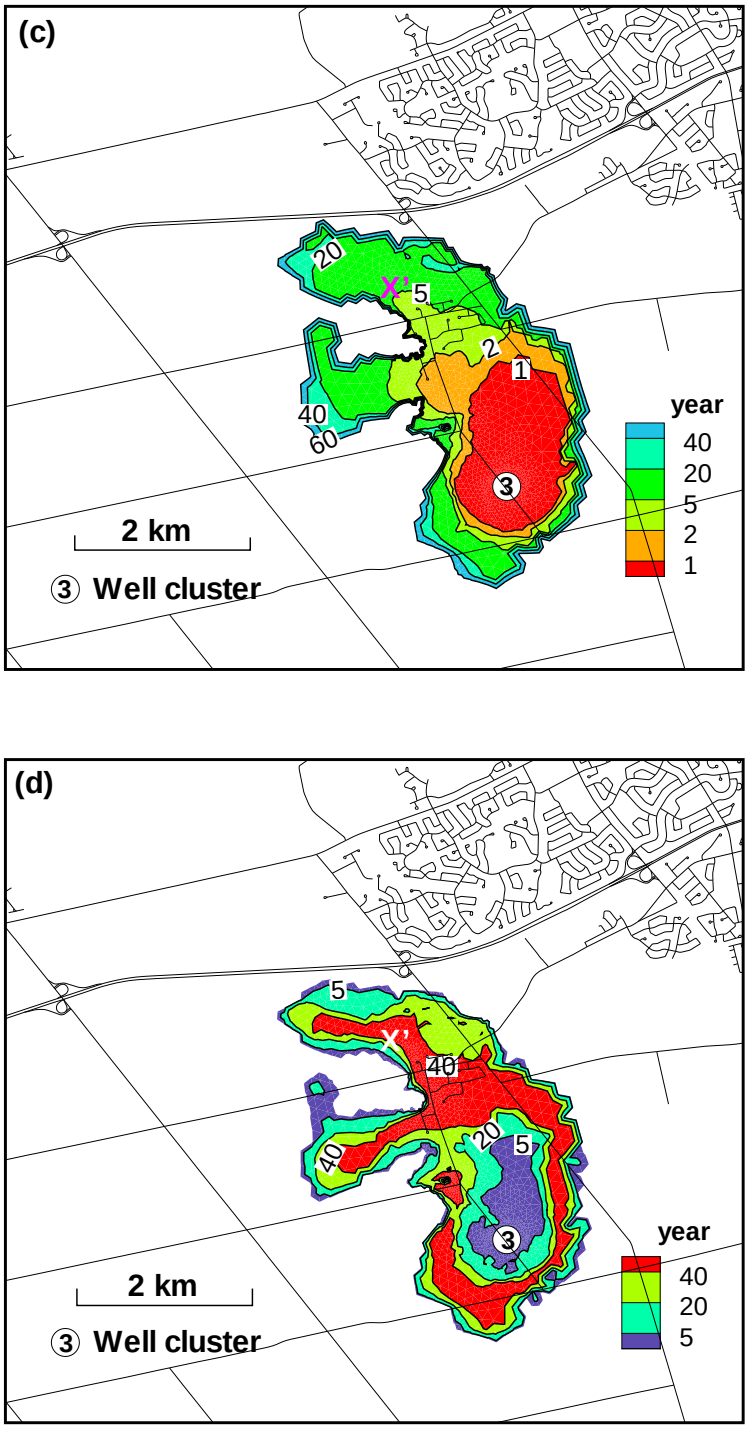

Figure 6.10: Well vulnerability maps for well cluster 3: (c) time taken to breach a threshold concentration of 10^{-9}, and (d) contaminant duration at the wells to above-threshold concentration.

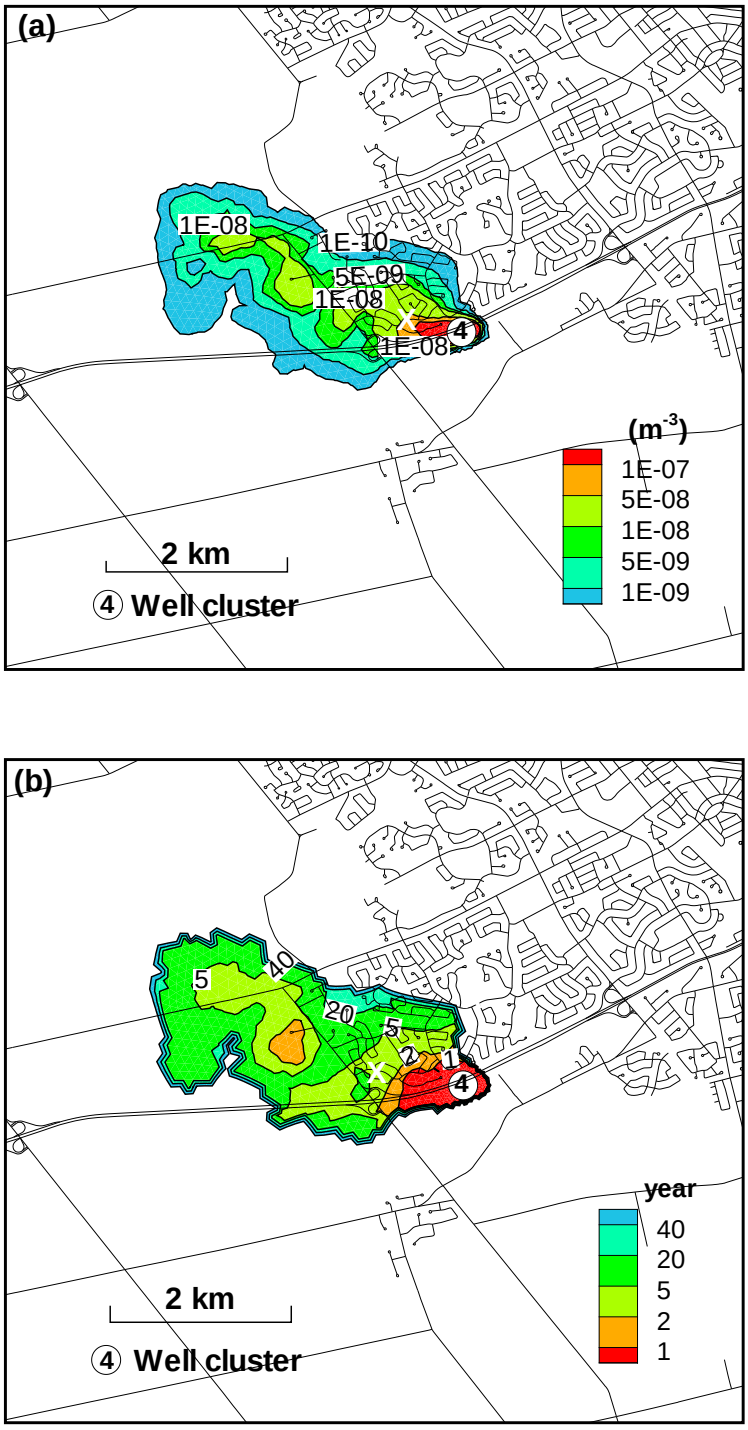

Figure 6.11: Well vulnerability maps for well cluster 4: (a) maximum expected concentration at the wells, and (b) time taken for the maximum concentration to reach the wells.

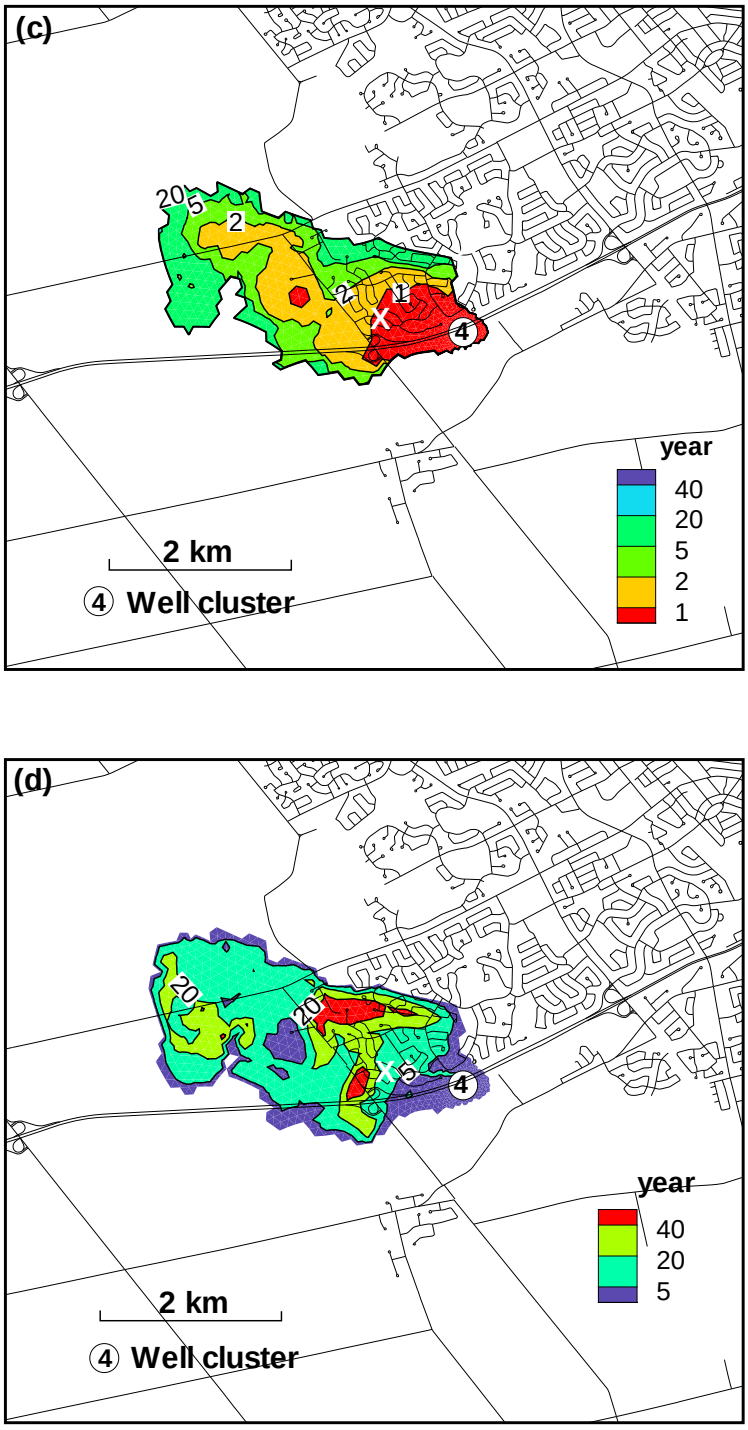

Figure 6.12: Well vulnerability maps for well cluster 4: (c) time taken to breach a threshold concentration of 10^{-9}, and (d) contaminant duration at the wells to above-threshold concentration.

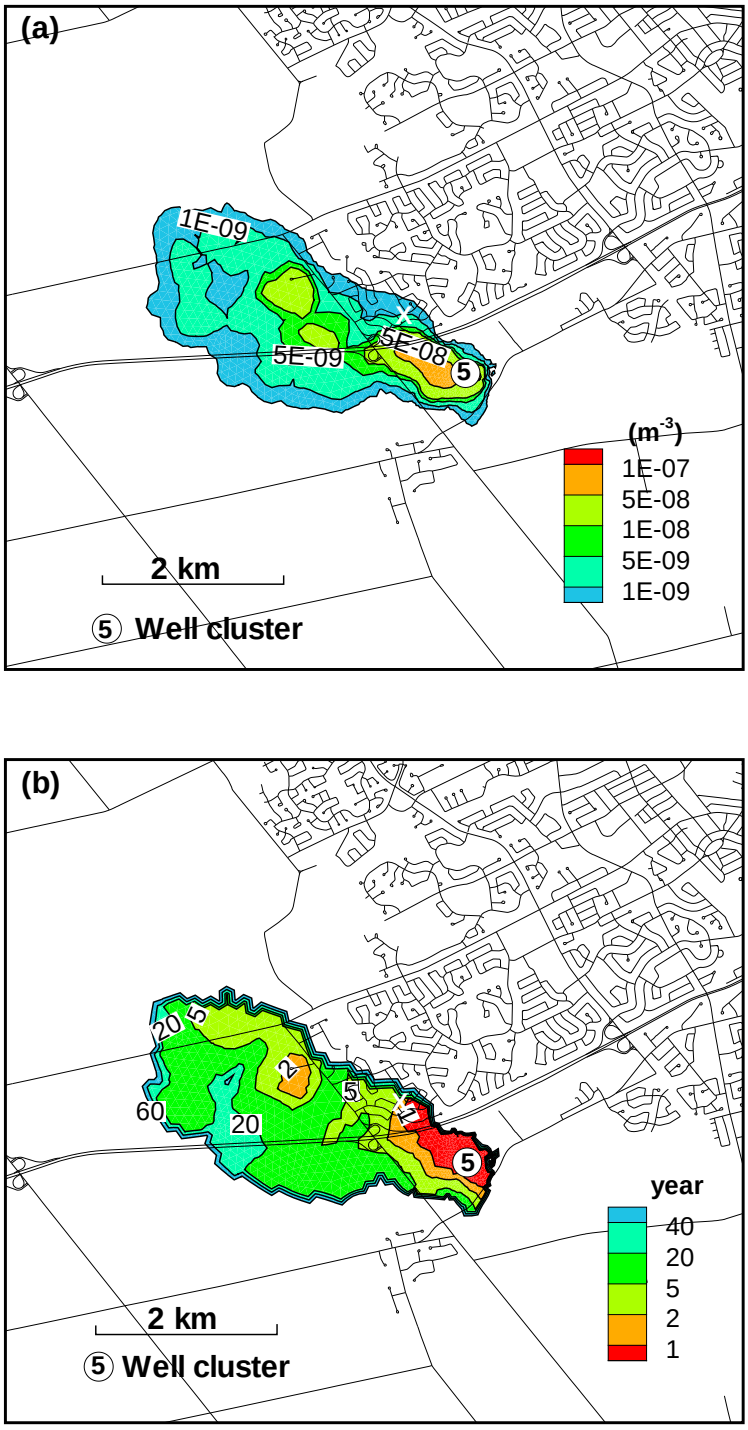

Figure 6.13: Well vulnerability maps for well cluster 5: (a) maximum expected concentration at the wells, and (b) time taken for the maximum concentration to reach the wells.

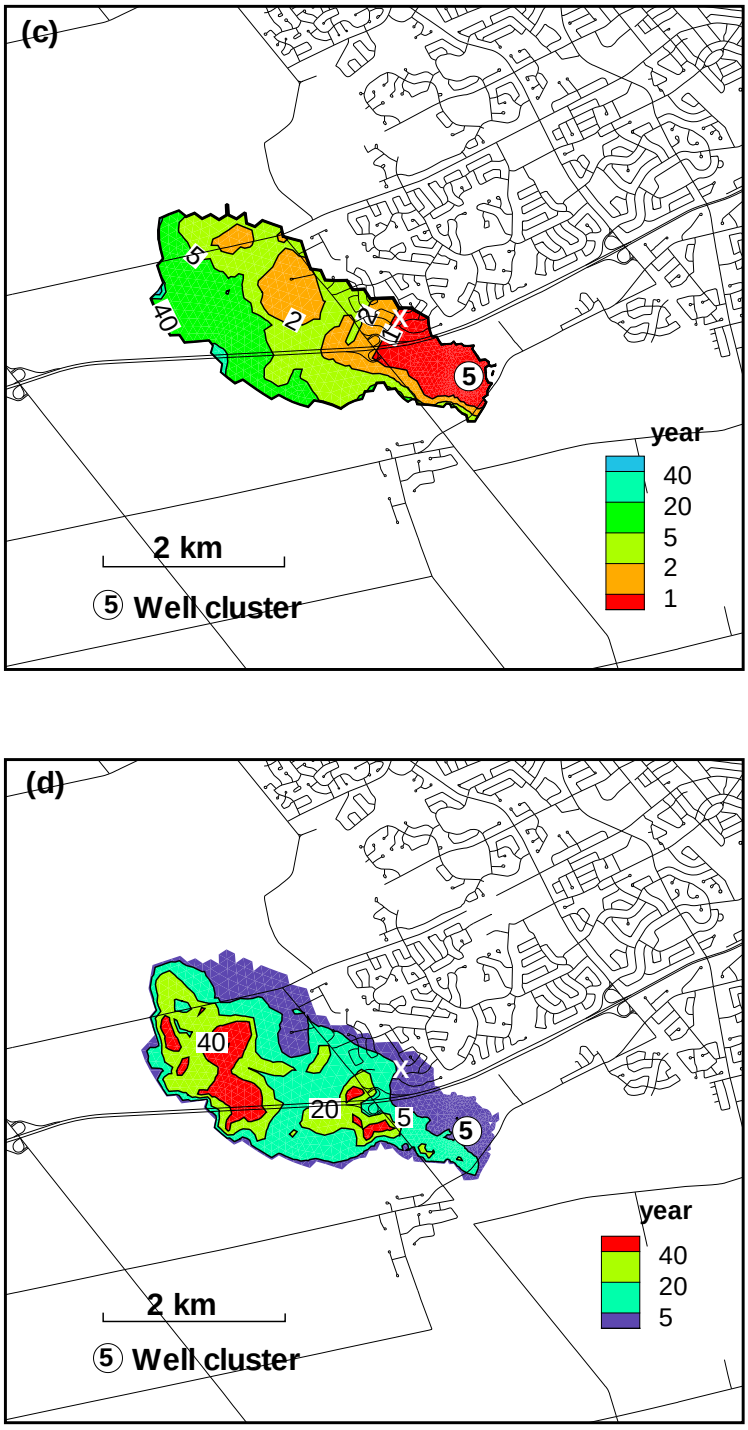

Figure 6.14: Well vulnerability maps for well cluster 5: (c) time taken to breach a threshold concentration of 10^{-9}, and (d) contaminant duration at the wells to above-threshold concentration.

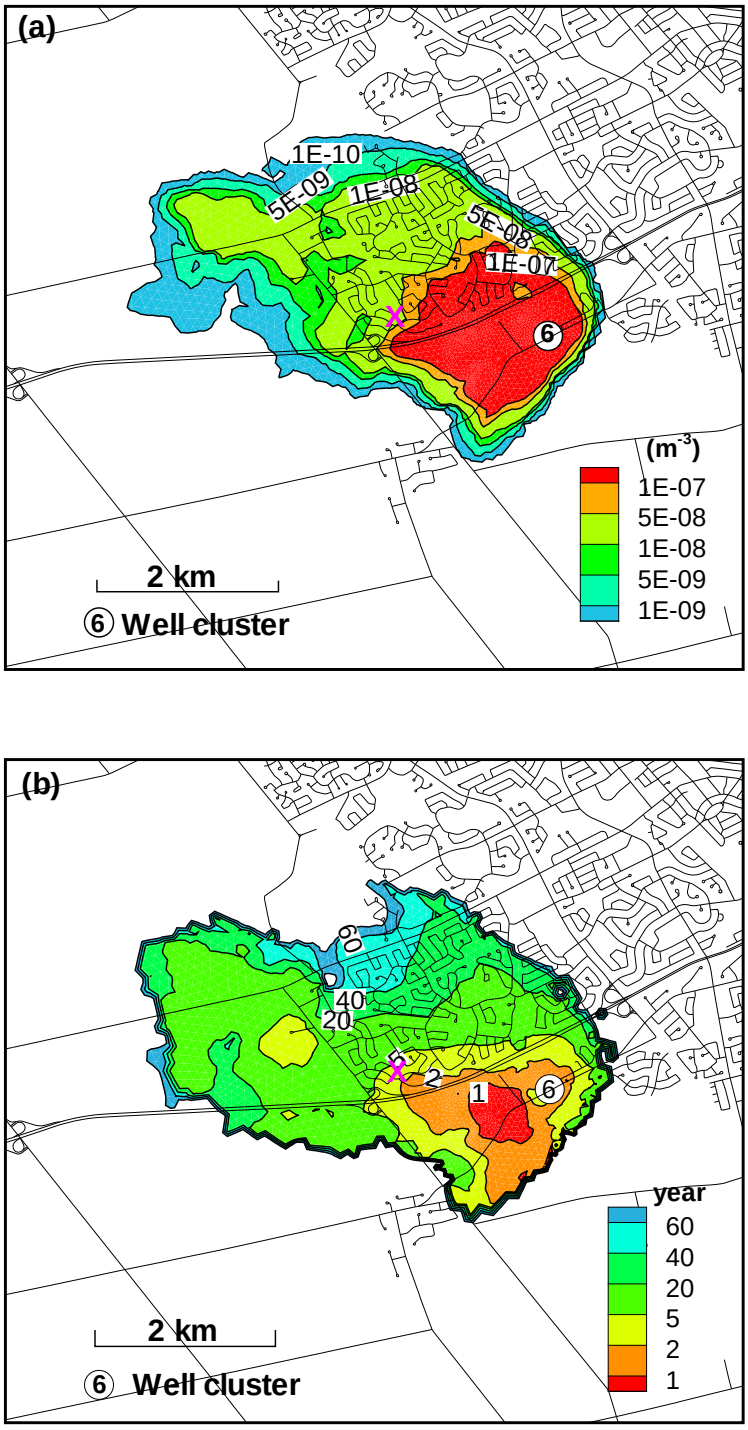

Figure 6.15: Well vulnerability maps for well cluster 6: (a) maximum expected concentration at the wells, and (b) time taken for the maximum concentration to reach the wells.

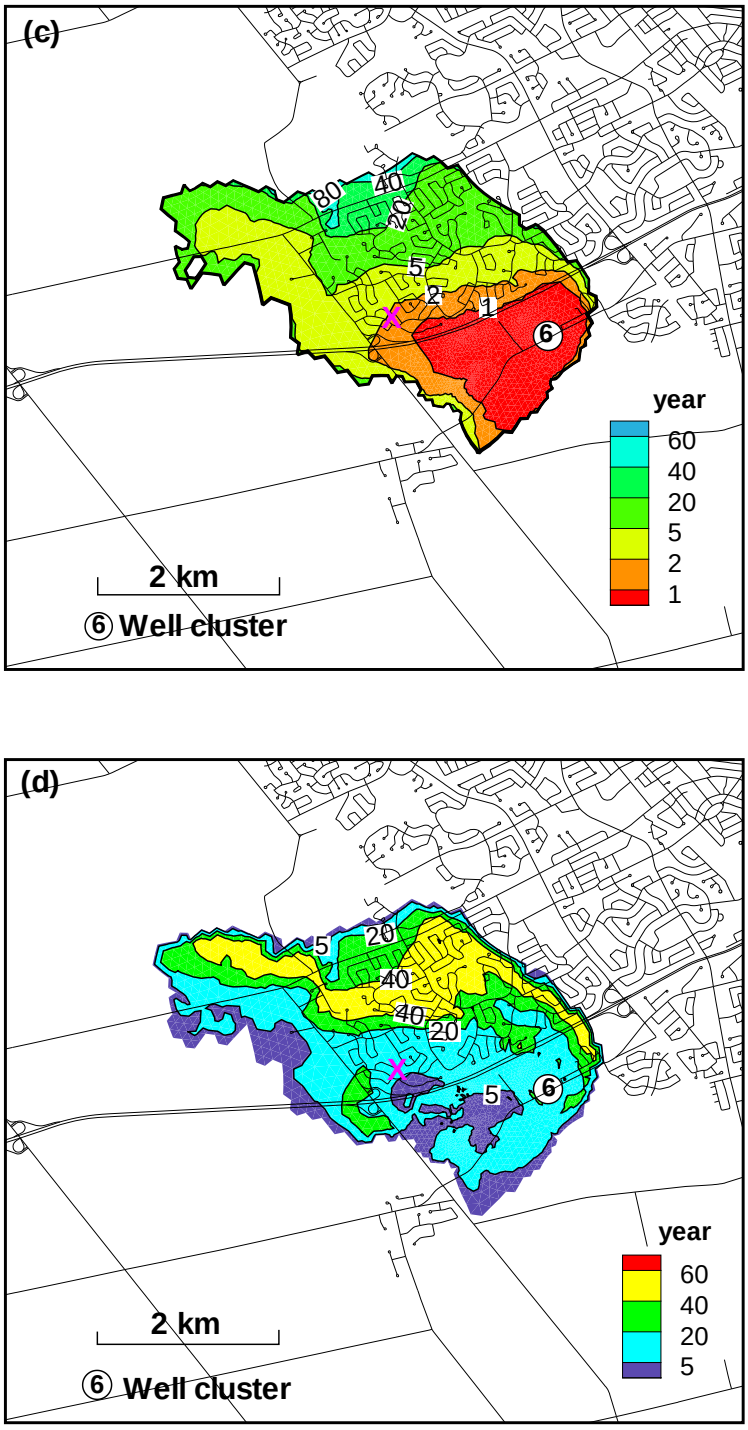

Figure 6.16: Well vulnerability maps for well cluster 6: (c) time taken to breach a threshold concentration of 10^{-9}, and (d) contaminant duration at the wells to above-threshold concentration.

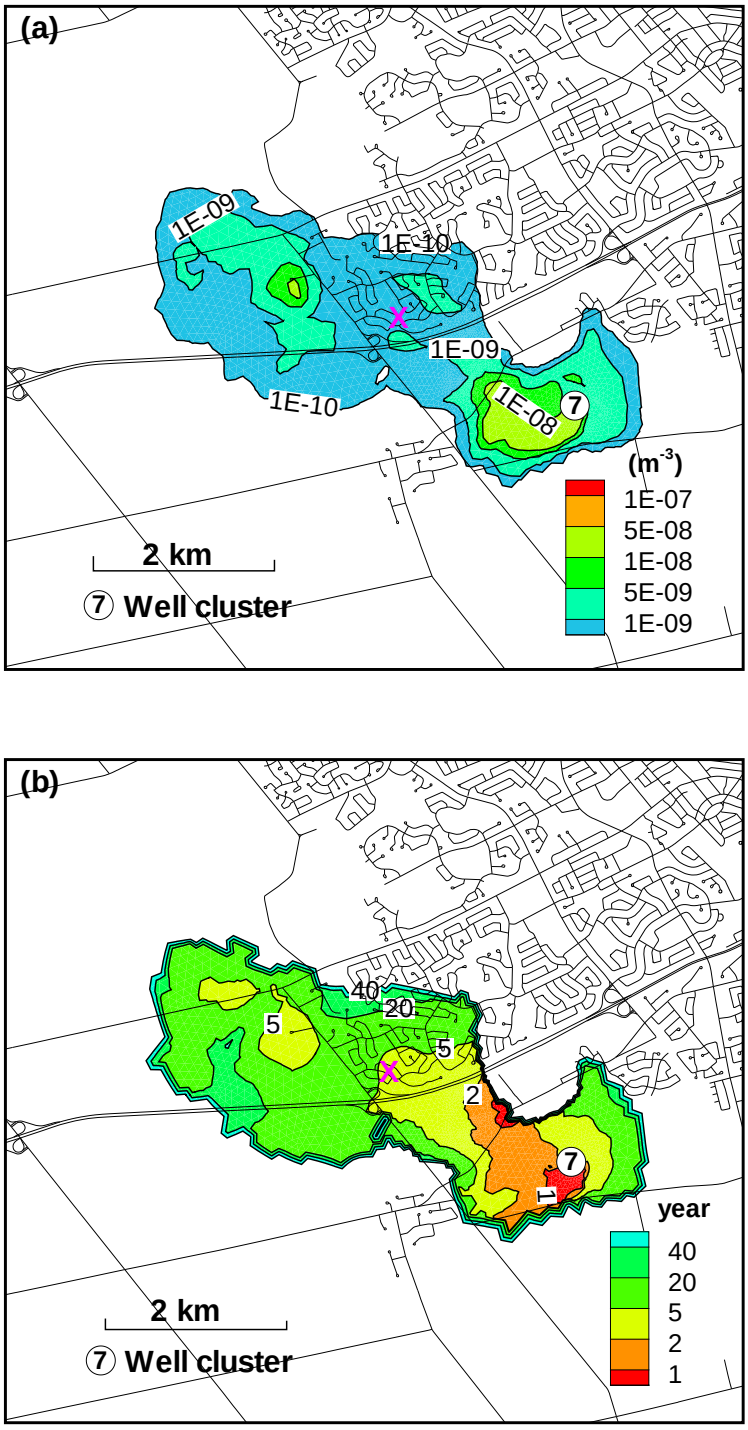

Figure 6.17: Well vulnerability maps for well cluster 7: (a) maximum expected concentration at the wells, and (b) time taken for the maximum concentration to reach the wells.

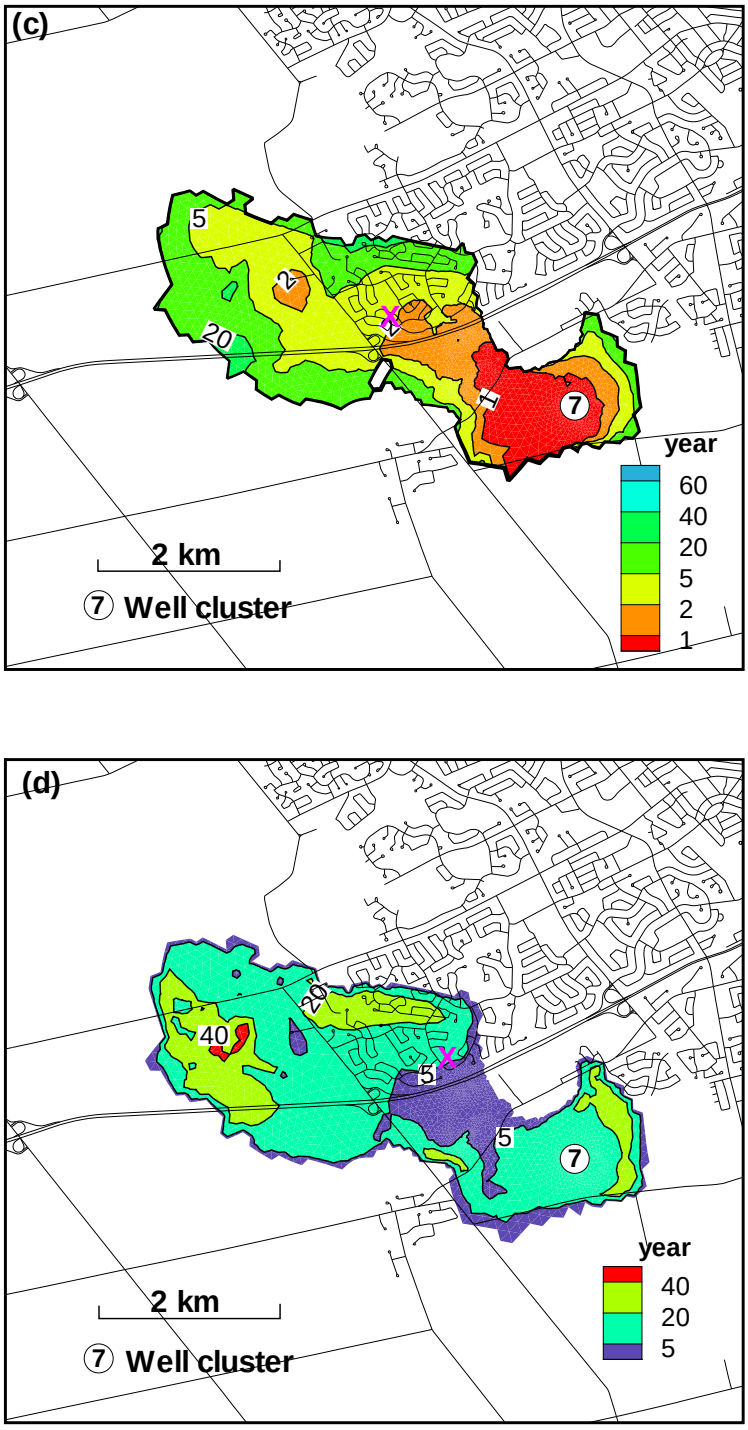

Figure 6.18: Well vulnerability maps for well cluster 7: (c) time taken to breach a threshold concentration of 10^{-9}, and (d) contaminant duration at the wells to above-threshold concentration.

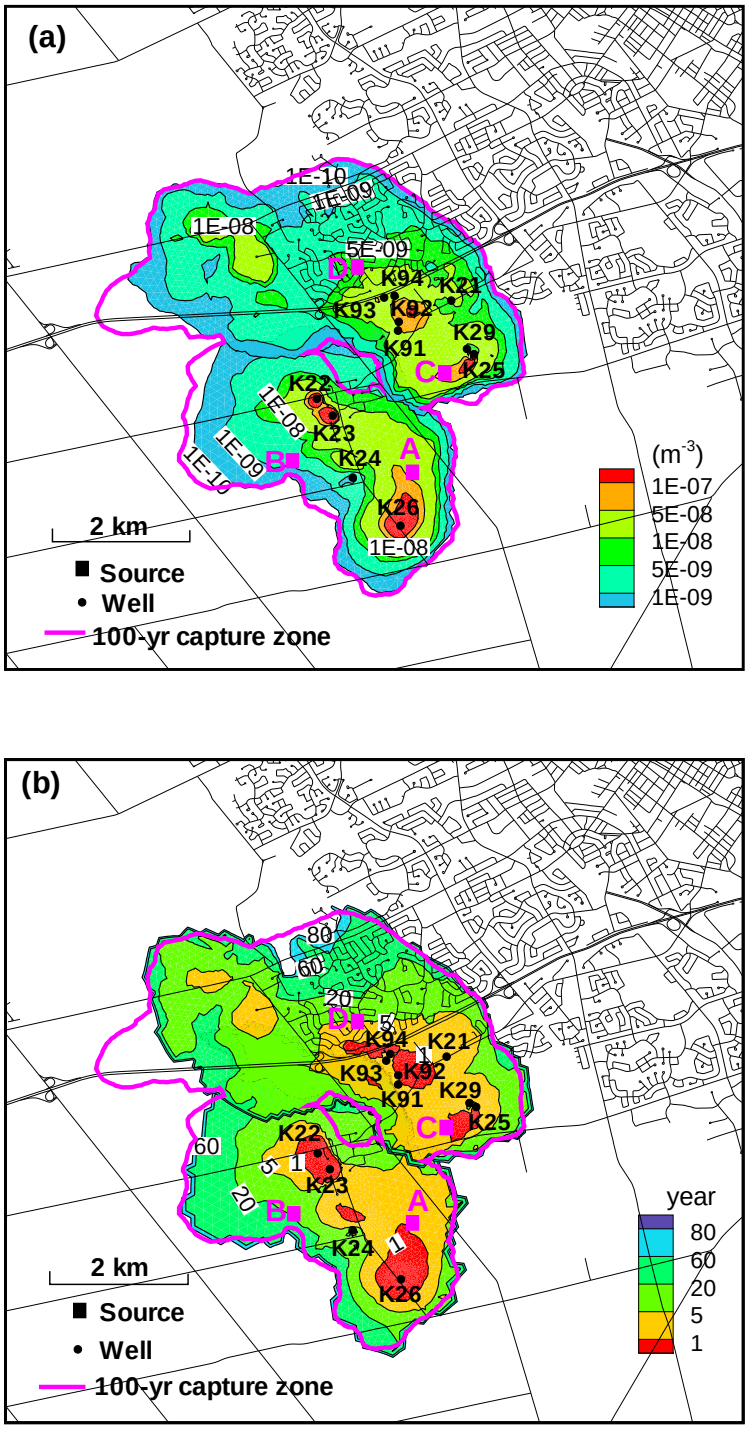

Figure 6.19: Vulnerability maps for the Mannheim well field, lumped approach: (a) maximum expected concentration at the wells, and (b) time taken for the maximum concentration to reach the wells.

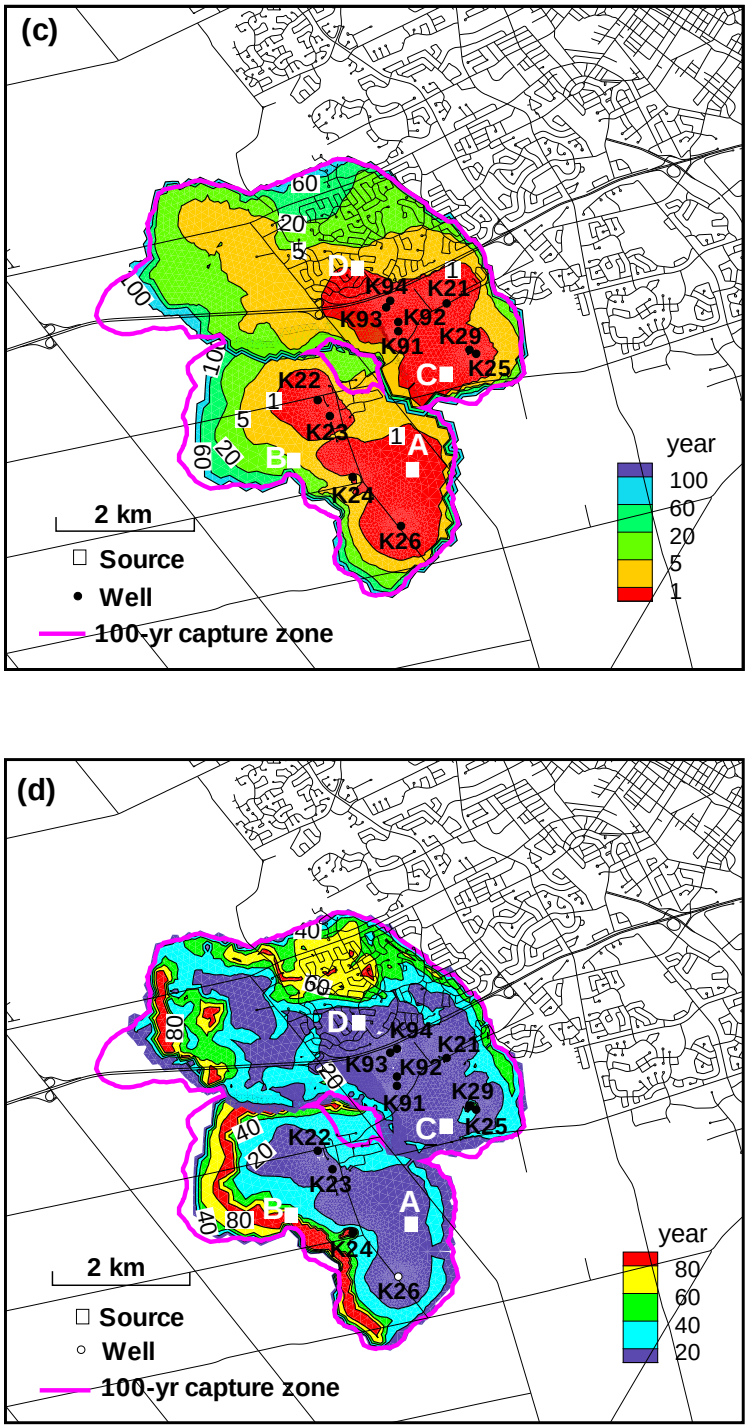

Figure 6.20: Vulnerability maps for the Mannheim well field, lumped approach: (c) time taken to breach a threshold concentration of 10^{-9}, and (d) exposure time to above-threshold concentrations.

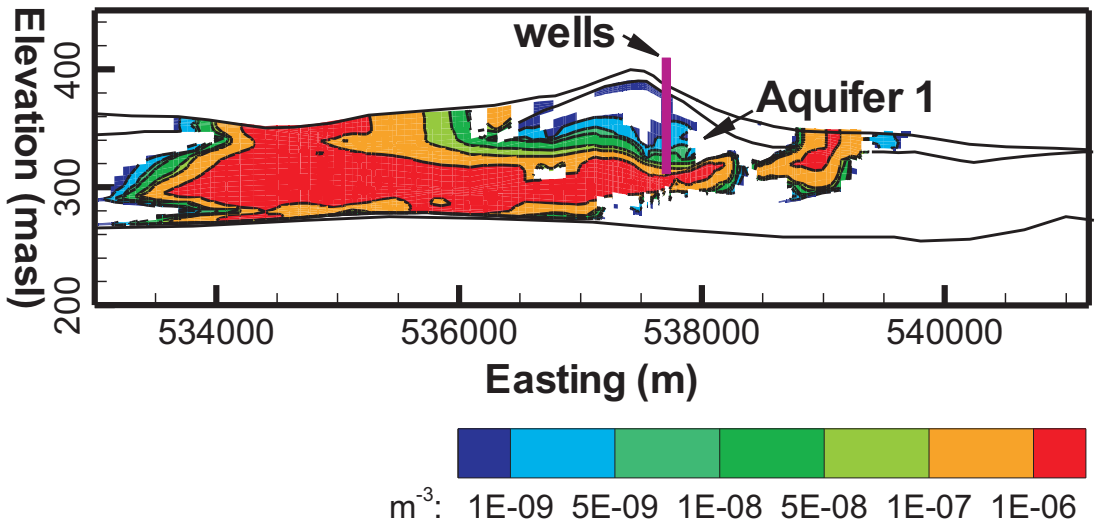

Figure 6.21: Vertical cross-section along the wells K93 and K94 (see Fig. 6.13(a)), showing contours of the backward travel time pdf at the Mannheim North well field.

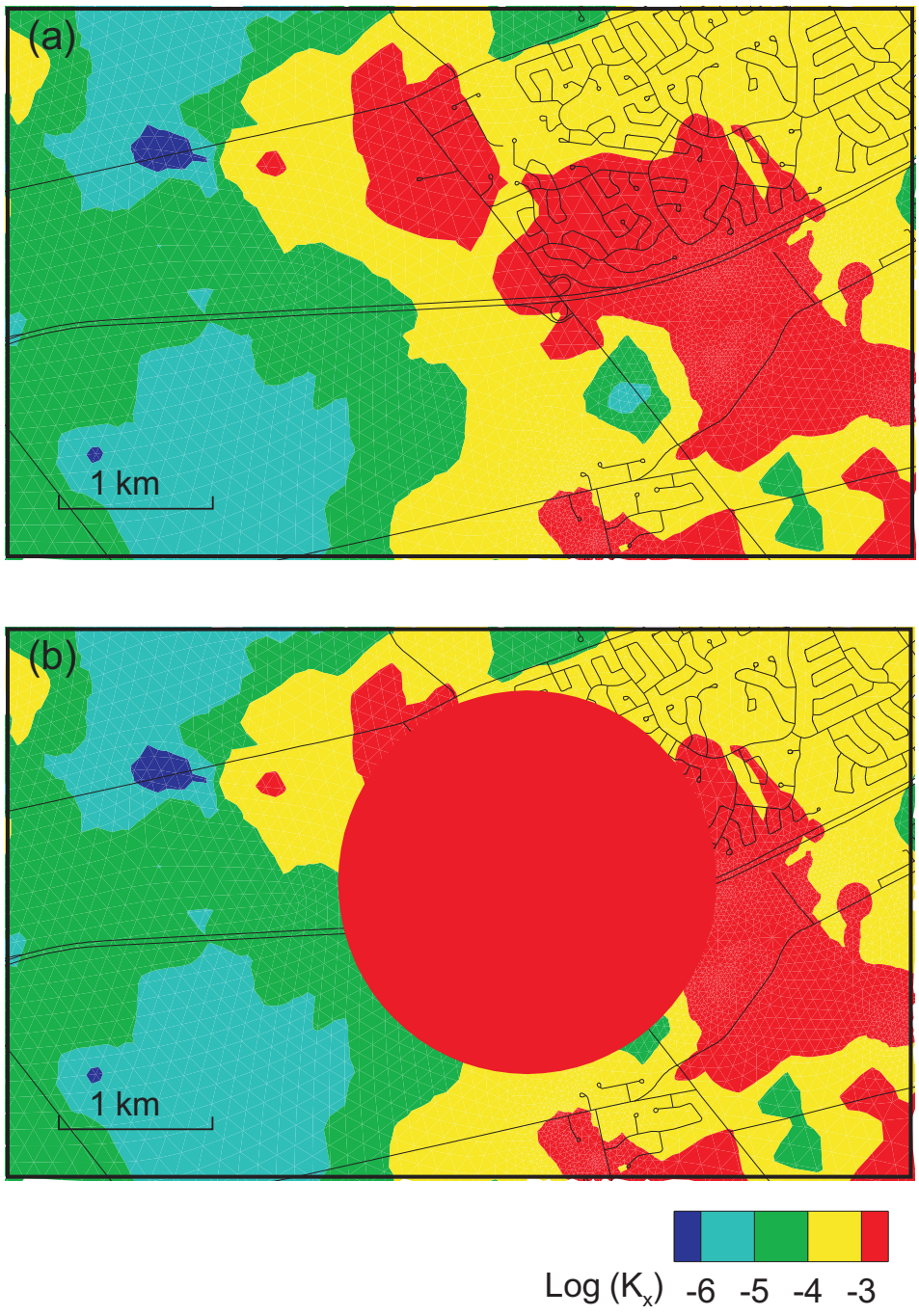

Figure 6.22: Hydraulic conductivity K_x of Aquifer 1 (K_x in m/s) within the areas of Cluster 5 in the Mannheim North well (a) original, (b) modified (as shown in red circle).

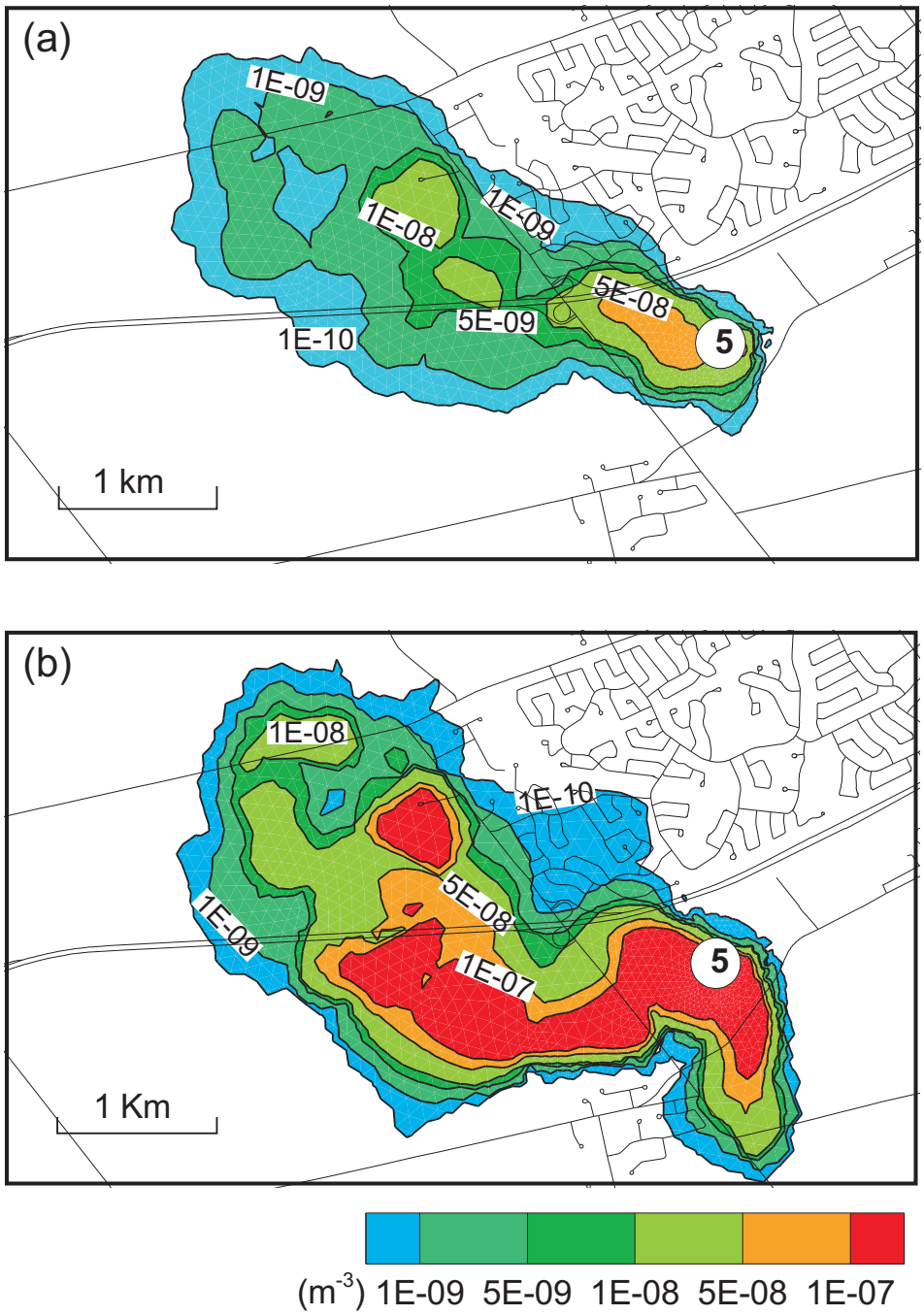

Figure 6.23: Maps of maximum expected relative concentration of well cluster 5: (a) before, (b) after adding high conductivity lenses.

Chapter 7

Quantitative Assessment of Risk

Risk assessment is formally defined as the "characterization of the potential adverse effects of human exposure to environmental hazards" [NRC, 1983]. Current approaches to assess the risk of groundwater contamination are essentially qualitative, where the risk may be defined subjectively, involving human judgment. For example, risk may be defined in a particular situation as low, moderate or high, requiring some standard to which the risk may be compared. Such approaches provide little information about the potential cost of well contamination.

In this chapter, we will explore a quantitative approach of risk assessment. Part of this work has been published in the proceedings of the IAH Groundwater Conference [Rahman et al., 2007].

7.1 Mathematical Definition of Risk

In mathematical terms, risk is defined as the probability of an event, multiplied by the consequence of the event. Risk can also be expressed as the expected loss associated with an event. In this study, risk is defined as the probability of a well becoming contaminated at some unacceptable level, multiplied by the cost of remediation or replacement of the well. The presence of potential contaminant sources within the WHPA that pose a threat to contaminating a drinking water supply well can be determined using the concept of well vulnerability. The method includes source mass characteristics, physical processes along the pathway from the source to a water supply well, and the concentration distribution in the well water. The results provide the exposure value and the time frame within which the well will

become contaminated, and can be used to estimate the cost of remediation or replacement of the well.

The shape of the concentration breakthrough curve at the well will depend on the source mass characteristics, i.e. the initial spatial and temporal distribution of the contaminant mass at ground surface, and the characteristic of the pathway from source to well. The magnitude of the contaminant concentration at the well depends on the amount of the source mass available to leach into the ground. If the amount is very low, it is likely that the critical concentration will never be observed at the well. On the other hand, if the mass of contaminant is very high, the expected concentration at the well will be higher and the duration of exposure can be longer.

The probability of a well becoming contaminated depends on the contaminant migration path from the source to the receptor. The factors which play an important role in contaminant migration are the physical characteristics of the aquifer, soil and geologic materials, the amount and nature of recharge and discharge into or out of the system, and the chemical characteristics of the contaminant and porous medium (i.e., sorption coefficient, degradation rate, solubility etc). The contaminant concentration in the well water includes well bore dilution due to mixing of contaminated water with clean water. Well bore dilution often significantly reduces contaminant concentrations in the well water as compared to concentrations in the aquifer [Einarson and Mackay, 2001]. The amount of dilution occurring at the well depends on the capacity of the well. Einarson and Mackay explain that the dilution factors are high in large capacity wells that draw in large amounts of clean water along with a contaminant plume. On the other hand, smaller wells may see little dilution if situated in the path of a plume.

A drinking water supply well will become contaminated if the expected concentration in the well water exceeds the maximum allowable concentration for a particular contaminant. The risk of contamination exceeding the allowable limit can be calculated by determining the exposure value according to [Archer and Shogren, 2001]:

$$Exposure\ value = \frac{Contaminant\ concentration}{Environmental\ benchmark} \tag{7.1}$$

An exposure value greater than unity indicates that the probable concentration will exceed the environmental benchmark, whereas an exposure value less than unity indicates that the contamination is within allowable limits. In this study, the ex-

pected contaminant concentration in the well water is estimated using the concept of well vulnerability.

The well vulnerability maps (as presented in Chapter 6) show the response to pulse sources of contamination that can be located anywhere within the well capture zone. The response represents the vulnerability of a well, which is defined as the vulnerability of the groundwater to contaminants, taking into account the inherent geological, hydrological, and hydrogeological characteristics, but independent of the nature of the contaminants [Vrba and Zoporozec, 1994]; [Brouyère et al., 2001]. For any particular contaminant or group of contaminants, including contaminants from distributed and time-varying sources in which the source mass and characteristics are known, but the location is unknown, the concentration distribution at the well can be evaluated by convoluting the source mass with the response of a pulse source. Convolution is a well-known and effective superposition method to deal with arbitrary inputs in time and space for linear systems. Detailed description of the convolution theory is given Appendix B.

For a known source mass of $M(t)$ distributed over a region of finite size Δ, the contaminant concentration at the well can be written as:

$$C(x_i,t) = \frac{1}{Q_w}\int_{\Omega}\left(\int_t \psi^*(x_i,\gamma)M(t-\gamma)d\gamma\right)\delta(x-x_i)d\Omega \qquad x_i\ \varepsilon\ \Delta \tag{7.2}$$

where $\psi^*(x_i,t)$ is the backward travel time pdf, and Q_w is the well pumping rate. The value of $C(x_i,t)$ in Eq. (7.2) can be interpreted as the probability of the well becoming contaminated to this value, due to a source applied at the given location (x_i).

For a known contaminant source mass, the concentration distribution at the well can be calculated by applying the forward ADE for each source. This approach requires a large number of simulation runs if there are many potential sources. The contaminant concentration at the well for the same known source mass can also be calculated using equation (7.2). Equation (7.2) simply convolute the known source mass with the results of the backward model without further use of the model. The backward model only requires one simulation run for all potential sources.

To demonstrate the equivalence of these two approaches, we use the conceptual domain presented in Chapter 5 (see Figure 5.1). The flow and transport boundary conditions are the same, except that the contaminant source releases a mass

of 1 kg/day for 300 days and 2 kg/day from 300 to 2000 days. The flow solution for this system is first developed using the 3D finite element model WATFLOW [Molson et al., 2002]. Using the steady-state head distribution, the concentration distribution at the well is calculated using the solute transport model WTC [Molson and Frind, 2004] in forward or backward mode. In the forward approach, the concentration breakthrough at the well is calculated using the standard ADE. In the backward model, the travel time pdf is first observed at the source location by applying a unit pulse conservative source at the well. The concentration breakthrough at the well is then calculated by convoluting the source mass with the travel time pdf using equation 7.2. Figure 7.1 shows that the concentration distribution at the well is the same for the two approaches. Equation (7.2) is used later in the chapter to obtain the concentration distribution of known potential contaminant sources located arbitrarily within the well capture zone.

7.2 Cost of Well Contamination

Selected information from the above distributions of well vulnerability can be used to develop a distributed expression of quantitative risk. We can merge the exposure value and the time taken to reach this value into a single quantity expressing risk in terms of the investment that must be made today to have the funds required for remedial action when needed. If the action can be staged or delayed, the cost is usually easier to manage. The present value of the investment can be estimated using the following equation:

$$P = \frac{E}{e^{r_c t}} \tag{7.3}$$

where E is the future cost of an alternative reduction measure based on the severity of the well contamination, r_c is the interest rate compounded annually, and P is the investment that has to be made today, so that amount E will be available after t years. Equation (7.3) allows calculation of the present value of investment in terms of the future cost of remediation.

7.3 Quantitative Risk Analysis

Wells K22 and K23 (cluster 1) within the Mannheim South well field are used to demonstrate the above approach. We assume a point source of contamination located arbitrarily within the 60-year capture zone of well cluster 1. The source

releases a mass of 100 kg/day continuously for 30 years.

The 3D groundwater flow model developed by Martin and Frind (1998) is used as a basis for simulating the concentration distribution at the wells. The description of the boundary conditions, recharge rate, well pumping rates, and hydraulic conductivity values in the aquifer and aquitard layers are given in Chapter 2 and Chapter 4. The concentration distribution at each well within well cluster 1 due to a source located arbitrarily within the capture zone is obtained by convoluting the response function with the source mass, using Equation (7.2).

The response function can be obtained from the vulnerability maps of well cluster 1, which can be developed using the backward-in-time transport model. The vulnerability maps for well cluster 1 developed in Chapter 6 are also reproduced here. The unit pulse source is first distributed between the wells based on the pumping ratio of the individual wells within the cluster to the total flow rate of the cluster. Using backward-in-time transport modelling, the impact of the pulse sources at the wells is expressed in terms of the maximum expected concentration in the well water (Fig. 7.2(a)) and the time required to reach the maximum expected concentration (Fig. 7.2(b)). The vulnerability maps generally show that wells are highly vulnerable to sources located near the wells and less vulnerable to sources further away. Exceptions as shown in Chapter 6 are associated with the presence of high conductivity lenses in Aquitard 1 overlying Aquifer 1.

The maximum exposure values of contamination at well cluster 1 can be determined from Equation (7.1). These are unitless measures of source concentrations normalized using the threshold value (i.e, drinking water standard (DWS)). In this case, we assume that DWS for the contaminant is 0.01 mg/L. With respect to risk, the most useful information consists of the exposure value (Eq. (7.1)) and the time taken to reach the exposure value. These values are shown in Figure 7.3. Figure 7.3(a) shows that under the given conditions, the exposure value of a point source will be exceeded for most source locations within the capture zone of wells K22 and K23. For the area within the 1-contour, which in this case includes most of the capture zone, some form of corrective action will be necessary, possibly in the form of blending the well water with cleaner water, treatment of the water, replacement of the well, or reducing the source mass input. For a source outside the 1-contour, no immediate remedial action is required, but the site would need monitoring.

The question is now whether all areas within the 1-contour should have the same priority with respect to remedial action. This question can be clarified by using the information from Figure 7.3(b), which shows the time taken to reach DWS of 0.01 mg/L. We can either use this time to determine a ranking of priorities, or to calculate the investment that must be made today in order to have the required funds available for remediation at the appropriate time.

Figure 7.4 shows the investment value required per dollar to remediate wells K22 and K23. The present value of investment varies between 0.37 to 0.95 within the contour of exposure value 1. For example at point X′, the present value of investment is 0.37. In this calculation, for simplicity we assume that the interest rate is equal to 5 percent and is compounded annually. Figure 7.3(b) shows the time frame, which is about 20 years. Thus we have the choice of postponing action for 20 years, or investing about 37 cents per dollar of the estimated cost of remediation now in order to have the required funds available in 20 years. In this way, the risk of the well becoming contaminated can be expressed quantitatively.

7.4 Conclusion

The concept of well vulnerability provides a basis for the quantitative assessment of the risk of well contamination. The concept is used to create exposure maps that quantify the threat to a well due to contaminant sources within the well capture zone. The exposure maps can then be integrated with the time element to create distributed maps of quantitative risk expressed in terms of the cost of remediation or replacement of the well. This approach should be useful for complementing present risk assessment methodologies based on subjective judgement.

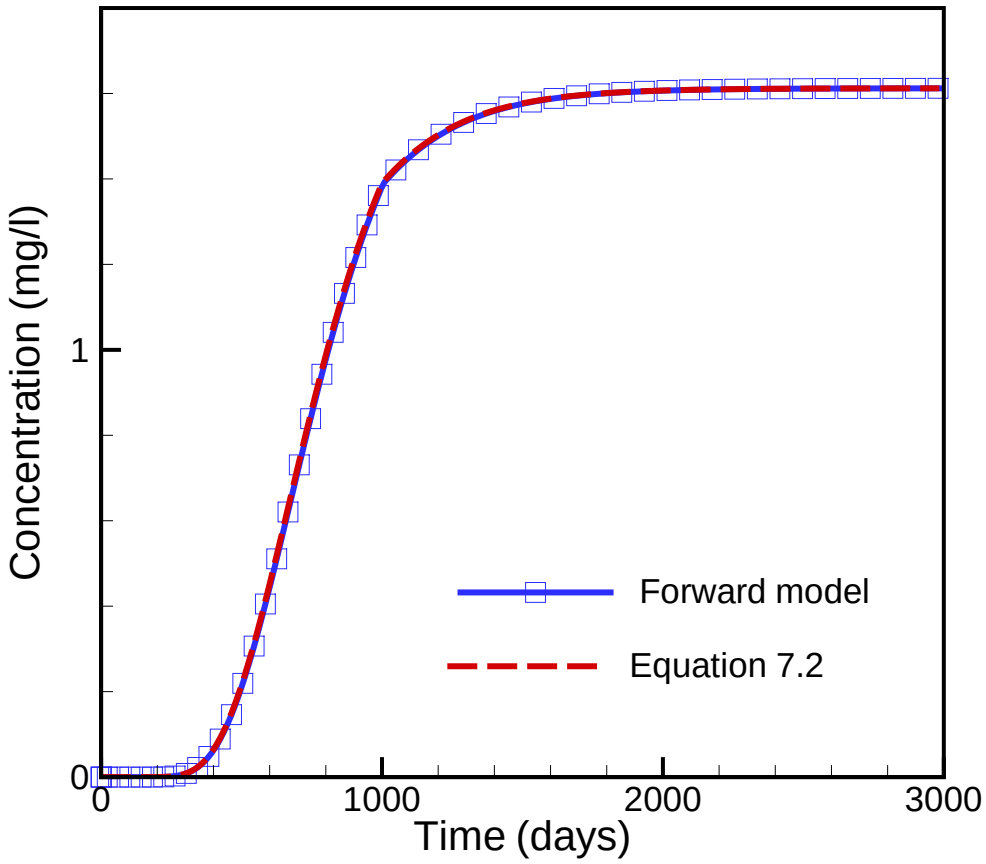

Figure 7.1: Forward and backward breakthrough for a time-varying conservative source.

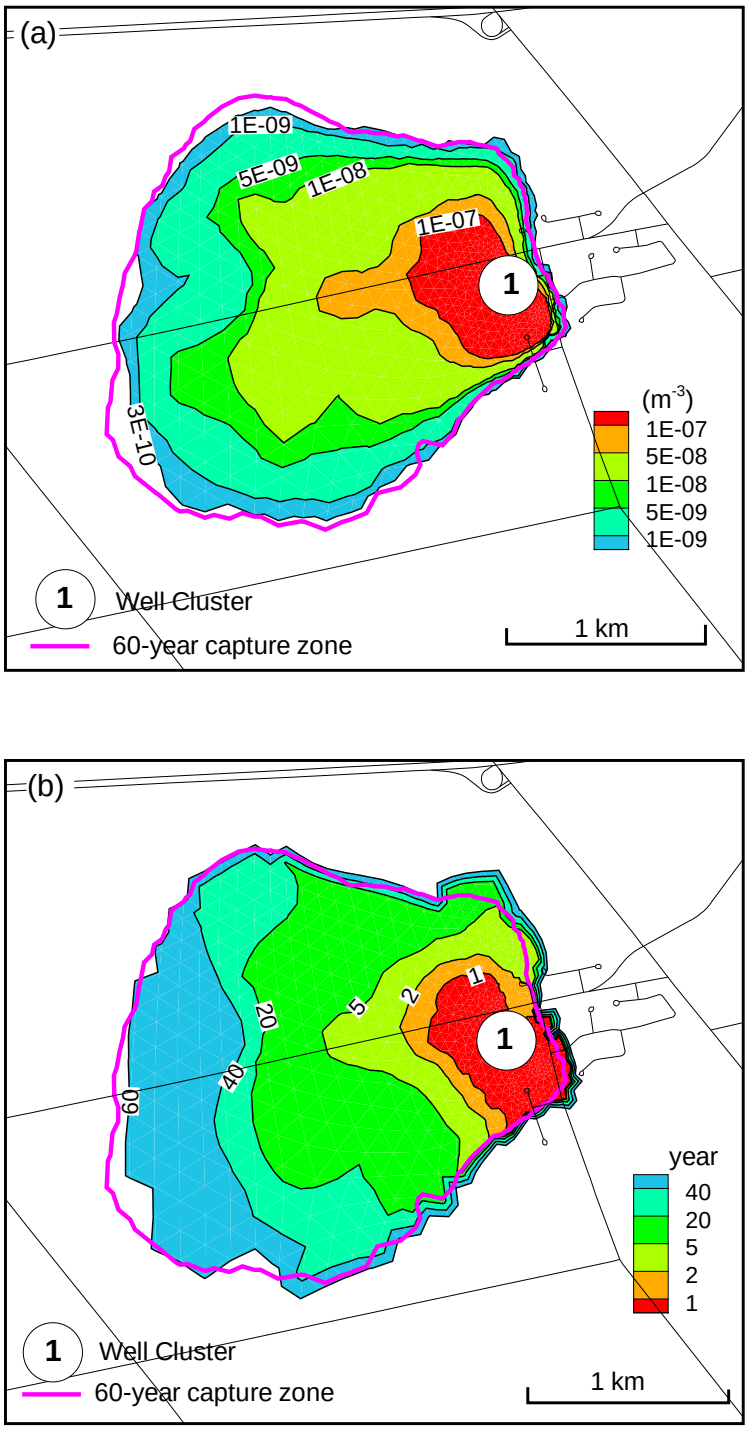

Figure 7.2: Well vulnerability maps for well cluster 1 due to unit pulse conservative sources: (a) maximum expected concentration at the wells, (b) time taken for the maximum concentration to reach the wells.

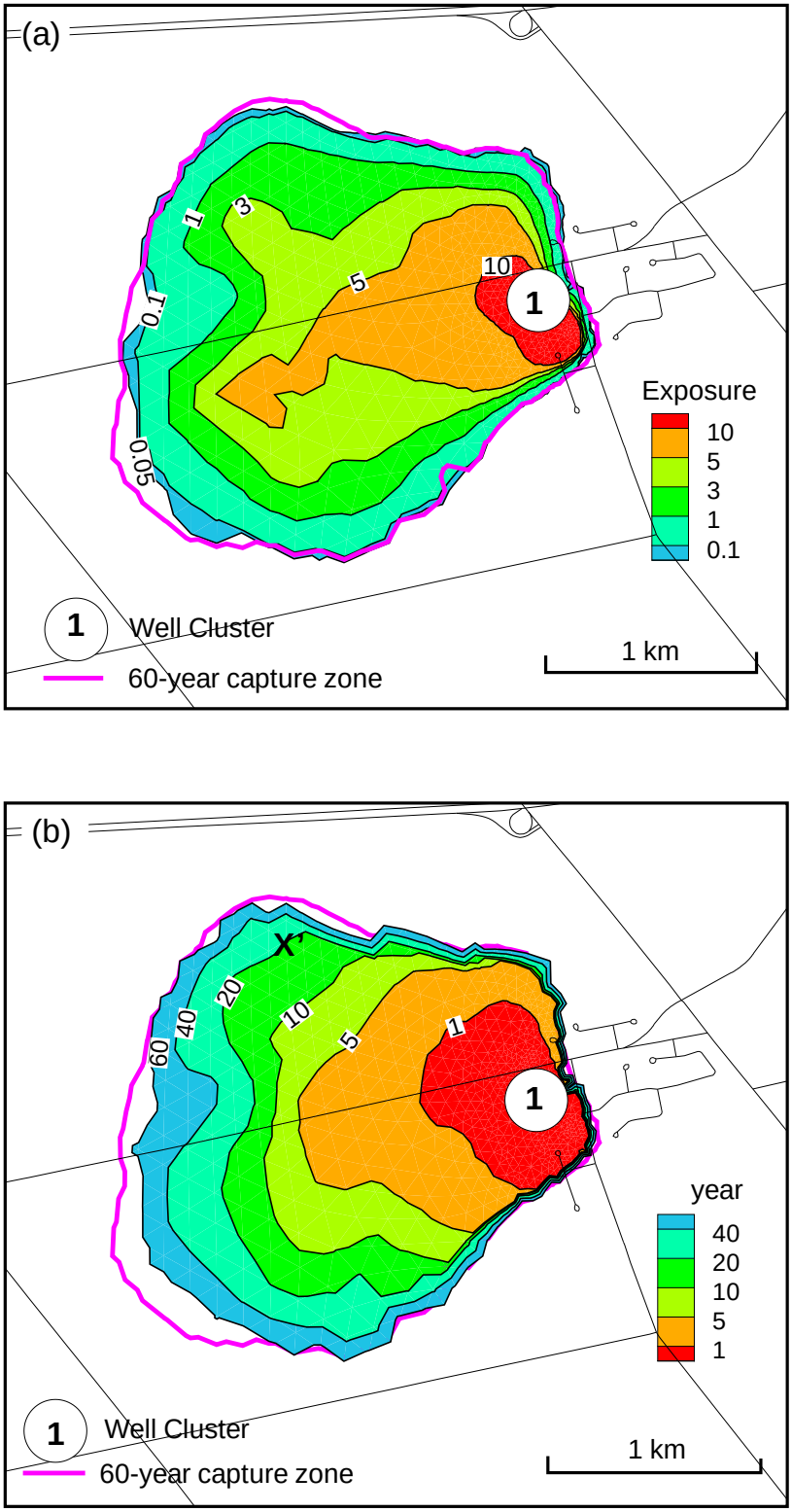

Figure 7.3: Quantitative risk assessment of point sources of contamination at well cluster 1: (a) maximum exposure value; (b) time required to reach the drinking water standard of 0.01 mg/L.

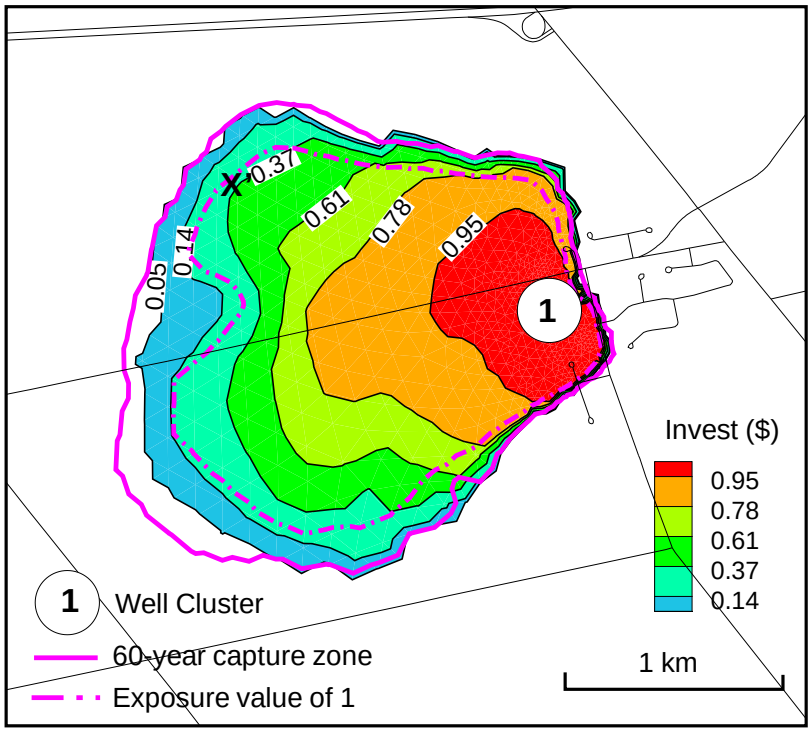

Figure 7.4: Investment value for well remediation of cluster 1, per dollar.

Chapter 8

Beneficial Management Practices

One of the options to reduce contaminant concentrations in the wells is to implement Beneficial Management Practices (BMPs) within WHPAs. In this study, the concept of well vulnerability is used to identify the best location within a WHPA to apply BMPs. The BMP investigated for this example is the reduction in nutrient land application rate as part of a routine crop fertilization program to reduce leaching below to root zone.

8.1 Impact of Nitrate Contamination at Well K26

The Mannheim South wells have historically exhibited high nitrate concentrations, in particular well K26 [CH2M-Hill, and Papadopulous and Associates Inc., 2003]. The primary land use within the Mannheim area is agriculture, which is also a potential source of nitrate. Short-term exposure to drinking water with a nitrate level at or just above the health standard of 10 mg/L nitrate-N is a potential health problem primarily, for infants. High levels of nitrate cause the condition known as methemoglobinemia, also known as "blue baby syndrome". The Mannheim South well field is located near the village of Mannheim and is a primary supply well field for the Region.

The land use map as presented in Figure 8.1 shows that most of the area within the capture zone of well K26 is used for agricultural activities. We assume that corn is the only crop planted within the area. The historical nitrogen fertilizer application rate for a corn field ranges from 157 to 190 kg-N/ha annually [Bekeris, 2007]. Figure 8.2 shows the dramatic increase of fertilizer consumption in Canada since the

1950s [Haslauer, 2005]. This increase in fertilizer consumption has resulted from an increase in average farm size, intensification of the farm process, and externalizing of farming costs to the detriment of the environment [Phipps, 1991]. Nitrogen fertilizer that is not taken up by crops is volatilized or carried away by surface runoff and the rest leaches to groundwater in the form of nitrate.

8.1.1 Modelling

For any known contaminant sources, the common approach is to use the standard advection-dispersion equation. Using equation (5.1) and the appropriate boundary conditions, the expected nitrate concentration at well K26 can be determined. The simulation was performed using nitrate concentrations ranging from 9.5 to 12.0 mg/L, which is estimated assuming a leaching rate of 23 to 30 kg-N per ha per year from corn land and using an average recharge rate of 250 mm/year. The recharge value was obtained from 3D flow model (WATFLOW) calibration. As mention in Chapter 4, an initial uniform recharge of 530 mm/yr is applied over the entire ground surface and of this potential recharge, approximately 260 mm/yr of recharge out of the system via stream runoff by means of a thin (0.1 m) highly permeable RSL. The rest about 250 mm/year recharges to the lower aquifer. In the transport model, these concentrations are entered as a mass flux boundary condition (i.e., Cauchy boundary condition), where the vertical Darcy flux is obtained from the element layer immediately below the RSL (which is removed from the transport grid). This flux varies spatially depending on the local conductivity and the flow system. According to a lab report (source: Region of Waterloo, 1969) the nitrate concentration in 1969 at well K26 was 2.5 mg/L. In this simulation, nitrate concentration of 9.5 mg/L is applied from year 1967 to 1969 to reach the initial nitrate concentration of 2.5 mg/L at well K26.

The major assumptions in the transport model are that the flow field is at steady state and nitrogen fertilizer is applied uniformly over time, rather than at a variable seasonal rate. The nitrate input rate is calculated by assuming an average annual recharge rate. Denitrification is not taken into account. The study also assumes that well K26 is pumping at a constant rate throughout the simulation period. In reality, the wells within the Mannheim well field pump into adjacent reservoirs at varying rates, and from there, water is delivered into the municipal water mains. Wells are normally pumped from early morning to early evening about 12 hours per day from October to April when the demand is relatively low. During the rest

of the year, demand is higher and wells are sometimes continuously pumped for several days.

In flow modelling, calibration is typically achieved by adjusting hydraulic conductivity and/or recharge to simulate hydraulic heads and base flows observed in the field. Calibration of large-scale flow models, however, is typically not sensitive to local scale changes in hydraulic conductivity. During the flow model calibration, errors in the simulated conductivity field near pumping wells may go unnoticed whereas they may have profound effects on the transport simulation (as shown in Chapter 5). The transport model simulation is based on adjusting the loading and the timing of application rates following the trends in the nitrogenous fertilizer consumption in Canada as shown in Figure 8.2. Bester (2002) calibrated a similar model for road salt impact by adjusting the salt input.

Figure 8.3 shows that the simulated nitrate concentration passes approximately through the center of the data points. The simulated results show that the nitrate concentration in the well water continue to increase up to 2006. The concentration profile shows a small jump about 2002 resulting from an increase in input concentration from 10.0 to 11.5 mg/L. The maximum expected concentration in the well water is below Ontario′s Maximum Acceptable Concentration (MAC) of 10 mg NO_3−N/L for nitrate in drinking water. The calibrated model is used to forecast the impact of the nitrate loading at well K26 for 20 years beyond 2006, using an input concentration of 12.0 mg/L. Figure 8.4 shows nitrate concentration increases only slightly beyond 2006, reaching steady-state in about 2010.

8.2 Implication of Beneficial Management Practices (BMPs)

In the Province of Ontario, many drinking water supply wells show increasing threat due to elevated nitrate concentrations. Regulators and water resource managers within the province have introduced both mandatory and voluntary standards for agricultural practice to reduce the nitrate losses [Bekeris, 2007]. The provincial nutrient management regulators have set up criteria for the land application of nutrients, such as set-backs from drinking water wells and restrictions on winter application [Nutrient Management Act, 2002]. Farmers are also encouraged to further enhance soil and water protection by implementing BMPs. These are improved

estimates of crop′s fertilizer needs, spatially adjusted and properly timed fertilizer application and the use of cover crops when commercial crops are not being grown (Ontario Ministry of Agriculture and Food [OMAF, 1994]). Padusenko (2001) estimated the time frame for changes in land-use management focussed on reducing nitrate to cause a decrease of nitrate concentration within the Thornton supply wells (which produces 50% of the drinking water for the city of Woodstock). Haslauer (2005) also investigated the effects of agricultural land-use changes within the 2-yr capture zone of the Thornton well field on the nitrate concentrations in the suppy wells of the Thornton well field.

8.2.1 Scenario Analysis

For the purpose of the analysis, we have applied BMPs immediately after 2003 (where well K26 sees a jump in concentration) for a period of 23 years to reduce the nitrate impact on well K26. The well vulnerability map showing maximum relative concentration (Fig. 8.5) is used to identify the locations for the application of BMPs. Four test areas (A,B,C,D), each of approximately 48 ha in size, are located within the capture zone of well K26, as shown in Figure 8.5. Several scenarios of BMPs were designed and described in Table 8.1.

Scenario 1 - Reduction of Nitrate Input from 12.0 to 8.8 mg/L

In this scenario, the nitrate concentration is reduced from 12.0 to 8.8 mg/L everywhere within the well capture zone after 2003. Initially the nitrate concentration in the well gradually decreases and then starts increasing slightly until the steady-state condition is reached at about 2023 (shown in Fig. 8.6). Scenario 1 reduces the nitrate concentration by up to 1.6 mg/L in the well water.

Scenario 2 - Eliminate Nitrate from Farm Area A

In Scenario 2, the nitrate input is eliminated in Area A and continued at 12.0 mg/L elsewhere. The nitrate concentration in well K26 (Figure 8.6) shows an immediate response to the reduction, as fresh water infiltrates and allows the nitrate to be diluted. The maximum reduction occurs after 1 year of application of BMPs. After 1 year, nitrate originating from the other areas reaches the well, and the nitrate concentration begins to rise. Steady-state conditions are reached in about 2024. Scenario 2 reduces the nitrate concentration by up to 3.8 mg/L in the well water.

Table 8.1: Predictive scenarios

Scenario	Title	Descriptions
1	Reduction of nitrate input from 12.0 to 8.8 mg/L	Apply lower nitrate concentration everywhere within the steady-state capture zone of well K26
2	Eliminate nitrate from farm area A	Farm Area A is located around the well (shown in Figure 8.5)
3	Eliminate nitrate from farm area B	Farm area B is located to the north of well K26 (shown in Figure 8.5)
4	Eliminate nitrate from farm area C	Farm area C is located to the west of well K26 (shown in Figure 8.5)
5	Eliminate nitrate from farm area D	Farm area D is located to the east of well K26 (shown in Figure 8.5)
6	Eliminate nitrate from farm areas B and C	Farm areas B and C are located within the vulnerable areas of well K26 (shown in Figure 8.5)

Scenario 3 - Eliminate Nitrate from Farm Area B

In Scenario 3, the nitrogen fertilizer is eliminated within the chosen farm area B. Initially, the nitrate concentration in well K26 sharply declines and reaches its minimum value in 2 years. After 2 years, the nitrate concentration begins to rise until the steady-state condition is reached about 2024 (Figure 8.6). Application of BMPs in the farm area B will lower the nitrate concentration in the well water by 2.0 mg/L.

Scenario 4 - Eliminate Nitrate from Farm Area C

In Scenario 4, the nitrate concentration in the well K26 follows the same trend as Scenario 3; the nitrate concentration slowly declines and reaches a minimum value after 6 years, and then increases until the steady-state condition is reached

about 2024 (Figure 8.6). Because area C is remote from the well, the effect of the reduction is not felt at the well until 4 years after inputing the change. Application of BMPs in the farm area C will lower the nitrate concentration in the well water by 1.6 mg/L.

Scenario 5 - Eliminate Nitrate from Farm Area D

In Scenario 5, the nitrate concentration also goes down due to reduction of nitrogen fertilizer on farm area D. The concentration distribution follows the same trend as shown in Figure 8.6. However in this scenario, the nitrate concentration is reduced by a maximum of 0.9 mg/L in the well water.

Scenario 6 - Eliminate Nitrate from Farm Areas B and C

In this scenario BMPs are applied within the farm areas B and C together. As more fresh water enters the system, the nitrate concentration in well K26 decreases more. The maximum reduction of the nitrate concentration in well K26 occurs after 8 years and the concentration then starts increasing slightly until steady-state condition is reached about 2024 (Figure 8.6). Scenario 6 has the same effect as Scenario 3 and 4 together, suggesting that impact due to BMPs applied to different areas may be additive under certain condition.

8.3 Discussion

In all scenarios, recharge entering the system at the surface allows fresh water to flush through the aquifer, reducing the nitrate concentration in the well water. However, the application of BMPs on farm area A, which surrounds the well, shows the most sensitive response to the nitrate reduction. The second most sensitive option is the reduction of nitrate application within farm area B. The simulation results suggest that within farm areas A and B, the pumped aquifer is hydraulically well-connected to the surface which allows fresh water to enter into the system and significantly dilute the nitrate plumes. The reduction of nitrate input on farm areas B and C together will also lower the concentration in the well water. Other scenarios give similar but less sensitive responses.

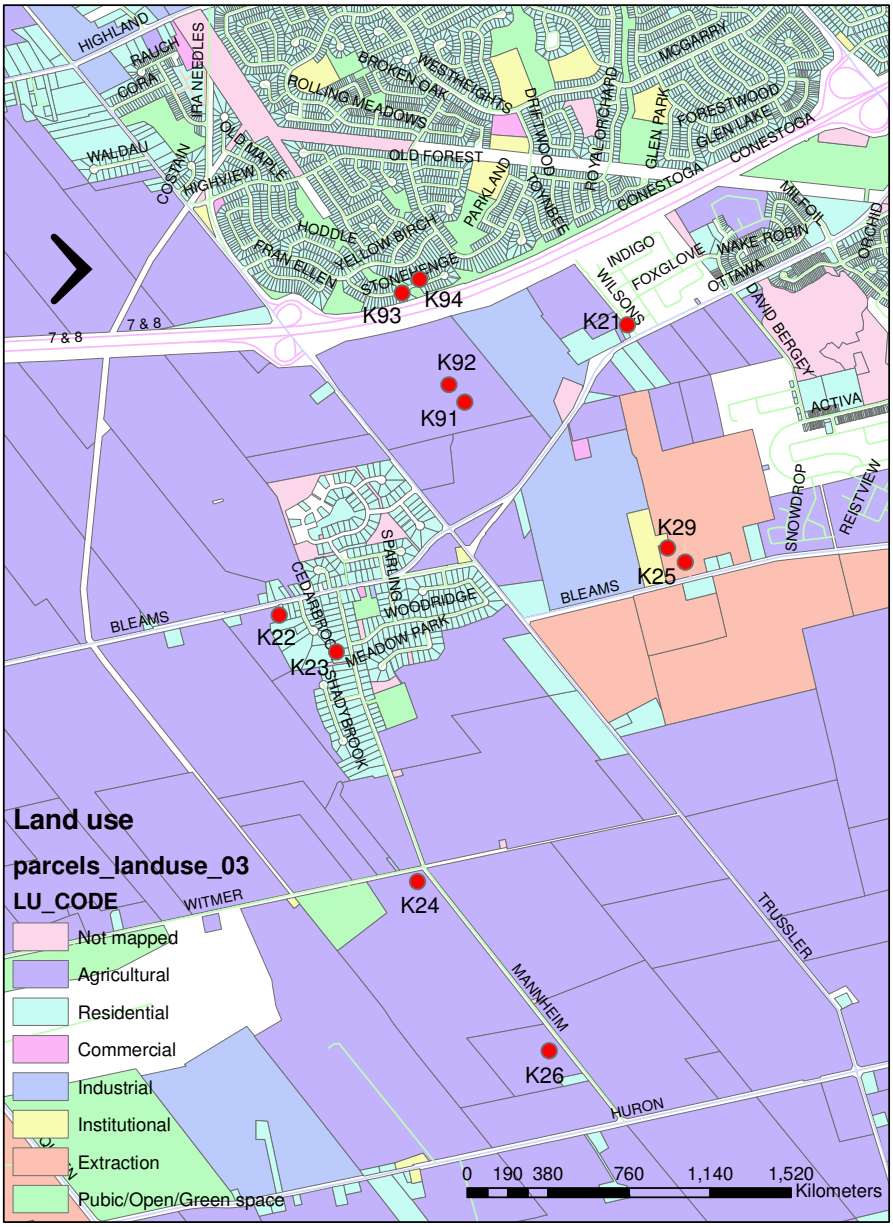

Figure 8.1: Land use map within the Mannheim well field (data from Teranet Waterloo).

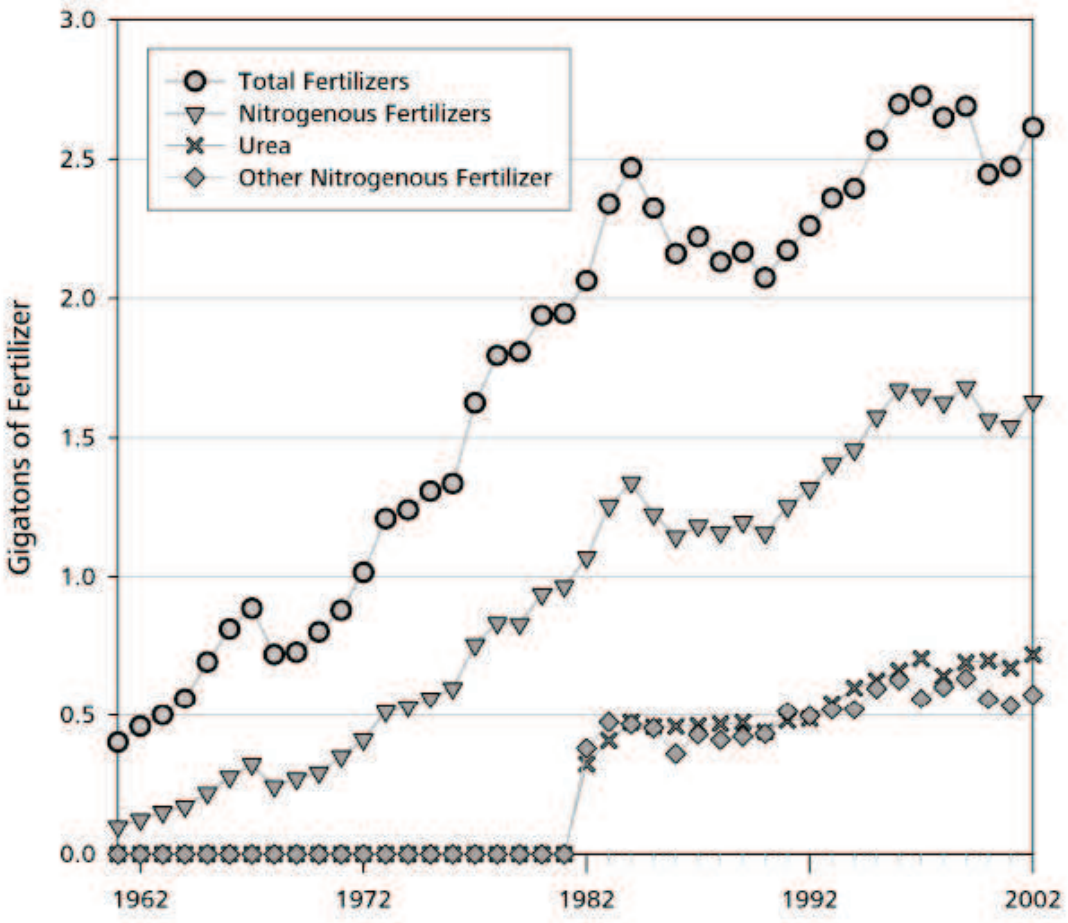

Figure 8.2: Development of fertilizer consumption in Canada. Some minor nitrogen−containing fertilizers, including calcium ammonium nitrate, are not shown. Data from the Food and Agriculture Organization of the United Nations, 2005.

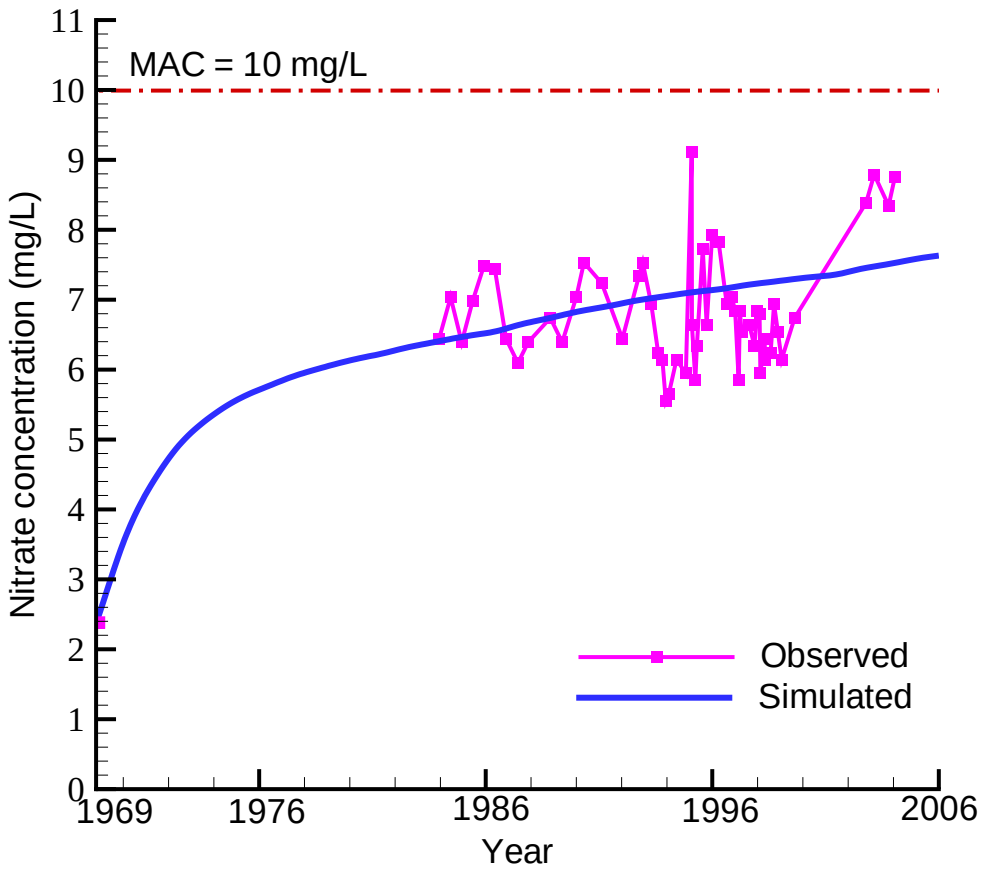

Figure 8.3: Expected nitrate concentration distribution at well K26.

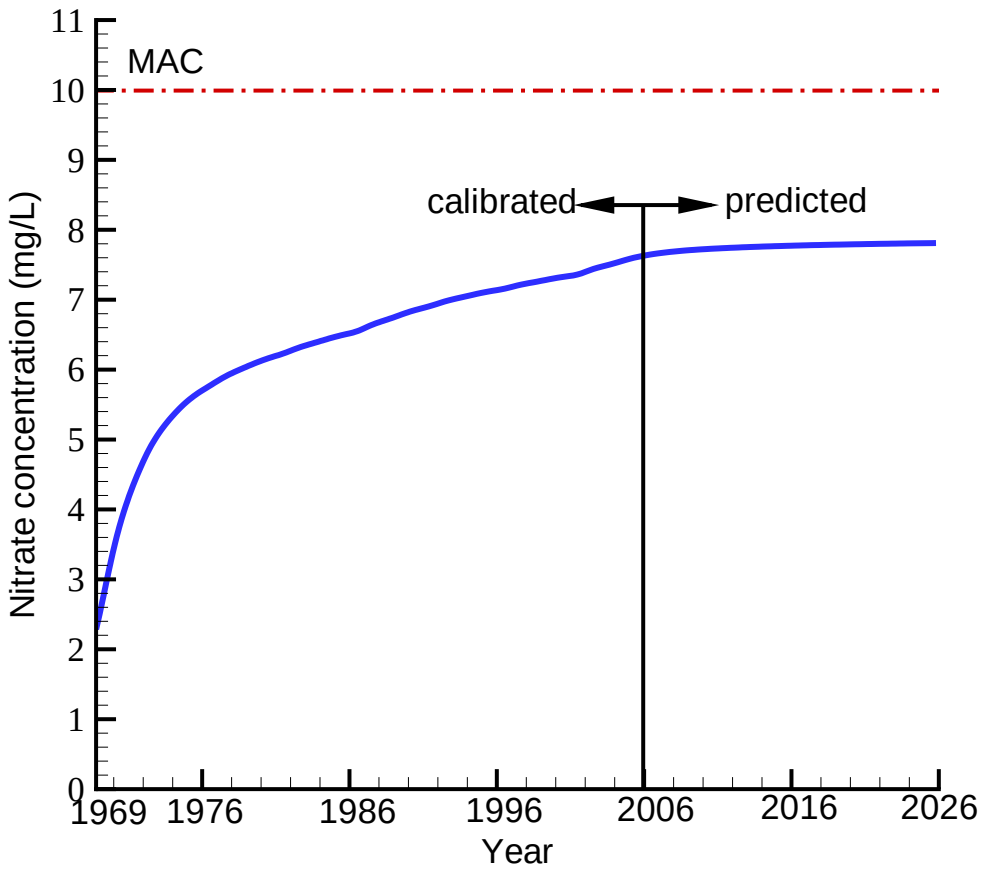

Figure 8.4: Predicted nitrate concentration at well K26 for 20 years from 2006.

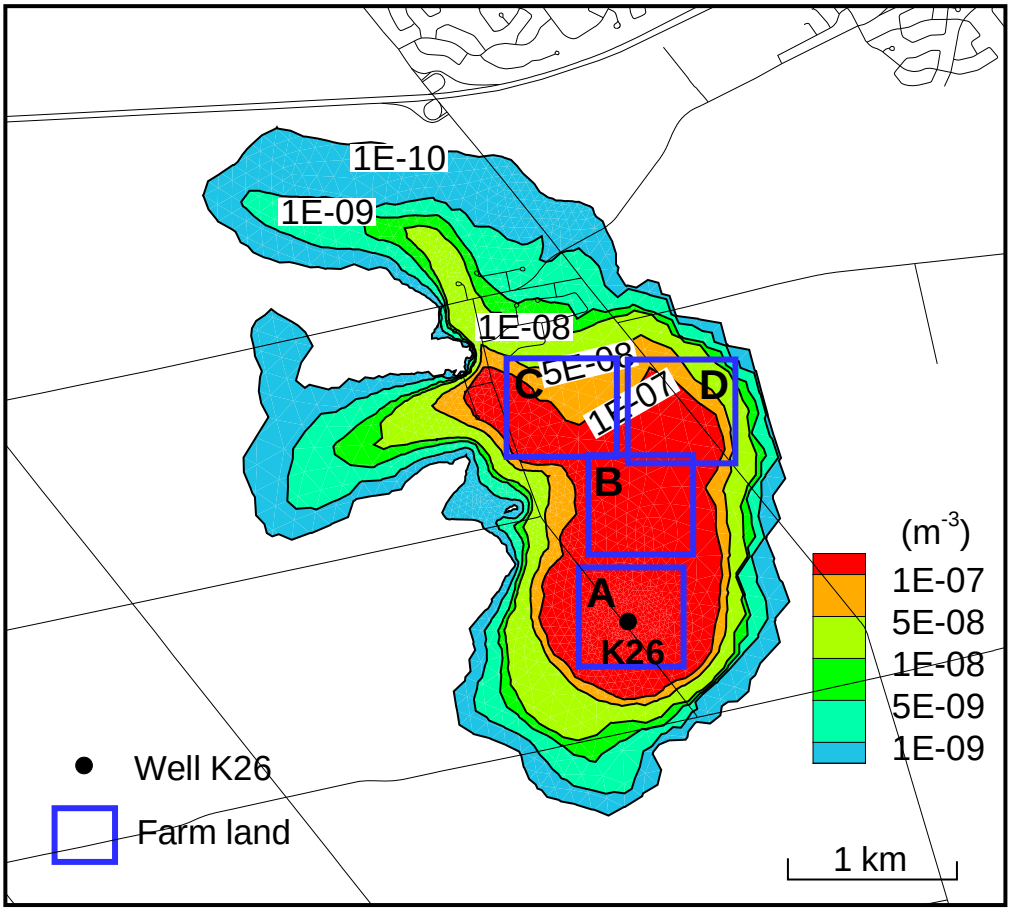

Figure 8.5: Location of farm areas within well cluster 3 showing maximum relative concentration.

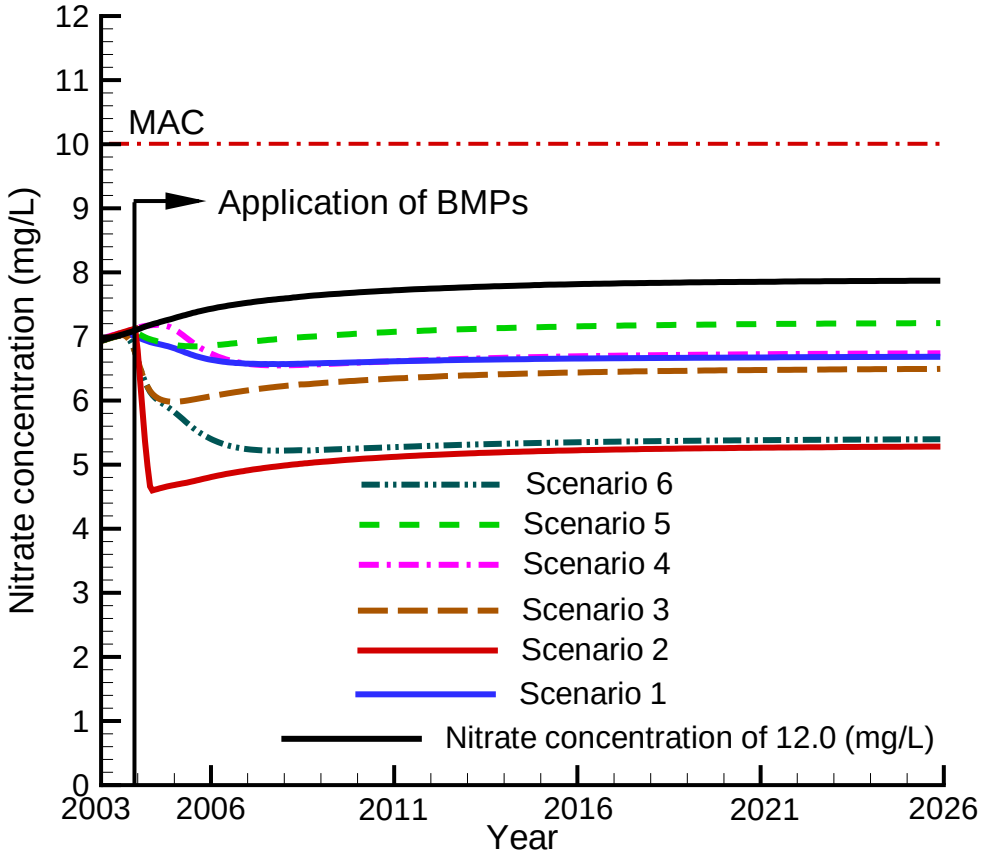

Figure 8.6: Expected nitrate concentrations at well K26 due to application of BMPs on the selected farm areas.

Chapter 9

Conclusions

9.1 Conclusions

This thesis focuses on the comparative evaluation of current tools for groundwater source protection and on the improvement of various aspects of source protection methodology. The methodology for source water protection (SWP) is centered on key concepts: aquifer vulnerability, the delineation of wellhead protection areas (WHPAs), well vulnerability, and the assessment of risk to wells.

Three approaches for assessing aquifer vulnerability are compared: the Intrinsic Susceptibility Index (ISI), the Hydraulic Resistance (HR), and the Surface to Aquifer Advection Time (SAAT). The comparison is made by applying these approaches to two key well fields in the Waterloo Moraine: the Mannheim well field, which extracts water from a partly unconfined aquifer, and the Greenbrook well field, which extracts water from a confined aquifer. For both scenarios, the ISI-values are dominated by the thickness of the overlying layers above the target aquifer while under-estimating the impact of the hydraulic conductivity. This suggests that the ISI method may give inaccurate results if the overlying layers consist of materials with widely varying hydraulic conductivity. HR uses the same data as ISI except for porosity, and gives a physically valid representation of vulnerability on the basis of time-invariant parameters of the system (i.e. not including flow system parameters). SAAT includes all relevant parameters and gives the most useful result in terms of advective time. SAAT has no meaning in areas of upward or zero gradients since water is not entering the system. In these situations the aquifer is considered not vulnerable. In cases of uncertain unsaturated-zone parameters, saturated conditions can be assumed throughout, which is a conservative assumption.

Under these assumptions, HR and SAAT give identical results except for a scale factor.

The standard approach to delineate WHPAs is in terms of Time of Travel (TOT) using backward particle tracking where a cloud of particles is inserted at the well and allowed to track upgradient. An alternative approach is to used backward 3D advective-dispersive transport modelling. The dispersive term in the transport modelling accounts for macrodispersion. Macrodispersion can be taken as representing the uncertainty in defining the hydrogeologic characteristics (e.g. hydraulic conductivity) of the aquifer [Gelhar and Axness, 1983], which is lacking in the particle tracking approach. Comparison of the 3D particle tracking and transport modelling shows that the maximum extent of the capture zone obtained by drawing an envelope around the respective particle tracks is smaller than the probabilistic capture zone using advective-dispersive transport modelling. The probabilistic capture zone can be easily converted into a standard capture zone outline.

Backward 3D particle tracking and 3D advective-dispersive transport are also compared by application to the Mannheim well field. For the Mannheim system, the capture zones obtained by transport modelling are somewhat larger than the TOT zones obtained by particle tracking with the largest differences in the upgradient areas towards the west. This is due to macrodispersion having its largest value in the longitudinal direction. The particle tracking approach also relies on the drawing of an envelope around the respective particle tracks, which requires considerable guess work. The advective-dispersive transport approach outlines the TOT zones using the mass balance approach where the pumping rate at the wells is balanced by the prevailing influx through the ground surface within the TOT zones. Therefore, the capture zone outline obtained using the advective-dispersive approach can arguably be taken to be more realistic than the particle tracks. In both approaches, the TOT zones are developed based on the steady-state pumping rates. The TOT zones will change if pumping rates change.

The methodologies for delineating WHPAs only provides the time of travel of the contaminant, however it does not quantify the actual threat to a well. The concept of well vulnerability can be used to quantify the actual impact of contaminant sources on a well. The well vulnerability concept includes all key characteristics and processes such as the nature of the source, the transport and fate of the contaminants along its path from the source to the receptor, and the interaction of

the well itself with the flow system. For a known source at a known location, the well vulnerability maps can be developed using standard advective-dispersive transport modelling. The technique is demonstrated by applying a unit-in-time pulse source within the Mannheim South well field and observing the concentration breakthrough at the wells. The four key parameters defining vulnerability, i.e., the maximum expected concentration and the time to reach maximum concentration, the time to reach a threshold value of the contaminant, and the exposure time of the concentration above the threshold value are determined using the resulting breakthrough curves. To map these key measures within the Mannheim well field, a number of similar sources need to be placed within the WHPAs. This approach would require a large number of forward transport model runs. A more efficient approach is to apply backward-in-time transport modelling, which only requires one simulation for all possible sources within the WHPAs.

In this study, we advance the concept proposed by Frind et al. (2006) by defining well vulnerability for multiple wells within a well field in terms of concentrations in the extracted well water. The expected contaminant concentration at the well is much lower than the concentration within the aquifer due to dilution with clean water [Einarson and Mackay, 2001]. The well vulnerability maps for the unit pulse sources within the capture zone of the Mannheim well field is developed using backward-in-time transport modelling. The steady-state flow field is used as a basis for the development of well vulnerability maps.

The backward transport modelling approach is demonstrated by applying it to the Mannheim well fields, using two approaches for representing the wells: (a) by treating wells in close proximity as well clusters, and (b) by lumping wells within a well field. The first approach gives the impact for the unit pulse sources located anywhere within the capture zone of the well field. In the second approach, the sources the impact is assumed to be the same for each well. However, in the first approach, it may be difficult to extract the overall vulnerability information for a point within the capture zone, while the second is simpler for well fields consisting of multiple wells. With either approach, the information gained from the vulnerability maps go much beyond that obtained from the conventional approach which is based on the advective time of travel of the contaminant and thus provides a sound basis for the quantitative management of contamination risk. A sensitivity analysis on the vulnerability maps shows that the presence of highly conductive lenses that control flow and transport can lead to a shorter time for contaminant migration to

the wells with a higher maximum relative concentration.

The well vulnerability maps also provide the basis for risk assessment of a well becoming contaminated due to potential sources within its capture zone. Here we advanced the presently available approaches of risk assessing by introducing a quantitative approach where risk is defined as the economic cost of remediation or replacement of a water supply well that has been contaminated. The approach is applied to one of the wells within the Mannheim well field, using hypothetical time-varying point sources located arbitrarily within the capture zone. The specific vulnerability of the well due to these sources is computed by convoluting the source mass with the results of the backward model. The major advantage of the convolution approach is that it does not require any model simulation run and is very computationally efficient. Using the information of the specific vulnerability we can further create the exposure map and the time map (time require to exceed the threshold value of the hypothetical sources). The exposure maps show which sources of contamination will lead to critical concentrations at the well, and the time map provides the information for the ranking of priorities to reduce contamination. The exposure information can then be integrated with the time element to create distributed maps of quantitative risk expressed in terms of investment that has to made today in order to have the funds for remediation or replacement of the well in the future. This approach should be useful for complementing present risk assessment methodologies based on subjective judgement.

The backward well vulnerability approach can be used to identify the optimal location to apply BMPs within the WHPAs. Application of BMPs can help to reduce contamination in drinking water supply wells. A scenario analysis shows where BMPs should be optimally focused to reduce the nitrate concentration at the target well. The results show that BMPs applied near the well have the greatest effect, but application at more distant areas can also be beneficial, provided such areas are located in areas of high well vulnerability. This information may be beneficial for regulators and water resource managers to purchase land within the WHPA of a well to reduce contamination.

9.2 Suggestions for Future Research

Future work may address the influence of fully transient flow and pumping history on WHPAs. Protection zones around surface water sources may also be developed

using the advective-dispersive transport model and vulnerable areas within the protection zones may be identified using the same principle of well vulnerability. This will require a coupling of surface water and groundwater modelling.

In this study, in the assessment of the risk from all possible contaminant sources within a well capture zone, we have only considered a first-order reaction rate. In case of the multi-component non-aqueous phase liquids (NAPL), which dissolve and can biodegrade in a porous aquifer, the concentration distribution at the well may be obtained using the advective-dispersive reactive transport equation.

Appendix A

Theoretical Development of the Backward Model

Continuous Theory

This section is concerned with the development of adjoint sensitivity equations for multidimensional contaminant transport in groundwater. The standard governing equation for advective-dispersive transport can be written as

$$\frac{\partial(RC)}{\partial t} = \frac{\partial}{\partial x_i}\left(D_{ij}\frac{\partial C}{\partial x_j} - v_i C\right) - \frac{q_0}{\theta}C + \frac{q_I}{\theta}C_I - R\lambda C \tag{A.1}$$

where $C(x,t)$ is resident concentration, t is time, x_i's are the spatial directions $(i = 1,2,3)$, $x = (x_1, x_2, x_3)$, D_{ij} is the i,j^{th} entry of the dispersion tensor, v_i is the groundwater velocity in the direction of x_i, q_0 is the outflow or sink rate per unit volume, q_I is the inflow or source rate per unit volume, and C_I is the source strength, and θ is the volumetric moisture content. In equation (A.1), R is the retardation factor.

In the backward model, the adjoint equation is derived based on the sensitivity analysis approach of Sykes et al. (1985). In a sensitivity analysis, a performance measure P that represents a state of the system is defined as

$$P = \int\int_{\Omega,t} h(\alpha, C) d\Omega dt \tag{A.2}$$

where $h(\alpha, C)$ is a functional state of the system, α is a parameter (such as v, D, q_I, or others), C is the resident concentration, Ω is the spatial domain, and t is the

time domain. The marginal sensitivity of this performance measure with respect to the parameter α is obtained by differentiating (A.2) with respect to α_k as

$$\frac{dP}{d\alpha_k} = \int\int_{\Omega,t} \left[\frac{\partial h(\alpha, C)}{\partial \alpha_k} + \frac{\partial h(\alpha, C)}{\partial C} \psi \right] d\Omega dt \tag{A.3}$$

where $\frac{dP}{d\alpha_k}$ is the marginal sensitivity, $\psi = \frac{\partial C}{\partial \alpha_k}$ is the state sensitivity. The state sensitivity in (A.3) can be evaluated for each parameter of interest using a sampling approach. For a system with a large number of parameters, this approach can be costly and time consuming. To eliminate ψ from (A.3), we first obtain a governing equation for ψ by differentiating the terms in (A.1) with respect to the parameter α_k.

$$\frac{\partial (R\psi)}{\partial t} = \frac{\partial}{\partial x_i} \left[D_{ij} \frac{\partial \psi}{\partial x_j} - v_i \psi \right] - R\lambda\psi - \frac{q_0}{\theta}\psi \tag{A.4}$$

$$\psi(x, 0) = \frac{\partial C_0}{\partial \alpha_k}$$

$$\psi(x, t) = 0 \qquad \Gamma_1$$

$$\left(D_{ij} \frac{\partial \psi}{\partial x_j} + \frac{\partial D_{ij}}{\partial \alpha} \frac{\partial C}{\partial x_j} \right) n_i = 0 \qquad \Gamma_2$$

$$\left(v_i \psi + \frac{\partial v_i}{\partial \alpha} C - D_{ij} \frac{\partial \psi}{\partial x_j} - \frac{\partial D_{ij}}{\partial \alpha} \frac{\partial C}{\partial x_j} \right) n_i = 0 \qquad \Gamma_3$$

If the parameter α_k is only related to the resident concentration, the other derivatives of D_{ij}, v_i, q_I, q_0, θ and C_I with respect to α_k will not appear in the boundary conditions.

Integrating equation (A.4) over the entire space and time domain after multiplying with respect to an arbitrary function ψ^* we obtain

$$\int\int_{\Omega,t} \left[-\psi^* \frac{\partial (R\psi)}{\partial t} + \psi^* \frac{\partial}{\partial x_i} (D_{ij} \frac{\partial \psi}{\partial x_j} - v_i \psi) - \psi^* \frac{q_0}{\theta} \psi - \psi^* R\lambda\psi \right] d\Omega dt = 0. \tag{A.5}$$

After using the product rule once on each of the first derivative terms and twice on the second derivative terms and adding (A.5) to the marginal sensitivity (A.3), we obtain

$$\begin{aligned} \frac{dP}{d\alpha} = \int\int_{\Omega,t} \Bigg\{ & \frac{\partial h(\alpha, C)}{\partial \alpha} + \psi \left[\frac{\partial h}{\partial C} + \frac{\partial (R\psi^*)}{\partial t} + \frac{\partial}{\partial x_i} \left(D_{ij} \frac{\partial \psi^*}{\partial x_j} \right) + v_i \frac{\partial \psi^*}{\partial x_j} \right. \\ & \left. - \frac{q_0}{\theta} \psi^* - R\lambda\psi^* \right] - \frac{\partial}{\partial t} (R\psi\psi^*) + \frac{\partial}{\partial x_i} \left[\psi^* D_{ij} \frac{\partial \psi}{\partial x_j} - \right. \\ & \left. \psi D_{ij} \frac{\partial \psi^*}{\partial x_j} - v_i \psi \psi^* \right] \Bigg\} d\Omega dt. \end{aligned} \tag{A.6}$$

Applying the divergence theorem ($\int_\Omega \nabla \dot{F} d\Omega = \int_\Gamma F \dot{n} d\Gamma$, where n is the outward normal direction on the boundary, Γ) to the last four terms of (A.6) and integrating the temporal divergence term, the marginal sensitivity becomes

$$\begin{aligned}\frac{dP}{d\alpha} &= \int\int_{\Omega,t} \frac{\partial h(\alpha, C)}{\partial \alpha} + \psi \left[\frac{\partial h}{\partial C} + \frac{\partial (R\psi^*)}{\partial t} + \frac{\partial}{\partial x_i}\left(D_{ij} \frac{\partial \psi^*}{\partial x_j} \right) + v_i \frac{\partial \psi^*}{\partial x_j} \right. \\ &\quad \left. - \frac{q_0}{\theta}\psi^* - R\lambda\psi^* \right] - \int_\Omega (R\psi\psi^*)|_{t=t_f}^{t=0} d\Omega + \int\int_{\Gamma,t} \left[\psi^* D_{ij} \frac{\partial \psi}{\partial x_j} \right. \\ &\quad \left. - \psi D_{ij} \frac{\partial \psi^*}{\partial x_j} - v_i \psi \psi^* \right] n_i d\Gamma dt, \end{aligned} \tag{A.7}$$

where t_f is the final time of the time domain and equal to the time of sampling. Substituting the initial and boundary conditions on ψ from (A.7), which are known values, we obtain

$$\begin{aligned}\frac{dP}{d\alpha} &= \int\int_{\Omega,t} \frac{\partial h(\alpha, C)}{\partial \alpha} + \psi \left[\frac{\partial h}{\partial C} + \frac{\partial (R\psi^*)}{\partial t} + \frac{\partial}{\partial x_i}\left(D_{ij} \frac{\partial \psi^*}{\partial x_j} \right) + v_i \frac{\partial \psi^*}{\partial x_j} \right. \\ &\quad \left. - \frac{q_0}{\theta}\psi^* - R\lambda\psi^* \right] - \int_\Omega \left[(R\psi\psi^*)|_{t=t_f} - \left(\psi^* \frac{\partial C_0}{\partial \alpha} \right) |_{t=t_0} \right] d\Omega \\ &\quad + \int\int_{\Gamma,t} \left[\psi^* D_{ij} \frac{\partial \psi}{\partial x_j} \right] n_i d\Gamma_1 dt - \int\int_{\Gamma,t} \left[\psi D_{ij} \frac{\partial \psi^*}{\partial x_j} + v_i \psi \psi^* \right] n_i d\Gamma_2 dt \\ &\quad - \int\int_{\Gamma,t} \left[\psi D_{ij} \frac{\partial \psi^*}{\partial x_j} \right] n_i d\Gamma_3 dt. \end{aligned} \tag{A.8}$$

In order to eliminate ψ from (A.8), the adjoint equation is chosen to satisfy the following equation and boundary conditions, known as the adjoint problem. If we define a new time variable, backward time, $\tau = t_f - t$, the initial condition on ψ^* in backward time is $\psi^*(x, \tau) = 0$ at $\tau = 0$. The complete adjoint equation in terms of backward time τ with initial and boundary conditions is defined as:

$$-\frac{\partial (R\psi^*)}{\partial \tau} + \frac{\partial}{\partial x_i}\left(D_{ij} \frac{\partial \psi^*}{\partial x_j} + v_i \psi^* \right) - \frac{q_I}{\theta}\psi^* - \lambda R \psi^* = -\frac{\partial h}{\partial C}. \tag{A.9}$$

The initial and boundary conditions are:

$$\psi^*(x, 0) = 0$$

$$\psi^*(x, \tau) = 0 \qquad \Gamma_1$$

$$(v_i \psi^* + D_{ij} \frac{\partial \psi^*}{\partial x_j}) n_i = 0 \qquad \Gamma_1$$

$$(D_{ij} \frac{\partial \psi^*}{\partial x_j}) n_i = 0 \qquad \Gamma_1 \cap \Gamma_0$$

Free exit boundary condition Γ_2

Using $\nabla.v = \frac{q_I}{\theta} - \frac{q_0}{\theta}$, the advection and sink terms in (A.8) are replaced with advection and source terms in (A.9).

Discrete Theory

The advection-dispersion equation defined by (A.1) can be solved accordingly: Equation (A.1) can be written in discrete form using the Galerkin finite element method as

$$[M]\{C\} = \{F_c(\alpha)\} \tag{A.10}$$

where $[M]$ is the transport matrix which assembles the advection, dispersion, decay and mass storage and boundary terms together and $F_c(\alpha)$ is the boundary vector. For any element, the dependent variables of the transport equation are approximated in terms of the nodal concentrations by

$$C = \{w\}^T\{C\}$$

The individual terms of the transport matrix $[M]$ and load term vector are

$$a_{ij} = \int_A \left(D\frac{\partial w_i}{\partial x}\frac{\partial w_j}{\partial x} - v\frac{\partial x_i}{\partial x}w_j + R\lambda w_i w_j \right) dA$$

$$F_i = \int_\Gamma \frac{q_0 C_0}{\eta}.\mathbf{n}w_i dB - \int_\Gamma \left(Dw_i\frac{\partial w_j}{\partial x} - v_n w_i w_j \right).\mathbf{n}w_i dB$$

The matrix form of the adjoint problem is found by differentiating both the performance measure and equation (A.10) with respect to a parameter α_k

$$\frac{dP}{d\alpha_k} = \frac{\partial P(\{\alpha\},\{C\})}{\partial \alpha_k} + \left[\frac{\partial P(\{\alpha\},\{C\})}{\partial \{C\}}\right]^T \{\psi\}_k \tag{A.11}$$

and

$$[M]\{\psi\}_k = \frac{\partial F\{\alpha\}}{\partial \alpha_k} - \frac{\partial [M\{\alpha\}]}{\partial \alpha_k}\{C\} = F_\psi(\{\alpha\},\{C\}). \tag{A.12}$$

Multiplying equation (A.12) by the arbitrary constant ψ^* and subtracting the result from equation (A.11) gives the marginal performance sensitivity as

$$\begin{aligned}\frac{dP}{d\alpha_k} &= \frac{\partial P(\{\alpha\},\{C\})}{\partial \alpha_k} + \left[\frac{\partial P(\{\alpha\},\{C\})}{\partial \{C\}}\right]^T \{\psi\}_k + \{\psi^*\}^T\{F_\psi\} \\ &\quad -\{\psi^*\}^T[M(\{\alpha\}]\{\psi\}_k.\end{aligned} \tag{A.13}$$

Now, we can eliminate ψ by letting

$$\{\psi\}_k^T \left[\frac{\partial P(\{\alpha\},\{C\})}{\partial\{C\}}\right] - \{\psi\}_k^T [M\{\alpha\}]^T \{\psi^*\} = 0. \tag{A.14}$$

The complete adjoint equation can be written as

$$[M(\alpha)]^T \{\psi^*\} = \frac{\partial P(\{\alpha\},\{C\})}{\partial\{C\}}. \tag{A.15}$$

The difference between equations (A.10) and (A.15) is the load term and the coefficient matrix $[M]^T$. Much of the computational structure involved in solving the forward problem may be utilized for the backward problem.

From equation (A.13), the marginal sensitivity of the performance measure becomes

$$\frac{dP}{d\alpha_k} = \frac{\partial P\{\alpha\},\{C\}}{\partial\alpha_k} + \{\psi^*\}^T \{F_\psi\}. \tag{A.16}$$

In equation (A.16), $\{F_\psi\}$ is defined as

$$\{F_\psi\} = \frac{\partial F\{\alpha\}}{\partial\alpha_k} - \frac{\partial[M\{\alpha\}]}{\partial\alpha_k}\{C\}. \tag{A.17}$$

The performance function P in equation (A.15) can be written in discrete form as [Thomson and Sykes, 1990]

$$P = \sum_{\substack{\text{time}\\ \text{levels}}} \sum_{node} w_i(m) h_i(m) \Delta t(m) \tag{A.18}$$

where h_i is the functional state of the system and w_i is the basis function having a value of 1 at the node points i and 0 at the other node points at time level m. For example, suppose the performance measure is the mass flux at the well, then the functional state becomes

$$h_i(\alpha, C) = q_w C(x_w, t)\delta(x - x_w)\delta(y - y_w)\frac{B_z(z_{wbot}, z_{wtop})}{z_{wtop} - z_{wbot}}\delta(t) \tag{A.19}$$

where q_w is the normal component of the fluid flux crossing the well screen, C is the resident concentration, $\delta(.)$ is a Dirac partial function, (x_w, y_w) are the coordinates of the center of the well, and z_{wtop} and z_{wbot} are the elevations of the top and bottom of the well screen, respectively. $B_z(z_{wbot}, x_{wtop})$ is a boxcar function which is 1 between the top and bottom elevations of the well and 0 otherwise. The performance measure P can be written as

$$P = \{w\}^T q_w \{C\}, \tag{A.20}$$

and the load term of the adjoint problem becomes

$$\frac{\partial P}{\partial C} = \{w\} q_w. \tag{A.21}$$

Using the load term defined by (A.21) the adjoint state sensitivity vector $\{\psi^*\}$ can be calculated from equation (A.15). The direct term in the marginal sensitivity (A.16) becomes

$$\frac{\partial P}{\partial \alpha_k} = \frac{\partial \{w\}^T}{\partial \alpha_k} q_w \{C\}. \tag{A.22}$$

In this case, since $\frac{\partial w_i}{\partial \alpha_k} = 0$, the direct contribution is zero. The marginal sensitivity is determined by using $\{\psi^*\}$ and $\{F\}$ from equation (A.16). The adjoint state $\{\psi^*\}$ represents the change in the value of the performance measure caused by a load at the well. The term $\{F\}$ represents the instantaneous point source anywhere within the system. The forward model is described as

$$\frac{\partial C^r}{\partial t} = -\nabla.qC^r + \nabla.D\nabla C^r \quad \text{in} \quad \Omega \tag{A.23}$$

$$C^r(x,0) = m^*\delta(x - x_i) \quad \text{in} \quad \Omega$$

$$[qC^r - D\nabla C^r].n = 0 \quad \text{on} \quad \Gamma^- \bigcup \Gamma_0$$

$$\text{Implicit Neumann condition} \quad \text{on} \quad \Gamma^+ \bigcup \Gamma_n$$

where m^* is the injected mass at $x = x_i$, Γ^- is the inlet zone, Γ^+ is the outlet zone and Γ_0 is the no-flow boundary. The Cauchy type boundary condition at $x = \Gamma^-$ prevents solute from migrating upgradient and the Dirac delta function $\delta(t)$ allows an instantaneous mass release at $t = 0$. The Implicit Neumann condition expresses a total mass continuity at the outlet. A total mass flux continuity at the outlet permits upgradient solute movement by dispersion from Γ^+. The implicit Neumann condition is not prescribed since the dependent variable is unknown, but the operator $D\nabla()$ is implicitly formulated.

The backward model is the adjoint of a forward model. Considering a Cauchy type condition at the outlet, the backward model can be defined as

$$\frac{\partial C_E}{\partial t} = \nabla.qC_E + \nabla.D\nabla C_E - Q_1 C_E \quad \text{in} \quad \Omega \tag{A.24}$$

$$[qC_E + D\nabla C_E].n = q.n\delta(t) \quad \text{on} \quad \Gamma_n$$

$$[qC_E + D\nabla C_E].n = 0 \qquad \text{on} \quad \Gamma_+$$

$$\text{Implicit Neumann condition} \qquad \text{on} \quad \Gamma^-$$

$$D\nabla C_E.n = 0 \qquad \text{on} \quad \Gamma_0.$$

Applying the Laplace transform to the forward and backward equations and then simplifying, one can obtain the following:

$$\int_{\Gamma_n} qC^r(x,t).nd\Gamma = m^* C_E(x_i,t) \tag{A.25}$$

Normalizing the equation (A.25) by the steady flow rate $F_{0,n}$ yields

$$\overline{C}^r_n(t) = \frac{1}{F_{0,n}} \int_{\Gamma_n} qC^r(x,t).nd\Gamma = \frac{m^* C_E(x_i,t)}{F_{0,n}} \tag{A.26}$$

where $C_E(x_i,t)$ is the life-expectancy-to-outlet pdf scaled by the outlet flow rate and C^r is the resident concentration. If the outlet is a pumping well ($\Gamma_n = \Gamma_w$, $F_{0,n}$ $= Q_w$), then for a unit mass input ($m^* = 1$) the forward and backward models are related through the following relationship [Cornaton, 2003]:

$$\frac{C^r(x_w,t)}{m^*} = \frac{C_E(x_i,t)}{Q_w}.$$

The flow rate scaled life-expectancy-to-well pdf $C_E(x,t)$ can be compared to the backward location probability of Neupauer and Wilson (2001).

Appendix B

Convolution Theory

Convolution is a well-known and effective superposition method to deal with arbitrary inputs in time and space for linear systems. It uses the response of a system caused by an excitation, i.e. a pulse, to subsequently simulate the effect of arbitrary space or time-varying input. For example, consider two functions $s(t)$ and $r(t)$, where $s(t)$ is a data or signal stream that goes on indefinitely in time and $r(t)$ is a response function that falls to zero in both directions from its maximum. The effect of convolution is to smear the signals which occur at time τ into the shape of the response function, but translated from time 0 to time τ as $r(t-\tau)$. A detailed description of the theorem can be found in various existing literature sources (see for example, Press et al., 1992).

Convolution of two functions denoted by $s * r$ is defined as in the continuous case as

$$s * r = \int_{-\infty}^{\infty} s(\tau) r(t-\tau) d\tau \tag{B.1}$$

In a discrete case, the signal $s(t)$ can be represented by its sample values at equal time intervals s_j. The response function is also a discrete set of numbers r_k. In case of a response function of finite duration M, the convolution of the response and signal function can be written in discrete form as:

$$(s * r)_j = \sum_{k=-\frac{M}{2}+1}^{\frac{M}{2}} s_{j-k} r_k \tag{B.2}$$

Convolution is generally applied to compute the dispersive transport of solutes from a time-varying source [Cornaton, 2003]; [Charbeneau, 2000]; [Carslaw and Jaeger, 1977].

In this thesis, the concentration distribution at a drinking water supply well due to the known contaminant source mass at an arbitrary location is obtained using the convolution approach. The development of this approach is presented in Figure B.1

For a source mass of $\Delta M(t)$ located at an unknown position, the concentration at a pumping well can be obtained using the product of the two functions, the backward travel time pdf (ψ^*) and $\Delta M(t)$. If $\Delta M(t)$ is not in a functional form, for example as shown in Figure B.2, it must be first discretized $\Delta M(t)$ into discrete steps.

Each of the discrete jumps in $\Delta M(t)$ are constants and can thus be taken outside the integral. The solution can be approximate as:

$$\begin{aligned} C(x_i,t) &= \left[\Delta M(0)\int_0^t \psi^*(x,t-\tau)d\tau + \Delta M(t_1)\int_{t_1}^t \psi^*(x,t-\tau)d\tau \right. \\ &\quad \left. + \Delta M(t_2)\int_{t_2}^t \psi^*(x,t-\tau)d\tau + ...\right] \end{aligned} \tag{B.3}$$

If we chose equal "panel" widths such that $t_i = i\Delta t$ in the discretization scheme, then Equation (B.3) can be written as:

$$C(x_i,t) = \left[\Delta M(0)\int_0^t \psi^*(x,t-\tau)d\tau + \sum_{i=1}^{\infty}\Delta M(i\Delta t)\int_0^t \psi^*(x,t-\tau)d\tau\right] \tag{B.4}$$

The convolution of the two functions can be performed efficiently using the Fast Fourier Transformation (FFT) [Press et al., 1992]. First, the discrete Fourier transform of the input function and response is done using the FFT algorithm. Second, the two transforms are multiplied together component by component, remembering that the transforms consist of complex numbers. Finally, using the FFT algorithm the inverse discrete Fourier transform of the products is obtained. The result is the convolution input$*$response. Convolution may be based on analytical solutions, but equally well on a numerical model, on time series analysis, or on any other means by which the impulse response can be obtained.

The convolution theorem assumes that the signal (i.e., input function) is periodic. Because of this assumption, it will falsely pollute the first output channel with some wrapped-around data from the far end of the data stream. The problem can be solved by creating a buffer zone of zero-padded values at the end of the signal vector, which will force the signal pollution to zero. The number of discrete

zero-points required to pad the data is equal to the maximum positive duration or maximum negative duration of the response function, whichever is larger. However, for a symmetric response function of duration M, only $\frac{M}{2}$ zero-points are required to pad the data. The convolution theorem assumes that the duration of the response function is the same as the signal. Almost always the response function is much shorter than the length of the signal. This problem can be solved by simply extending the response function to the length of the signal by padding it with zeros.

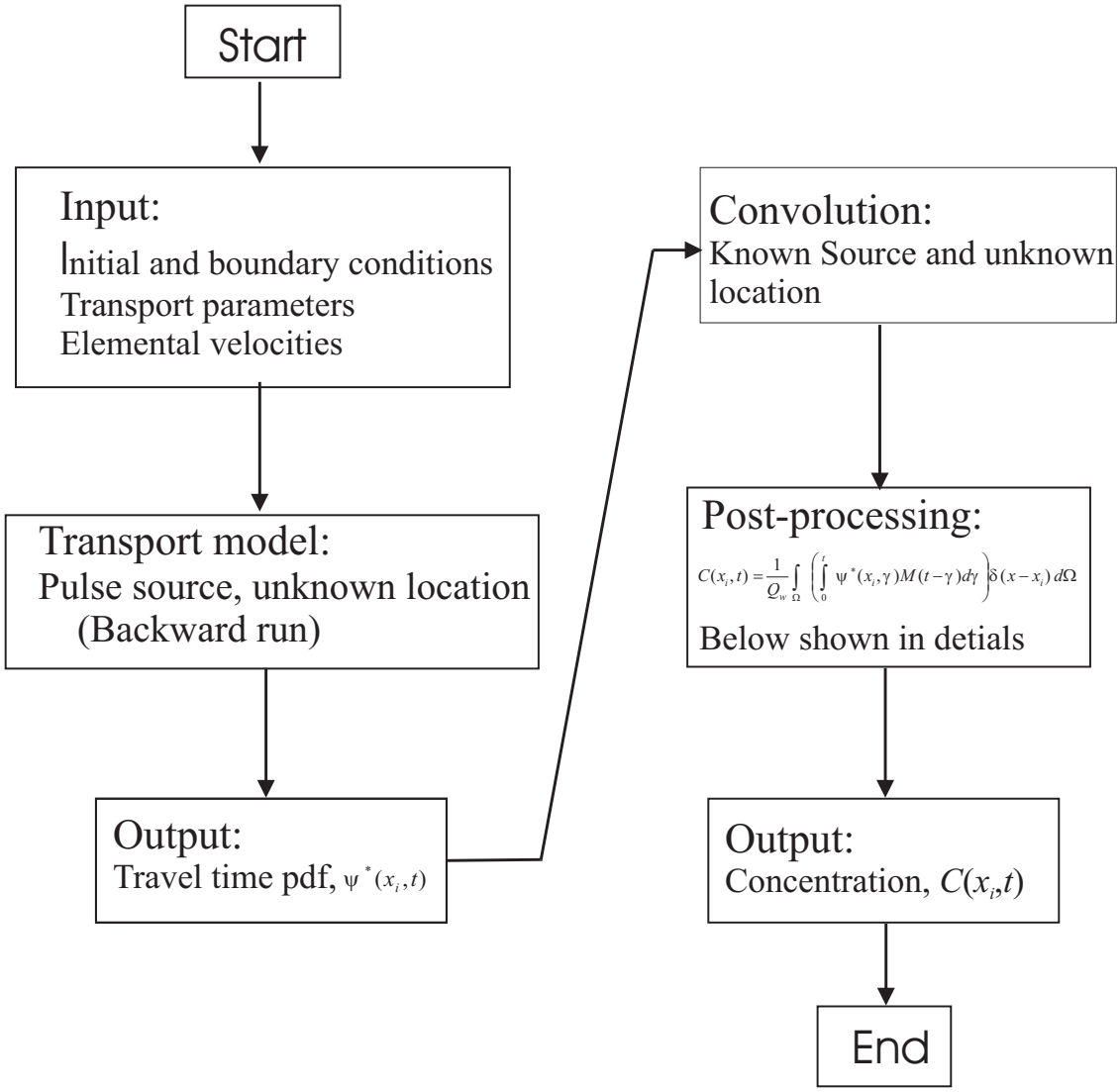

Figure B.1: Algorithm for the solution of the convolution approach.

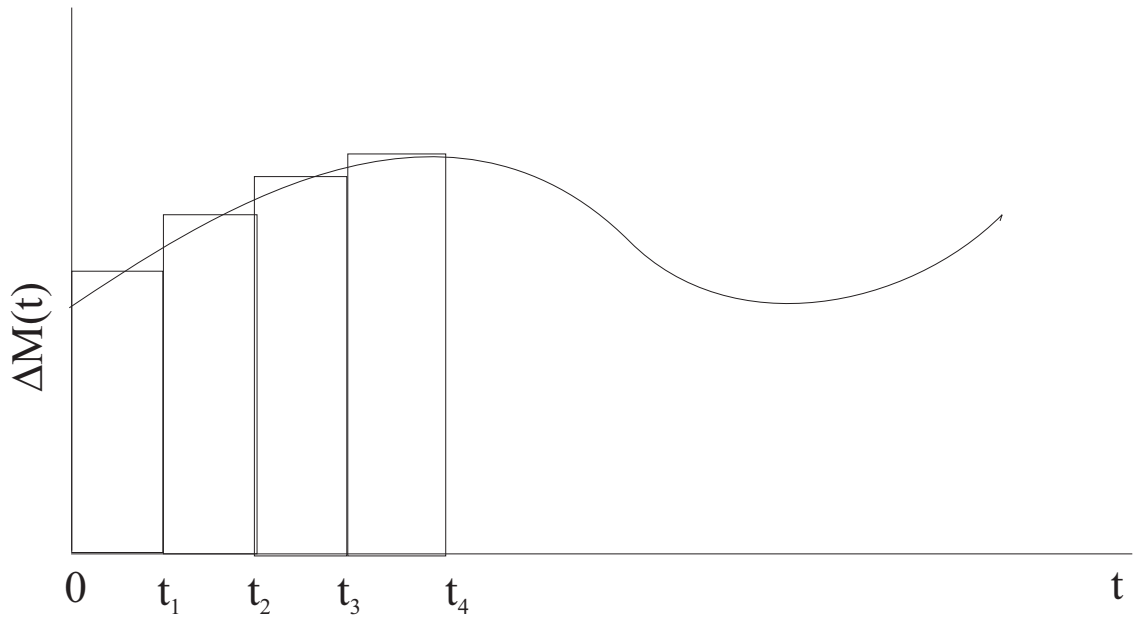

Figure B.2: Time-varying source mass distribution.

References

[Aller et al., 1987] Aller, L., Bennett, T., Lehr, J. H., Petty, R., and Hackett, G. (1987). *DRASTIC: A standardized system for evaluating ground water potential using hydrogeological settings.* 22

[Archer and Shogren, 2001] Archer, D. W. and Shogren, J. F. (2001). Risk-indexed herbicide taxes to reduce ground and surface water pollution: an integrated ecological economics evaluation. *Ecological Economics*, 38:227–250. 128

[Bagtzoglou et al., 1992] Bagtzoglou, A., Dougherty, D., and Thompson, A. (1992). Application of particle methods to reliable identification of groundwater pollution sources. *Water Resource Mgmt*, pages 15–23.

[Barlow, 1994] Barlow, P. (1994). Two and three-dimensional pathline analysis of contributing areas to public-supply wells of Cape Cod, Massachusetts. *Ground Water*, 32(3):399–410.

[Bear, 1972] Bear, J. (1972). *Dynamics of Fluids in Porous Media.* Americal Elsevier, NewYork, NY. 10, 27, 29

[Beckers, 1998] Beckers, J. (1998). *Modeling the Oro Morain multi-system-aquifer system: Role of geology, numerical model, parameter estimation, and uncertainity.* Ph.D. Thesis, Deptartment of Earth and Environmental Sciences, University of Waterloo. 11, 12

[Beckers and Frind, 2002] Beckers, J. and Frind, E. O. (2002). Simulating groundwater flow and runoff for the Ore moraine aquifer system. PartII. Automated calibration and mass balance calculations. *Journal of Hydrology.* 12

[Bekeris, 2007] Bekeris, L. (2007). *Field-scale evaluation of enhanced agricultural management practices using a novel unsaturated zone nitrate mass load approach.* M.Sc. Thesis, Deptartment of Earth and Environmental Sciences, University of Waterloo. 137, 139

[Bester, 2002] Bester, M. L. (2002). *Numerical simulation of road salt impact at the Greenbrook well field, Kitchener, Ontario*. M.Sc. Thesis, Deptartment of Earth and Environmental Sciences, University of Waterloo.

[Bester et al., 2006] Bester, M. L., Frind, E. O., Molson, J. W., and Rudolph, L. D. (2006). Numerical investigation of road salt impact on an urban wellfield. *Ground Water*, 44(2):165–175. 10

[Bouchard et al., 1992] Bouchard, D. C., Williams, M. K., and Surampalli, R. Y. (1992). Nitrate contamination of groundwater sources and potential health effects. *American Water Works Association*, 84(9):85–90. 1

[Brouyère et al., 2001] Brouyère, S., Jeannin, P. Y., Dassargues, P., Goldscheider, N., Popescu, I. C., Sauter, M., Vadillo, I., and Zwahlen, I. (2001). Evaluation and validation of vulnerability concepts using a physically based approach. *In Sci. Tech. Envir., Mém., Proceedings of the 7th Conference on Limestone Hydrology and Fissured Media, Besancon. Universitié de Franche-Comte, Sciences et Techniques de l'Environment, Besancon*, 13:67–72. 23, 24, 129

[Burnett and Frind, 2002] Burnett, R. D. and Frind, E. O. (2002). Simulation of contaminant transport in three dimensions: The Alternating Direction Galerkin Technique. *Water Resources Research*, 24(3):683–694. 61, 85

[Butt and Oduyemi, 2003] Butt, T. E. and Oduyemi, K. O. K. (2003). A holistic approach to contamination assessment of hazards in the risk assessment of landfill leachate. *Environmental International*, 28:597–608.

[CH2M-Hill, and Papadopulous and Associates Inc., 2003] CH2M-Hill, and Papadopulous and Associates Inc. (2003). *Alder Creek groundwater study:final report*. Prepared for the Regional Municipality of Waterloo, special volume 2 edition. 64, 137

[Chapman and Putnam, 1984] Chapman, L. J. and Putnam, D. F. (1984). *The physiography of Southern Ontario*. Ontario Geological Survey, special volume 2nd edition edition.

[Charbeneau, 2000] Charbeneau, R. J. (2000). *Groundwater Hydraulics and Pollutant Transport*. ISBN 0-13-975616-7. Upper Saddle River, New Jersey: Prentice Hall. 161

[Chin and Chittaluru, 1994] Chin, D. and Chittaluru, P. (1994). Risk management in wellhead protection. *Water Resour Plan Mgmt*, 120:294–315.

[Cornaton, 2003] Cornaton, F. (2003). *Deterministic models of groundwater age, life expectancy and trasmit time distributions in advective-dispersive systems*. Ph.D. Thesis, University of Neuchâtel. 160, 161

[Daly et al., 2002] Daly, D., Dassargues, A., Drew, D., Dunne, S., Goldscheider, N., Nepale, S., Popescu, I. C., and Zwahlen, F. (2002). Main concepts of the European approach to karst groundwater vulnerability assessment and mapping. *Journal of Hydrology*, 10:340–345.

[Daus et al., 1985] Daus, A. D., Frind, E. O., and Sudicky, E. A. (1985). Comparative error analysis in finite element formulations of the advective-dispersive equation. *Advances in Water Resources*, 8:86–95. 13

[Einarson and Mackay, 2001] Einarson, D. M. and Mackay, M. D. (2001). Predicting impacts of groundwater contamination. *Environmental Geology*, 35(3):1657–1668. 59, 128

[Environmental Protection Agency (EPA), 1990] Environmental Protection Agency (EPA) (1990). *Risk assessment management and communication of drinking water contamination*. EPA/625/4-89/024. Washington, DC: EPA office of research and development.

[Feyen et al., 2001] Feyen, L., Beven, K. J., de Smedt, F., and Freer, J. (2001). Stochastic capture zone delineation within the generalized likelihood uncertainity estimation methodology: conditioning on head observations. *Water Resources Research*, 37(3):625–638. 4

[Focazio et al., 2002] Focazio, M. J., Reilly, T. E., Rupert, M. G., and Helsel, D. R. (2002). Assessing ground-water vulnerability to contamination: providing scientifically defensible information for decision makers. *U.S. Geological Survey Circular 1224*.

[Fogg, 1986] Fogg, G. E. (1986). Groundwater flow and sand body interconnectedness in a thick, multiple-aquifer system. *Water Resources Research*, 22(5):679–694. 57

[Foster and Hirata, 1992] Foster, S. and Hirata, R. (1992). Groundwater pollution risk assessment. World Health Organization. Pan American Heath Organization. Pan American Center for Sanitary Engineering and Environmental Sciences (CEPIS). Lima, Peru. 22

[Foster, 1987] Foster, S. S. D. (1987). Fundamental concepts in aquifer vulnerability pollution risk and protection strategy. Proceedings of International Conference: Vulnerability of soil and Groundwater to Pollutants. Noordwijk, The Netherlands. 22

[Foster et al., 1991] Foster, S. S. D., Hirata, R. G., DEllia, M., and Paris, M. (1991). Analysis and evaluation of the pumping test data. international institute for land reclamation and improvement. 22

[Freeze and Cherry, 1979] Freeze, A. R. and Cherry, A. J. (1979). *Groundwater*. Prentice Hall Inc., Englewood Cliffs, NJ.

[Frind, 1988] Frind, E. O. (1988). Solution of the advection-dispersion equation with free exit boundary. *Numerical Methods for Partial Diffential Equations*, 4:301–313. 61, 86

[Frind, 1997] Frind, E. O. (1997). Groundwater modelling (numarical methods). Lecture notes. *Deptartment of Earth and Environmental Sciences, University of Waterloo*. 13, 29

[Frind and Molson, 2004] Frind, E. O. and Molson, J. W. (2004). A new particle tracking algorithm for finite element grids. *FEM-MODFLOW Conference, Carlsbad, Czech Republic*. 63, 65

[Frind et al., 2006] Frind, E. O., Molson, J. W., and Rudolph, L. D. (2006). Well vulnerability: A quantitative approach for source water protection. *Ground Water*, 44(5):732–742. 4, 60, 95

[Frind et al., 2002] Frind, E. O., Muhammad, D. S., and Molson, J. W. (2002). Delineation of three-dimensional well capture zones for complex multi-aquifer systems. *Ground Water*, 40(6):586–598. 3, 59, 60, 67, 101

[Gelhar and Axness, 1983] Gelhar, L. W. and Axness, C. L. (1983). Three-dimensional stochatic analysis of macro dispersion in aquifers. *Water Resources Research*, 19(1):161–180. 59, 150

[Gelhar et al., 1992] Gelhar, L. W., Welty, C., and Rehfeldt, K. R. (1992). A critical review of data on field-scale dispersion in aquifers. *Water Resources Research*, 10(7):1955–1974. 67

[Guadagnini and Franzetti, 1999] Guadagnini, A. and Franzetti, S. (1999). Time-related capture zones for contaminants in randomly heterogeneous formations. *Ground Water*, 37(2):253–260.

[Harman et al., 2001] Harman, W. A., Allan, C. J., and Forsythe, R. D. (2001). Assessment of potential groundwater contamination sources in a wellhead protection area. *Journal of Enviroonmantal Management*, 62:271–282. 5

[Haslauer, 2005] Haslauer, P. C. (2005). *Hydrogeologic analysis of a complex aquifer system and impacts of changes in agricultural practices on nitrate concentrations in a municipal well field: Woodstock, Ontario.* M.Sc. Thesis, Deptartment of Earth and Environmental Sciences, University of Waterloo. 2, 138

[Howard et al., 1993] Howard, K. W. F., Boyce, J. I., Livingston, S. J., and Salvatori, S. (1993). Road salt impacts on groundwater quality - the worst is still to come. *GSA Today*, 3:319–321. 2

[Huyakorn and Pinder, 1983] Huyakorn, P. S. and Pinder, G. F. (1983). *Numerical Methods in Subsurface Flow.* Academic Press.

[Jones et al., 1986] Jones, P. H., Jeffrey, B. A., Walter, P. K., and Hutchon, H. (1986). *Environmental impact of road salting − state of the art, Ministry of Transportation and Communications.* Downsview, Ontario. 2

[Karrow, 1987] Karrow, P. F. (1987). *Quatenary Geology of the Hamilton-Cambridge Area, Southern Ontario.* Ontario Geological Survey Report. 9

[Karrow, 1993] Karrow, P. F. (1993). Quatenary geology, stratford-conestoga area.

[Kinzelbach et al., 1992] Kinzelbach, W., Marburger, M., and Chaing, W. H. (1992). Determination of groundwater catchmant areas in two and three spatial dimensions. *Journal of Hydrology*, 134:221–246.

[Kruseman and de Ridder, 1990] Kruseman, G. P. and de Ridder, N. A. (1990). *Groundwater quality protection: a guide for water utilities, municipal authorities and environmental agencies.* The World Bank, Washington D C. 27

[Kunstmann and Kinzelbach, 2000] Kunstmann, H. and Kinzelbach, W. (2000). Computation of stochastic well-head protection zones by combining the first-order second-moment method and Kolmogorow backward equation analysis. *Journal of Hydrology*, 237:127–146. 60, 96

[Leismann and Frind, 1989] Leismann, H. M. and Frind, E. O. (1989). A symmetric-matrix time integration scheme for the efficient solution of advection-dispersion problems. *Water Resources Research*, pages 1133–1139.

[Marquis and Stewart, 1992] Marquis, S. A. J. and Stewart, E. (1992). *The delineation of wellhead protection areas in fractured bedrock terrains using groundwater flow models*. California: McLaren/Hart Environmental Engineering. 58

[Martin, 1994] Martin, P. J. (1994). Modelling of the north Waterloo multi-aquifer system. *M.Sc. Thesis, Deptartment of Earth and Environmental Sciences, University of Waterloo*. 12

[Martin and Frind, 1998] Martin, P. J. and Frind, E. O. (1998). Modeling a complex multi-aquifer system: The Waterloo Moraine. *Ground water*, 36(4):679–690. 12, 58

[McLaren, 1999] McLaren, R. G. (1999). GRIDBUILDER: A pre-processor for 2D traingular element, finite-element programs. User's Guide. *Department of Earth Sciences, University of Waterloo*. 11

[Merry et al., 2000] Merry, A. G., Martin, P. J., and Middleton, T. (2000). Application of advanced modelling tools to evaluate uncertainty in modelling prediction. *Joint CGS/IAH-CNC Groundwater Conference*. 102

[Molson et al., 2002] Molson, J. W., Beckers, J., Frind, E. O., and Martin, P. J. (2002). WATFLOW 3D version 4.0, A Three-Dimensional Groundwater/Surface Water Flow Model, Users Guide. *Ontario, Canada: Department of Earth Sciences, University of Waterloo*. 10, 62, 63, 64, 87, 97, 130

[Molson and Frind, 2004] Molson, J. W. and Frind, E. O. (2004). WTC: The Waterloo Transport Code, Version 3.0. An advective-dispersive mass transport model in three dimensions. *Ontario, Canada: Department of Earth Sciences, University of Waterloo*. 13, 67, 87, 97, 130

[Mualem, 1976] Mualem, Y. (1976). A new model for predicting the hydraulic conductivity of unsaturated porous media. *Proceedings, 59th Canadian Geotechnical and 7th Joint CGS/IAH-CNC Groundwater Specialty Conf., Vancouver*, 12(3):513–522. 12

[National Research Council (NRC), 1983] National Research Council (NRC) (1983). *Risk Assessment in the Federal Government: Managing the Process*. National Academy Press, Washington, DC.

[National Research Council (NRC), 1993] National Research Council (NRC) (1993). *Groundwater vulnerability assessment: contamination potential under conditions of uncertainties*. National Academy Press., Washington, D.C.

[Neupauer and Wilson, 1999] Neupauer, R. M. and Wilson, J. L. (1999). Adjoint method for obtaining backward-in-time location and travel time probabilities of a conservative grounwater contaminant. *Water Resources Research*, 35(11):3389–3398. 4

[Neupauer and Wilson, 2001] Neupauer, R. M. and Wilson, J. L. (2001). Adjoint-derived location and travel time probabilities for a multidimensional groundwater system. *Water Resources Research*, 37:1657–1668. 95, 96

[Neupauer and Wilson, 2002] Neupauer, R. M. and Wilson, J. L. (2002). Backward probabilistic model of groundwater contamination in non-uniform and transient flow. *Advances in Water Resources*, 25:733–746.

[Nobre et al., 2007] Nobre, R. C. M., Rotunno, O. C., Mansur, W. J., Nobre, M. M. M., and Cosenza, C. A. N. (2007). Groundwater vulnerability and risk mapping using GIS, modeling and a fuzy logic tool. *Contaminant Hydrogeology*, 94(3-4):277–292.

[Nutrient Management Act, 2002] Nutrient Management Act (2002). *S.O., c.4*. 139

[OMAF, 1994] OMAF (1994). *See Ontario Ministry of Agriculture and Food and Agriculture Canada*. 140

[Ontario Ministry of Environment (MOE), 2006] Ontario Ministry of Environment (MOE) (2006). *Assessment report: draft guidance module 3 - groundwater vulnerability analysis. For use with source protection technical studies*. Ontario, Canada. 27

[Padusenko, 2001] Padusenko, G. (2001). *Regional hydrogeologic evaluation of a complex glacial aquifer system in an agricultural landscape: implications for nitrate distribution*. M.Sc. Thesis, Deptartment of Earth and Environmental Sciences, University of Waterloo.

[Paradis et al., 2007] Paradis, D., Martel, R., Karanta, G., Lafebvre, R., Michaid, Y. Therrien, R., and Nastev, M. (2007). Comparative study of methods for WHPA delineation. *Ground Water*, 45(2):158–167. 57

[Phipps, 1991] Phipps, T. T. (1991). Commercial agriculture and the environment. *Northeastern Journal of Agriculture and Resource Economics*. 138

[Piersol, 2005] Piersol, J. (2005). *Evaluating groundwater supply sustainable capacity and pollution threats for an urban well field in a semi-arid coastal region: Aguadulce, Panama*. M.Sc. Thesis, Deptartment of Earth and Environmental Sciences, University of Waterloo.

[Pollock, 1994] Pollock, D. W. (1994). A particle tracking post-processing package for MODFLOW, the U.S. Geological Survey Open-File Report. *User's Guide for MODPATH/MONPATH-PLOT, version 3*, 6:94–464. 60, 63

[Press et al., 1992] Press, H. W., Flannery, P. B., Teukolsky, A. S., and Vetterling, T. W. (1992). *Numerical Recipes in Fortran 77, The Art of Scientific Computing*. Volume 1. 162

[Rahman et al., 2006] Rahman, R., Frind, E. O., Molson, J. W., and Rudolph, D. L. (2006). Development of well vulnerability maps for multiple wells using backward-in-time transport modelling. *Proceedings, 59th Canadian Geotechnical and 7th Joint CGS/IAH-CNC Groundwater Specialty Conf., Vancouver*. 94

[Rahman et al., 2007] Rahman, R., Frind, E. O., Rudolph, D. L., Thomson, N. R., and Molson, J. W. (2007). Well vulnerability maps: an approach to measure the impact of contaminants on wells. *The 8th Joint CGS/IAH-CNC Groundwater Conference, Ottawa*. 127

[Region of Waterloo, 2006] Region of Waterloo (2006). *A low-salt diet for Ontario's roads and rivers*. RiverSides Stewardship Alliance and Sierra Legal Defence Fund. 2

[Region of Waterloo, 2007] Region of Waterloo (2007). *Sources of supply, Living in the Region of Waterloo*. Source: http://www.region.waterloo.on.ca. 1

[Roos et al., 2003] Roos, A., Ward, M., Lynch, C., and Cantor, K. (2003). Nitrate in public water supplies and the risk of colon cancer and Rectum cancers. *Epidemiology*, 14(6):640–649. 2

[Schmidt, 1987] Schmidt, R. R. (1987). Groundwater contamination susceptibility in Wisconsin. Wisconsin's groundwater management plan report. *Madison, Wisconsin: Wisconsin Department of Natural Resources, PUBL-WR-177-87*, 5.

[Schroeder et al., 1994] Schroeder, P. R., Lloyd, C. M., Zappi, P. A., and Aziz, N. M. (1994). The hydrologic evaluation of landfill performance (HELP) Model: users guide for version 3. EPA/600/R-94/168a. *U.S. Environmental Protection Agency Risk Reduction Engineering Laboratory, Cincinnati, OH*. 31

[Springer and Bair, 1994] Springer, A. E. and Bair, E. S. (1994). Comparison of methods used to delineate capture zones of wells: 2 Stratified-drift buried-valley aquifer. *Ground Water*, 30(6):908–917. 58

[Sudicky, 1989] Sudicky, E. A. (1989). The Laplace transform Galerkin technique: A time continuous finite element theory and application to mass transport in groungwater. *Water Resources Research*, 25:1933–1846. 11

[Technical Experts Committee, 2004] Technical Experts Committee (2004). Watershed-based source protection planning: Science-based decision-making for protecting Ontario's drinking water resources. *Ministry of the Environment, Canada*.

[Thomson and Sykes, 1990] Thomson, N. R. and Sykes, J. F. (1990). Sensitivity and uncertainity analysis of a short-term sea ice motion model. *Geophysical Research*, 95:1713–1739. 158

[Thornthwaite, 1948] Thornthwaite, C. W. (1948). An approach toward a rational classification of climate. *Geographical Review*, 38:55–94. 31

[Trotta, 1985] Trotta, L. C. (1985). The potential for contamination of ground water based on hydrogeology - A geographical information system application. Abstract. *In Annual Midwest Ground Water Conference 30th October 23-25. St. Paul, Minnesota, 19*. 3

[Uffink, 1989] Uffink, G. J. M. (1989). Application of Kolmogorov's backward equation in random walk simulations of groundwater contaminant transport. *Contaminant Transport in Groundwater (ed. by H. E. Kobus and W. Kinzelbach). A. A. Balkema, Rotterdam, The Netherlands*. 59, 60, 96

[U.S. Environmental Protection Agency (EPA), 1987] U.S. Environmental Protection Agency (EPA) (1987). *Guidelines for delineation of wellhead protection areas*. Office of Water, Report EPA-4405-93-001.

[U.S. Environmental Protection Agency (EPA), 1997] U.S. Environmental Protection Agency (EPA) (1997). *State Source Water Assessment and Protection Program Guidance: Final Guidance*. Office of Water, Report EPA 816-R-97-009.

[Van Genuchten, 1986] Van Genuchten, M. T. (1986). A closed-form equation for predicting the hydraulic conductivity of unsaturated soils. *Soil Science Society of American Proceedings*, 44:892–898. 11

[Van Leeuwen et al., 1998] Van Leeuwen, M., te Stroet, C. B. M., Butler, A. P., and Tompkins, J. A. (1998). Stochastic determination of well capture zone. *Water Resources Research*, 34(9):2215.

[Van Stempvoort et al., 1992] Van Stempvoort, D. R., Ewert, D. L., and Wassenaar, L. (1992). AVI: A method for groundwater protection mapping in the prairie provinces of Canada. Prairie Provinces Water Board Report 114, Regina, SK. 24

[Vassolo et al., 1998] Vassolo, S., Kinzelbach, W., and Schafer, W. (1998). Determination of well head protection zone by inverse stochastic moodeling. *Journal of Hydrolody*, 206:168–280.

[Vrba and Zoporozec, 1994] Vrba, J. and Zoporozec, A. (1994). Guidebook on mapping groundwater vulnerability. *International Contributions to Hydrology, H.Heise Plublisher, Hannover*. 129

[Ward et al., 2003] Ward, M., Riley, D., Merkle, S., and Lynch, C. (2003). Nitrate in public water supplies and risk of bladder cancer. *Epidemiology*, 14(2):183–190. 2

[Waterloo Hydrogeologic Inc., 2000] Waterloo Hydrogeologic Inc. (2000). *Delineation of well field capture zones within the Waterloo Moraine final report to the Regional Municipality of Waterloo*. Ontario, Canada.

[Weyer et al., 2001] Weyer, P., Cerhan, J., Kross, B., Hallberg, G., Kantamneni, J., Breuer, G., Jones, M., Zheng, W., and Lynch, C. (2001). Municipal drinking water nitrate level and cancer risk in older women: The Iowa Women′s Health Study. *Epidemiology*, 12(3):327–338.

[Wilson and Liu, 1995] Wilson, J. L. and Liu, J. (1995). Backward tracking to find the source of the pollution in waste management: From Risk to Reduction, edited by R. Bahda. *Albuquerque, New Mexico: ECM Press*, pages 181–199. 4, 59, 60, 96

[Worrall et al., 2000] Worrall, F., Wooff, A. H. S., and Coolen, F. P. A. (2000). New approaches to assessing the risk of groundwater contamination by pesticides. *Journal of the Geological Society*, 157(4):877–884.